Fundamental Studies of the Structures, Energetics and Collision Dynamics of Large Molecules in the Gas Phase

Thesis by

Elaine M. Marzluff

In Partial Fulfillment of the Requirements

for the Degree of

Doctor of Philosophy

California Institute of Technology

Pasadena, California

1995

(Submitted December 28, 1994)

ACKNOWLEDGMENTS

This work described in this thesis would not have been possible without the help of a number of people who deserve mention here. Professor Jack Beauchamp has served as my advisor and especially deserves thanks for the useful discussions and encouragement of this work. Group dinners sponsored by Jack and Pat and always featuring good food will be much missed.

The members of the Beauchamp group have contributed to this work with helpful discussions and participation in many agonizing hours of instrument building and maintenance. Sherrie Campbell, Mary Rodgers and Jim Smith played active roles in the research described in this thesis. The other members of the Beauchamp group, past and present, deserve acknowledgment and include Karl Irikura, Srihari Murthy, Edmund Fowles, Manuel de Piedade, Shu Li, Marcel Widmer, Kevin Crellin and Hakno Lee.

I have made many friends here and the social opportunities, including hiking, mountain biking and skiing, which they allowed me to participate in provided an often needed break from work. These fun times with Teri Longin, Steve O'Connor, Bob Terbrueggan, Mark McCleskey, Christine Nelson, Faiz Kayyem, Bob Blake, Ariel and Marni Anbar, Jim Smith, Pin Chen, and Sakae Suzuki will be well remembered.

ABSTRACT

The construction and application of an external source Fourier transform ion cyclotron resonance mass spectrometer equipped with a fast atom bombardment source for studies of biological molecules is described. The instrument features an octopole ion guide, Shulz-Phelps ionization gauge and 7-Tesla superconducting magnet and has been specifically designed for quantitative studies of biological molecules. The primary focus of the work described here has been the development of chemical and physical probes to examine the properties and structures of biomolecules in the gas phase.

The results of a complete study of the low energy dissociation pathways using off resonance collisional activation of deprotonated peptides is presented. The dissociation pathways are governed by the site of charge and yield partial C-terminus sequence information in favorable cases. Application of statistical RRKM calculations to these systems allows a qualitative understanding of the energetic changes associated with the observed dissociation processes. The bimolecular reactivity of these species was investigated. Several reactions taking advantage of the nucleophilicity of the deprotonated carboxylic group were observed. This is particularly noteworthy as there are few previously reported instances of bimolecular reactions (other than proton transfer) involving biological species in the gas phase.

The results of the above study identified a homologous system of deprotonated peptides which dissociate with similar activation parameters. This was used as a model system to investigate the effect of molecular size on the collisional

activation process. Contrary to the common belief that it is inherently harder to activate large molecules and induce dissociation, it was discovered that molecules with many degrees of freedom dissociate more readily than molecules with fewer degrees of freedom. This is attributed to the ability of these molecules to easily deform and efficiently convert translational energy into internal excitation.

The mechanism of the collisional energy transfer was investigated using trajectory calculations with a molecular mechanics force field. The collisions appear to be impulsive in nature and energy transfer occurs on a timescale similar to a vibrational period. Large molecules have the ability to undergo several encounters with the collision gas in a single collision event, each encounter resulting in a significant amount of internal energy being transferred into internal modes.

A master equation analysis was applied to the off resonance collisional activation process in an attempt to obtain a more quantitative understanding of the dissociation energetics of large molecules. This analysis takes into account all processes contributing to the change in ion internal energy. The primary result of this analysis was the observation that a significant fraction of the ions formed in the collisional activation process have a large internal energy and are slow to collisionally relax under conditions employed in our experiments. A more thorough knowledge of this energy distribution is required before an analysis such as this can be used.

TABLE OF CONTENTS

Introduction

Recent advances in ion source technology have made possible the study of large biological molecules in the gas phase by mass spectrometry. Techniques such as fast atom bombardment (FAB),[1] liquid secondary ion mass spectrometry (LSIMS),[2] matrix assisted laser desorption ionization (MALDI),[3] and electrospray ionization (ESI)[4] have proven to be efficient vaporization and ionization techniques for creating quasimolecular (i.e., protonated, deprotonated and metalated) peptides and protein ions in the gas phase. Molecules with molecular weights exceeding 5,000,000 daltons have been successfully ionized and detected.[5]

The primary focus of the research described in this thesis has been the development of chemical and physical probes to examine the properties and structures of biomolecules in the gas phase. To carry out these studies an external source Fourier Transform Ion Cyclotron Resonance Mass Spectrometer (FT-ICR) interfaced with a Liquid SIMS source was constructed. Several recent reviews cover the general theory and use of ICR for the study of ion-molecule reactions.[6] FT-ICR is a rapid, sensitive technique for obtaining high resolution mass spectra. Ions are trapped in a magnetic field and detected in a non-destructive manner, making it an ideal method for carrying out laser dissociation, collisional activated dissociation (CAD) and chemical reactivity studies.

Chapter 1 of this thesis describes in detail the design and construction of an external source FT-ICR equipped with a Liquid SIMS source. Much of this instrument was fabricated by IonSpec. Corporation (Irvine, CA) to our specifications.

Chapter 1 gives particular attention to the parts of the instrument designed, constructed and installed in our laboratory. These include the octopole ion guide, Shulz-Phelps ionization gauge, and laser access window, as well as associated electronics. Examples of the use of the instrument for obtaining mass spectra of a variety of molecules are given. Appendix 1 includes a description of the care and maintenance of the Oxford 7-Tesla superconducting magnet.

One of the initial applications of this instrumentation was a complete study of the low energy collisional activation products of small deprotonated peptides.[7] This is the subject of Chapter 2. Sustained off resonance collisional excitation was used as the primary activation technique.[8] Application of a radio frequency pulse slightly off resonance from the frequency of the selected ion cause the ion to oscillate with low (< 5 eV center of mass), bounded translational energies. In the presence of a collision gas the ion undergoes multiple collisions, each one resulting in some of the translational energy being transferred into internal excitation. The internal energy of the ion will slowly increase until the ion undergoes unimolecular dissociation. This allows the determination of low energy fragmentation pathways. For deprotonated peptides, the dissociation pathways are governed by the site of charge and yield partial c-terminal sequence information in favorable cases. The bimolecular reactivity of these species was also investigated. Several reactions taking advantage of the nucleophilicity of the deprotonated carboxylic group were observed. This is particularly noteworthy as there are few previously reported instances of bimolecular reactions (other than proton transfer) involving biological species in the gas phase.

Chapter 3 describes a preliminary study of the dynamics and mechanism of the collisional activation process.[9] Such studies have been limited due to the lack of ideal model systems. The studies carried out in Chapter 2 led to the identification of a homologous series of deprotonated peptides which dissociate with similar activation parameters. These peptides were used to investigate the effect of molecular size on the efficiency of collisional activation. Contrary to the common belief that it is inherently harder to activate large molecules and induce dissociation, it was discovered that molecules with many degrees of freedom dissociate more readily than molecules with fewer degrees of freedom. This is attributed to the ability of these molecules to undergo collisions resulting in up to 100% of the center of mass kinetic energy being converted into internal excitation. Preliminary trajectory calculations using molecular mechanics force fields support the observed experimental patterns.

Chapter 4 details the use of computational methods, particularly RRKM and molecular mechanics collision trajectory calculations for further understanding the process of collisional activation of large molecules. In part I of this chapter, the assumptions and methodology for carrying out RRKM calculations are described in detail. Such calculations are relatively easy to perform and enable estimates of activation energies and experimental collision efficiencies to be determined. They are also useful for determining the likelihood that observed product distributions are the result of sequential or competitive dissociation pathways.

In part II of Chapter 4 the results of ion molecule collision trajectory calculations using molecular mechanics are described. These calculations support the high efficiency of collision energy transfer experimentally observed in Chapter 3.

The amount of energy transferred is a strong function of molecule size and relative collision energy. Increasing either the size of the molecule or the collision energy results in more efficient energy conversion into internal modes during the collision, to the point where collisions of bradykinin (a nonapeptide with 444 degrees of freedom) results in typical energy conversions of greater than 90% at a relative energy of 50 eV. The amount of energy transferred in any given collision is a function of where the molecule strikes the peptide. The collisions appear to be impulsive in nature and energy transfer occurs on a timescale similar to a vibrational period. It is observed that with larger molecules the collision partners can undergo multiple distinct encounters in each collision event, with each one transferring a significant fraction of energy into internal modes. Trajectory calculations indicate that the use of a fast ion in place of a neutral collision partner still results in high energy conversion efficiencies.

The understanding of the collision events from the experiments and calculations described in Chapter 3 and 4 led us to pursue the idea of applying a master equation analysis to the collisional activation process in an attempt to obtain more quantitative information. This is the subject of Chapter 5. A master equation analysis was performed on the dissociation of the deprotonated peptide gly-gly-ile taking into account all of the processes which can add or remove energy from the ion population. This analysis yielded a qualitatively correct energetic picture using the parameters for collisional activation determined from the trajectory calculations in Chapter 4. However, the primary result obtained from these calculations was that a significant fraction of the ions are formed in the SIMS process with very high internal

energies. It appears that radiative relaxation plays a significant role. To obtain quantitative information more detailed information about the initial internal energy distribution of the ions is necessary.

Chapter 6 describes the interface of an electrospray ionization source with a quadrupole mass spectrometer. This chapter is intended as a guide to future users of this instrument, and includes drawings of electronic wiring and fabricated vacuum components required for the interfacing. Examples of spectra obtained with this instrument are included. A description of easily implementable modifications to the instrument to allow a variety of studies included collisional activation and ion mobility experiments is included.

REFERENCES

[1] Barber, M.; Boddoli, R.D.; Sedgwick, R.D.; Tyler, A.N. *J. Chem. Soc. Chem. Commun.* **1981**, 325.

[2] McCullough, S.M.; Gard, E.; Lebrilla, C.B. *Int. J. Mass Spec. Ion Proc.* **1991**, 107, 91.

[3] a. Hillenkamp, F.; Karas, M.; Beacis, R.C.; Chait, B.T. *Anal. Chem.* **1991**, 63, 1193A. b. Castro, J.A.; Koster, C.; Wilkens, C. *Rapid Comm. Mass Spec.* **1992**, 6, 239. C. McIver, R.T.; Li, Y.Z.; Hunter, R.L. *Rapid Comm. Mass Spec.* **1994**, 8, 237-241.

[4] Fenn, J.B.; Mann, M.; Meng, C.K.; Wong, S.F.; Whitehouse, C.M.; *Science*, **1989**, 246, 64.

[5] Bruce, J.E.; Cheng, X.; Bakhtiar, R.; Wu, Q.; Hofstadler, S.A.; Anderson, G.A.; Smith, R.D. *J. Am. Chem. Soc.* **1994**, 116, 7839-7847.

[6] a. Marshall, A.G.; Grosshans, P.B.; *Anal. Chem.* **1991**, 63, 215-229A. b. Nibbering, N.M.M. Acc. Chem. Res. 1990, 23, 279-285. c. Burlingame, A.L.; Malthy, D.; Russell, D.H.; Holland, P.T. *Anal. Chem.* **1988**, 60, 294R.

[7] Marzluff, E.M.; Campbell, S.; Rodgers, M.T.; Beauchamp, J.L. *J. Am. Chem. Soc.* **1994**, 116, 7787-7796.

[8] Gauthier, J.W.; Trautman, T.R.; Jacobsen, D.B. *Anal. Chim. Acta.* **1991**, 246, 211-225.

[9] Marzluff, E.M.; Campbell, S.; Rodgers, M.T.; Beauchamp, J.L. *J. Am. Chem. Soc.* **1994**, 116, 6947.

Chapter 1

Design, Construction and Implementation of Beckman Institute External Source Fourier Transform Ion Cyclotron Resonance Mass Spectrometer

A modified IonSpec (Irvine, CA) external source instrument equipped with a fast atom bombardment source (FAB) and specifically designed for quantitative studies of biomolecule reaction dynamics was used to carry out these studies. The instrument, shown schematically in Figure 1-1, has three differentially pumped regions containing an ion source, octopole ion guide and analyzer cell. An Oxford Mark II 7-Tesla superconducting magnet is used to supply the homogeneous magnetic field. A more complete description of the use and care of the magnet is included in Appendix I. APD cryopumps (APD-6 1000 liters/second) provide pumping in each of the three regions of the vacuum chamber with operating pressures of 5×10^{-10} torr as measured by an internal Granville-Phillips Ionization Gauge above the pump adjacent to the magnet. Due to the proximity of the magnetic field, the cryopump motors are shielded with cold rolled steel. Prior to shielding, the cryopump motor on the pump located closest to the magnet failed after about 1 1/2 years of operation. (The motor had material in it which had become magnetized, causing it to cease proper operation.) Unique features of the instrument include an octopole ion guide, a split injection electrode to improve the efficiency of ion trapping, and an ionization gauge designed to measure pressures at the analyzer cell in the high magnetic field. The instrument is designed to carry out fundamental studies of the energetics and reactivity of biological molecules.

Fast Atom Bombardment Ion Source. The ion source region is equipped with an Antek cesium ion gun (Model 160-250B) controlled with a PS4 power supply. Samples are transferred into vacuum through an interlock using an MDC high vacuum motion feedthrough assembly. The gun is mounted on a cube consisting of

Figure 1-1. Schematic Diagram of Beckman Institute external ion source FT-ICR, showing location of ion source, pumping regions, octopole ion guide, analyzer cell and gas inlet system.

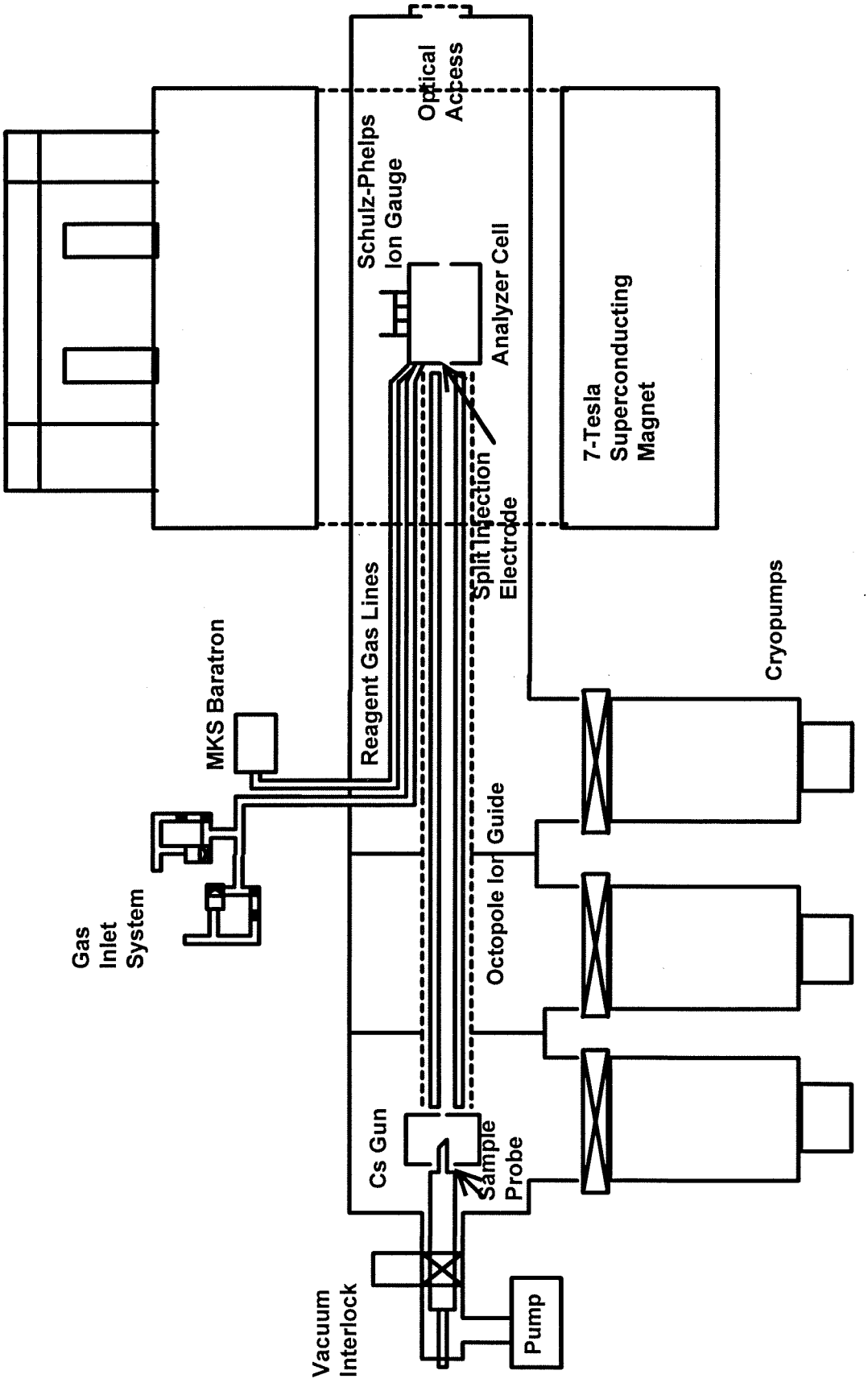
Optical Access
Schulz-Phelps Ion Gauge
Analyzer Cell
7-Tesla Superconducting Magnet
Split Injection Electrode
Reagent Gas Lines
MKS Baratron
Gas Inlet System
Octopole Ion Guide
Cryopumps
Cs Gun
Sample Probe
Vacuum Interlock
Pump

six independently controllable lenses for ion beam directing and extracting. The gun and source are shown schematically in Figure 1-2. Typical voltages are set on the controller with the MS Accel at 8.25 kV, the lens at 1.375 kV and the extractor at 430 volts with respect to the anode. This results in a beam of cesium ions about 2 mmx2mm with 1-2 microamps intensity. Ions are typically extracted from the source regions with potentials of 350 to 500 volts. The source is reasonably durable; however, accidental exposure of the high voltage power supplies to high pressures can cause arcing and has several times caused the destruction of the extractor power supply. Replacement supplies can be obtained from Bertan (PMT-1500N). The cesium pellet is good for about three months of experiments; replacement pellets are available from Antek. Depending on the use of the source, cleaning should be performed every one to three months to avoid permanent damage to the ceramic pieces. It will not necessarily look visibly dirty when it is time for its periodic cleaning; instructions on cleaning the source are included with the Antek manuals.

Figure 1-3a shows potential contours and low energy ion trajectories of a 45 degree probe tip in the ion source cube calculated using SIMION.[1] Typical extractor and repeller potentials of 400 volts are used in this simulation. Ions (with energies of 2-4 volts) which are desorbed normal from the surface feel potentials that are not optimum for ion extraction. Initial studies required the use of a thin shield around the 1/8" copper probe tips to mimic a probe tip with a 90 degree desorption surface. This results in flattened electric potential contours around the probe tip and allows efficient extraction of low energy ions, as shown in Figure 1-3b. The optimum probe tip angle and size for operation without the addition of a shield has been determined to be a 36

Figure 1-2. Schematic diagram of Cesium Ion Gun Source. Typical voltages are MS Accel=8.25 kV, Lens=1.375 kV, and Extractor (on gun)=430 Volts. The source cube repeller varies from 0-400 Volts, and the source cube extractor is typically set at 350-500 Volts. The pairs of side plates opposite each other in the source cube can be used to steer the beam and are typically set close to 100 Volts.

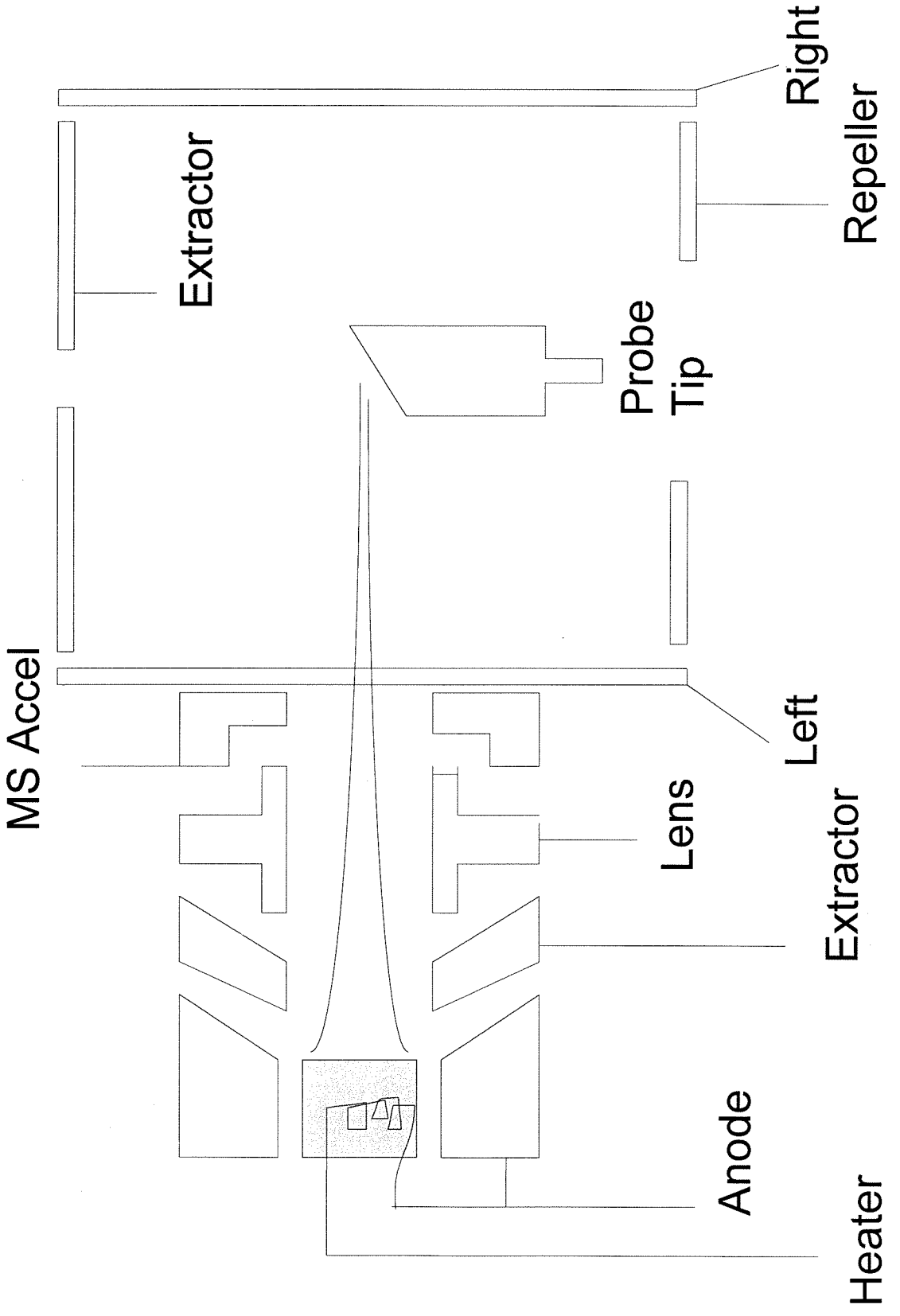
Right
Repeller
Extractor
Probe
Tip
MS Accel
Left
Lens
Extractor
Anode
Heater

Figure 1-3. SIMION potentials and trajectories for low energy ions desorbed from probe tips with different geometries. For this simulation the ions were given initial energies of 2-4 volts, and the extractor=400 volts, the repeller=-400 volts, and the side plates were left at ground. a. Trajectories of ions from a 45 degree probe tip show that ions desorbed normal from the surface with energies up to 10 volts are not efficiently extracted from the source region. b. Trajectories of ions desorbed from a 90 degree probe tip show flattened electrical potentials around the probe tip allowing efficient ion extraction from the source region.

a.

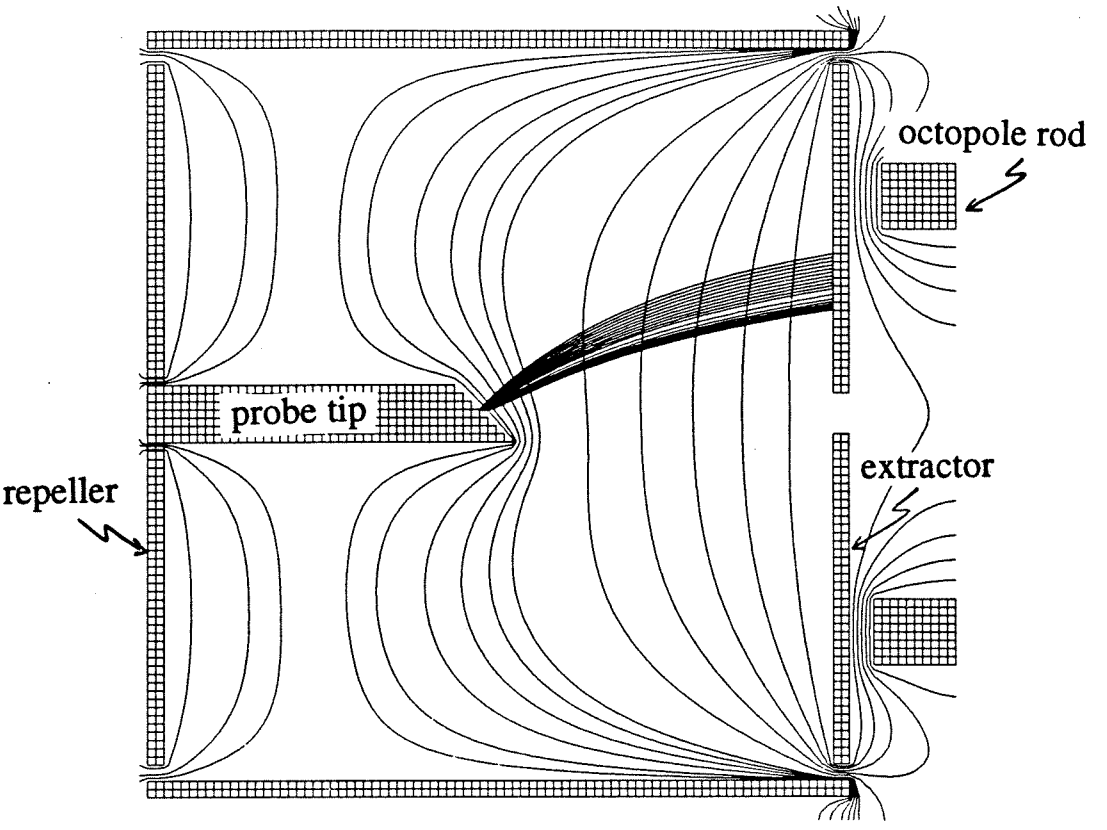
octopole rod
probe tip
extractor
repeller

b.

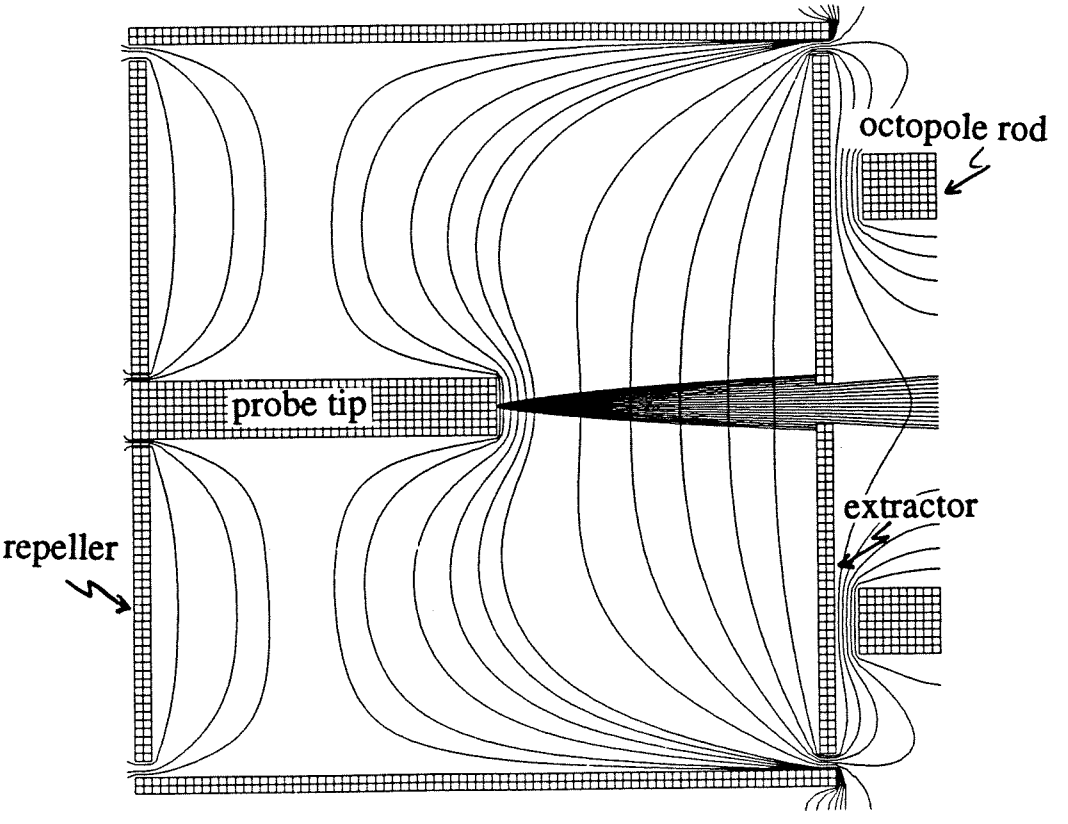
octopole rod
probe tip
extractor
repeller

degree surface with respect to the extractor plate on a 1/4" copper rod (stainless steel rapidly oxidizes with the acidic conditions employed in a typical matrix).

To determine the longitudinal kinetic energies of the ions transmitted to the analyzer cell, a kinetic energy analyzer was constructed and mounted on the rear plate of the cell as shown in Figure 1-4. The energy analyzer consists of three closely spaced grids constructed with 95% transmittance copper mesh. The outer two maintain a constant electric field around the central retarding field grid used to slow down the ions. When not in use the energy analyzer does not otherwise interfere with instrument operation. To measure positive ion kinetic energies, the source and octopole ion guide are turned on continuously. The cell plates are biased at -5 volts to allow transmittance of ions through the cell to the energy analyzer. The two grids around the retarding grid are biased at -9 volts. A picoampmeter that can be biased with respect to ground is used to measure the ion current at the collector plate as a function of retarding grid voltage, and this gives a measure of the ion kinetic energies.

An insertion probe that can be independently biased at positive or negative offset voltage was also constructed. Energy curves for cesium iodide with the probe tip biased at 5 volts, 0 volts and -5 volts are shown in Figure 1-5. Most of the ions have kinetic energies that range from 5 to 15 eV and these energies are not affected by the probe bias voltage. Changing the energy and intensity of the primary Cs^+ desorption beam has little effect on the curves obtained. Instead the amount of current observed varies depending on the probe voltage although the shape of the curve does not change (Figure 1-5b). The spectra obtained with probe tip voltages of -5, 0 and 5 volts are shown in Figure 1-6. They are similar in quality though the

Figure 1-4. Schematic diagram of energy analyzer mounted on rear of analyzer cell.

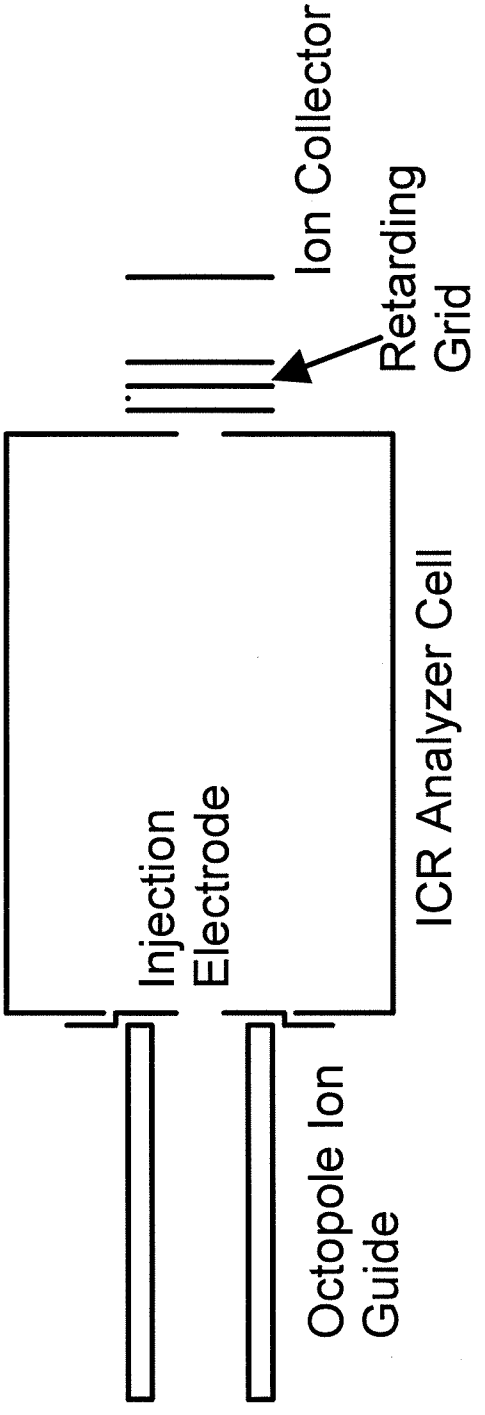
Ion Collector
Retarding Grid
ICR Analyzer Cell
Injection Electrode
Octopole Ion Guide

Figure 1-5. Energy distribution curves as measured by the stopping grid for Cesium Iodide with the probe tip biased at 5 Volts, 0 Volts and -5 Volts.

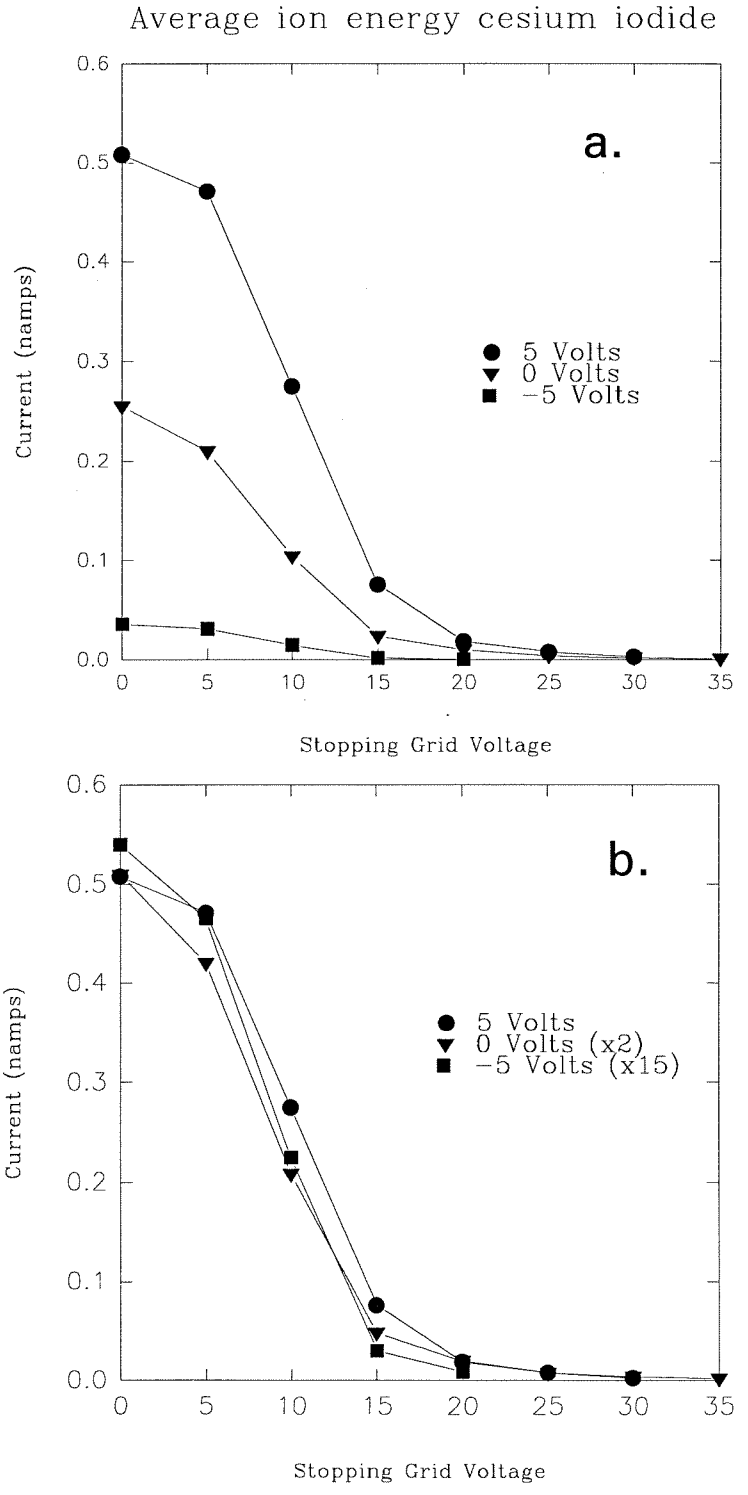
Average ion energy cesium iodide
a.
5 Volts
0 Volts
−5 Volts
Current (namps)
Stopping Grid Voltage
b.
5 Volts
0 Volts (x2)
−5 Volts (x15)
Current (namps)
Stopping Grid Voltage

Figure 1-6. Cesium Iodide Spectra at various probe tip voltages. a. +5 Volts. b. 0 Volts. c. -5 Volts.

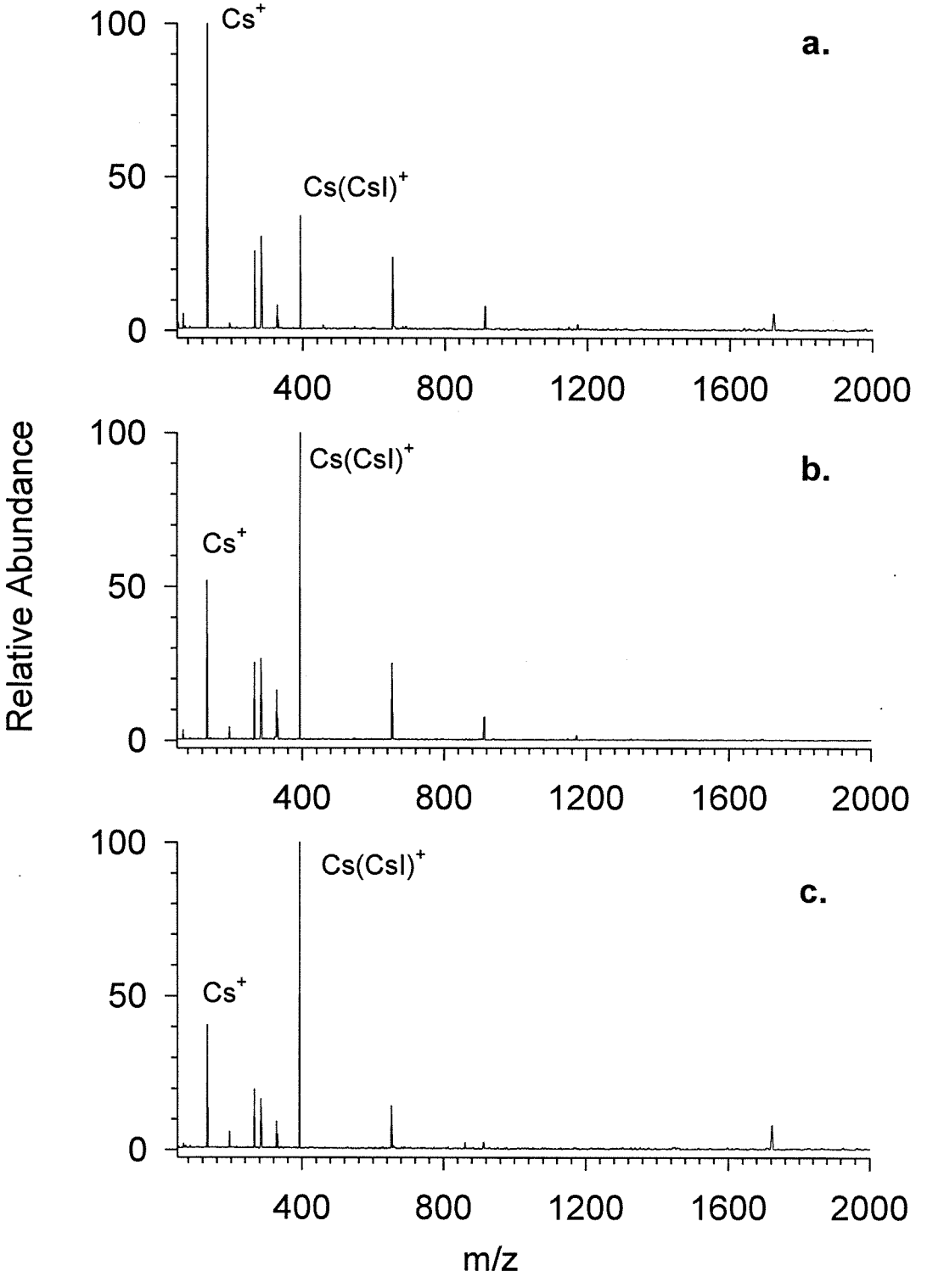
Relative Abundance
100
50
0
Cs+
Cs(CsI)+
a.
b.
c.
400
800
1200
1600
2000
m/z

spectrum with the probe at +5 volts contains a lot more of the bare Cs^+ as compared to the others. The higher current at positive probe bias voltages is thus attributed to more Cs^+ ions being present in the beam of ions extracted from the source region. The small effects observed from changing the probe conditions when operating with a cesium iodide sample (which, unlike peptides, is not run out of a liquid matrix) is hypothesized to be a result of reflection of the primary Cs^+ beam, accounting for the high energy ions observed.

The energy curves for the simple protonated peptide gly-gly-ile (m/z 246) are shown in Figure 1-7. Unlike the cesium iodide clusters, the kinetic energy of these ions is affected by the probe bias voltage. When the probe is at ground (normal operation), the protonated peptide ions have significantly less kinetic energy and narrower energy distributions than the desorbed cesium iodide clusters. Most of the ions have kinetic energies ranging between 2 and 4 eV. This is the preferred range of energies where ions can be efficiently trapped. Despite the fact that the energy distributions and observed ion current changes dramatically as the probe bias is changed, the mass spectra obtained when the probe is biased at 0 volts and 5 volts are virtually identical.

Sample Preparation. In a typical experiment the peptide is dissolved in a thin layer of glycerol coated on the copper probe tip. For protonated positive ions a small amount of triflouroacetic acid is then added; for deprotonated negative ions a small amount of ammonium hydroxide is added. If the peptide is not soluble in the matrix, it is first dissolved in water and then added to the glycerol. For cesium iodide samples, the cesium iodide is dissolved into a saturated water solution. This is placed

Figure 1-7. Energy distribution curves for the protonated peptide gly-gly-ile as a function of probe tip voltage.

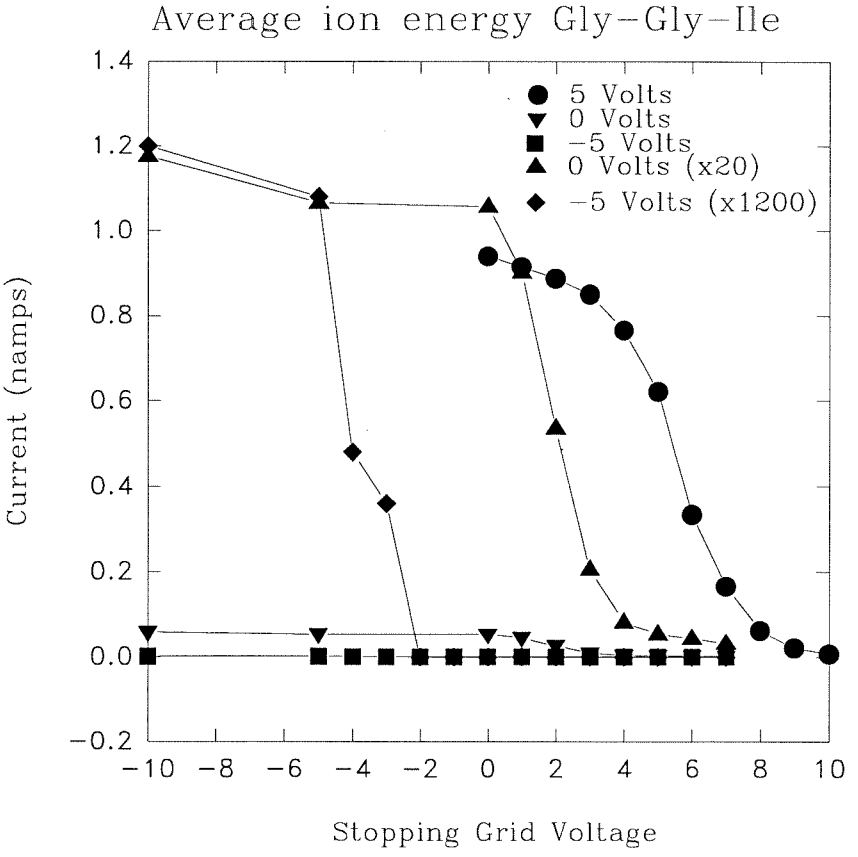
Average ion energy Gly-Gly-Ile
5 Volts
0 Volts
−5 Volts
0 Volts (x20)
−5 Volts (x1200)
Current (namps)
1.4
1.2
1.0
0.8
0.6
0.4
0.2
0.0
−0.2
−10
−8
−6
−4
−2
0
2
4
6
8
10
Stopping Grid Voltage

on the probe tip and the water allowed to evaporate prior to loading into the ion source. Porphyrin samples are typically dissolved in nitrobenzyl alcohol on the probe tip. It is not necessary to add acid or base to the porphyrin samples.

Octopole Ion Guide. To transport ions from an external source into an analyzer cell in a high magnetic field, it has been shown that care must be taken to avoid magnetic mirror effects which reflect ions from the high magnetic field region. Both Smalley type lenses[2] and quadrupole ion guides[3] have been successful in delivering ions through the magnetic fringing fields to the detector cell. Theoretical calculations predict an octopole ion guide has several advantages over these conventional lenses.[4] The octopole permits a more efficient transfer of ions with large off-axis translational energies from the external source to the detector cell. An octopole ion guide, designed and constructed in our laboratory, allows ions to be transported efficiently from the source region to the analyzer cell 47 inches away in the high magnetic field. The octopole is constructed with 1/8 inch stainless steel rods 47 inches in length and supported in a flight tube with six ceramic rings spaced along its length on a diameter of 0.465 inches. The end on assembly including dimensions is shown in Figure 1-8. Two extra ceramics have been machined and are available in the event of breakage. Because of the design limitations of the counterbore in the ceramic and the thickness of the rods, the 0-80 allen head screws that hold the rods in place need to be cut to a length of 0.339 inches.

The octopole is powered by an ENI power amplifier (Model 2100L) driven by a Wavetek function generator (Model 190). A schematic diagram of the electronic circuit is shown in Figure 1-9. The higher radio frequency (rf) voltages required to

Figure 1-8. Schematic diagram of octopole ion guide designed and constructed in our laboratory for use in this instrument.

Thru hole and countersink
for 0-80 screws

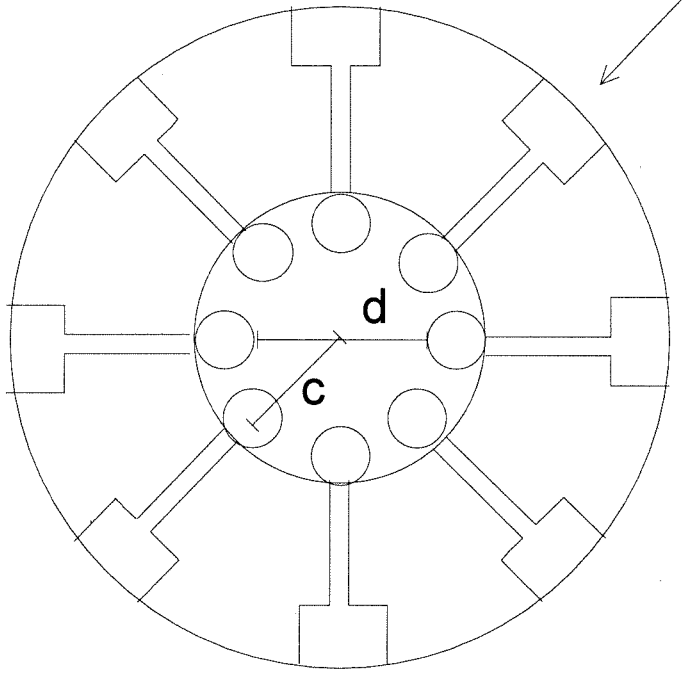

Ceramic O.D.=1.360"
Ceramic I.D.=0.590"
Rods are 1/8" diameter
c=0.2325"=5.91 mm
d=0.340"=8.64 mm
Counterbore=.109"

Figure 1-9. Schematic diagram of electronic circuit designed to provide rf and dc to the octopole ion guide.

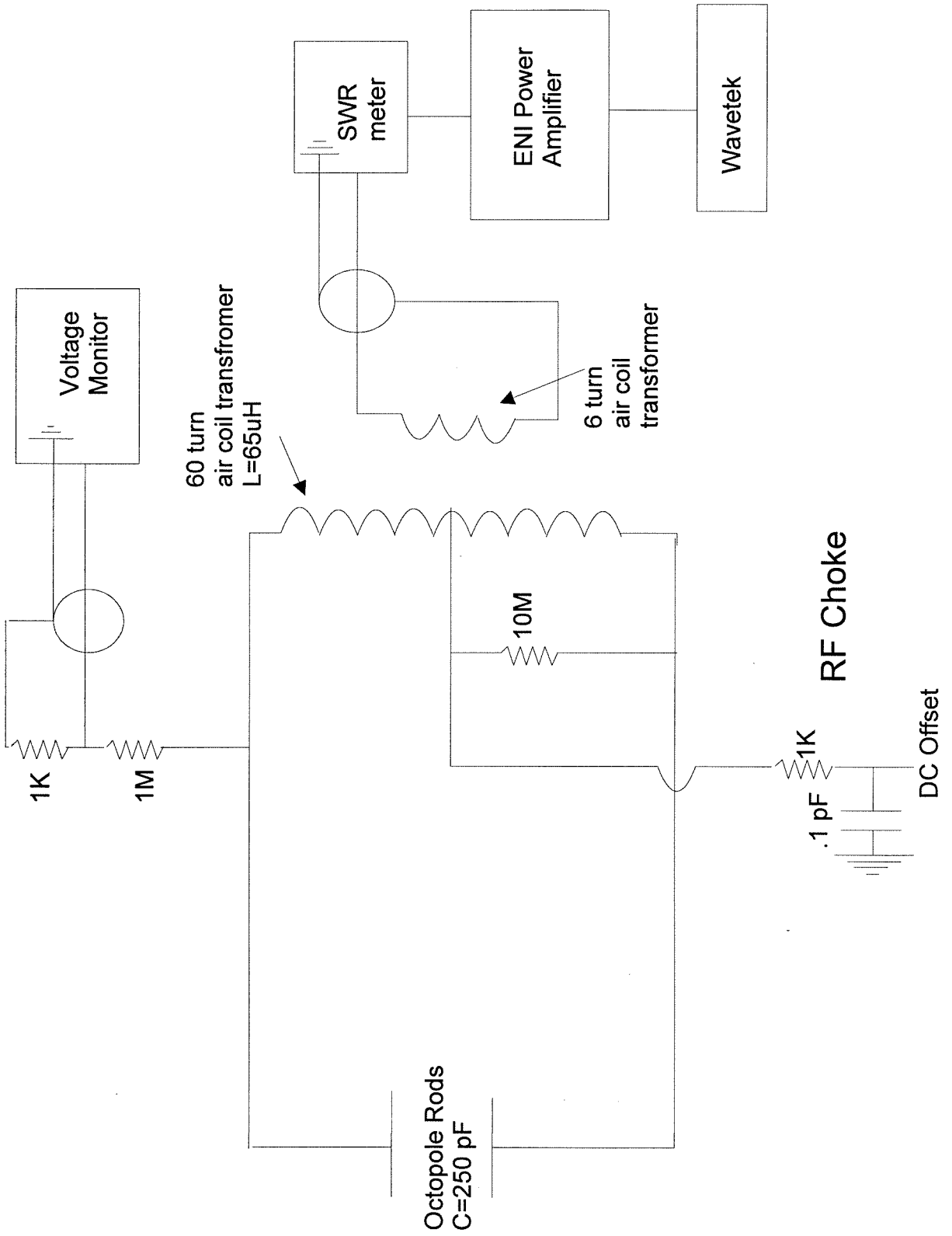
Wavetek
ENI Power Amplifier
SWR meter
Voltage Monitor
60 turn air coil transfromer L=65uH
6 turn air coil transformer
10M
1K
1M
RF Choke
1K
.1 pF
DC Offset
Octopole Rods C=250 pF

drive the octopole are derived from an air coil transformer with the secondary coil forming a tuned *L.C.* circuit with the octopole rods resonating at 1.2 MHz. The octopole rods have a measured capacitance of 250 picofarads. The inductance is provided by an air coil transformer. The air coil transformer provides a times ten voltage gain and consists of a primary coil of six turns of copper wire hand wound over a length of 2 inches around a secondary coil of 60 turns (8 turns/inch) with a diameter of 2 1/2 inches. The inductance of such an air coil can be calculated using Equation 1 where L=inductance in microhenrys; d=coil diameter in inches (2.5), l=coil length in inches (60/8=7.5); n=number of turns=60. Plugging in typical values gives an inductance of 65 microhenrys.[5]

$$L(\mu H) = \frac{d^2 n^2}{18d + 40l} \qquad (1)$$

The theoretical resonance frequency can also be calculated. It is given in Equation 2, and plugging in L=65x10^{-6} Henrys and C=250x10^{-12} farads yields a calculated resonance frequency of 1.25 MHz.

$$f = \frac{1}{2\pi}\sqrt{\frac{1}{LC}} \qquad (2)$$

DC offset is applied to the rods through an rf choke to the center tap of the secondary coil. A 1000:1 voltage divider is used for output of the voltage for monitoring on an oscilloscope. The circuit has such a high Q that it is necessary to detune the circuit by application of a 10 MΩ resistor across the secondary coil to achieve resonance by hand adjustment. To avoid grounding loops that seem to develop between the ENI power amplifier, the chassis and the oscilloscope the electrical inputs are brought in

by isolated grounds that are wired as shown. Typically for good ion transmission below m/z 1000, a 50-150 volt pulse at 1.2 MHz is applied to the octopole rods. The voltage from the ENI power amplifier is passed through a standing wave reflector (SWR) to measure the efficiency of transfer. If it is necessary in the future to change the resonance frequency, this can be done by changing the inductance of the air coil by either adding or removing coil turns or by adding capacitance across the octopole rods.

The octopole guide acts as a broadband mass filter passing a range of masses dependent on the applied frequency and voltage. For more details of the effect of the magnetic field and the non-ideality of the constructed octopole ion guide, see reference 4. The effective potential felt by ions in an ideal octopole ion trap is given by Equation 3 where V_o is the applied rf voltage (0-peak), q is the charge, m is the mass, ω is the frequency and r_o is the inside radius of the octopole. Figure 1-10 shows the potential for a variety of ions and voltages. The potential well is characterized by its uniform potential well and high trapping potentials.

$$U_{eff} = 4\frac{r^6 q^2 V_0^2}{m\omega^2 r_o^8} \qquad (3)$$

The octopole typically is operated with a dc offset of less than 20 volts (negative for positive ions, positive for negative ions). Ions from the FAB source are typically accelerated to 450 volts. As they pass from this region of high potential to the low potential of the guide, trajectory calculations carried out with SIMION (Figure 1-11a) demonstrate that they acquire large amounts of off axis energy. The

Figure 1-10. Effective potentials experienced by ions in the octopole as a function of m/z and applied rf voltage (0-peak). a. Effective potential experienced by an ion with m/z 100 and applied voltage of 50 V. b. Effective potential experienced by an ion with m/z 1000 and applied voltage of 200 V. c. Effective potential experienced by an ion with m/z 2000 and applied voltage of 300 V.

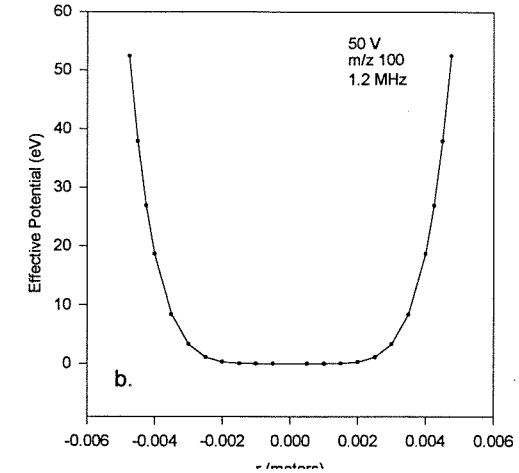
50 V
m/z 100
1.2 MHz
Effective Potential (eV)
b.
60
50
40
30
20
10
0
-0.006
-0.004
-0.002
0.000
0.002
0.004
0.006

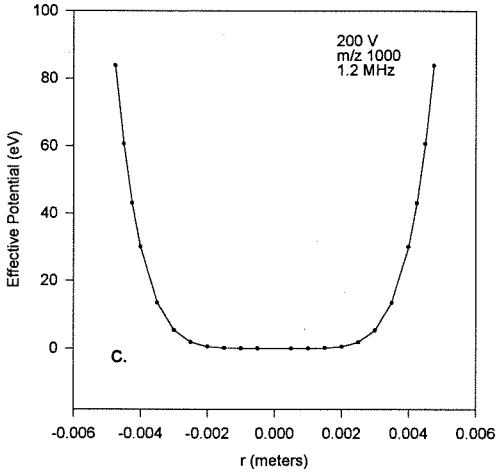
200 V
m/z 1000
1.2 MHz
Effective Potential (eV)
c.
100
80
60
40
20
0
-0.006
-0.004
-0.002
0.000
0.002
0.004
0.006
r (meters)

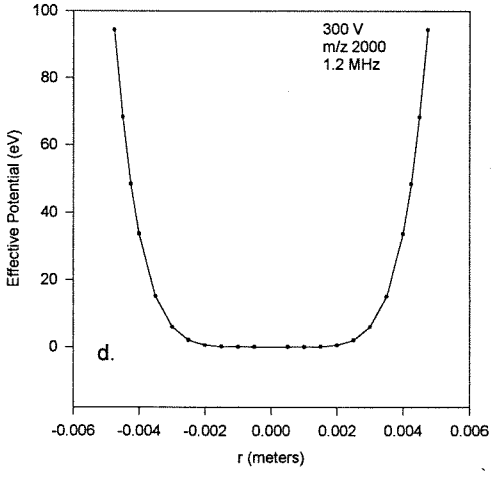
300 V
m/z 2000
1.2 MHz
Effective Potential (eV)
d.
100
80
60
40
20
0
-0.006
-0.004
-0.002
0.000
0.002
0.004
0.006
r (meters)

Figure 1-11. Effect on ion off axis energy for ions traveling from a region of high potential (extractor at -400 Volts) to low potential (octopole at -20 Volts). b. Effect of additional lens (potential at -150 Volts) on reducing this off axis energy gain.

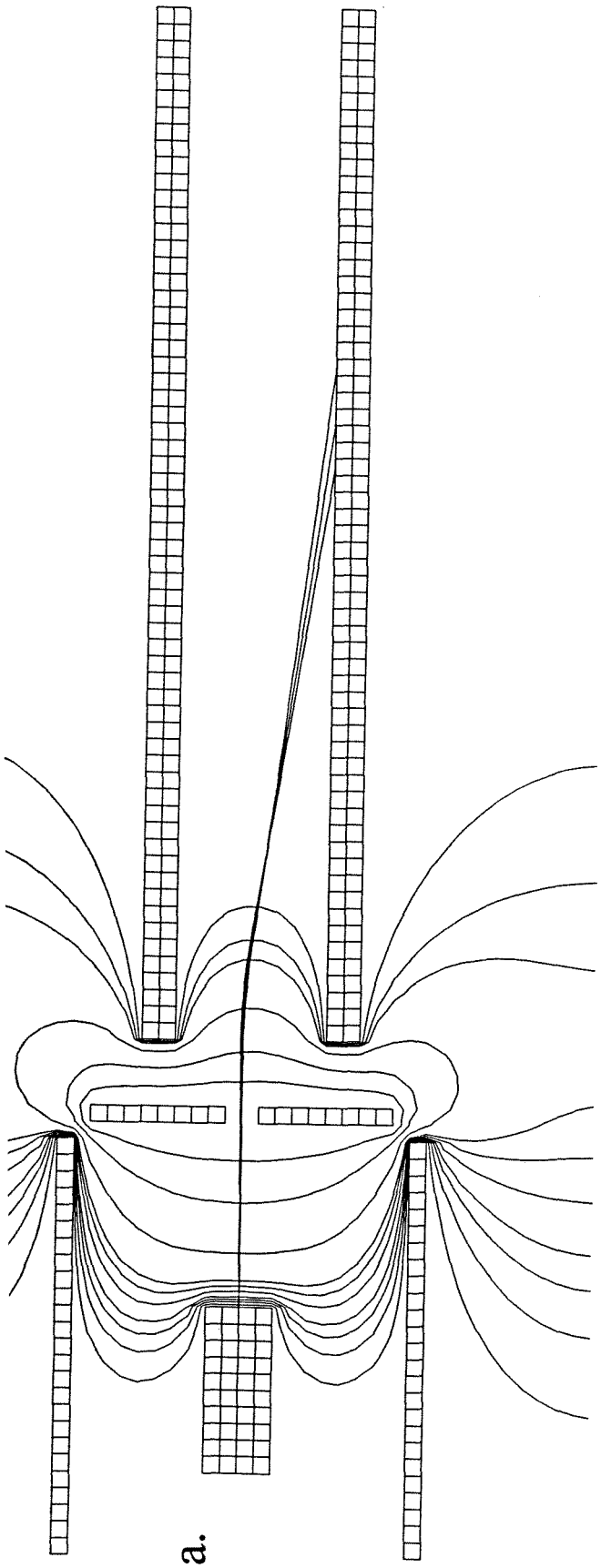

a.

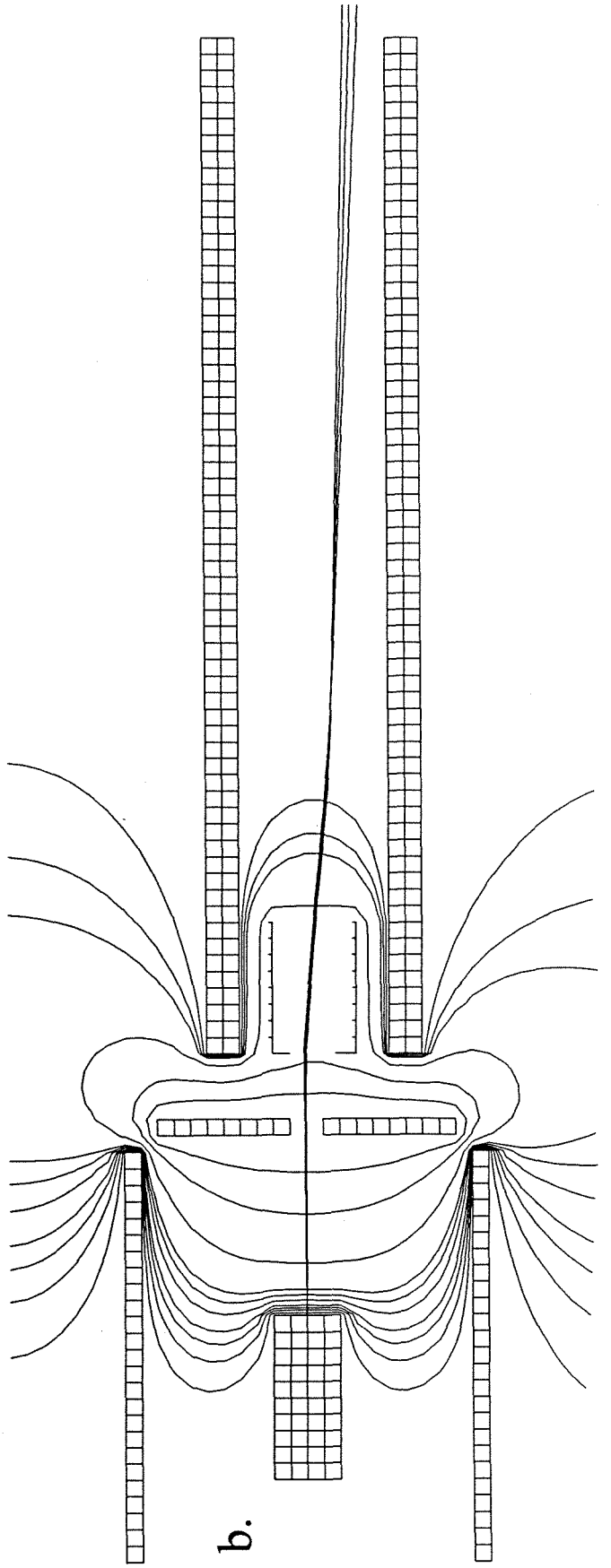

b.

deep potential well of the octopole still allows these ions to be effectively contained within the ion guide. To prevent this large off axis energy gain, an additional lens can be used to provide a more gradual voltage gradient (Figure 1-11b). A design of such a lens which can be incorporated into our existing instrument design is shown in Figure 1-12. This lens has recently been constructed but has not yet been implemented.

The effect of octopole voltage on the mass of ions transmitted is shown in Figure 1-13 for cesium iodide, where the only parameter that has been changed is the applied rf voltage. As the rf voltage is increased, higher mass ions are transmitted and lower masses are excluded. Experimental measurement of ion currents entering and exiting the octopole imply a typical transmission efficiency of 30%. Though careful studies have not been carried out, the observations made in Figure 1-13 imply that this is certainly somewhat dependent on octopole rf voltage. This feature is useful for experiments utilizing a fast atom bombardment source, which generates intense low mass peaks from a liquid matrix. The ions generated with cesium iodide were shown previously (Figure 1-5) to range between 5 and 15 Volts, well above what we can easily trap. Ion energy in the octopole is determined by the DC bias voltage, and with typical offset voltages ions will have flight times in the octopole of 0.1 to 1 milliseconds. For reference Table 1 has the flight times of ions as a function of mass and energy in the octopole. To attempt to slow down these ions, a square wave 2 volts 0-peak with a period of 1.25 milliseconds (800 Hz) was applied to the rods in addition to a low DC offset (-5 volts). Ions which are in the flight tube when the square wave changes should subsequently exit the octopole with either 2 volts

Figure 1-12. Lens designed for mounting over front of octopole.

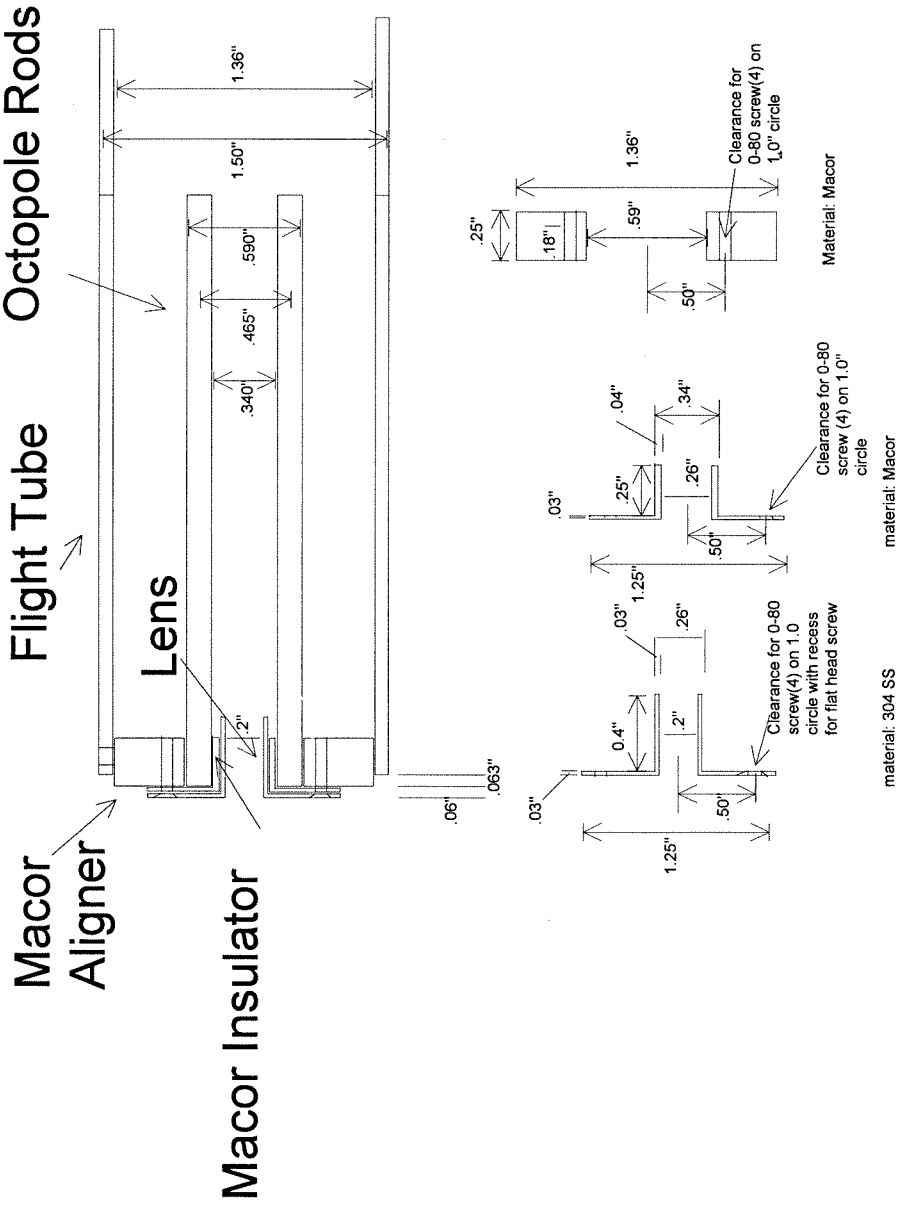
Macor Aligner
Flight Tube
Octopole Rods
Lens
Macor Insulator
1.36"
1.50"
.590"
.465"
.340"
.2"
.063"
.06"
.25"
.18"
.59"
.50"
1.36"
Clearance for 0-80 screw(4) on 1.0" circle
Material: Macor
.04"
.34"
.03"
.25"
.26"
.50"
1.25"
Clearance for 0-80 screw (4) on 1.0" circle
material: Macor
.03"
.26"
0.4"
.2"
Clearance for 0-80 screw(4) on 1.0 circle with recess for flat head screw
.50"
1.25"
material: 304 SS

Figure 1-13. Effect of octopole voltage on ion mass transmitted for Cesium Iodide ($Cs(CsI)^+$) clusters. a. Octopole at 50 Volts (peak to peak) b. 100 Volts (peak to peak) c. 200 Volts (peak to peak).

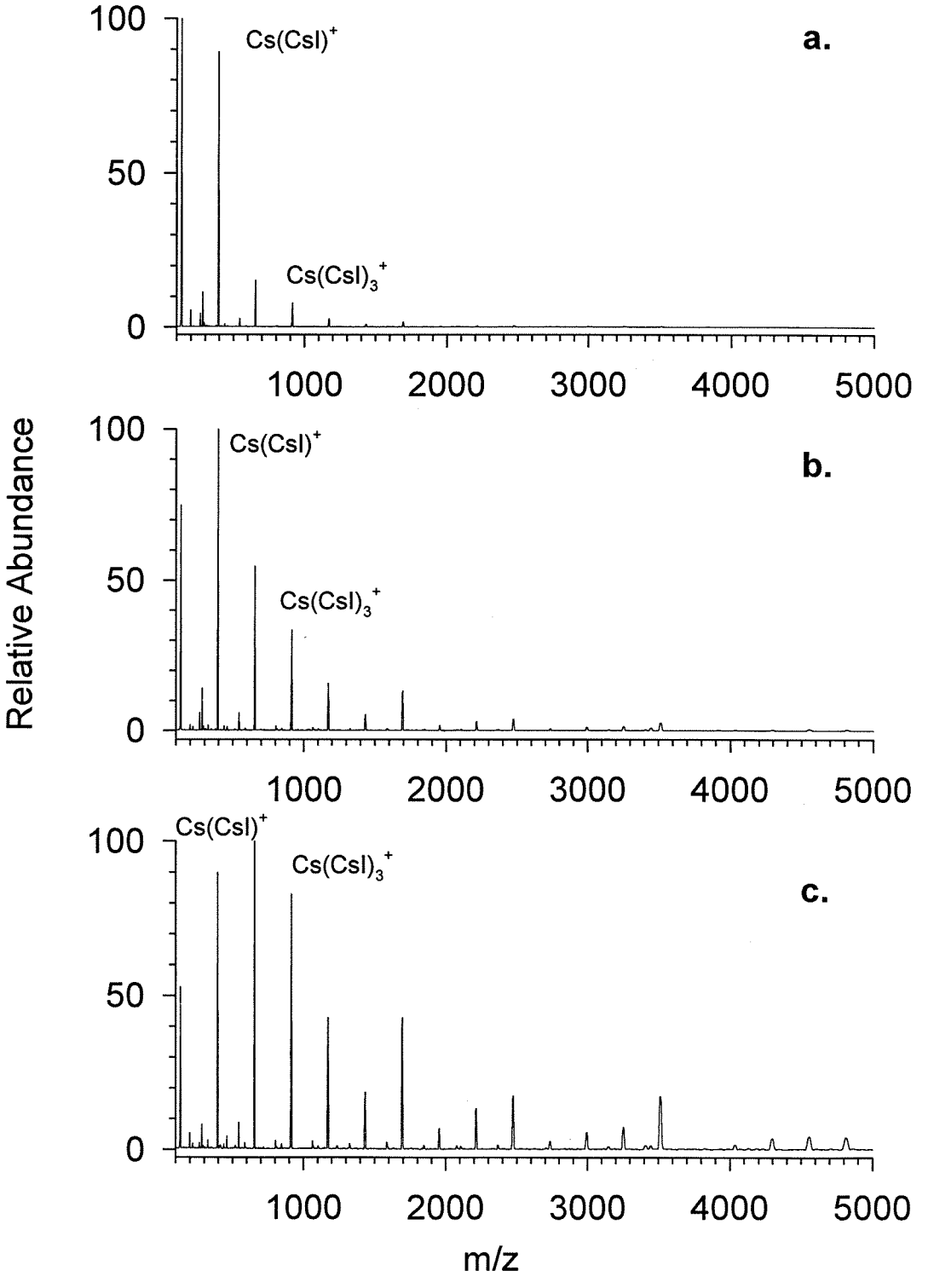
Relative Abundance
100
50
0
Cs(CsI)+
Cs(CsI)3+
a.
b.
c.
1000
2000
3000
4000
5000
m/z

Table 1: Flight time of ions inside the octopole as a function of ion mass and ion energy. For Reference ion frequencies in a 7 Tesla magnetic field are given.

m/z	Ion Energy: 5 eV	10 eV	20 eV	Frequency
100	0.38 ms	0.27 ms	0.19 ms	1.07 MHz
500	0.85 ms	0.60 ms	0.42 ms	215 kHz
1000	1.20 ms	0.85 ms	0.60 ms	107 kHz
1500	1.47 ms	1.04 ms	0.73 ms	71.7 kHz
2000	1.69 ms	1.20 ms	0.85 ms	53.8 kHz
10000	3.83 ms	2.71 ms	1.92 ms	10.8 kHz
20000	5.42 ms	3.83 ms	2.71 ms	5.3 kHz

more or 2 volts less than they would otherwise have. Examples of spectra obtained with and without this square wave applied are shown in Figure 1-14. Application of a square wave slows down enough of the ions to cause the signal to noise of the spectra to increase by a factor of two. In addition more of the low mass ions were trapped, implying that the smaller clusters of cesium iodide are formed with more energy than the larger ones.

Analyzer Cell. The stainless steel analyzer cell with dimensions 2x2x3 inches is centered in the homogenous region of an Oxford instruments MarkII, 7-Tesla superconducting magnet. Replacing all of the cell materials with copper does not result in any observable change in spectra or resolution. An inlet manifold equipped with two Varian (Model 951-5106) and two General Valve (series 9) pulsed valves is configured to deliver gas directly to the analyzer cell through 3/8 inch OD tubing. The General Valve pulsed valves are solenoid driven and do not perform well in the high magnetic fields generated by our magnet. This necessitates locating them several feet from the cell. A schematic diagram of the pulsed valve controller which accepts a TTL input pulse to trigger the valves is shown in Figure 1-15. This controller will work with any solenoid driven device that does not require a time resolution of greater than 2-3 milliseconds. The combination of plumbing and electronic limitations makes obtaining a short burst of gas over a controlled time difficult with the current set-up. Typical pump out times for a high pressure (1×10^{-6} torr) burst of gas are 1-3 minutes. The gas is let into the cell and out to the Baratron through two holes in the front plate of the cell 5/16 inches in diameter covered with mesh (20 lines/inch). These holes do not perturb the effective trapping potential

Figure 1-14. Effect of application of square wave offset on octopole rods during ion loading. a. Constant DC offset applied. b. Application of a square wave of 2 Volts 0-peak with a period of 1.25 milliseconds offset with a same DC voltage as in a.

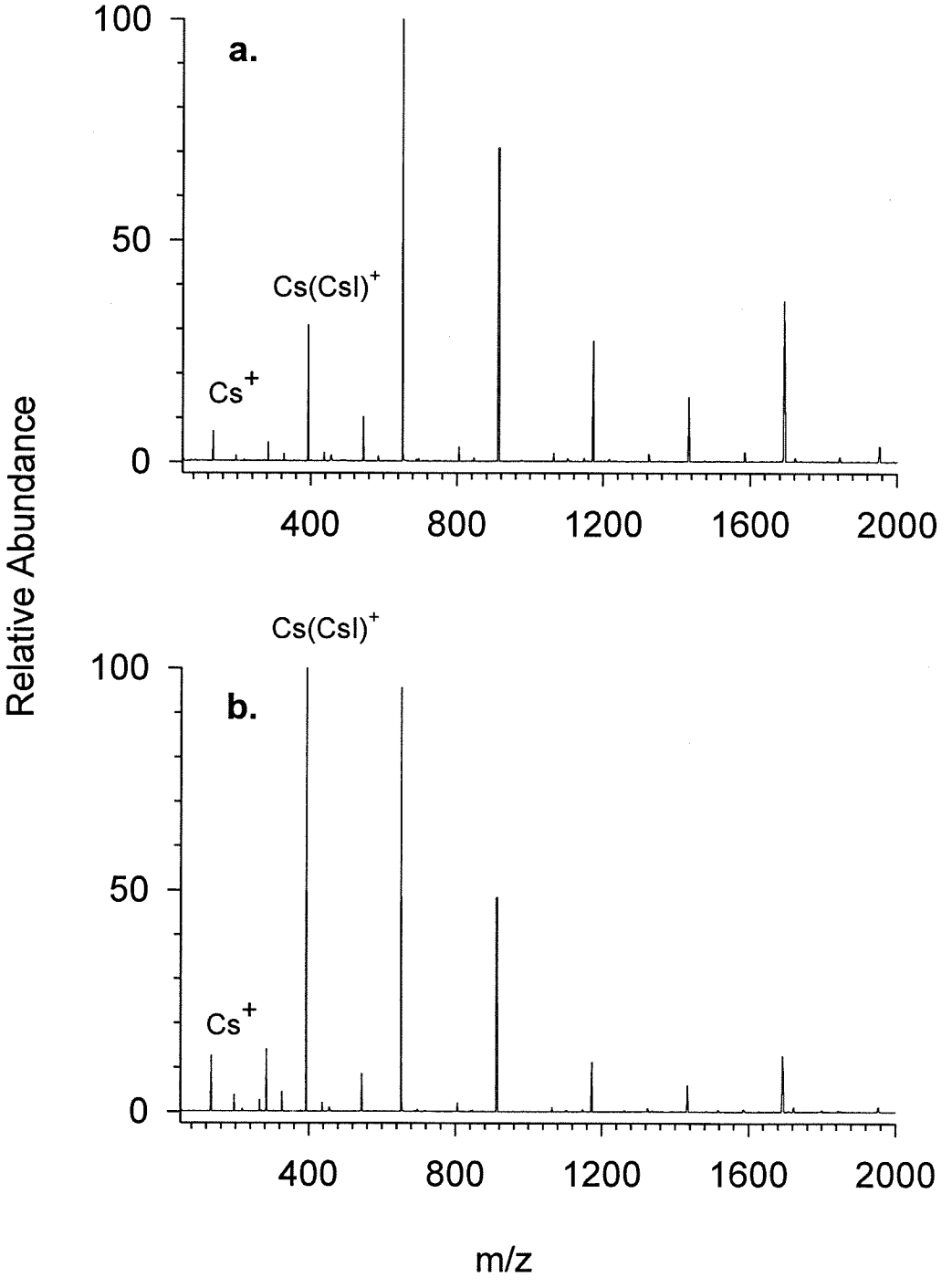
a.
b.
Cs(CsI)+
Cs+
100
50
0
400
800
1200
1600
2000
Relative Abundance
m/z

Figure 1-15. Schematic Diagram of pulsed valve controller circuit that can be operated manually or by computer provided TTL.

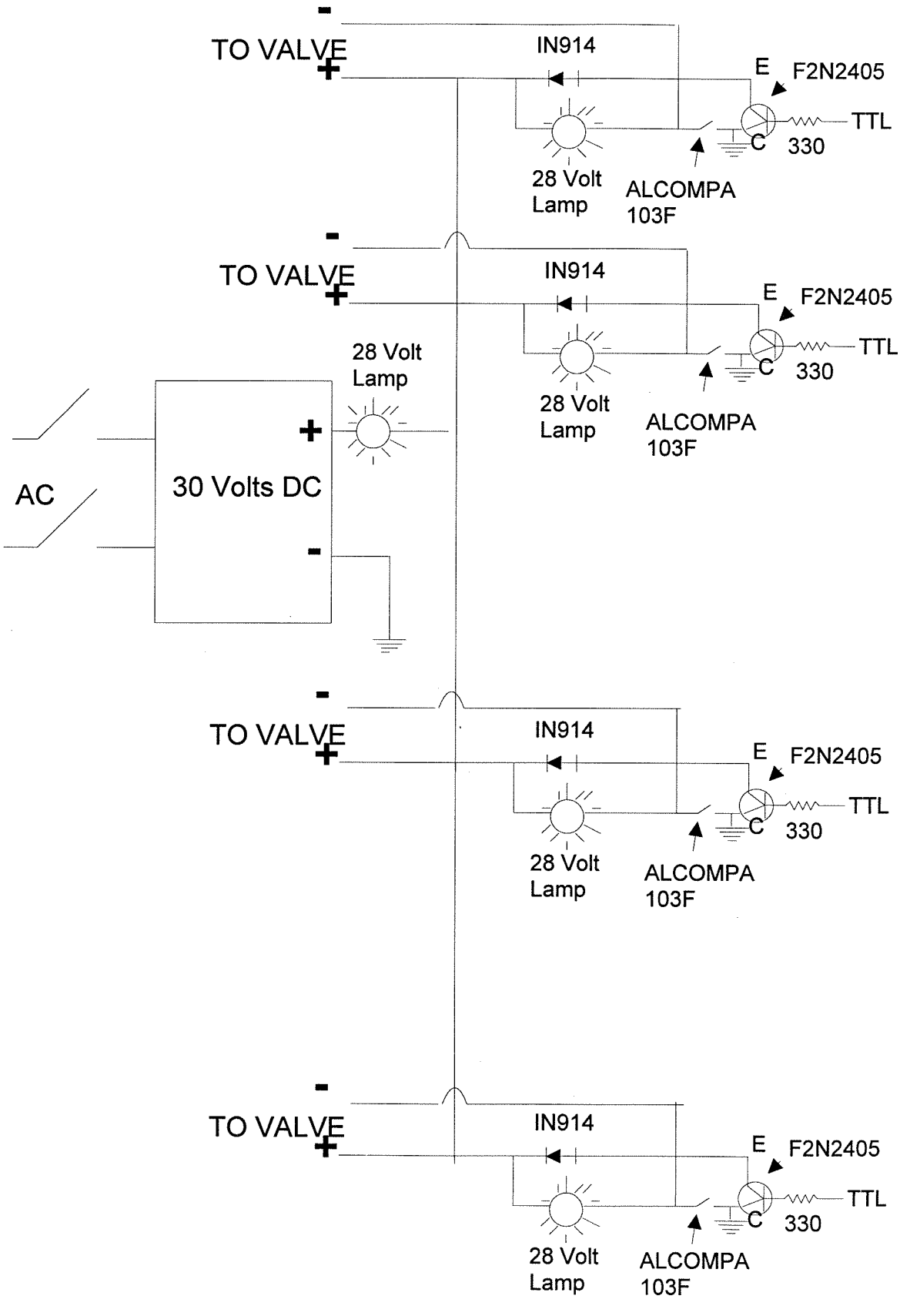
TO VALVE
IN914
E
F2N2405
TTL
C
330
28 Volt Lamp
ALCOMPA 103F
TO VALVE
IN914
E
F2N2405
TTL
C
330
28 Volt Lamp
28 Volt Lamp
ALCOMPA 103F
AC
30 Volts DC
TO VALVE
IN914
E
F2N2405
TTL
C
330
28 Volt Lamp
ALCOMPA 103F
TO VALVE
IN914
E
F2N2405
TTL
C
330
28 Volt Lamp
ALCOMPA 103F

enough to have a noticeable effect on our ability to trap ions. Ions are normally trapped with 1.0-2.5 volts of trapping potential and the receiver and transmitter plates are left at ground.

Split Injection Electrode. Efficient trapping of ions generated with external source instruments is a difficult task. A variety of injection methods have been used including voltage ramps[6], injection electrodes[7], off axis injection[6], and front door injection cycles. [8] To trap ions it is necessary either to apply a differential bias voltage on the transmitter plates of the analyzer cell or to employ an injection electrode consisting of two plates around the ion entrance that can be independently biased to create a differential bias during ion loading. Simple trajectory calculations with SIMION show that, in the absence of collisions or external fields, any ions that have enough energy to enter the analyzer cell will not be trapped. FT-ICR works best when trapping low energy ions created with a narrow energy distribution, preferably with energies around 2 eV. However, it is desirable to leave the transmitter plates at ground during detection and, until recently, it has not been possible to change those voltages during an experiment. As a result, the cell has been modified to incorporate a split injection electrode directly opposite the octopole ion guide exit.

A variety of electrode designs were evaluated and the two most commonly implemented in the FAB experiments performed here are shown in Figure 1-16. The upper design is mounted on a trapping plate with a 1 inch hole, and the injection field is felt by the ions both as they enter the cell and once they are in the cell. The lower design uses a cell plate with a smaller opening (.25 inches square) and the field is felt by the ions primarily as they pass through the gap of the electrode (0.20 inches) as

Figure 1-16. Schematic diagram of split injection electrode designs used. a. Round type. b. Square type.

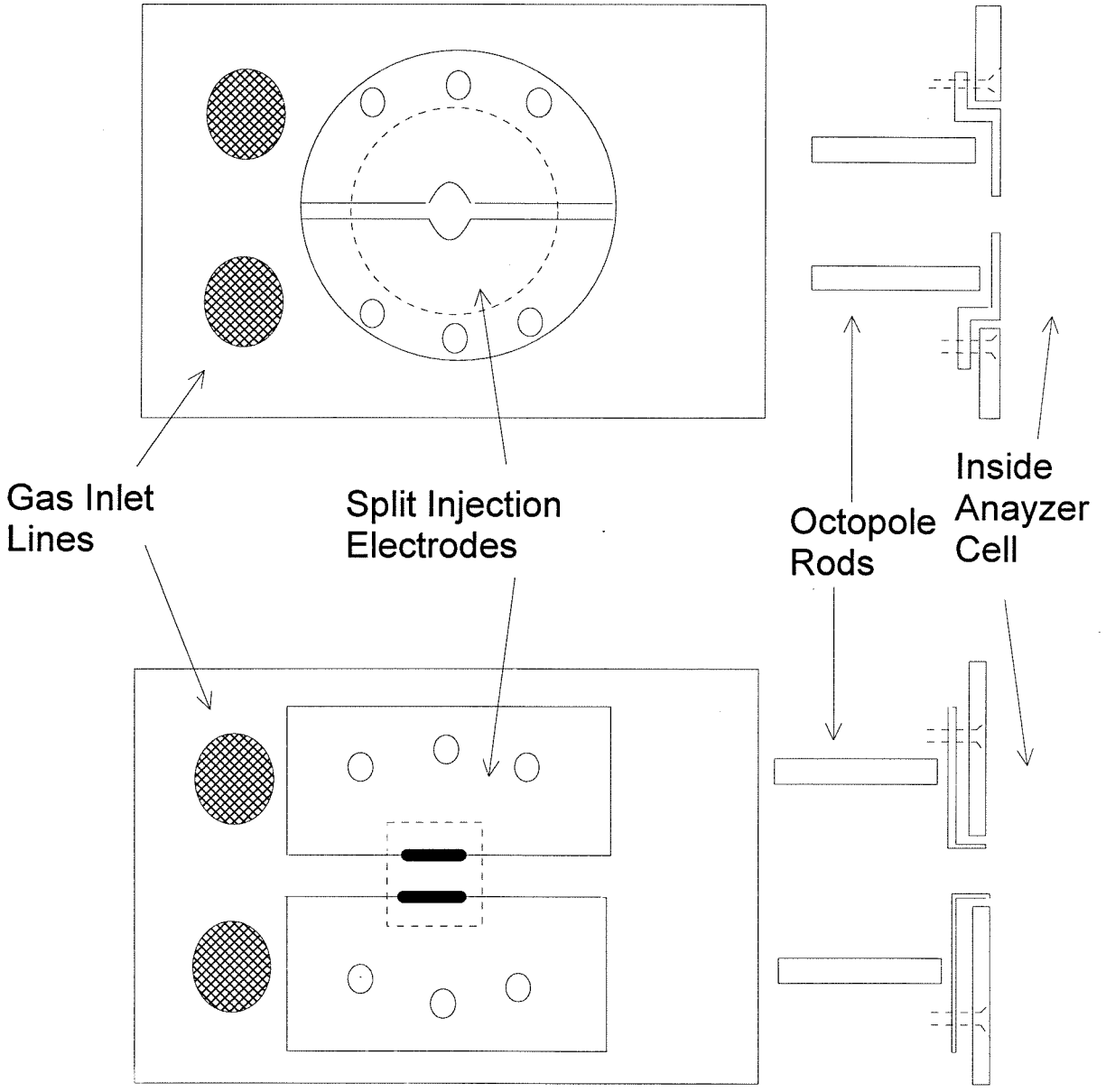
Gas Inlet Lines
Split Injection Electrodes
Octopole Rods
Inside Anayzer Cell

they enter the cell. The thickness of the electrode that the ions travel through is longer in the lower than in the upper case. The differences in the ion intensities and resolution of the spectra resulting from the two different designs are indistinguishable. However, it is thought that the lower design should be better as the trapping potential felt by the ions in the cell is more ideal during ion loading.

Initial control of the electrode was through the home built circuit shown in Figure 1-17. A TTL pulse triggered a relay which alternately applied adjustable voltages to the top and bottom electrode plates from voltages supplied by two 9 volt batteries for a maximum differential input of 18 volts during ion loading. An OMRON relay requiring a 12 volt input to close (65V-2-H-DC12V) was found to demonstrate the good response and reproducibility necessary for this application. Recent upgrades in the electronic interface now allow these voltages to be supplied by two independent 10 volt DACs that are under computer control.

Typically a total of 2 nanoamps of ion current is generated by the FAB source. This can be measured by looking at the total ion current collected on the octopole rods using a picoampmeter biased to allow efficient ion collection. Under optimum conditions up to 0.5 namps of current can be detected at the analyzer cell, corresponding to 3×10^{10} ions/second. In 100 milliseconds (typical ion loading and injection field application times) 3×10^{9} ions reach the analyzer cell. With a trapping efficiency of only 1%, this would mean that 3×10^{7} ions would be stored. Since this is near or above the space charge limit, it is likely that 3×10^{5} ions are typically trapped and generate good signal to noise mass spectra. This corresponds to a trapping efficiency of only 0.01%. In an attempt to increase this efficiency,

Figure 1-17. Schematic diagram of electronic circuit to control voltages to split injection electrode.

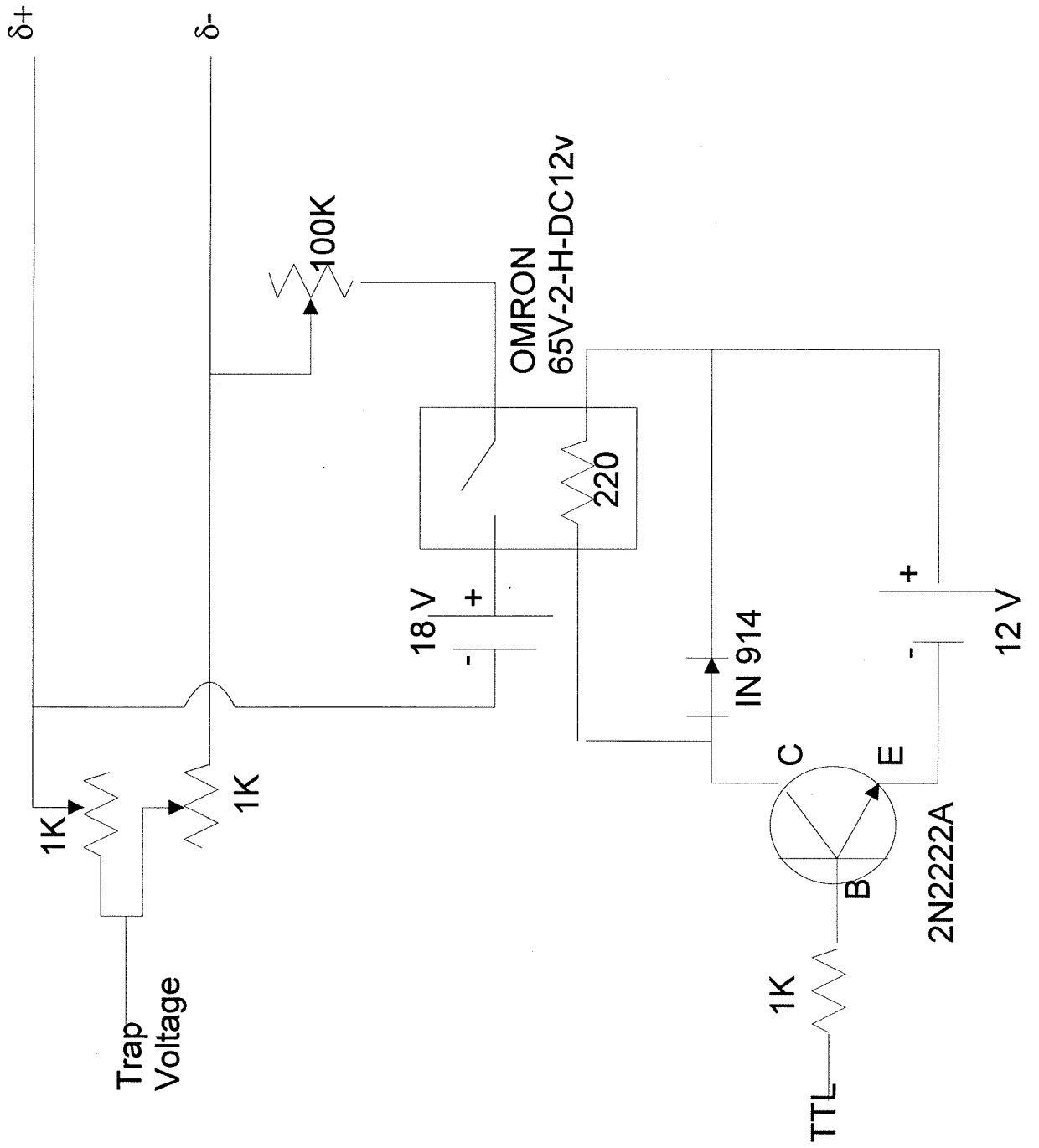
δ+
δ-
100K
OMRON
65V-2-H-DC12v
220
18 V
+
-
IN 914
+
12 V
-
1K
1K
C
E
B
2N2222A
1K
TTL
Trap
Voltage

experiments were performed with a solid plate at the rear of the cell held at a slightly lower potential than the front plate to investigate the possibility of slowing and trapping ions by surface collisions. Unfortunately, a large amount of the higher energy ion current from the FAB source is due to the presence of Cs^+ ions and these attempts only led to more efficient trapping of Cs^+.

Shulz-Phelps Ionization Gauge. Pressures in the analyzer cell are measured by a home built ionization gauge of the Shulz-Phelps geometry[9] mounted directly on the cell and calibrated against a MKS (Model 390) pressure transducer, configured to work in a high magnetic field. The commercial electronics contain a relay on the electronics mounted on the head; this relay was used only for testing procedures and was removed and overridden by MKS at our request. A schematic diagram of the ionization gauge is shown in Figure 1-18. A diagram of the electronic circuit to control the gauge is shown in Figure 1-19. Because the wires carrying current to the filament are subject to a large force by the magnetic field (enough to move them 1/2" or more), they are shielded with fiberglass and macor insulators. The ion collector and filament were initially mounted on the same ceramic. However, as the gauge was used and the ceramic got dirty, conducting paths developed, resulting in a new design locating the ion collector on a separate piece of ceramic. The electrical leads to the ion and electron collectors utilize shielded MHV vacuum electrical feedthroughs. Typical emission currents to measure the low pressures typically employed in our experiments are 50-100 microamps.

IR Laser Studies. Laser access to the cell is available through the rear trapping plate. A laser window is mounted on the flange at the end of the arm inside the

Figure 1-18. Schematic diagram of Shulz Phelps ionization gauge. Electrons accelerated from the filament ionize neutral gas molecules prior to striking the electron collector. Positive ions formed are accelerated in the opposite direction and their current is measured on the ion collector. The ion current measured is proportional to pressure of neutral molecules.

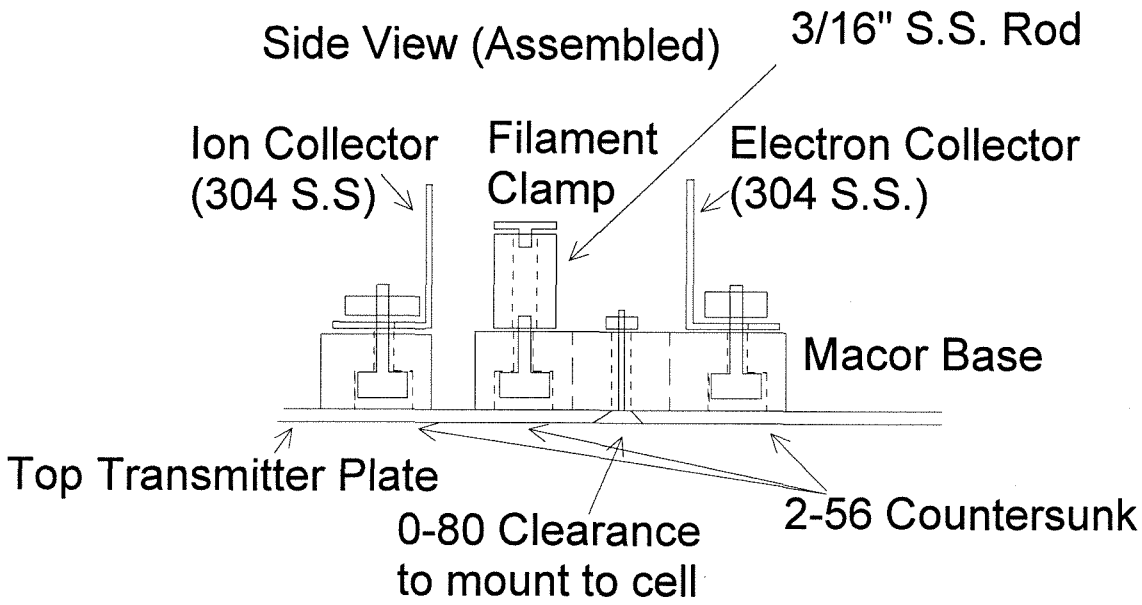
Side View (Assembled)
3/16" S.S. Rod
Ion Collector
(304 S.S)
Filament
Clamp
Electron Collector
(304 S.S.)
Macor Base
Top Transmitter Plate
0-80 Clearance
to mount to cell
2-56 Countersunk

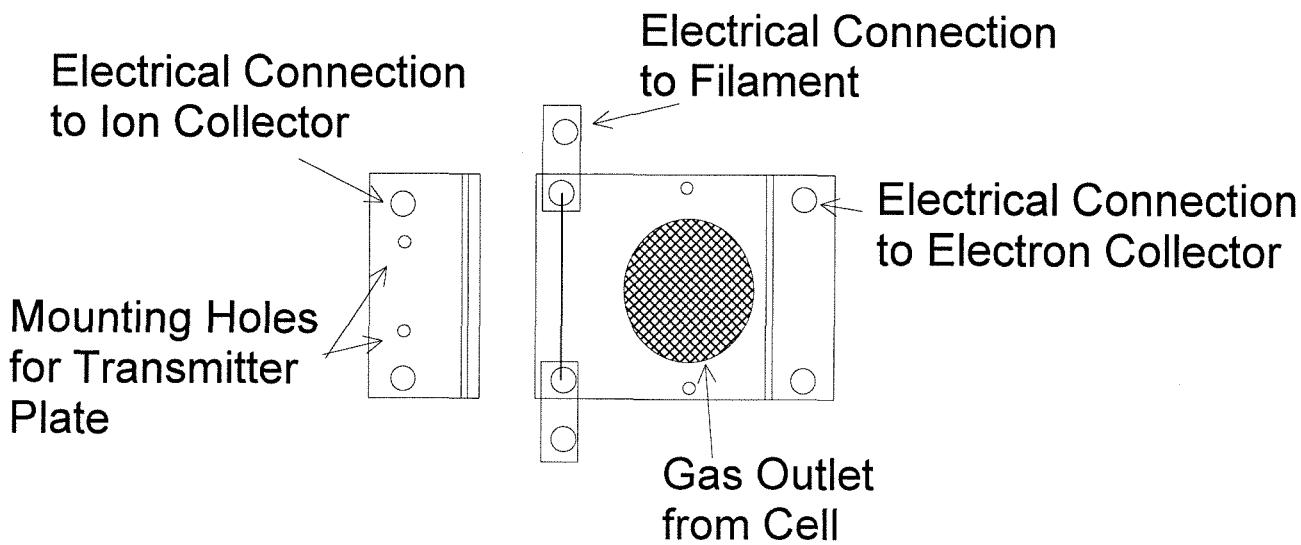
Electrical Connection
to Ion Collector
Electrical Connection
to Filament
Electrical Connection
to Electron Collector
Mounting Holes
for Transmitter
Plate
Gas Outlet
from Cell

Figure 1-19. Schematic diagram of controller for Shulz-Phelps ionization gauge. The electron emission current is regulated by a feedback circuit which adjusts the filament current to maintain constant emission current. Switch provides for full scale meter readings of 1, 10 and 100 microampheres.

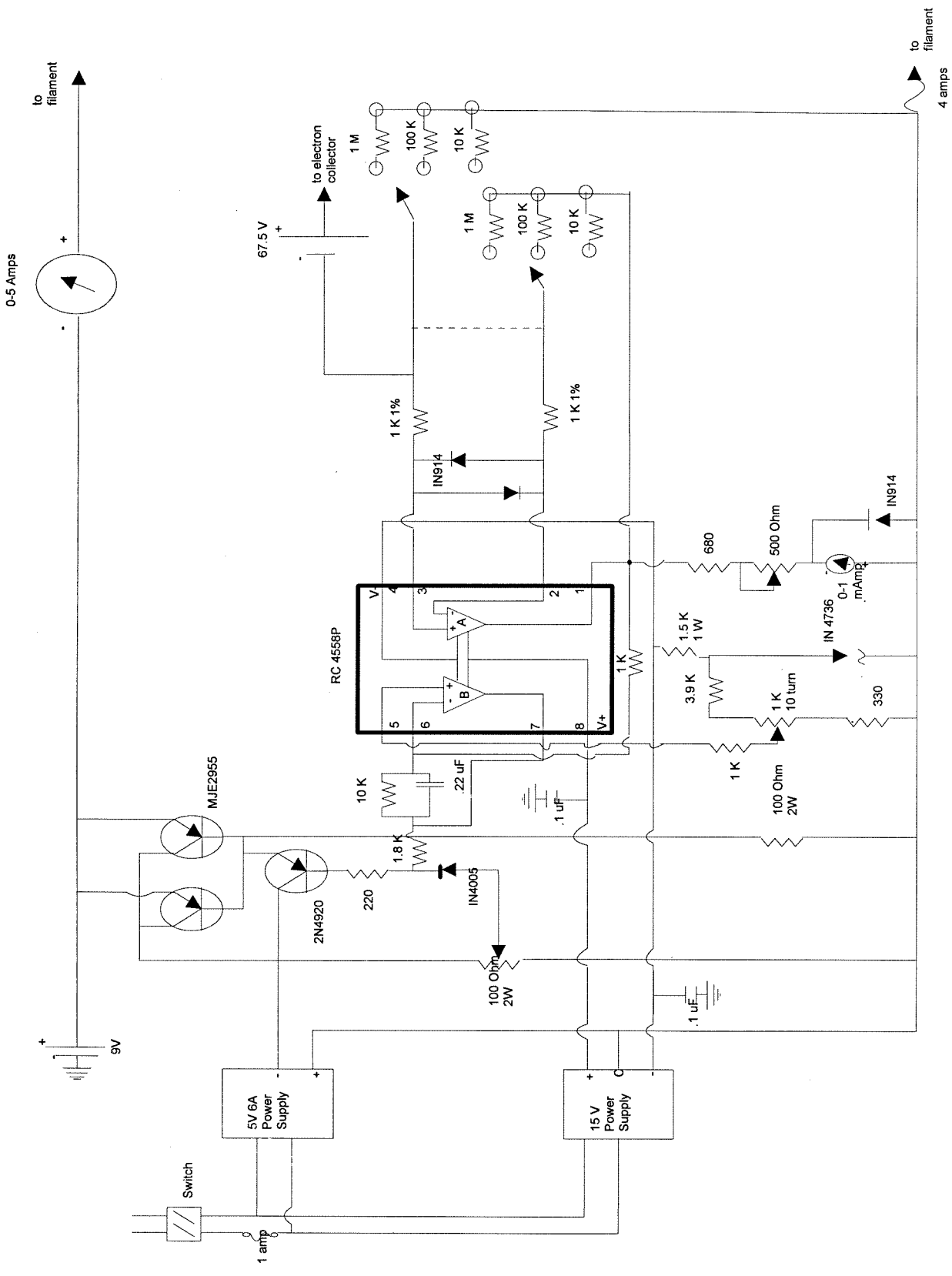
to filament
0-5 Amps
9V
5V 6A Power Supply
15 V Power Supply
Switch
1 amp
MJE2955
2N4920
220
1.8 K
IN4005
100 Ohm 2W
10 K
.22 uF
.1 uF
RC 4558P
V-
V+
1 K
1 K 1%
IN914
67.5 V
to electron collector
1 M
100 K
10 K
680
500 Ohm
0-1 mAmp
IN 4736
1.5 K 1 W
3.9 K
1 K 10 turn
330
100 Ohm 2W
to filament 4 amps

magnet. The window mount is via an o-ring (Figure 1-20) allowing flexibility of window material. The difficulty with these experiments lies in laser alignment; unfortunately, since the arm and the analyzer cell and the floor of the lab are not all parallel, care must be taken to align the laser. It is desirable to pass the laser beam through both the laser window and all the way through the analyzer cell to encompass the ion cloud. The most efficient way to accomplish this is to vent the instrument, remove the arm and physically verify the laser light travels into and through the cell. The laser window can most easily be mimicked by a piece of cardboard cut to the magnet bore size with a hole in the center the size of the window. This can be mounted in the magnet bore at the position typical of the window. The more elegant way to align the laser is to use a HeNe laser and look for the visible light in the ion source region, which has a window. Aligning the laser beam of interest collinear with the HeNe beam will assure that the laser is passing through the cell. In practice, although it takes a day to pump out the instrument, the former method is more effective.

Preliminary studies using a CO_2 laser were carried out; peak power of the laser is currently about 10 Watts. This was not enough to effect dissociation of a protonated peptide, but it could dissociate a dimer of a peptide, which is held together through weaker hydrogen bonds. In addition, dissociation of the Co-C bond in coenzyme B_{12} could be effected using IR laser irradiation as shown in Figure 1-21. The structure of coenzyme B_{12} and the Co-C bond which is cleaved is shown in Figure 1-22. This bond is known to be a weak bond (Bond Dissociation Energy = 26 kcal mol^{-1}), and the mass measurements shown here imply that homolytic cleavage is

Figure 1-20. Schematic diagram of laser window mounting flange.

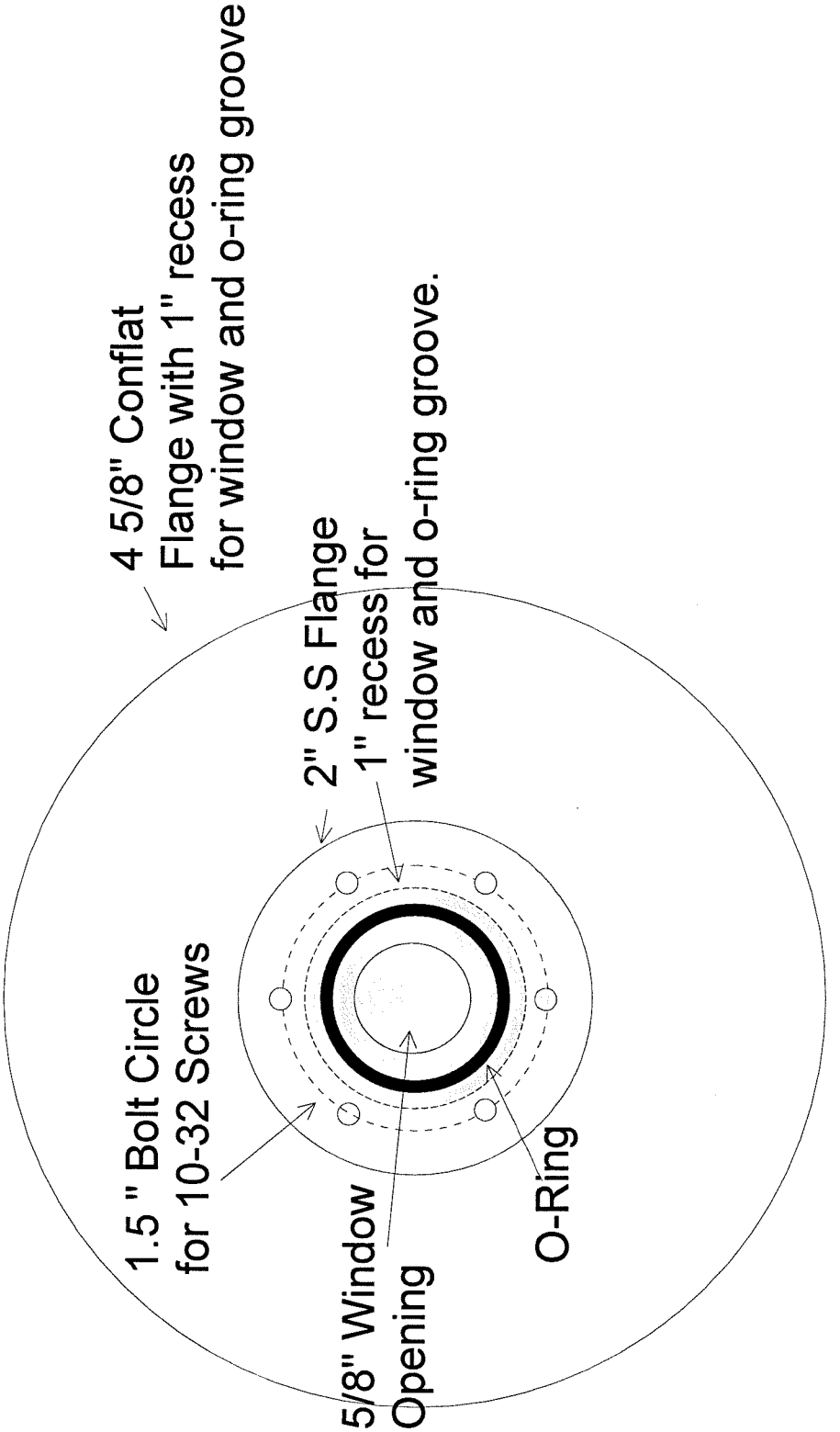
4 5/8" Conflat
Flange with 1" recess
for window and o-ring groove
2" S.S Flange
1" recess for
window and o-ring groove.
1.5 " Bolt Circle
for 10-32 Screws
5/8" Window
Opening
O-Ring

the primary dissociation pathway.[10] It is possible that repositioning the laser closer to the magnet would allow more of the laser energy to be transmitted into the cell. A more efficient and selective dissociation method is described next.

Off Resonance Excitation. Low energy pathways for unimolecular dissociation can be investigated using off resonance excitation,[11] which has been shown to emulate infrared multiphoton excitation. Application of a radio frequency pulse to the cell transmitter plates slightly off resonance from the frequency of a selected ion causes the ion to oscillate with low (typically <5 eV COM) bounded translational energies. As a result excitation can be carried out for long time periods (> 1 second). In the presence of a collision gas the ion undergoes multiple collisions, each one resulting in some of the translational energy being transferred into internal excitation. The internal energy of the ion will slowly increase over time until the ion undergoes unimolecular dissociation. Generally, for singly charge ions, the products are further off resonance and are not excited by the radio frequency field. Instead they collisionally relax.

The energetics of this process can be quantified. The amount of translational energy that the ion gains is given by Equation 4, where ω_c is the cyclotron frequency of the ion and ω and E_o are the frequency and electric field used for excitation. Tests show that exciting at a frequency below the resonance frequency (higher mass) gave better results, though in principle the amount of energy absorbed should be the same. The translational energy of the ion oscillates with an average value given by Equation

5. The total number of oscillations in a time t (seconds) is given by Equation 6. The translational energy in the center of mass is given by Equation 7.

$$E_{tr} = \frac{E_o^2 q^2 \sin^2\left(\frac{(\omega - \omega_c)t}{2}\right)}{2m(\omega - \omega_c)^2} \qquad (4)$$

$$\langle E_{tr} \rangle = \frac{E_o^2 q^2}{4m(\omega - \omega_c)^2} \qquad (5)$$

$$n = t\left(\frac{\omega}{2\pi} - \frac{\omega_c}{2\pi}\right) \qquad (6)$$

$$\langle E_{com} \rangle = \langle E_{tr} \rangle \left[\frac{m_{gas}}{m_{gas} + m_{ion}}\right] \qquad (7)$$

Typical operating conditions use t = 500-5000 milliseconds, ω-ω_c = 1000-3000 Hz, and E_o = 0.949*V/(0.0508)^2 where V is the applied rf voltage in volts (measured peak to peak, or 0-peak times 2 since there are two plates to which the voltage is applied). 0.0508 is the cell electrode spacing in meters and 0.949 is a correction factor for the effective electric field at the center of the cell (determined using SIMION). The number of ion energy oscillations, given by Equation 6, is typically 1000-3000 per second. The typical inert collision gas of choice is nitrogen since it is effectively pumped by the cryopumps and cheaply and easily available.

Figure 1-21. IR laser dissociation of coenzyme B_{12}. a. Isolated molecular parent ion at m/z 1579.6. b. Fragment at m/z 1329 corresponding to homolytic cleavage of the Co-C bond with IR irradiation at 10.6 microns with 8 watts cm^{-2} laser output for 6 seconds.

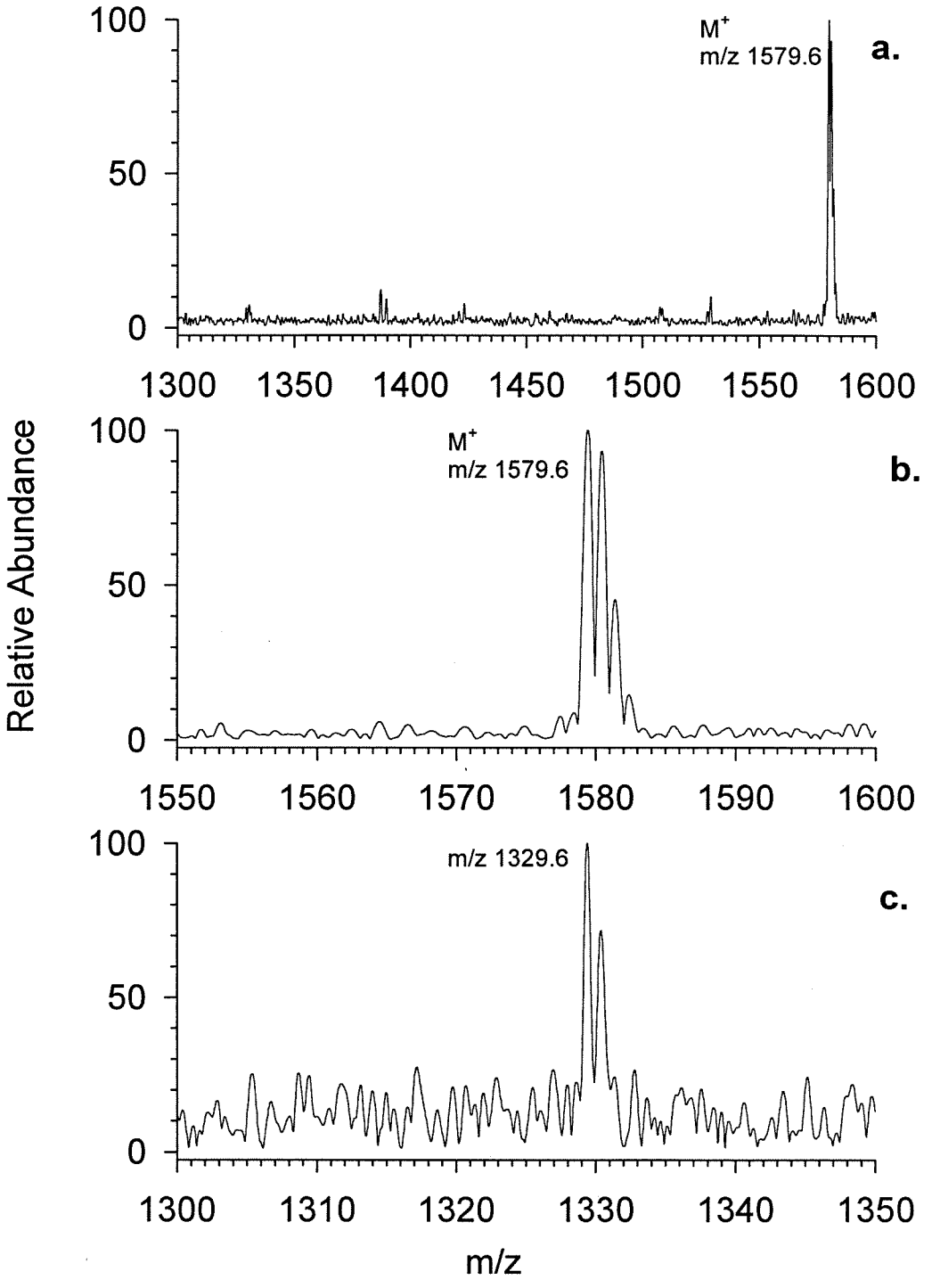
100
50
0
M+
m/z 1579.6
a.
1300
1350
1400
1450
1500
1550
1600
Relative Abundance
100
50
0
M+
m/z 1579.6
b.
1550
1560
1570
1580
1590
1600
100
50
0
m/z 1329.6
c.
1300
1310
1320
1330
1340
1350
m/z

Figure 1-22. Structure of coenzyme B_{12}. The low energy dissociation pathway is homolytic cleavage of the Co-C bond.

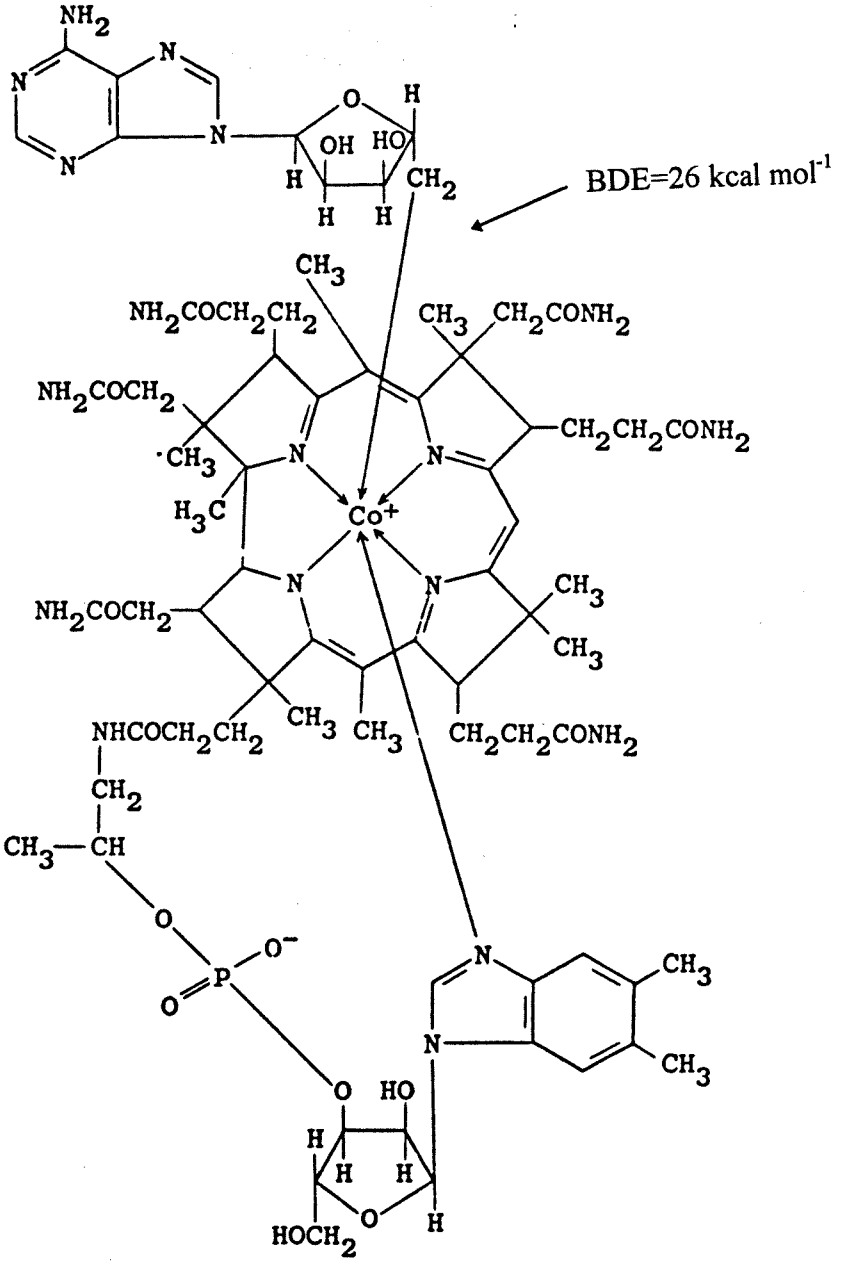
BDE=26 kcal mol-1

Typical pressures when a static gas is used are 0.5-2.0 x 10^{-7} torr (2-12 collisions/second) and when a pulsed gas is used are 1-5 x 10^{-6} torr (30-200 collisions/second). The large number of oscillations compared with the number of collisions justifies the use of an average translational energy as given by Equation 5. The amount of fragmentation and, therefore, the amount of excitation of the molecule is a function of the average ion translational energy and independent of frequency of excitation over a range of frequencies from 1.5-3.5 kHz.

Typical dissociation using off resonance excitation (also referred to as collisional activated dissociation or CAD) are shown for met-enkephalin in Figure 1-23. For comparison a high energy spectra taken by Michael Gross and coworkers for the same molecule is also shown.[12] Salient features include the observation of a primary dissociation pathway (the B_4 ion shown) and the ability to induce 100% dissociation of the parent ion. This facilitates dissociation studies of the fragment ions which are usually formed in large abundance and are easy to isolate for further study. In this example, further fragmentation of the b_4 ion yields the A_4 ion and it is likely that the small amount of A_4 ion observed in Figure 1-23 arises from sequential dissociation of the B_4 ion, which is initially formed with an excess of internal energy. More examples of the use and applications of this method of activation are covered in greater detail in later chapters.

Experimental Sequence. Control pulses for the ion source, radio frequency octopole guide, and FTMS analyzer cell are generated by an OMEGA data system manufactured by IonSpec Corporation which digitizes and processes the transients collected. All control is through a 486 computer which allows storage and

Figure 1-23. a. Isolation of the protonated peptide met-enkephalin (tyr-gly-gly-phe-met). b. Off resonance excitation of protonated methionine enkephalin at an average E_{com}=0.335 eV for 3 seconds at a pressure 1x10-6 torr. b. Spectra of same molecule using single collision high energy collision induced dissociation (spectra taken from reference 11).

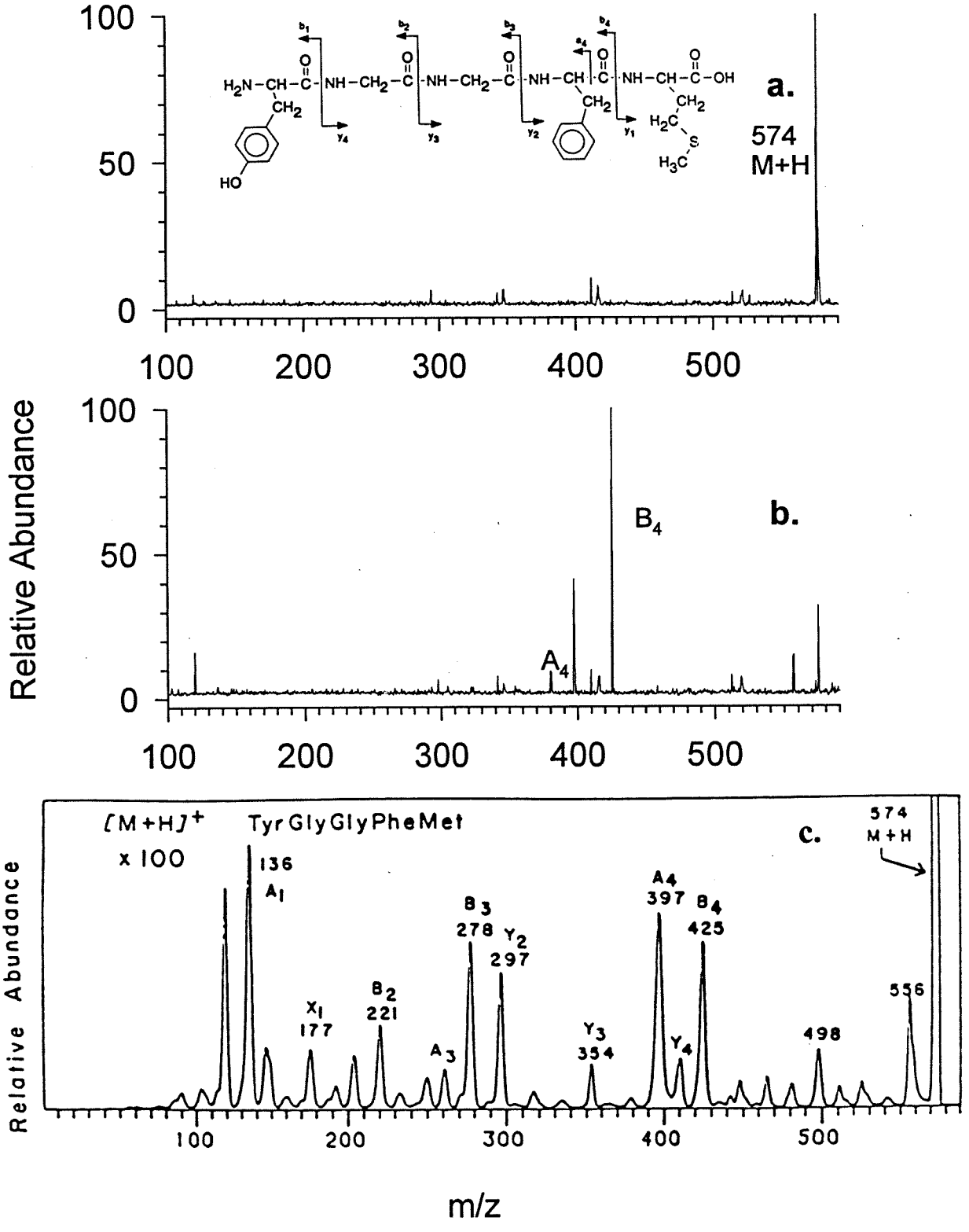
a.
574
M+H
b.
B_4
A_4
Relative Abundance
[M+H]+
x 100
Tyr Gly Gly Phe Met
c.
574
M+H
136
A_1
B_3
278
Y_2
297
B_2
221
X_1
177
A_3
Y_3
354
A_4
397
B_4
425
Y_4
498
556
m/z

manipulation of the data. A typical experimental pulse sequence is shown in Figure 1-24. A quench pulse is used to remove any ions from previous experiments from the cell. The sample is desorbed by a pulse of Cs^+ ions. Concurrently, rf voltage is applied to the octopole rods and a differential voltage is applied to the split injection electrode. After ion storage the ion of interest is isolated by applying a series of ejection pulses. After this ion activation can be carried out either through application of an off resonance excitation pulse or by turning on a laser. Application of a detection pulse and acquisition of signal can occur at any time and ions have been stored for periods of several minutes with no degradation of signal intensity. For FAB spectra, longer detect delays and the presence of low pressure of a collision gas typically results in better signal intensity; this has been observed by other groups as well, and has been postulated to be due to the relaxation of any excess translational energy the ions gain during formation and injection into the analyzer cell.

High Resolution Spectra. To obtain maximum resolution it is necessary to drop the trapping plate voltages during detection. The effect of this on resolution of a porphyrin ion generated by FAB with mass 1036.15 is shown in Figure 1-25. Dropping the trapping plate voltages to 0.25 volts after application of the excitation pulse and prior to detection results in longer signal transients. This results in better resolution and signal intensity. If the same length transient is collected, there is an observed decrease in ion intensity and signal to noise. This is probably due to loss of ions along the z-axis after excitation due to insufficient trapping. Dropping the trapping plates during detection results in an increase in transient length that can be collected; this results in overall better signal intensity. It is very critical to experiment

Figure 1-24. Typical experimental control pulse sequence for FT-ICR experiments.

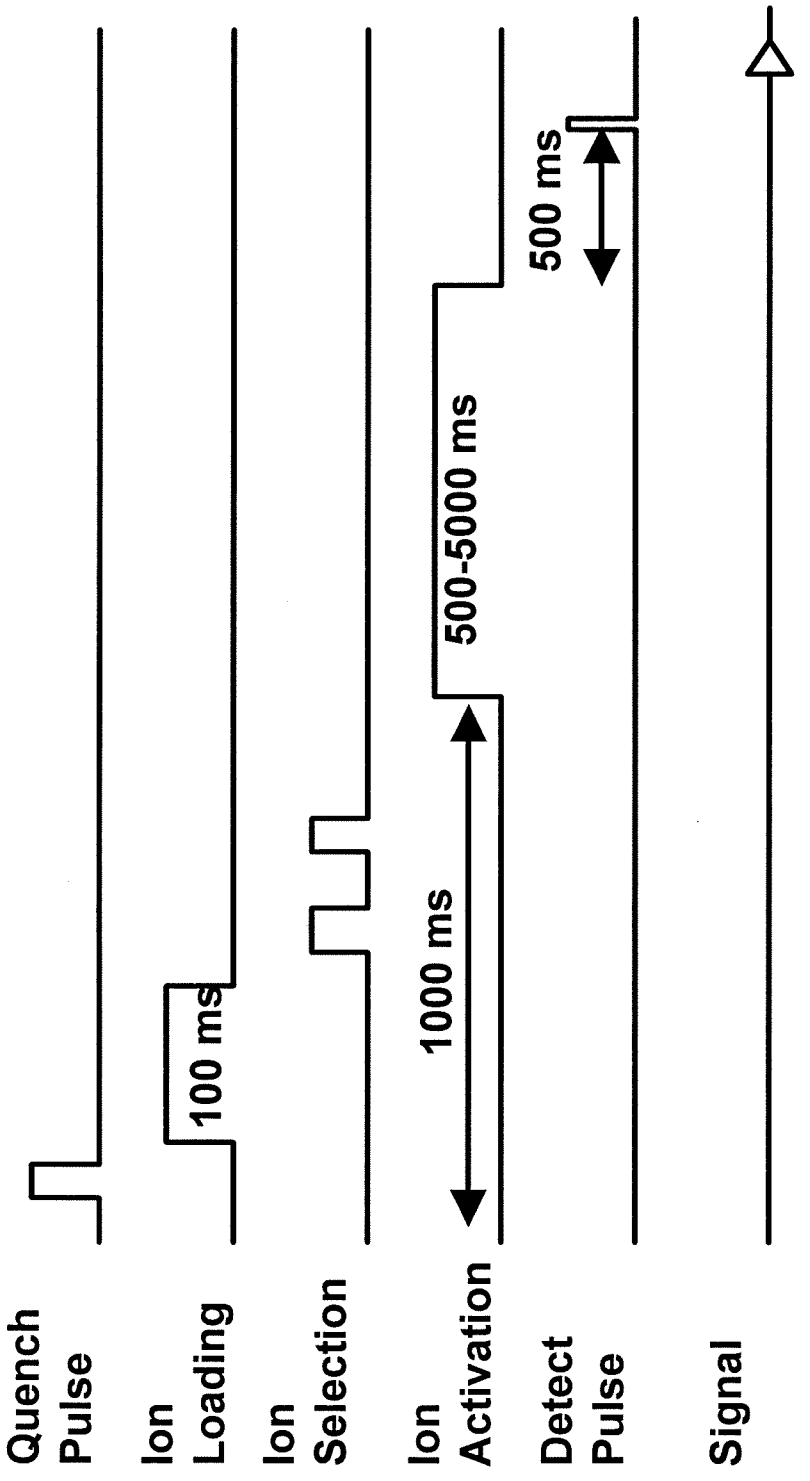
Quench Pulse
Ion Loading
100 ms
Ion Selection
Ion Activation
1000 ms
500-5000 ms
Detect Pulse
500 ms
Signal
Time

Figure 1-25. Effect of trapping plate potential on ion resolution for porphyrin ions. a. Trapping potential at 2.2 volts during detection. b. Trapping potential dropped to 0.25 Volts after excitation and prior to ion detection, resulting in longer transients and higher resolution.

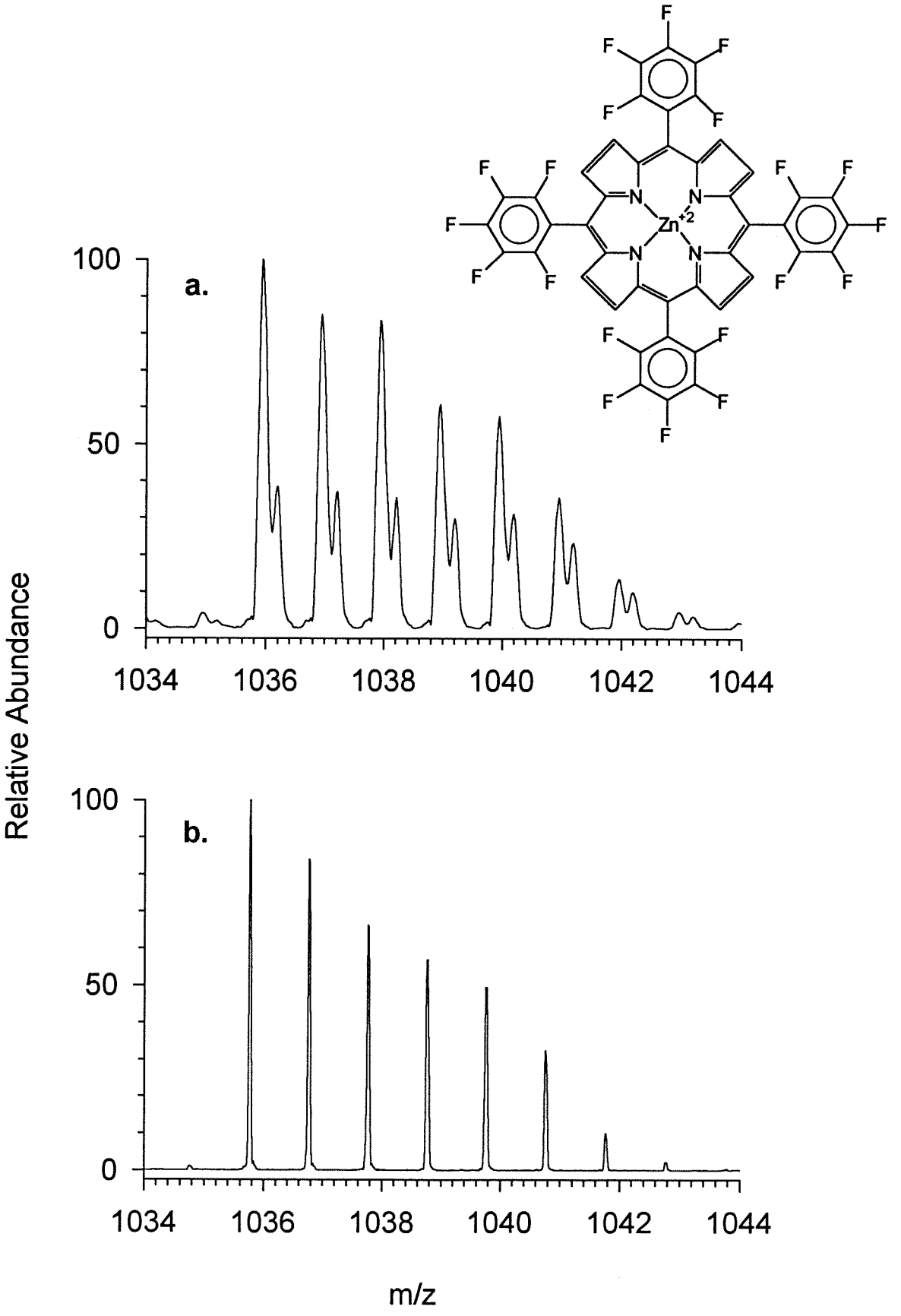
a.
b.
100
50
0
1034
1036
1038
1040
1042
1044
Relative Abundance
m/z
F
N
Zn+2

with the interplay of timing and voltages to take full advantage of this capability. The shift in mass with the dropping of the trapping voltage observed here is due to the fact that the system was calibrated with trapping potential of 2.5 volts.

APPENDIX 1.

7-Tesla Superconducting Magnet. The Oxford Mark II superconducting magnet is very stable over time but requires constant maintenance. It is important to check the flow meters and liquid levels daily if possible. The gas flow meters are always connected; however, the level meters should be left off when not in use. The typical boil off rate for nitrogen is 5.1 liters/minute and for helium is 250 cc/min. Barometric pressure changes can cause this to vary by as much as 20-30% daily. For mass accuracy of several PPM, it is necessary to re-calibrate the mass ranges of interest every few months using a well established calibration compound; cesium iodide works well for this. The magnet requires filling with nitrogen about every five days; typically a fill is done when the level meter reads about 50%. This is well above the safety level of 20% recommended by Oxford. At this fluid level the magnet requires about 40 Liters volume to fill plus whatever is required to cool down the transfer lines. Helium is filled every 21 days or so, typically when the meter reads 78%. At this point it requires about 25 liters to fill, and a 30 liter dewar is adequate. This is again conservative with respect to the recommended refill level of 40%, which would require 35 liters and the ordering of a 60 liter dewar. Excessive boil off of helium could indicate a leak into the vacuum space which may require running down the magnet and warming the cryostat before a cure can be effected. This is a typical condition for older magnets and is something to watch for after the magnet has been in use for 10 years or more.

If either nitrogen or helium boil off falls to zero, it is important to check for icing in the cryostats. Total ice blockages can lead to pressurized reservoirs, and if

this goes unattended the pressure may rise to a point where it ruptures the wall of the can, allowing liquid to spray out, causing damage to virtually every component in the cryostat, and potential harm to anyone standing in the vicinity of the magnet. The most effective way to prevent an ice blockage is to carefully inspect all o-rings sealing the system during each fill period and replace if necessary. For this reason it is important to make sure that at all times spare o-rings are available. If an o-ring looks at all worn, replace it; they are relatively inexpensive compared to the price of a magnet. The o-rings will occasionally fail due to their inability to constantly deal with an excessive number of freeze and thaw cycles.

If an ice blockage is present, the best thing is to call Oxford immediately. They are able to provide very good advice about removal of ice blockages. If they are unreachable, the user can attempt to melt the ice blockage, which is typically frozen air. If the ice blockage occurs in the helium fill port (the most likely place as it is opened and closed for filling, although this procedure will also work for the nitrogen fill port), a warm hollow tube the same diameter as the transfer tube can be inserted into the port in an attempt to melt the ice. Such a tube is available in the lab; it is made of copper for good heat transfer. It is important that this be a hollow tube so that any pressure that has built up can escape; the user should be prepared for this eventuality (a face shield is recommended) so that they do not drop the tube. Because the tube will rapidly cool, care must be taken to ensure that it does not freeze during insertion into the port. The tube should be removed and heated with a hair dryer and dried of condensation and the procedure repeated. It will probably be necessary to repeat this several times to clear the ice. It is important the tube merely be warm

(very easy to handle) and not too hot as too much heat may cause excessive boil off. While performing this procedure if it is thought likely that the magnet may quench or build up a lot of pressure, it is advisable to remove one of the burst disks and place a rubber stopper loosely across the opening. In the event of a quench, it takes less pressure to remove this stopper, resulting in less probable damage to the magnet. This is only for temporary use as it is not a permanent seal.

The magnet will attract any magnetic material that is brought near it including gas cylinders and nitrogen dewars. All helium dewars should be supplied non-magnetic; it is recommended that they be wheeled close to the magnet slowly to verify this prior to use. In the event something large gets stuck to the magnet, it is advisable to try to remove it as soon as possible. Just as it is attracted to the magnet, the magnet itself, which is somewhat free floating in the dewar, will be attracted to it and will move inside the dewar. The boil off rate will probably go up and, again, it is advisable to temporarily open a port to avoid over-pressurization of the dewar. In the event it is necessary (i.e., if someone is trapped), an emergency run down unit is available to quench the magnet. This should always be kept within easy access to the magnet. In the event the magnet quenches (or is quenched), it is advisable to refill the dewar with liquid helium immediately if possible to keep it cold and to maintain the vacuum.

Liquid Helium Fills. As mentioned, liquid helium fills are necessary every 30 days. For volumes of 30 liters the order must be placed by 2 p.m. on the day prior to the desired delivery day. Currently, deliveries are made Monday, Wednesday and Friday only. When placing the order, verify that there is also a cylinder of helium gas

available. Before beginning the fill gather together near the magnet the helium transfer line, extra plastic seal for magnet, gas pressurization inlet for helium dewar, correct tubing to connect this to a cylinder of helium gas, ladder, and towel. The seal where the transfer line enters the dewar does not always fit correctly as supplied and it may be necessary to use the one we have separately purchased.

First purge the transfer line with helium gas. Then, it is necessary to cool the transfer line prior to helium transfer. First, put the extra plastic seal and o-ring onto the transfer line. Connect the helium gas to the gas inlet port on the helium dewar. Lower transfer line **slowly** into the dewar, being careful not to build up too much pressure. The pressure can be monitored on the gas pressurization inlet gauge. As the warm transfer line contacts the liquid helium, it rapidly converts it to gas and builds up pressure, forcing liquid into the transfer line and cooling it. During the cool down period and transfer it will probably be necessary to close the vent valve on the dewar to maintain the necessary adequate pressures. Remember this is available, and if the pressure gets too high (above 2.5 psi) anytime during the cool down or helium transfer, immediately open this valve to relieve the pressure. The transfer line is ready for use when a visible plume of gas emerges from the tip and ice freezes on the tip.

Wipe ice off with towel and remove both the plastic stopper where the transfer line goes in **and** the one-way helium vent valve on the magnet. Slowly lower transfer line into magnet. Do not do this unless the vent valve has also been removed or too much pressure will build up in the magnet, possibly causing problems. To insert the transfer line, it will probably be necessary to remove it part way from the helium

dewar to have the necessary flexibility. Insert the transfer line as far as it will go into the magnet and then raise it about 3/4 of an inch. Tighten the plastic seal. Open the valve on the dewar gas inlet slowly and let in helium gas until the pressure is about 2 psi in the dewar. This will force the liquid out of the dewar and into the magnet. The magnet should fill in about 15 minutes. When it is full the plume of helium coming from the magnet will become significantly larger. At this time release the gas pressure on the dewar, remove the transfer line and reseal both that entrance and the vent valve entrance to the magnet. During the fill, check the o-rings on both of those seals and replace if they look at all worn. It will be necessary to check these about 15 minutes later and retighten as the metal magnet dewar warms up. The helium boil off will probably be higher than usual for a few hours, but should return to normal within a day.

If, while filling, the plume of helium gas becomes smaller and the pressure in the dewar decreases, this means the helium dewar has been emptied. Release the pressure and stop the fill immediately, as described above. If, during the fill, the transfer line becomes cold, or if condensation forms on it, the vacuum has probably gone "soft" and this is a sign that it should be pumped out again before the next fill. This is usually most easily accomplished by using the helium leak detector for pumping. If it is cold and the fill seems to be proceeding unusually slow or necessitates unusually high transfer pressures, abort the fill, reseal the magnet, and pump out the transfer line before continuing with the helium fill.

Energization of Magnet. The Oxford manual contains a complete description of the procedures necessary for re-energizing and shimming the magnet.

REFERENCES

[1] SIMION PC/PS2 Version 4.0 is an electrostatic lens modeling program available free of charge from David Dahl at the Idaho Engineering Laboratory.

[2] Alford, J.M.; Williams, P.E.; Trevor, D.J.; Smalley, R.E. *Int. J. Mass Spectrom and Ion Proc.* **1986**, 72, 33-51.

[3] Lebrilla, C.B.; Amster, I.J.; McIver, R.T. *Int. J. Mass Spectrom and Ion Proc.* **1989**, 87, 7-13.

[4] Deem, M.W.; Beauchamp, J.L. submitted to *Int. J. Mass Spectrom and Ion Proc.*

[5] For more information on rf devices, see The ARRL Handbook, published by the American Radio Relay League.

[6] Koster, C.; Castoro, J.A.; Wilkins, C.L. *J. Am. Chem. Soc.* **1992**, 114, 7572-7574.

[7] Caravatti, P. Patent # 4924089.

[8] Smalley, R.E. *Analytical Instrumenation.* **1988**, 17, 1-21.

[9] Schulz, G.J., Phelps, A.V. *Rev. Sci. Instrum.* **1957**, 28, 1051-1054.

[10] Halpern, J.; Kim, S-H.; Leung, T.W.; *J. Am. Chem. Soc.* **1984**, 106, 8317-8319.

[11] Gauthier, J.W.; Trautman, T.R.; Jacobsen, D.B. *Anal Chim. Acta.* **1991**, 246, 211-225.

[12] Grese, R.P.; Cerny, R.L.; Gross, M.L. *J. Am. Chem. Soc.* **1989**, 111, 2835-2842.

Chapter 2

Low Energy Dissociation Pathways of Small Deprotonated Peptides in the Gas Phase

Low Energy Dissociation Pathways of Small Deprotonated Peptides in the Gas Phase

Elaine M. Marzluff, Sherrie Campbell, M.T. Rodgers, and J.L. Beauchamp*

Beckman Institute, California Institute of Technology, Pasadena, CA 91125

Contribution # 8834

Accepted for publication in the Journal of the American Chemical Society

*Author to whom correspondence should be addressed

ABSTRACT

The unimolecular dissociation dynamics of small deprotonated peptides generated with an external fast atom bombardment source have been investigated using Fourier transform ion cyclotron resonance mass spectrometry. Because the charge site is well defined in peptides lacking strongly acidic side chains, deprotonated peptides present a good model system for investigating the unimolecular dissociation dynamics of "large" molecules. Off resonance collisional activation was used to determine the low energy fragmentation pathways available to the peptides, which greatly contrast those of higher energy dissociation techniques. Dissociation is governed by the site of deprotonation, and yields partial sequence information in favorable cases. Almost all observed pathways were brought about by charge induced mechanisms. The lowest energy dissociation pathway for all peptides without acidic side chains is elimination of the conjugate base of the C-terminus amino acid as the ionic fragment. This generally occurs in up to 100% yield with no competition. For peptides with acidic side chains, alternate pathways are also observed. However, in most cases, through competing or sequential dissociation processes, the C-terminus amino acid could be determined. Calculations were carried out at the AM1 level to determine the minimum energy configurations of these species. Intramolecular hydrogen bonding to solvate and stabilize the charge is observed to be prevalent. The calculations provide further support for the dissociation mechanisms presented. Application of statistical RRKM calculations to these systems allows a qualitative understanding of the energetic changes associated with the observed dissociation processes, distinguishing in particular processes arising from competitive as opposed to sequential dissociations. The bimolecular reactivity of deprotonated peptides was also investigated. Several reactions taking advantage of the nucleophilicity of the deprotonated carboxylic group were observed.

INTRODUCTION

Relatively little is known about the *low energy* dissociation pathways of biopolymers in the gas phase. Yet an understanding of these processes is critical to developing methods for obtaining sequence specific information of peptides by collisional activation techniques. The majority of previous investigations have utilized high energy collision induced dissociation of quasimolecular ions to obtain sequence information.[1] The dissociation pathways exhibited by many peptides appear to be controlled by the site of charge, but for many protonated and cationized species the charge site is not well known or necessarily localized. Calculations on amino acids and simple peptides to determine the most likely site of protonation or cationization have been reported.[2] The most stable form does not necessarily represent a reactive configuration, which could be energetically less favorable yet easily accessed when the molecule is activated. Solvation of the charge site by other basic functional groups in the molecule results in further complications. The major conclusion from these studies is that for many protonated or cationized peptides, there tend to be a variety of sites close in energy where the charge could reside. Even though the experimental methodology often yields useful sequence information, this makes obtaining a systematic understanding of the actual high or low energy dissociation dynamics for these species difficult.

Deprotonated peptides, which can be formed easily by the same methods employed for positive ions (fast atom bombardment or laser desorption), circumvent this charge localization problem. The site of charge in the absence of acidic side chains will be the carboxyl terminus, which can be solvated by internal hydrogen bonding. A consistent pattern of charge localization is expected to result in specific and perhaps predictable dissociation pathways. Of particular interest then is determination of the most energetically favorable pathway(s) for dissociation of

deprotonated peptides. Studies of deprotonated peptides have been somewhat more limited. Bowie and co-workers have published a series of papers on the high energy fragmentation patterns of dipeptides, in which they observe that some sequence information can be obtained from these patterns.[3a-e] More recently, Adams and co-workers have carried out studies on anionic complexes of serine and threonine containing peptides, both deprotonated and complexed with calcium. They looked at both the high energy CID, as well as the metastable decay processes of these peptides. For most peptides both groups observe multiple fragmentation pathways.[3f]

Fourier transform ion cyclotron resonance (FT-ICR) spectroscopy is a powerful tool both for studies of negative ions and for studies of low energy collision dynamics. Low energy pathways for unimolecular dissociation can be investigated using off resonance excitation.[4] Application of radio frequency excitation slightly off resonance from the frequency of a selected ion causes the ion to oscillate with low (<5 eV center of mass), bounded translational energies. As a result excitation can be carried out for long time periods (> 1 second). In the presence of a collision gas, the ion undergoes multiple collisions, each one resulting in some of the translational energy being transferred into internal excitation. The internal energy of the ion will slowly increase until the ion undergoes unimolecular dissociation. Generally, the products are further off resonance and so are not excited by the radio frequency field. Instead they collisionally relax. Thus off resonance excitation allows determination of the low energy fragmentation pathways. Energetic requirements for the systems studied can be specified by an RRKM analysis, which provides a better understanding of observed sequential and competitive dissociation processes.

Very few bimolecular reactions of peptides other than proton transfer reactions have been reported.[5] In the gas phase a peptide is a fairly inert species, at least while in its protonated or cationized form. However, a peptide deprotonated on the carboxyl terminus possesses a reasonably nucleophilic site. As a result

bimolecular reactions with reagents subject to nucleophilic attack are likely to be observed.

In the present work we have investigated the low energy dissociation pathways of a range of deprotonated peptides of varying complexity. The effect of adding acidic side chains, and hence varying the site of charge was probed. AM1 geometry calculations and RRKM statistical calculations were carried out to further understand the mechanisms of unimolecular dissociation. In addition, the bimolecular reactivity of simple deprotonated peptides was studied using a variety of traditional reagents which are susceptible to nucleophilic attack.

EXPERIMENTAL

A modified IonSpec Corporation external source FT-ICR equipped with a fast atom bombardment (FAB) source and specifically designed for quantitative studies of biomolecule reaction dynamics was used to carry out these studies. The instrument, schematically shown in Figure 2-1, has three differentially pumped regions containing an ion source, octopole ion guide and analyzer cell. APD cryopumps (APD-6, 1000 L/sec each) provide pumping in each of the three regions of the vacuum chamber with operating pressures of $5x10^{-10}$ torr as measured by an internal Granville-Phillips ionization gauge located above the pump adjacent to the magnet. Due to the proximity of the magnetic field, the cryopump motors are shielded with cold rolled steel. The ion source region is equipped with an Antek Cesium Ion gun (Model 160-250B) with a PS4 power supply. Samples are transferred into vacuum through an interlock using an MDC High Vacuum motion feed through assembly. The octopole ion guide, designed and constructed in our laboratory, allows ions to be transported efficiently from the source region to the analyzer cell 47 inches away in the high magnetic field. The octopole with 1/8" rods is powered by an ENI power amplifier

Figure 2-1. Schematic Diagram of external ion source FT-ICR.

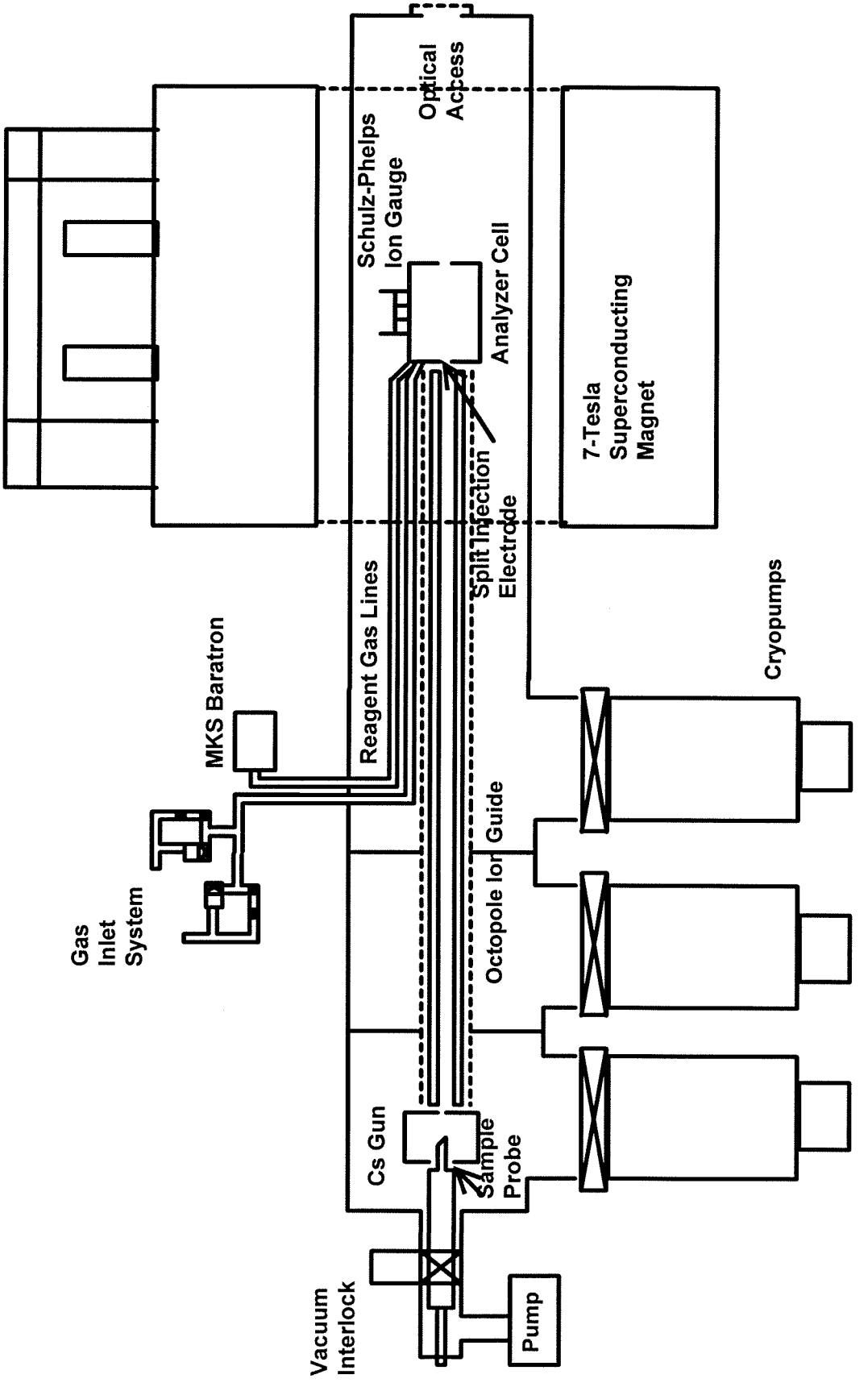
Optical Access
Schulz-Phelps Ion Gauge
Analyzer Cell
7-Tesla Superconducting Magnet
Split Injection Electrode
Reagent Gas Lines
MKS Baratron
Gas Inlet System
Octopole Ion Guide
Cryopumps
Cs Gun
Sample Probe
Vacuum Interlock
Pump

(Model 2100L) driven by a Wavetek function generator (Model 190). The higher voltages required to drive the octopole are derived from an air coil transformer with the secondary coil forming a tuned LC circuit with the octopole rods which resonates at 1.2 MHz. The stainless steel trapped ion analyzer cell with dimensions 2x2x3 inches is centered in the homogeneous region of an Oxford Instruments MarkII, 7-Tesla superconducting magnet. An inlet manifold equipped with two Varian (Model 951-5106) leak valves and two General Valve (series 9) pulsed valves is configured to deliver gas directly to the analyzer cell. The General Valve pulsed valves do not perform well in the high fringing fields generated by our magnet, and this necessitates locating them several feet from the cell. Thus, obtaining a short burst of gas over a controlled period of time is not possible with our current set-up. Pressures in the source region are measured by a home built ionization gauge of the Schulz-Phelps geometry[6] mounted directly on the cell and calibrated against a MKS (Model 390) pressure transducer, configured to work in a high magnetic field. A static gas tap from the pressure transducer to the cell allows accurate measurement of the gas pressures to the cell. The cell has been modified to incorporate a split injection electrode directly opposite the octopole ion guide exit.[7] Control pulses for the ion source, radio frequency octopole ion guide and FTMS analyzer cell are generated by an OMEGA data system manufactured by IonSpec Corporation which digitizes and processes the transients collected. The data system allows for transients up to 256 kilobytes in length to be recorded. All control is through a 486 computer which allows storage and manipulation of the data.

In a typical experiment the peptide is dissolved in a thin layer of liquid matrix (usually 2:1 glycerol and ammonium hydroxide) coated on a copper tip. The sample is then desorbed by a 100 ms pulse of 6-8 keV cesium ions. Concurrently, a 50-150 Volts, 1.2 MHz radio frequency electric field is applied to the octopole rods and a 9-18 Volt differential is applied to the split electrode. Ions are typically trapped with

1.0-2.5 Volts trapping potential and the transmitter and receiver plates are left at ground. Spectra are derived from averaging 5-10 transients. For systems giving weaker signal intensity, as many as 50 transients were averaged. All peptides and other reagents were obtained from Sigma and used as received. The time allowed before detection was dependent on the experiment being performed.

In all of the collision activated dissociation studies reported here, nitrogen was used as the collision gas. The species of interest was isolated through a series of ejection pulses and could be stored for several minutes with no loss of signal. Detection delays up to several seconds often resulted in better signal intensity and resolution, probably the result of relaxation of any excess translational energy the ions gain during formation and injection into the analyzer cell. Species were activated 1-4 kHz off resonance at lower frequency (higher mass) for 1000 ms with a radio frequency pulse 1.0-5.0 Volts zero-to-peak. Dissociation was carried out against both static ($0.5\text{-}1.0\times10^{-7}$ torr) and pulsed ($1.0\text{-}5.0\times10^{-6}$ torr) gases. For static experiments the total delay time was 5 seconds, whereas for pulsed experiments a 3 minute detect delay was necessary to allow the gas to be fully pumped away. In general the energies for excitation were higher for static experiments (compared to pulsed) since lower pressures resulted in fewer collisions during the reaction period. It is noteworthy that none of the energies employed excite the ions to radii of more than a few millimeters, so resolution should not be greatly affected. The average ion energy was varied by changing the frequency of excitation and the amplitude of the radio frequency field.

Geometry optimization calculations were carried out on using the Hyperchem program suite (Autodesk, Inc.) on an IBM 486 DX33 computer. Structures were initially optimized using molecular mechanics, typically with AMBER force fields. Final further optimization was carried out using semi-empirical methods at the AM1 level. The AM1 model has been found to be a fast and accurate calculation method

Table 1. Product distributions[a] observed for the low energy collision activated dissociation of a variety of simple peptides.

a.) Non Acidic and Slightly Acidic Side Chains

Peptide	m/z deprotonated peptide	C-terminus product	Other products
gly-gly	131.0451	100	
gly-leu	187.1083	100	
gly-ala	145.0613	100	
gly-gly-ala	202.0828	100	
gly-gly-ileu	244.1298	100	
gly-gly-gly	188.0672	100	
gly-gly-val	230.1141	100	
ala-leu-ala	272.1610	100	
gly-gly-phe	278.1141	100	
met-leu-phe	408.1957	100	
ala-leu-ala-leu	385.2451	100	
val-ala-ala-phe	405.2137	100	
tyr-gly-gly	294.1090	75	25 m/z 219[b]
thr-val-leu	330.2029	20	80 m/z 286[b]
leu-ser-phe	364.1872	25	75 m/z 334[b]
leu-ser	217.1188	0	82 m/z 187[b] 18 m/z 74 gly-H^-

b.) Very Acidic Side Chains

gly-trp	260.1035	78	22 m/z 131
gly-his	211.0831	30	27 m/z 149 -(CO_2+H_2O) 27 m/z 74 gly-H^- 7.5 m/z 193 -H_2O 7.5 m/z 110[b]
glu-leu	259.1294		90 m/z 128[a] 10 m/z 241 -H_2O
gly-glu	203.0668		54 m/z 185 -H_2O 17 m/z 128[b] 14 m/z 74 gly-H^- 10 m/z 141 -(CO_2+H_2O) 5 m/z 159 -CO_2
val-gly-ser-glu	389.1672		44 m/z 260[b] 31 m/z 128[b] 25 m/z 173[b]

a. Reported as percent of total products.
b. See text for details.

for ions as well as neutrals. It has also been demonstrated to be able to accurately handle intramolecular hydrogen bond interactions.[8]

RESULTS

Unimolecular Reactions: Non Acidic Side Chains. Table 1 summarizes the low energy dissociation patterns observed for all peptides studied. Collisional activation of all peptides with non-acidic side chains results in exclusive elimination of the conjugate base of the C-terminus amino acid as the observed product ion. The type of data obtained for these experiments are illustrated for the case of the deprotonated peptide gly-gly-ile in Figure 2-2. The reactant ion is isolated with a series of radio frequency ejection pulses. Collision gas is pulsed into the system, and off resonance excitation of the isolated ion results in controlled fragmentation with only one product. The proposed mechanism for this dissociation is shown in Reaction 1. While the secondary structure of deprotonated peptides in the gas phase is not known, the only reasonable site of deprotonation for molecules with simple side chains is the carboxyl terminus, as depicted here. We propose a mechanism in which dissociation is

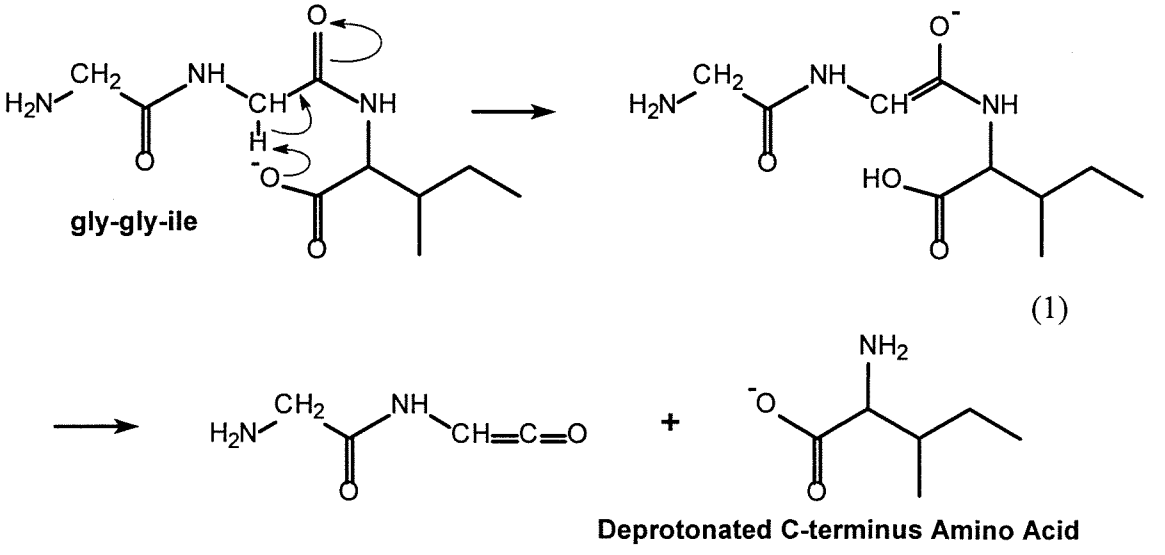

(1)

Figure 2-2. Low energy collision induced dissociation of the deprotonated peptide gly-gly-ile (m/z=244.1). a.) Isolated spectrum of the parent peptide. b.) Irradiation with $\Delta\omega/2\pi$=4400 Hz (m/z=246.5) and $<E_{com}>$=0.24 eV at a pressure of $1x10^{-6}$ torr for 1 second (approximately 100 collisions) yields partial dissociation of the parent to give the c-terminal amino acid. (m/z=130.1) c.) Irradiation with $<E_{com}>$= 0.42 eV at a pressure of $1.5x10^{-6}$ torr for 1 second (approximately 150 collisions) yields 100% dissociation. The small peaks in the spectrum are not products but can be assigned either to noise or to incomplete isolation of the selected ion.

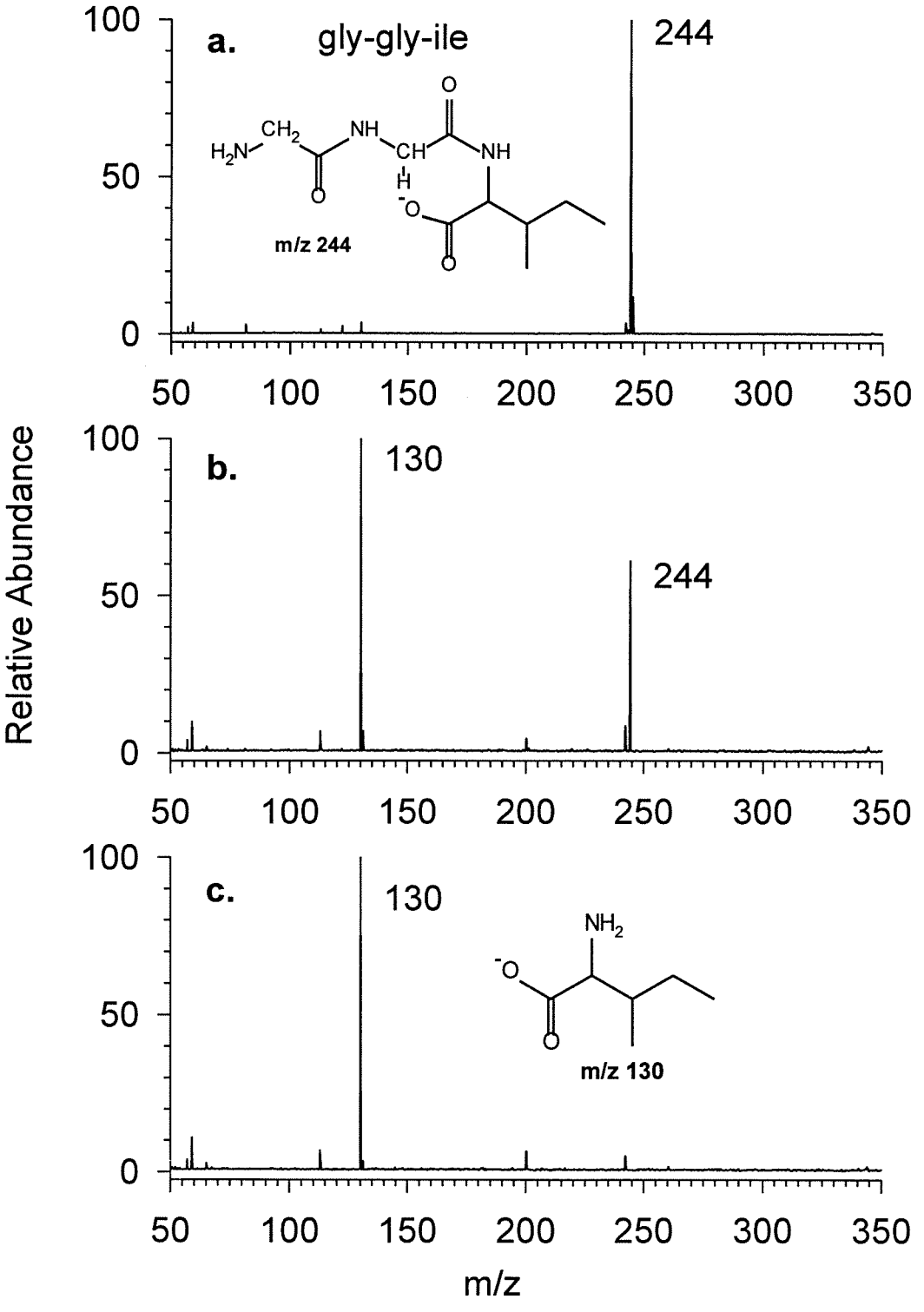
a.
gly-gly-ile
244
m/z 244
b.
130
244
c.
130
m/z 130
Relative Abundance
m/z
100
50
0
50
100
150
200
250
300
350

initiated by proton abstraction from the adjacent amino acid through a favorable seven member ring intermediate. Simple analysis based on the approximate relative acidities of the sites predict this step to be endothermic by about 30 kcal mol^{-1} (1.3 eV)[9]. This initial abstraction is followed by rapid rearrangement to yield the C-terminus amino acid as the charged product. The overall endothermicity of the process is estimated from bond strengths to be approximately 40 kcal mol^{-1} (1.7 eV). Labeling studies by Bowie et al.[3a] on dipeptides confirm that the proton we propose is initially abstracted is present in the final product.

It should be noted that the observed products in Reaction 1 could also result from a simple 4-center elimination reaction, as has been proposed for the related compound acetamide as shown in Reaction 2.[10] This reaction has measured activation parameters of $\log_{10}A=14.7$ and $E_a=73.4$ kcal mol^{-1} (3.2 eV).[10a] However, as discussed by Benson et al.,[10b] these numbers are not consistent with a four center elimination reaction, which should have a tight transition state and a lower A-factor than observed. They suggest that

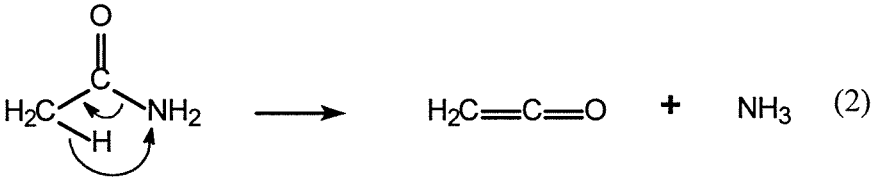

(2)

for the 4-center elimination reaction $\log_{10}A=13.0$ and $E_a=68$ kcal mol^{-1} (2.9 eV) are more appropriate values.

In the studies of deprotonated peptides without acidic side chains, cleavage occurs only at the C-terminus amino acid. This means that the charge localization at the C-terminus necessarily plays a key role in determining the site specificity of the reaction. If a charge remote four center elimination reaction was possible in this low energy dissociation regime, then dissociation at every amide bond should be equally

possible, but for all the peptides without acidic side chains investigated, dissociation at the C-terminus amino acid is exclusively observed. In the proposed dissociation mechanism in Reaction 1, the carboxylate anion can be considered a catalyst for the four-center elimination reaction. The estimated E_a of 68 kcal mol^{-1} for the four-center process can be considered a reasonable upper limit for the activation energy of the observed catalyzed process. AM1 calculations reveal the lowest energy geometry of peptides without acidic side chains containing at least three amino acids to be a structure with hydrogen bonding interactions between the deprotonated C-terminus and the N-terminus and/or other amide hydrogens. However, the amide and N-terminus hydrogens are not particularly acidic and dissociation pathways involving deprotonation of these sites would be necessarily a much higher energy process than hydrogen abstraction from the adjacent amino acid. However, in the collisional activation process, enough energy is added to the molecule so that all of the lower energy structures will be easily accessible.

The energetics of the off resonance excitation process can be quantified. The amount of translational energy that the ion gains is given by Equation 3 where ω_c is the cyclotron frequency and ω and E_o are the frequency and electric field used for excitation.[11]

$$E_{tr} = \frac{E_o^2 q^2 \sin^2\left(\frac{(\omega - \omega_c)t}{2}\right)}{2m(\omega - \omega_c)^2} \qquad (3)$$

Experimentally, exciting at a frequency below the resonance frequency (higher mass) gave better results, though in principle the amount of energy absorbed should be the same. The translational energy of the ion oscillates with time with an average value given by Equation 4. The total number of oscillations in a time t (seconds) is given by Equation 5.

$$\langle E_{tr} \rangle = \frac{E_o^2 q^2}{4m(\omega - \omega_c)^2} \tag{4}$$

$$n = t\left(\frac{\omega}{2\pi} - \frac{\omega_c}{2\pi}\right) \tag{5}$$

The translational energy in the center of mass frame is given by Equation 6.

$$\langle E_{com} \rangle = \langle E_{tr} \rangle \left[\frac{m_{gas}}{m_{gas} + m_{ion}}\right] \tag{6}$$

Typical operating conditions are those used to obtain the data shown in Figure 2-2. Irradiation of gly-gly-ile with $\Delta\omega/2\pi$=4400 Hz at $<E_{com}>$=0.24 eV at a pressure of $1x10^{-6}$ torr for 1 second yields partial dissociation (Figure 2-2b). These conditions correspond to approximately 100 collisions with 4400 oscillations. This large number of oscillations compared with the number of collisions justifies the use of an average translational energy as given by Equation 4. Increasing $<E_{com}>$ to 0.42 eV and the pressure to $1.5x10^{-6}$ torr results in 100% dissociation of the peptide with no other product channels observed (Figure 2-2c). For most experiments the amount of fragmentation was varied by changing E_O and/or by varying the pressure. The extent of fragmentation can also be finely controlled by varying the frequency (ω) of excitation and the time (t) of excitation. Figure 2-3 demonstrates this for gly-gly-ile. In Figure 2-3a dissociation was examined at three different frequencies. The energy was varied by changing the applied radio frequency pulse amplitude. Figure 2-3a shows that the extent of dissociation is a function of the average ion energy and independent of the frequency chosen for excitation over a frequency range of 1.5-3.5 kHz of the frequency chosen for excitation. Figure 2-3b shows that, as expected, the extent of dissociation increases as the time of excitation increases. A small fraction of the ions always dissociate under very low energy conditions. This is attributed to a

Figure 2-3. a.) Dissociation of deprotonated gly-gly-ile at various excitation energies. Three different frequencies for excitation were examined. For each frequency the ion translational energy was varied by varying the amplitude of the applied radio frequency electric field. Excitation was for one second at a pressure of $9x10^{-8}$ torr. b.) Extent of fragmentation of deprotonated gly-gly-ile as a function of excitation time. Irradiation with at $\Delta\omega/2\pi$=4400 Hz (m/z=246.5) and $<E_{com}>$= 1.57 eV at a pressure of $8x10^{-8}$ torr results in increasing dissociation with time.

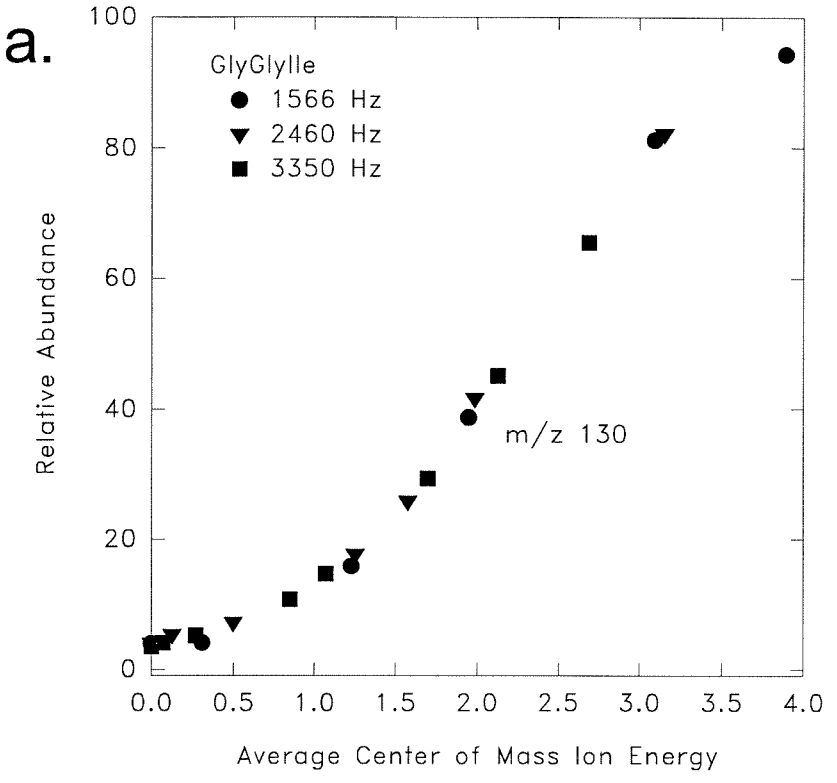
a.
GlyGlyIle
1566 Hz
2460 Hz
3350 Hz
m/z 130
Relative Abundance
Average Center of Mass Ion Energy
0
20
40
60
80
100
0.0
0.5
1.0
1.5
2.0
2.5
3.0
3.5
4.0

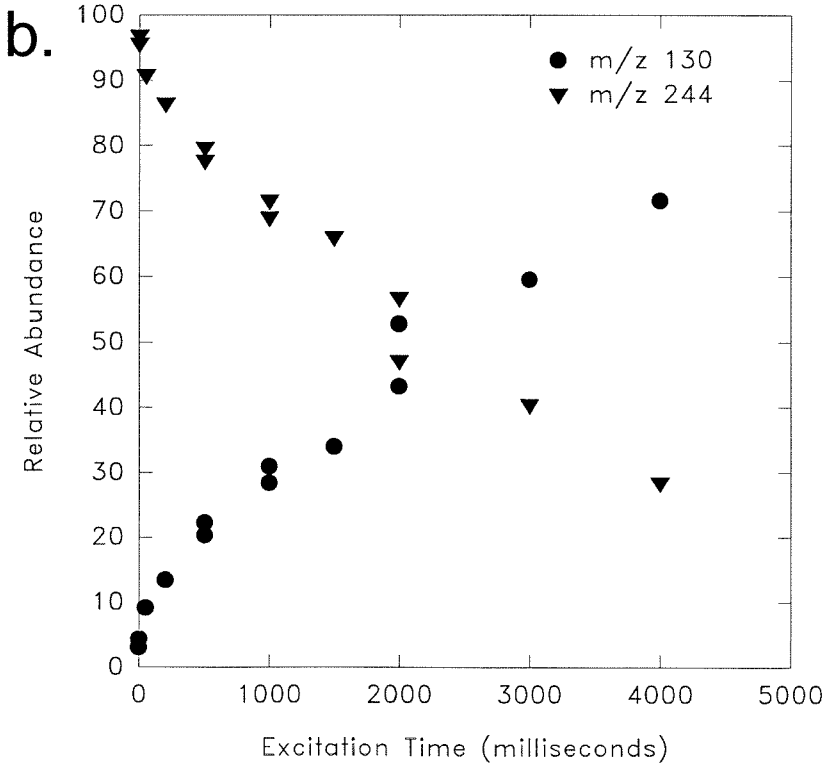
b.
m/z 130
m/z 244
Relative Abundance
Excitation Time (milliseconds)
0
10
20
30
40
50
60
70
80
90
100
0
1000
2000
3000
4000
5000

fraction of the ion population being formed initially in the FAB desorption process with high internal energies. A more complete analysis of the kinetic data will be the subject of a separate paper.[12]

Unimolecular Reactions: Weakly acidic side chains. For reference, Table 2 contains estimated acidities (ΔH_{acid}) of the various amino acid side chains. These values were estimated from comparison of similar compounds with known acidities available in the literature.[13] Also noteworthy is that ΔH_{acid} has been experimentally determined by bracketing techniques for glycine and alanine to be 342.4 and 340.7 kcal mol^{-1}, respectively.[14] Recently the acidities of all the amino acids have been determined by kinetic methods, and are in good agreement with these values.[15] These measured values are also included in Table 2. From these a value of about 342 kcal mol^{-1} for the acidity of a generic peptide with no acidic side chains which deprotonates on the C-terminus is estimated. Further stabilization from hydrogen bonding with the side chain is possible for some of the larger amino acids, which would be reflected by an increased acidity.

Peptides containing tyrosine, serine and threonine, all of which are moderately acidic, exhibit slightly different behavior compared to the compounds with non-acidic side chains studied. Peptides containing tyrosine, which is comparable in acidity to the carboxyl terminus (347 kcal mol^{-1} vs. 342 kcal mol^{-1}) yield two products upon collisional activation, as shown in Reaction 7 for the deprotonated peptide tyr-gly-gly. The lowest energy structure is one which adopts a conformation allowing intramolecular hydrogen bonding between the tyrosine side chain and C-terminus amino acid, as shown. AM1 calculations show this structure to be more stable by 9.3 kcal mol^{-1} than the open form of the peptide and more stable by 2.4 kcal mol^{-1} than a structure with hydrogen bonding between a N-terminus hydrogen and the deprotonated C-terminus.

Table 2. Estimated side chain acidities for the amino acids and measured aciditiy values of the amino acids.[c] For reference the accepted abbreviations and monoisotopic molecular weights are also given.

Peptide	Abbrev-iation		$NH_2CHRCOOH$ Structure of R	MW	Acidities ΔH_a(kcal mol^{-1}) Side Chain	Amino Acid[a]
Glycine	Gly	G	-H	75.0321	>390[b]	342.0
Alanine	Ala	A	$-CH_3$	89.0477	>390[b]	341.2
Valine	Val	V	$-CH(CH_3)_2$	117.0790	>390[b]	339.4
Leucine	Leu	L	$-CH_2CH(CH_3)_2$	131.0947	>390[b]	339.1
Isoleucine	Ile	K	$-CH(CH_3)CH_2CH_3$	131.0946	>390[b]	338.8
Methionine	Met	M	$-CH_2CH_2SCH_3$	149.0511	>390[b]	335.8
Proline	Pro	P	$-CH_2CH_2CH_2-$	115.0634	>390[b]	340.3
Lysine	Lys	L	$-CH_2CH_2CH_2CH_2NH_2$	146.1056	>390[b]	337.5
Arginine	Arg	R	$-CH_2CH_2CH_2NHC(NH)NH_2$	174.1117	>390b	331.9
Phenylalanine	Phe	F	$-CH_2Ph$	165.0790	380[b]	336.5
Serine	Ser	S	$-CH_2OH$	105.0426	375[b]	332.7
Threonine	Thr	T	$-CH(OH)CH_3$	116.0583	373[b]	332.1
Asparagine	Asn	N	$-CH_2CONH_2$	132.0535	362[b]	331.7
Glutamine	Gln	Q	$-CH_2CH_2CONH_2$	146.0692	362b	331.7
Cysteine	Cys	C	CH_2SH	121.0198	355[b]	332.9
Histidine	His	H	d	155.0695	353[c]	331.0
Tryptophan	Trp	W	e	204.0899	352[c]	336.9
Tyrosine	Tyr	Y	$-CH_2PhOH$	181.0739	347[b]	336.4
Aspartic Acid	Asp	D	$-CH_2COOH$	133.0375	345[b]	---
Glutamic Acid	Glu	E	$-CH_2CH_2COOH$	147.0532	344[b]	---

a.) From Reference 14.
b.) From Reference 12b.
c.) From Reference 12a.
d.) 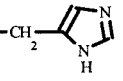
e.) 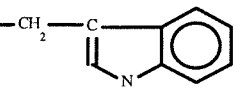

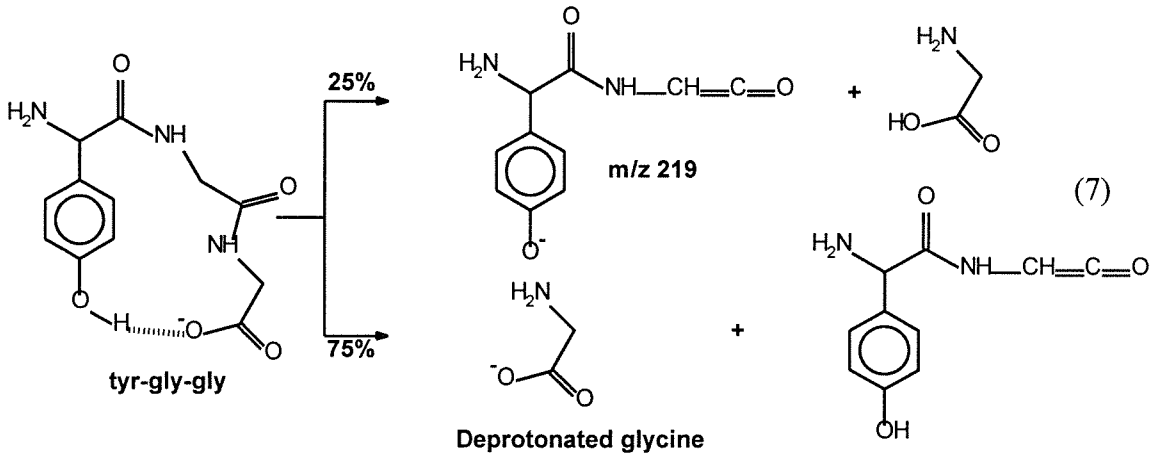

Dissociation occurs by the same mechanism as shown for gly-gly-ile and the two products could then arise from a competition of charge retention between the two acidic sites of the molecule. When the C-terminus is deprotonated, typical dissociation behavior yielding deprotonated glycine as the product ion is observed. When the tyrosine side chain retains the charge, the product at m/z 219 is observed. The observation of these two products arising form a competitive proton transfer reaction implies the possibility of formation of a long-lived dissociation complex.

Peptides containing smaller alcoholic groups like serine and threonine also yield two products. An example with the peptide thr-val-leu is shown in Figures 2-4 and 2-5. The reason for the differences in these spectra is discussed later. One product corresponds to the loss of the side chain yielding an ion at m/z 286 and the other is the expected C-terminus amino acid, in this case deprotonated leucine at m/z 130. Because the resulting

Figure 2-4. Low energy dissociation of the deprotonated peptide thr-val-leu (m/z=330.2) against a pulsed gas pressure. a.) Isolated parent ion. b.) Irradiation with $\Delta\omega/2\pi$=1866 Hz (m/z=332) and $<E_{com}>$=0.29 eV at a pressure of 10^{-6} torr for 1 second (approximately 100 collisions) yields partial dissociation and two products. c.) Increasing irradiation at $<E_{com}>$=0.41 eV yields 100% dissociation.

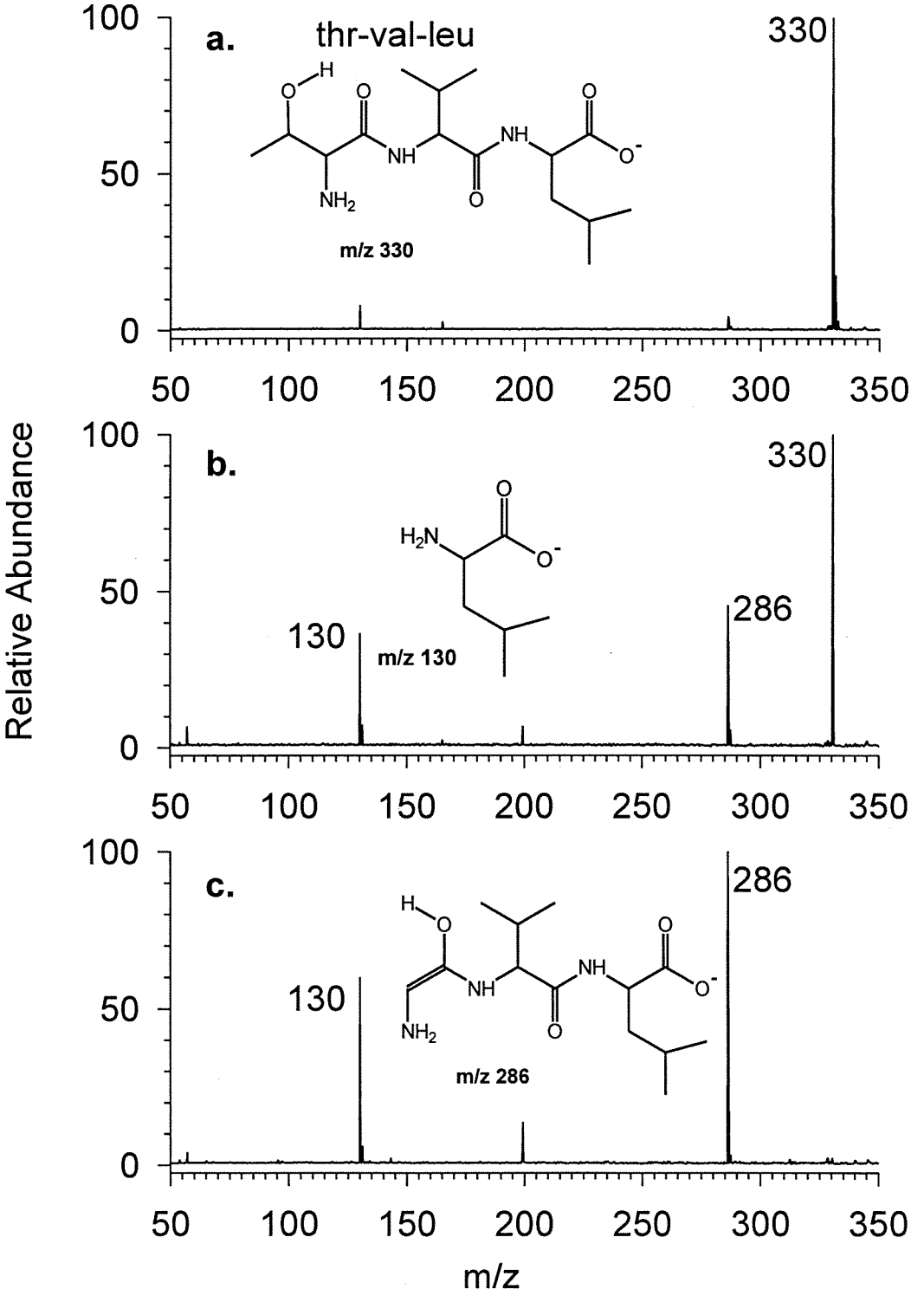
a.
thr-val-leu
330
m/z 330
b.
330
286
130
m/z 130
c.
286
130
m/z 286
Relative Abundance
m/z
100
50
0
50
100
150
200
250
300
350

Figure 2-5. Low energy dissociation of the deprotonated peptide thr-val-leu (m/z=330.2) against a static gas pressure. a.) Isolated parent ion. b.) Irradiation with $\Delta\omega/2\pi$=1866 Hz (m/z=332) and $<E_{com}>$=1.50 eV at a pressure of 10^{-7} torr for 1 second (approximately 10 collisions) yields partial dissociation and two products. c.) Increasing irradiation to $<E_{com}>$=2.16 eV yields 100% dissociation.

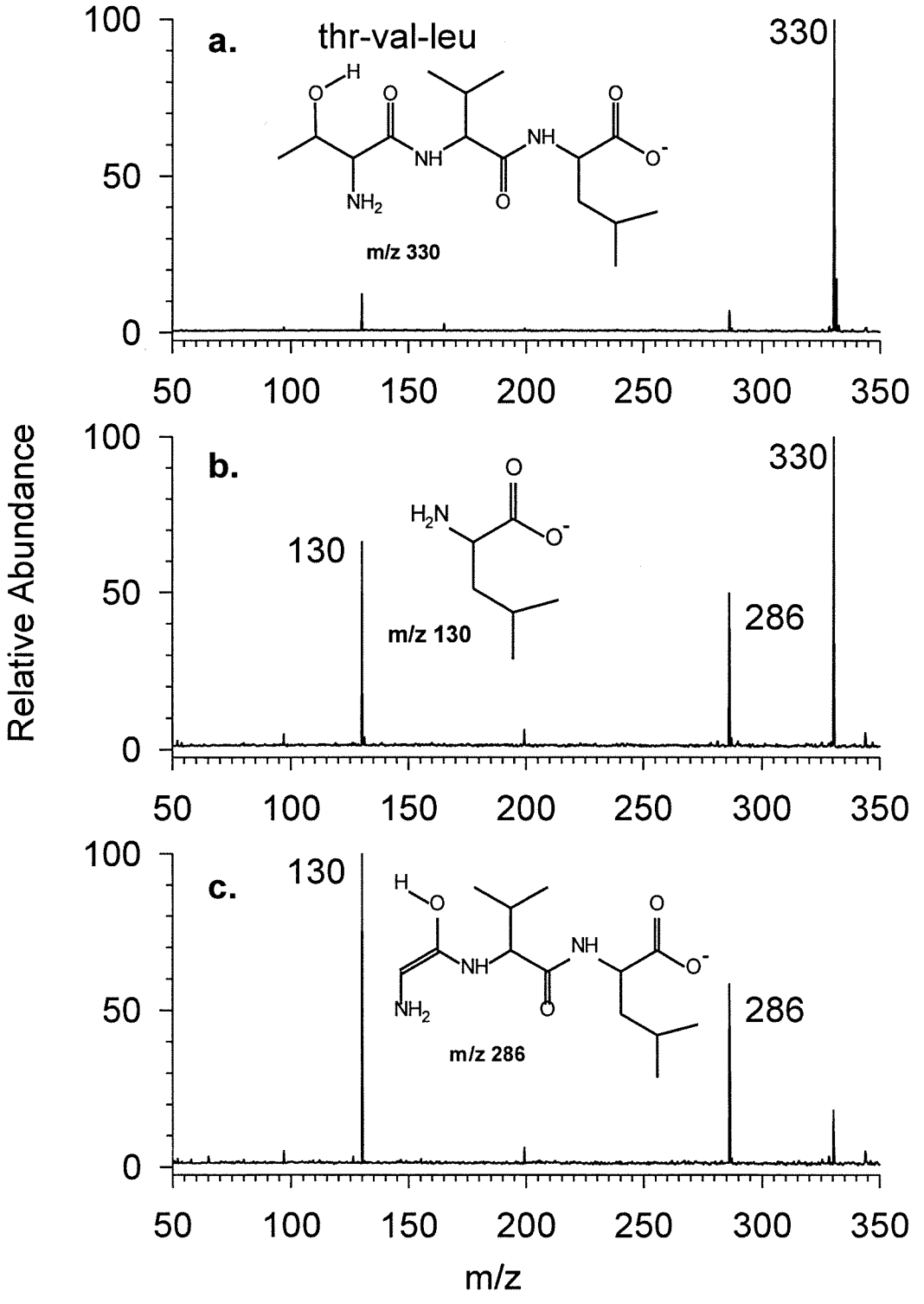
a.
thr-val-leu
330
m/z 330
b.
330
130
286
m/z 130
c.
130
286
m/z 286
100
50
0
50
100
150
200
250
300
350
Relative Abundance
m/z

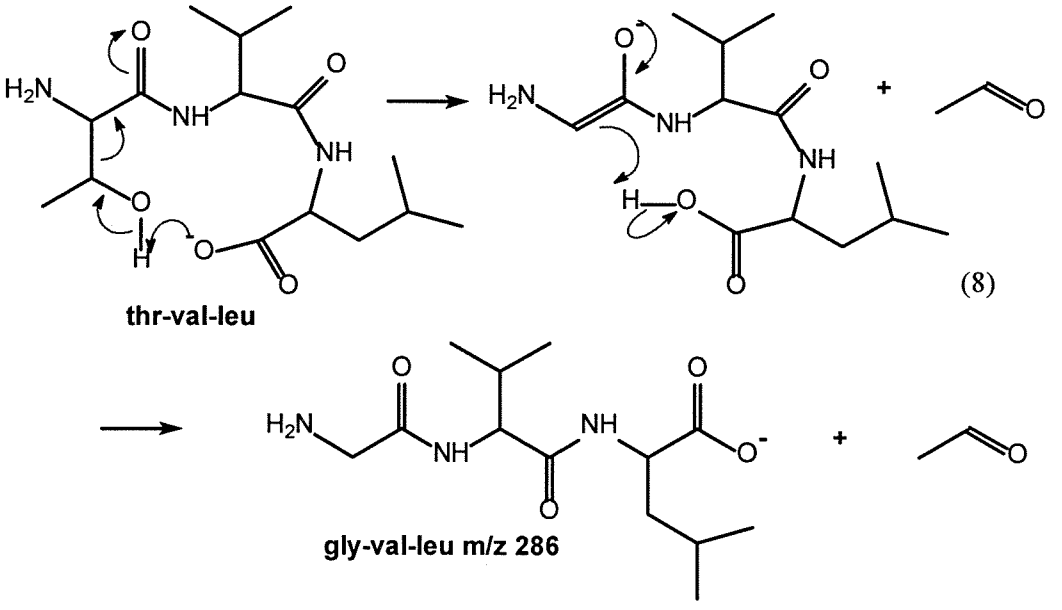

fragment at m/z 286 corresponds to peptide with glycine in the place of threonine, further dissociation should yield the deprotonated C-terminus amino acid. Off resonance collisional activation of the m/z 286 fragment from thr-val-leu yielded deprotonated leucine as expected. This is shown in Figure 2-6. If the alcoholic amino acid is at the C-terminus (i.e., leu-ser) the peptide should then first lose the aldehyde from the side chain and then sequentially eliminate deprotonated glycine. This process was also confirmed by initial product isolation and further collisional activation of deprotonated leu-ser. With leu-ser no deprotonated serine was observed confirming that loss of the side chain is the lowest energy process. This implies that the pathway to yield the C-terminus amino acid occurs exclusively through a sequential process, and not through two competing processes. The initial loss of the side chain is thought to arise through either a charge-induced mechanism (shown in reaction 8) or charge remote rearrangement (shown in reaction 9). As discussed by Adams,[3f] either of these mechanisms can account for the

Figure 2-6. a.) Isolation of the daughter ion of m/z 286 from the dissociation of thr-val-leu. b.) Off resonance excitation with $\Delta\omega/2\pi$=2370 Hz (m/z=288) and $<E_{com}>$= 0.43 eV at a pressure of 10^{-6} torr for 1 second (approximately 100 collisions) yields complete fragmentation to give the C-terminus amino acid (m/z=130).

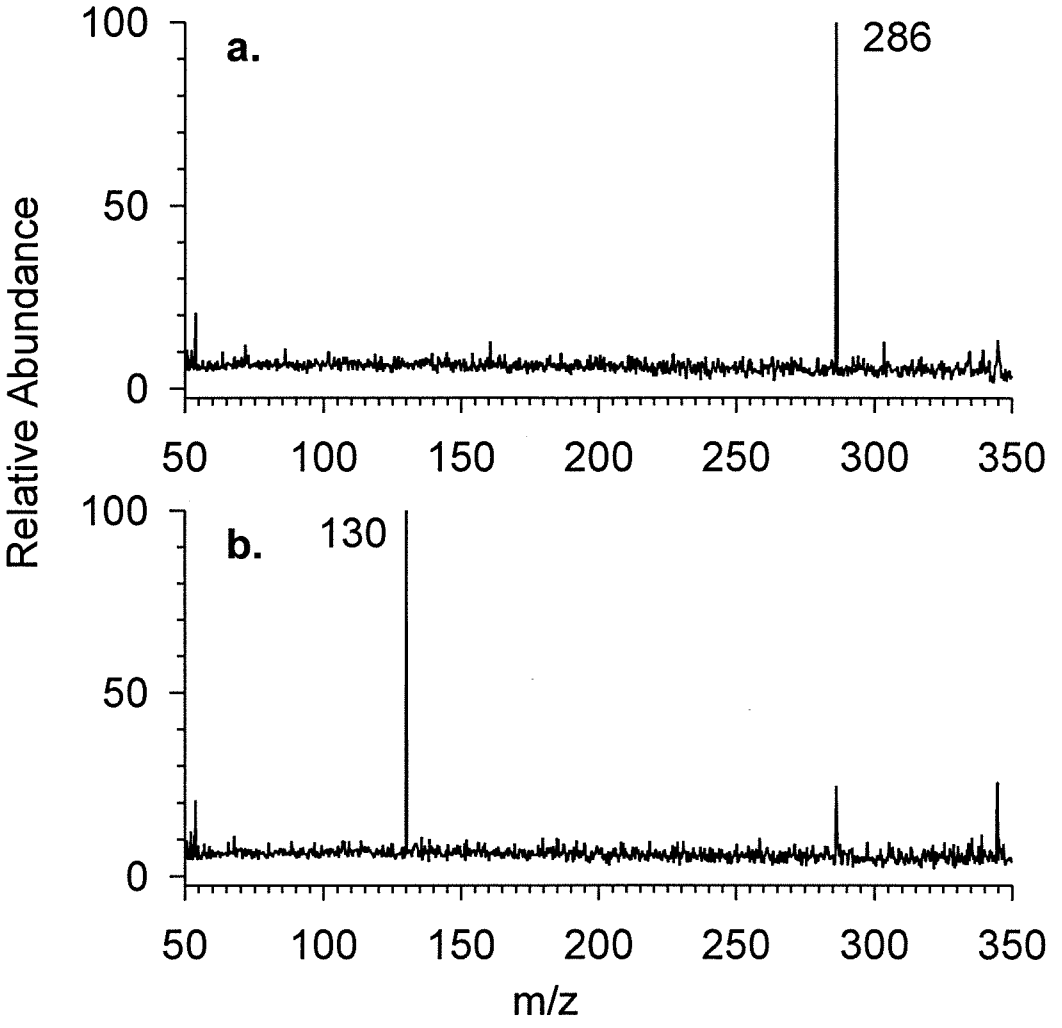
a.
286
b.
130
100
50
0
Relative Abundance
50
100
150
200
250
300
350
m/z

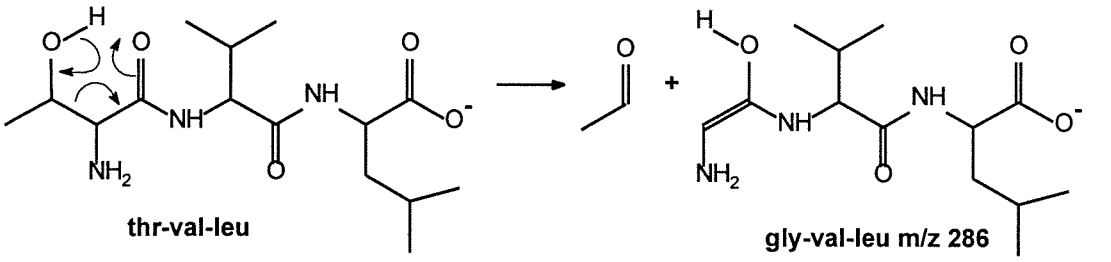

(9)

observed products. We have no additional experimental evidence to support one or the other of the mechanisms, but Adams showed that for peptides with threonine where the deprotonated C-terminus was bound to a Ca^{2+} ion that the loss of the side chain was still observed, supporting the charge-remote mechanism of reaction 9. Molecular mechanics calculations by Adams on deprotonated thr-val-leu showed that the lowest energy structure mimics that shown in reaction 8 with hydrogen bonding between the deprotonated C terminus and the side chain. However, we have done further calculations at the AM1 level and observe that a structure with hydrogen bonding between the deprotonated C-terminus and the N-terminus and terminal amide bond and a hydrogen bond between the hydroxyl group of the side chain and the adjacent carbonyl is lower in energy than a structure with a hydrogen bond between the deprotonated C-terminus and the hydroxyl group by 2.0 kcal mol^{-1}. Though all the structures will be accessible with the energy available from collisional activation, this is further support for the charge remote mechanism. As will be further mentioned in the discussion, a charge remote mechanism fits the general trend of dissociation mechanisms observed. In addition, the thermal rearrangement of 4-hydroxy-4-methyl-2-pentanone, which occurs by a mechanism analogous to the mechanism in reaction 9, has known activation parameters of E_a=32.3 kcal mol^{-1} (1.4 eV) and $A=10^{12}$ sec^{-1}.[10c]

Unimolecular Reactions: Strongly Acidic Side Chains. Preliminary studies were carried out on peptides containing amino acids with acidities comparable to the C-terminus carboxyl group. For even the simple dipeptides containing such

functionalities, determination of the C-terminus amino acid was often not possible, and multiple fragmentation patterns were usually observed. Peptides containing histidine and tryptophan side chains, which are estimated to be slightly less acidic than the carboxyl terminus, still yield the deprotonated C-terminus amino acid as one of their dissociation pathways. Peptides containing tryptophan in addition eliminate the tryptophan side chain, while peptides with histidine also lose CO_2 and/or H_2O.

Peptides containing glutamic acid yield dissociation patterns similar to the high energy spectra.[3e] Two types of products observed for a more complicated peptide, in this case val-gly-ser-glu, are indicated in Reaction 10. Two products probably arising from a competitive dissociation process are observed. This again suggests the existence of a long lived dissociation complex. With peptides having glutamic acid at the C-terminus position, the major product of chemical interest observed is an intact peptide less the C-terminus amino acid as shown for val-gly-ser-glu in Reaction 10. In this case an ion of m/z 260 proposed to correspond to the simpler deprotonated peptide val-gly-ser is observed. Further dissociation of this product confirms its identity and yields an ion of m/z 230

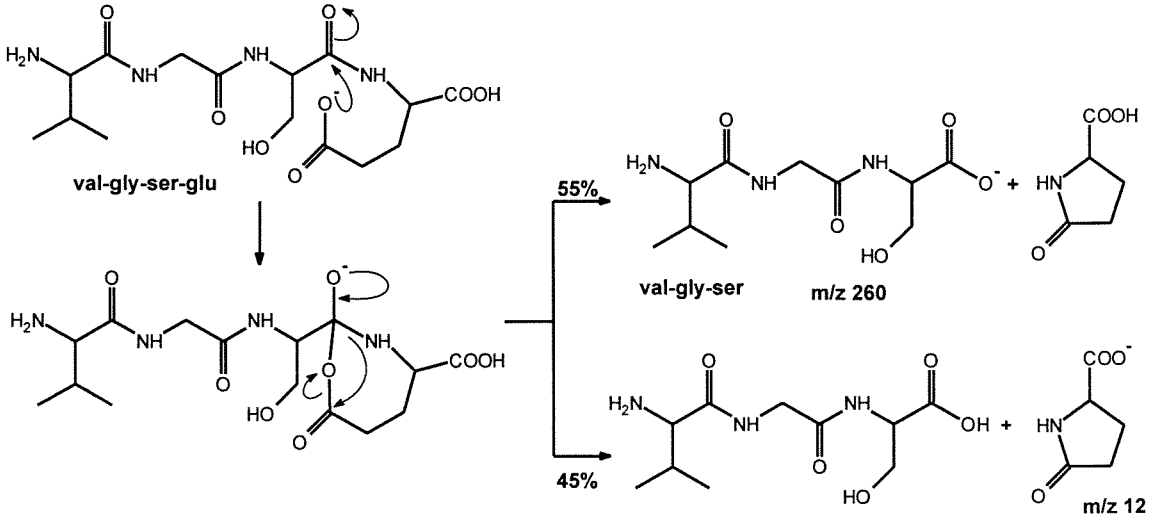

corresponding to loss of formaldehyde from the serine side chain. An ion corresponding to m/z 173 was also observed (both by us and by Bowie et al.[3]), but we were unable to assign a reasonable structure. Likewise, in the case of gly-glu, deprotonated glycine is observed. In all glutamic acid containing peptides, an ion of m/z 128 was observed. When glutamic acid is at the C-terminus, this ion is proposed to correspond to the product shown in Reaction 10. This structure was confirmed by Bowie et al. by MS/MS experiments.[3e] When glutamic acid is at the N-terminus, the ion at m/z 128 was also observed ion and is proposed to arise as shown in Reaction 11 deprotonated glu-leu. This mechanism is

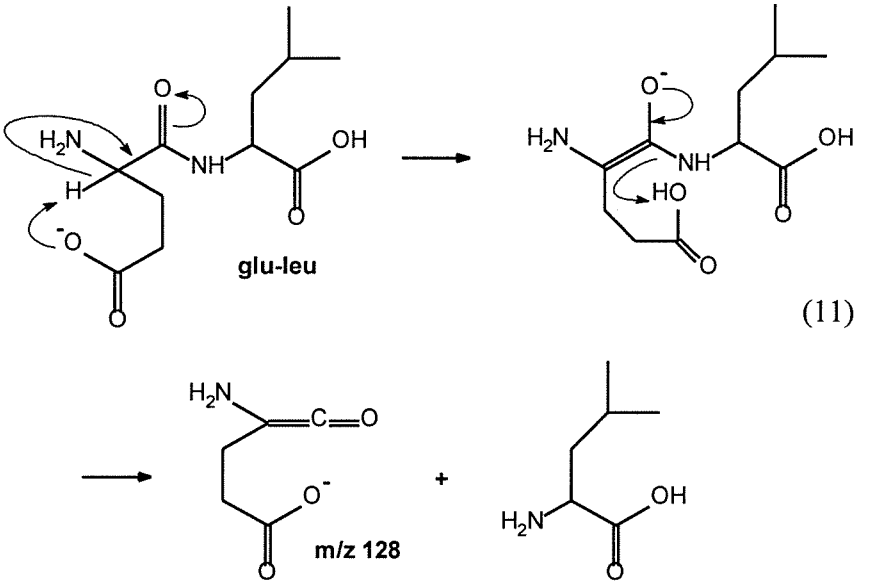

(11)

analogous to the reactions exhibited by peptides without acidic side chains, except the ion observed corresponds to the fragment containing the glutamic acid side chain, which is deprotonated. In addition, the smaller peptides with acidic side chains often showed water and/or carbon dioxide loss, a process never observed for peptides without acidic side chains.

Bimolecular Reactions. Simple deprotonated peptides were exposed to various reagents susceptible to nucleophilic attack to see if any bimolecular reactivity could be observed. Table 3 provides a summary of reagents tried and reactivity

Table 3. Reagents tested to probe bimolecular reactivity of amino acids and peptides.

Reagent	Observed Reactions
o-CH_3-Ph-N=C=O	none
CH_3-N=C=S	none
Acetone CH_3COCH_3	none
CH_3COCl	none
Ethylene Oxide	none
Formaldehyde	none
Acetic Anhydride CH_3CO-O-$COCH_3$	m/z 119
Triflouroacetic anhydride CF_3CO-O-$COCF_3$	m/z 113
Phenylsilane $SiPhH_3$	proton transfer
Acetic Acid	proton transfer
$Fe(CO)_5$	adduct formation and $Fe(CO)_4^-$ formation
Triflouroacetic acid	proton transfer

observed. Most bimolecular reactions of deprotonated peptides with other reagents are expected to be endothermic, and off resonance excitation was employed to promote product formation. A variety of reactive electrophiles exhibited no reactivity, including formaldehyde, ethylene oxide and p-tolyl-isocyanate. Species with labile protons like acetic acid, triflouroacetic acid, and phenylsilane tended to undergo fast proton transfer as shown in Reaction 12. Transition metal carbonyl complexes, like iron pentacarbonyl, known to be reactive with carboxylic acids[16] formed dimer complexes with the peptides as shown in Reaction 13.

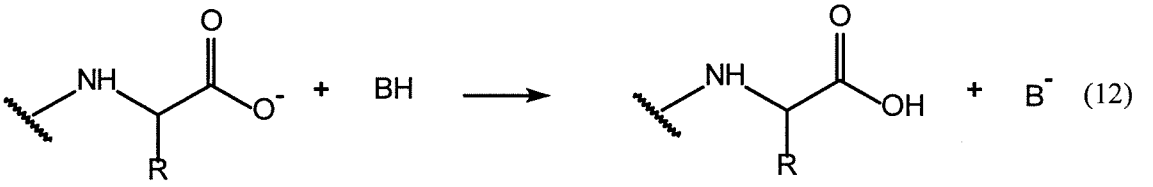

(12)

In ten seconds the reaction time at an iron pentacarbonyl pressure of $5x10^{-8}$ torr the reaction goes to completion with the resulting product distribution shown in Reaction 13.

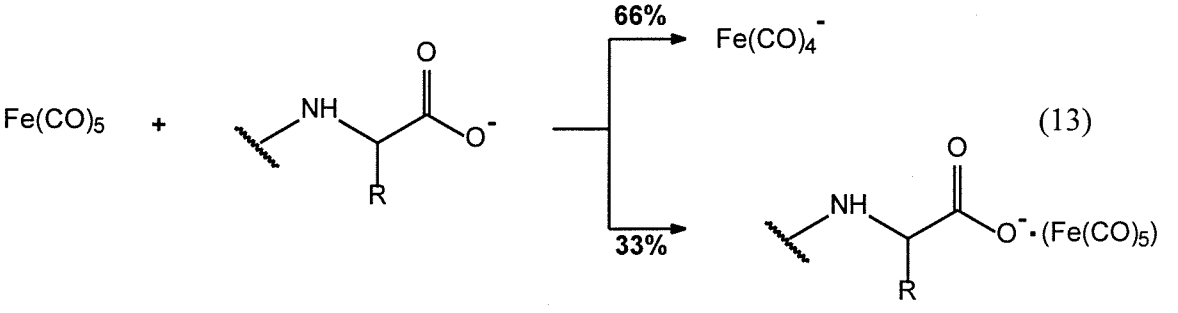

(13)

Bimolecular reactivity of anyhydrides at a reasonable rate without any excitation was observed, specifically with acetic and triflouroacetic anhydride. Reactions 14 and 15

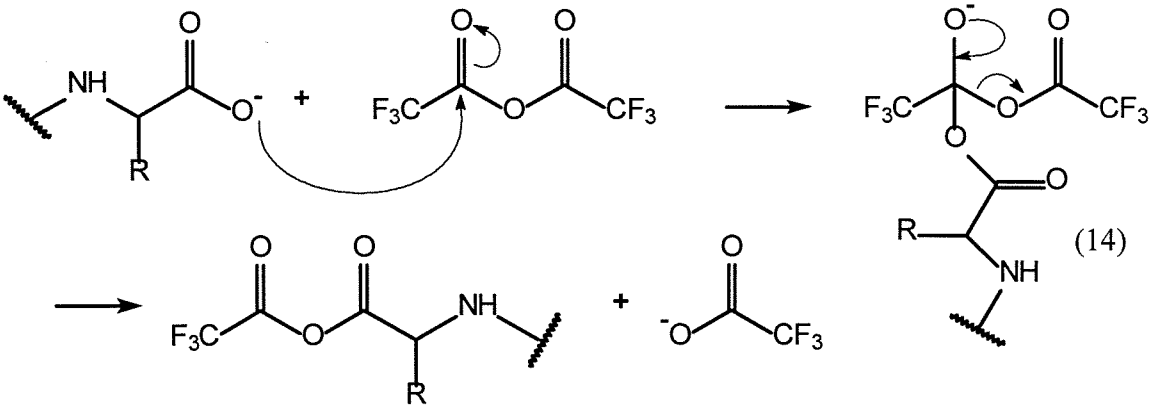

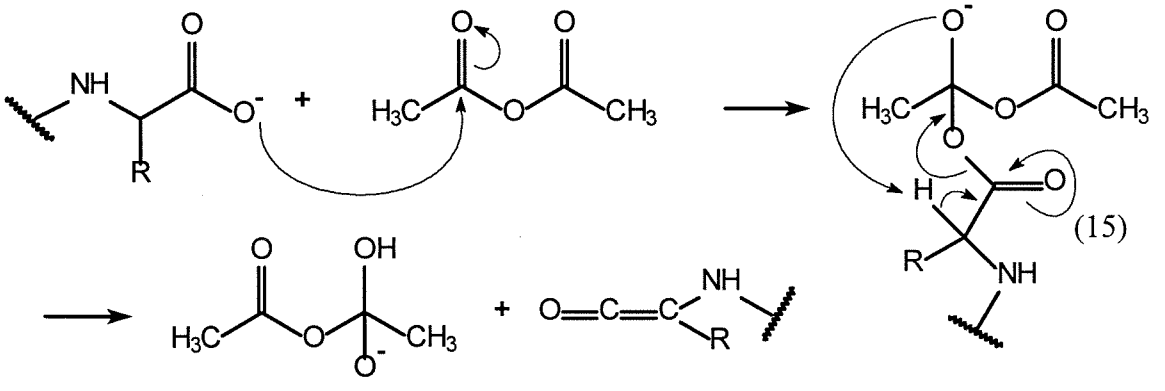

exemplify reaction pathways observed for a typical peptide reacting with triflouroacetic anhydride and acetic anhydride, respectively. These reactions are in good agreement with known gas phase reactivity of anhydrides with simple carboxylic acids.[17] Though none of the observed processes yielded any useful sequence information, these results are noteworthy since other than isotopic hydrogen exchange and proton transfer processes, there are few previously reported instances of bimolecular reactions of biomolecular ions with small molecules in the gas phase.

DISCUSSION

Off resonance excitation has been previously demonstrated to be a simple method with which to effect low energy dissociations of ions in an ICR cell.[4] Here we have shown its applicability to studying simple deprotonated peptides. The example of the dissociation of gly-gly-ile given in Figures 2 and 3 and Reaction 1 shows many of the key features of the technique being used. The amount of fragmentation can be finely controlled by varying the average ion translational energy, the length of the excitation period and the collision gas pressure. Complete fragmentation can be obtained with efficient collection and detection of the nascent fragment ions. This is in contrast to high energy collision induced dissociation techniques where to obtain fragmentation significant attenuation of the ion beam, accompanied by a loss of fragment ion signal intensity, is necessary. Off resonance excitation is highly selective and only ions with resonance frequencies close to the applied excitation frequency are excited. The products generally are far enough off resonance that they are not excited and instead collisionally relax. High energy collision induced dissociation (CID) is usually conducted under multiple collision conditions and fragments may be further excited in energetic encounters with the collision gas. This aspect of the experiment also provides advantages over infrared multiphoton dissociation (IRMPD)[18] and other photoexcitation methods[19] where everything trapped in the cell (products and reactants) is subject to excitation if the wavelengths employed are absorbed by the ions.

RRKM calculations have been carried out for several of the systems studied, and are shown in Figure 2-7 for the simple peptides gly-gly-ile, thr-val-leu and gly-val-leu. Appendix 1 details the assumptions made and equations used in carrying out the RRKM analysis on these large molecules. Though it is difficult to obtain quantitative information, a more thorough qualitative understanding of the energetics of dissociation of these molecules can be obtained. Because the activation energies

Figure 2-7. RRKM calculations for the dissociation of small deprotonated peptides as a function of internal energy for various activation energies. These results indicate that internal energies significantly in excess of threshold are required for large molecules to obtain an appreciable dissociation rate. a.) Rates of dissociation of gly-gly-ile to form deprotonated isoleucine. b.) Rates of dissociation of deprotonated thr-val-leu to form deprotonated gly-val-leu (m/z 286). c.) Rates of dissociation of deprotonated gly-val-leu to yield deprotonated leucine (m/z 130).

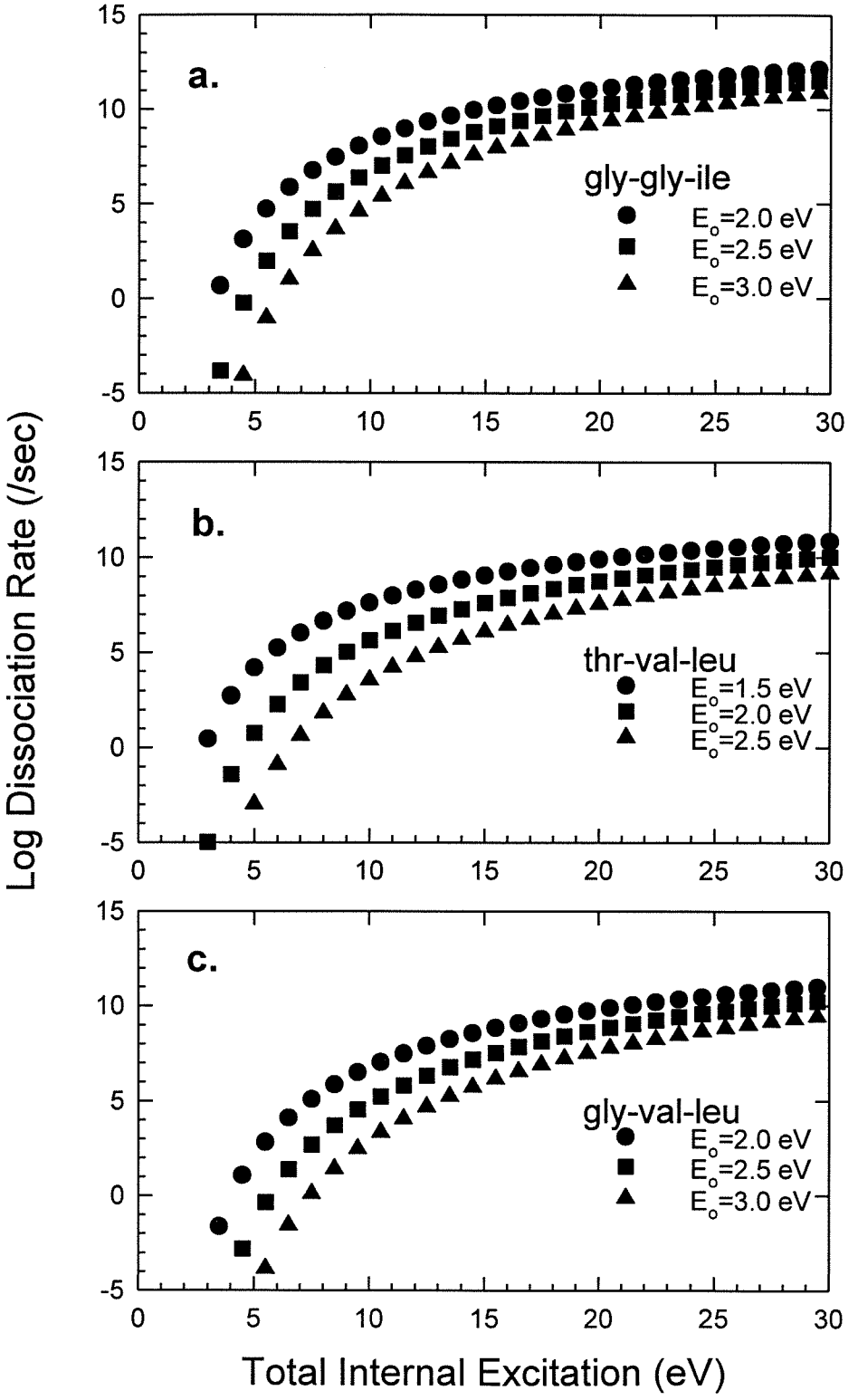
a.
gly-gly-ile
E_o=2.0 eV
E_o=2.5 eV
E_o=3.0 eV
b.
thr-val-leu
E_o=1.5 eV
E_o=2.0 eV
E_o=2.5 eV
c.
gly-val-leu
E_o=2.0 eV
E_o=2.5 eV
E_o=3.0 eV
Log Dissociation Rate (/sec)
Total Internal Excitation (eV)

are not known, the calculations were initially carried out for gly-gly-ile at a variety of activation energies ranging typically from 2 to 3 eV (46-69 kcal mol^{-1}). These numbers are about one and a half to two times the estimated reaction endothermicity and, based on the parameters for acetamide,[10] are probably reasonable guesses. One of the most important things that immediately becomes apparent in these calculations is that internal energies significantly in excess of the activation energy are required to obtain dissociation rates of 10 sec^{-1} (an appropriate rate for the time scales associated with our experiments) even for the small peptides being studied here. Despite this requirement for high internal energy, reasonably selective fragmentation patterns are observed. For gly-gly-ile, Figure 2-7a shows that to obtain a dissociation rate of 10 sec^{-1} with an assumed E_0 (threshold or activation energy) of 2.5 eV will require a total of 5 eV of internal excitation, or 2.5 eV excess energy over the threshold energy. This is in comparison to high energy CID experiments, where to observe dissociation with the same activation parameters requires a dissociation rate of at least 10^6 which would require at least 9 eV of internal excitation, or 6.5 eV of excess energy over threshold. Figure 2-3 shows that to obtain almost complete dissociation requires an $<E_{com}>$ of 4.0 eV for 9 collisions. This implies an average efficiency for conversion of translational to internal vibrational energy of at least 14% for each collision [about 13 kcal mol^{-1} (0.56 eV) $collision^{-1}$] to accumulate the required internal energy.

Only in the reactions of peptides with acidic side chains were multiple products observed. In the case of tyr-gly-gly competing processes were observed. Competition was postulated to arise by one dissociation pathway with the products resulting from placing the proton on two sites comparable in acidity. This proton transfer competition probably results in the multiple products observed for peptides involving strongly acidic side chains as well. However, it is observed and expected from an RRKM analysis that if multiple major products from two different dissociation pathways are observed, they tend to arise due to sequential rather than

competitive pathways. This is the case with peptides containing threonine and serine (i.e., thr-val-leu, leu-ser-phe and leu-ser). The initial fragmentation pathway involves elimination of the alcoholic side chain. As we have shown, the resulting fragment ion can then be further dissociated to yield the deprotonated C-terminus amino acid. Since no deprotonated serine is observed in the dissociation of leu-ser, we propose that the process to yield the deprotonated C-terminus amino acid occurs exclusively by sequential fragmentation after loss of the hydroxyl side chain. The fragment ion intensities observed for thr-val-leu at two different pressures are shown in Figures 4 and 5. Figure 2-4 shows that at higher pressures (in this case 10^{-6} torr), more of the fragment arising from side chain elimination is observed. In contrast, at the lower pressure used to obtain the spectra in Figure 2-5, the deprotonated C-terminus amino acid is the more abundant ion observed. RRKM analysis can also be used to explain the different branching ratios observed at different pressures. RRKM calculations for a variety of activation energies are shown for the two processes in Figure 2-7b and 7c. When dissociation first occurs the fragments are still vibrationally excited. The charged fragment (m/z 286 in this case) retains a substantial fraction of the initial internal energy deposited in excess of the threshold energy and can further dissociate. In this case, the second dissociation process, leading to the deprotonated C-terminus amino acid, can occur on a time scale comparable to collisional or radiative relaxation, provided it has a similar (or slightly higher) activation energy. Since it is not efficiently excited by the off resonance pulse, it will also slowly lose energy (at pressures of 10^{-6} torr collisional relaxation can become significant on a 10 ms time scale). The product distributions observed for unimolecular dissociation at 10^{-6} torr (Figure 2-4) compared with those observed at $5x10^{-8}$ torr (Figure 2-5) further support this postulated sequential process. Collisional relaxation of the product(s) occurs faster at the higher pressures of the former experiment, and so significantly less of the deprotonated C-terminus amino acid is observed. Hence, to determine low energy

dissociation pathways, a pulsed gas experiment which allows higher collision pressures to be obtained is more appropriate. An idea of the necessary energetics can be determined by considering the RRKM calculations shown in figure 2-7 b and c for thr-val-leu and gly-val-leu. For example, if E_0 for the loss of the threonine side chain is 1.5 eV and the internal excitation is 3.5 eV, the fragment ion can retain an average internal vibrational energy of almost 2.0 eV, meaning no extensive further dissociation would be observed. This means that to observe dissociation the loss of the C-terminus amino acid must have an activation energy of less than 2.0 eV. Collisional energy transfer processes of large molecules is not well understood. To rationalize the observed product distributions with the energetic data available, it seems likely that a fraction of the molecules are dissociating with even higher internal energies than those postulated here. These highly excited molecules would then more readily undergo sequential dissociation on the time scales of our experiments and yield the observed product distributions.

There are salient features which characterize almost all of the dissociation processes considered in this study. The dissociations are controlled by the site of charge, whether it is on the C-terminus of the peptide or on the side chain of an amino acid in the peptide, except perhaps for the threonine and serine containing peptides. The importance of the size of the internal ring formed to bring about the dissociation is also apparent. The general mechanism for dissociation of peptides without acidic side chains (Reaction 1) involves formation of a seven member ring. This ring size selectivity is also evident when considering the dissociation of the deprotonated peptide val-gly-ser-glu (Reaction 9) and comparing it to the observed dissociations of other peptides containing glutamic acid (Reaction 10). The fragment resulting from the dissociation pathway of Reaction 1 is never observed. If the charge is on the glutamic acid side chain for this peptide, an eight member ring would be required to abstract the appropriate proton. The major products observed result from the initial

formation of a more favorable seven member ring. Likewise, the major product observed for the deprotonated peptide glu-leu is proposed to result from a six member ring transition state (Reaction 10). Water loss is a process observed for many of the smaller peptides with acidic side chains, and it seems likely this corresponds to cyclization of the peptide. In the case of dipeptides, this would result in formation of rings with six to eight members. It is evident water loss is not exclusively due to the presence of acidic side chains as it is not an observed product from deprotonated val-gly-ser-glu, which would form a much larger ring upon cyclization. The importance of ring size formed in the transition state provides further evidence that the decomposition of the serine and threonine containing peptides occurs by a charge remote mechanism, which would have a six member ring transition state. Further work probing the fragmentations of model compounds and peptides of various composition is needed to understand more thoroughly these dissociation mechanisms.

Off resonance collisional activation of deprotonated peptides is a useful technique for simple systems because it allows identification of the C-terminus amino acid in many instances. However, most of the molecule is lost as a neutral, making the determination of further sequence information impossible. A more ideal experiment would leave the neutral fragment as an ion with an intact C-terminus mimicking the parent ion. Then sequential dissociations could allow the sequence of the peptide to be rapidly determined. The simplest way to do this would be by a bimolecular reaction with some reagent that would add to the C-terminus prior to collisional activation to yield the desired product. Something that would add to mimic the chemistry of glutamic acid on the C-terminus would be ideal, for as was shown in reaction 10, these peptides undergo a potentially useful dissociation pathway to yield a peptide with an intact C-terminus. Though none of the reactions investigated afforded any sequence information, they are noteworthy because there are few previously reported studies of bimolecular reactions of peptides in the gas

phase. Understanding the bimolecular reactivity of quasimolecular ions formed from peptides can aid in development of methods to obtain sequence specific information for these species.

CONCLUSIONS

It has been demonstrated that collisional activation of deprotonated peptides can yield useful but limited sequence information. In general the low energy pathway for dissociation of peptides without acidic side chains is elimination of the deprotonated C-terminus amino acid. This reaction pathway is controlled and catalyzed by the deprotonated carboxyl group. Peptides with acidic side chains exhibit more complex behavior but still yield useful sequence information. Statistical analysis using RRKM theory of these systems aids in the qualitative understanding of the energetics of the various processes. Further work to understand the mechanisms of collisional activation in the off resonance excitation process and obtain more quantitative energetic information is in progress. In particular, it is possible to use a series of deprotonated peptides to form a homologous set of molecules that dissociate with similar activation parameters. This can then be used to probe the effect of size on the collisional activation process.

APPENDIX 1.

RRKM Calculations. RRKM calculations to model the unimolecular dissociation dynamics were carried out using the Whitten-Rabinovitch approximation.[20] External rotations were assumed to be inactive. In this case the functional form of the sum of states, $G(E^{\neq})$ as a function of the excess energy in the activated complex, $E^{\neq}$, is given by Equation 16. The density of states, N(E), as a function of total internal energy, E, for the reactant species is given by Equation 17. $E_z^{\neq}$ is the zero point energy (ZPE) of the activated complex, E_z is the ZPE of the reactant species, s is the number of degrees of freedom of the reactant species and $\nu_i^{\neq}$ and ν_i are the vibrational frequencies of the activated and reactant species. The activated complex is assumed to have one less degree of freedom than the reactant molecule.

$$G(E^{\neq}) = \frac{\left(E^{\neq} + a^{\neq}E_z^{\neq}\right)^{s-1}}{(s-1)!\prod_{i=1}^{s-1} h\nu_i^{\neq}} \tag{16}$$

$$N(E) = \frac{\left(E + aE_z\right)^{s-1}}{(s-1)!\prod_{i=1}^{s} h\nu_i} \tag{17}$$

The rate expression can then be simplified to the form shown in Equation 18.

$$k = \frac{G\left(E^{\neq}\right)}{hN\left(E\right)} = \left(\frac{E^{\neq} + a^{\neq}E_z^{\neq}}{E + aE_z}\right)^{s-1} \frac{\prod_{i=1}^{s}\nu_i}{\prod_{i-1}^{s-1}\nu_i^{\neq}} \tag{18}$$

For "large" molecules the ZPE and sum and density of states are very large. For example, the ZPE of a 5 unit glycine polymer is about 10 eV. To carry out the actual calculation, a reasonable mechanism and activated complex is first proposed.

Vibrational frequencies are estimated from known frequencies for groups functionally similar to those found in peptides. Any additional frequencies not directly assignable were assumed to be low energy modes, and internal rotations were constrained in the cyclic transition states. Typical frequency factors were 10^{13} sec^{-1}. To test the accuracy of the Whitten-Rabinovitch approximation, we also performed calculations using a direct count algorithm in the case of gly-gly-ile for comparison. For rate constants of less than 10^{8} sec^{-1}, very good agreement was observed. This justifies using the simpler (and faster) approach outlined here to obtain unimolecular dissociation rate constants in the energy regime in which we are interested.

ACKNOWLEDGMENTS

We gratefully acknowledge the financial support of EMM from a Rainin Fellowhip and a NIH-NRSA Human Genome fellowship, and of SC from a NIH-NRSA traineeship in Biotechnology. We are indebted to the Beckman Foundation and Institute for the initial funding and continuing support of the research facilities. This work was supported in part by the National Science Foundation under grant CHE-9108318. Funds for instrument development have also been provided by ARPA (Advanced Research Projects Agency) and the DOD-URI program (ONR-N0014-92-J-1901).

REFERENCES

(1) (a) Lippstreu-Fisher, D.L.; Gross, M.L. *Anal. Chem.* **1985,** 57, 1174-1180. (b) Johnson, R.S.; Martin, S.A.; Biemann, K. *Int. J. Mass Spec. and Ion Proc.* **1988**, 86, 137-154. (c) Grese, R.P.; Cerny, R.L.; Gross, M.L. *J. Am. Chem. Soc.*. **1989**, 111, 2835-2842. (d) Teesch, L.M.; Adams. J. *J. Am. Chem. Soc.*. **1991**, 113, 812-820. (e) Biemann, K. *Annu. Rev. Biochem.* **1992**, 61, 977-1010.

(2) (a) Leary, J.A.; Zhou, Z.; Ogden, S.A.; Williams, T.D. *J. Am. Soc. Mass Spectrom.* **1990**, 1, 473-480. (b) Jensen, F. *J. Am. Chem. Soc.*, **1992**, 114, 9533-9537.

(3) (a) Eckersley, M.; Bowie J.H.; Hayes, R.N. *Org. Mass Spectrom.* **1989**, 24, 597-602. (b) Eckersley, M.; Bowie, J.H.; Hayes, R.N. *Int. J. Mass Spec. and Ion Proc.* **1989**, 93, 199-213. (c) Waugh, R.J.; Eckersley, M.; Bowie, J.H.; Hayes, R.N. *Int. J. Mass Spec. and Ion Proc.* **1990**, 98, 135-145. (d) Waugh, R.J.; Bowie, J.H.; Hayes, R.N. *Int. J. Mass Spec and Ion Proc.* **1991**, 107, 333-347. (e) Waugh, R.J.; Bowie, J.H.; Hayes, R.N. *Org. Mass Spectrom.* **1991**, 26, 250-256. (f) Reiter, A.; Teesch, L.M.; Zhao, H.; Adams, J. *Int. J. Mass Spec. and Ion Proc.* **1993**, 127, 17-26.

(4) Gauthier, J.W.; Trautman, T.R.; Jacobsen, D.B. *Anal. Chim. Acta.* **1991**, 246, 211-225.

(5) (a) Orlando, R.; Fenselau, C; Cotter, R.J. *Org. Mass Spectrom.* **1989**. 24, 1033-1042. (b) Orlando, R.; Murphy, C.; Fenselau, C.; Hansen, G.; Cotter, R.J. *Anal. Chem.* **1990**, 62, 125-129. (c) Orlando, R.; Fenselau, C.; Cotter, R.J. *Rapid Comm.*

Mass Spectrom. **1990**, 4, 259-262. (d) Orlando, R.; Fenselau, C.; Cotter, R.J. *J. Am. Soc. Mass Spectrom.* **1991**, 2, 189-197.

(6) Schulz, G.J.; Phelps, A.V. *Rev. of Sci. Instrum.* **1957**, 28, 1051-1054.

(7) In initial experiments we found that a differential bias voltage on the transmitter plates of the icr analyzer cell was required to maximize ion trapping efficiency. This acts to slow down the ions as they traverse the cell but skews the ion orbits in the analyzer cell. To avoid distortion of the electrostatic potentials in the cell, a split injection electrode consisting of two plates at the ion entrance to the cell that can be independently biased during ion injection was incorporated.

(8) (a) Dewar, M.J.S.; Zoebisch, E.G.; Healy, E.F.; Stewart, J.J.P. *J. Am. Chem. Soc.*, **1985**, 107, 3902-3909. (b) Dewar, M.J.S.; Dieter, K.M. *J. Am. Chem. Soc.*, **1986**, 8075-8086.

(9) The endothermicity can be estimated from the difference in acidities between a carboxylic acid site and a model ketone (CH_3CONMe_2 has acidity of 375 kcal mol^{-1} from reference 12b). Likewise the total exothermicity for the reaction was estimated by a thermodynamic analysis of the bonds broken and formed during reaction.

(10) (a) Hunt, M.; Kerr, J.A.; Trotman-Dickensen, A.F. *J. Chem. Soc.* **1965**. 5074-5080. (b) Benson, S.W.; O'Neal, H.E. in *Kinetic Data on Gas Phase Unimolecular Reactions.* National Bureau of Standards. United States, 1970. (c) Smith, G.G., Yates, B.L. *J. Org. Chem.* **1965** (30) 2067.

(11) For our cell geometry E_0 is 0.949*V/.0508 where V is the applied rf voltage and 0.0508 is the cell electrode spacing in meters.

(12) Marzluff, E.M.; Beauchamp, J.L., to be submitted.

(13) (a) Meot-Ner, M. *J. Am. Chem. Soc.* **1988**, 110, 3071-3075. (b) Lias, S.G.; Bartmess, J.E.; Liebman, J.F.; Holmes, J.L.; Levin, R.D.; Mallard, W.G. *Gas Phase Ion and Neutral Thermochemistry, Journal of Physical and Chemical Reference Data.* **1988**, 17, supplement 1. (c) Bartmess, J.E.; McIver, R.T. Jr. in *Gas Phase Ion Chem. Vol 2.* ed. Bowers, M.T. Academic Press: Orlando, FL, 1979; pp 87-121.

(14) Locke, M.J.; McIver, R.T. Jr. *J. Am. Chem. Soc.*. **1983**, 105, 4226-4232.

(15) O'Hair, R.A.J.; Bowie, J.H.; Gronert, S. *Int. J. Mass Spec. and Ion Proc.* **1992**, 117, 23-36.

(16) Lame, K.R.; Sallans, L.; Squires, R.R.; *J. Am. Chem. Soc.*, **1986**, 108, 4368-4378.

(17) (a) Bowie, J.H. *Aust. J. Chem.* **1975**, 28, 559-562. (b) Bowie, J.H.; Williams, B.D. *Org. Mass Spectrum.* **1975**, 10, 141-145.

(18) (a) Moini, M.; Eyler, J.R. *Int. J. Mass Spec. and Ion Proc.* **1987**, 76, 47-54. (b) Moini, M.; Eyler, J.R. *Int. J. Mass Spec. and Ion Proc.* **1989**, 87, 29-40.

(19) (a) Bowers, W.D.; Delbert, S.; Hunter, R.L.; McIver, R.T. Jr. *J. Am. Chem. Soc.*. **1984**, 106, 7288-7289. (b) Bowers, W.D.; Delbert, S.; McIver, R.T. Jr. *Anal. Chem.* **1986**, 58, 969-972.

(20) (a) Whitten, G.Z.; Rabinovitch, B.S. *J. Chem. Phys.* **1963**, 38, 2466-2473.

Chapter 3

Collisional Activation of Large Molecules is an Efficient Process

Collisional Activation of Large Molecules is an Efficient Process

Elaine M. Marzluff, Sherrie Campbell, M.T. Rodgers and J.L. Beauchamp*

Beckman Institute, California Institute of Technology, Pasadena, CA 91125

Contribution # 8936

Accepted for publication in the Journal of the American Chemical Society

as a Communication

*Author to whom correspondence should be addressed

ABSTRACT

The activation efficiency of large molecules has been investigated using off resonance excitation in the presence of an inert collision gas with an external source Fourier transform ion cyclotron resonance mass spectrometer. A homologous series of deprotonated peptides which dissociate with similar activation parameters has been used to investigate the effect of molecular size on the efficiency of collisional activation. Contrary to the common belief that it is inherently harder to activate large molecules and induce dissociation, it is demonstrated that under identical activation conditions large molecules with many internal degrees of freedom dissociate more readily than molecules with fewer degrees of freedom. This is attributed to an increase in cross section with molecular size and, more significantly, an ability for these molecules to undergo collisions resulting in up to 100% of the center of mass kinetic energy being converted to internal excitation. Trajectory calculations using a molecular mechanics force field have been carried out which support this idea and show that large molecules with many degrees of freedom can easily deform and efficiently convert translational energy to internal energy during a collision. Various collision gases have been investigated. Nitrogen, carbon dioxide and cyclohexane all exhibit similar activation efficiencies. The only polar gas investigated, ammonia, is even more efficient at activating these molecules. These results are in stark contrast to collision dynamics of small, rigid molecules where collisions typically involve transfer of only a few percent of the relative translational energy into internal excitation.

It is a common perception that as molecules become larger they become inherently more difficult to activate and dissociate in the gas phase, especially under low energy collision induced dissociation (CID) conditions.[1] In addition to the trivial consideration of reduced center of mass (COM) collision energies for a given collision gas, this difficulty has been attributed both to the inefficiency of the collisional activation process[1a,b] and to the requirement of higher levels of internal excitation to induce dissociation.[1c] A serious consequence of this supposition is the implied difficulty of using CID methods to sequence peptides and proteins.

A thorough understanding of the collisional activation dynamics of large molecules has been difficult to obtain due to lack of a simple model system. We have discovered a candidate for such studies in an investigation of the low energy dissociation pathways exhibited by deprotonated peptides.[2] In particular, deprotonated peptides without acidic side chains dissociate at low collision energies to yield exclusively the deprotonated C-terminus amino acid. This system provides a homologous series of molecules which undergo unimolecular dissociation with similar activation parameters. Here this set of molecules is used as a model system to investigate the effect of molecular size on low energy collisional activation processes.

The instrument and methodology of the collisional activation experiments have been previously described in detail.[2] An IonSpec (Irvine, CA) external source Fourier transform ion cyclotron resonance mass spectrometer (FT-ICR) equipped with an Antek cesium ion gun (Model 160-250B) was used in all the experiments. The deprotonated parent peptide was isolated with a series of radio frequency (rf) ejection pulses.

Activation of the peptide was initiated by the application of rf excitation slightly off resonance from the cyclotron frequency of the selected species.[3] This causes the ion to oscillate with low (typically <5 eV COM) bounded translational energy. In the presence of a collision gas, the ion undergoes multiple collisions with the internal energy of the ion increasing over time until it undergoes unimolecular dissociation.[4] In typical experiments, species were activated 1-4 kHz off resonance at lower frequency (higher mass) for 0.5-5.0 seconds with rf excitation of 1.0-5.0 volts zero-to-peak. A variety of collision gases were employed including nitrogen, carbon dioxide, cyclohexane and ammonia at static pressures of $0.5\text{-}2.0\text{x}10^{-7}$ torr. To determine the efficiency of the collisional activation process, the extent of dissociation of the activated ion was monitored as the translational energy, excitation time, and collision gas were varied.

Collisional activation of deprotonated peptides without acidic side chains yields exclusively the deprotonated C-terminus amino acid.[2] In this study we have used a total of ten peptides which exclusively dissociate in this manner with between 51 and 174 internal degrees of freedom. The proposed mechanism to account for their dissociation is illustrated in Scheme 1.[2] Dissociation is initiated by proton abstraction from the adjacent amino acid through a favorable seven member ring intermediate. Simple analysis of the relative acidities of the sites indicate this reaction is endothermic by approximately 30 kcal mol^{-1} (1.3 eV).[2] Proton abstraction is followed by rapid rearrangement to form the deprotonated C-terminus amino acid as the charged product. This process is estimated to have a threshold energy of 2.5 eV and a pre-exponential factor of 13.2.[2] While the activation parameters for the peptides investigated probably differ slightly depending on

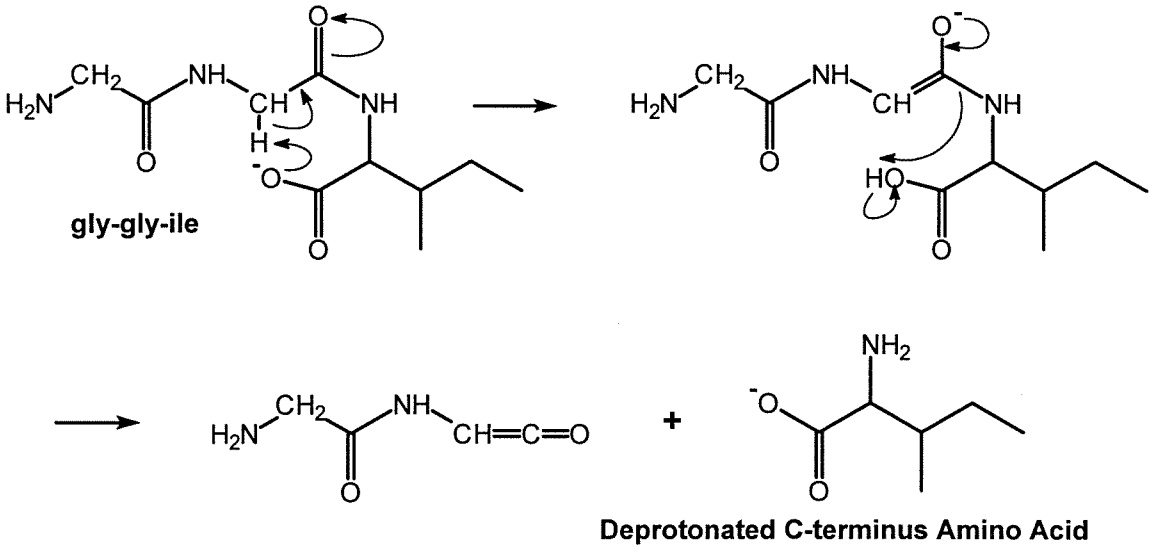

Scheme 1

the amino acid present at the position adjacent to the C-terminus, they are expected to be similar. Larger molecules will require more internal energy to produce dissociation at the same rate. A simple RRKM rate calculation demonstrates this for a series of deprotonated alanine polymers with an assumed threshold energy of 2.5 eV as shown in Figure 3-1.[5] Typical rates of dissociation for the time scale of our experiments using off resonance collisional activation are in the range of 1-10 sec^{-1}. The amount of energy over threshold (excess energy in the activated complex) required to obtain equal rates of dissociation increases as the number of degrees of freedom of the molecule increases. Because of the low collision energies employed in these studies, the activation process is expected to yield a statistical energy distribution in the ion (i.e., the energy should randomize among all the internal modes of the molecules faster than dissociation is effected).

Figure 3-2a shows the extent of dissociation observed for each peptide with 1 second of excitation at a COM collision energy of 1.25 eV and a nitrogen collision gas pressure of $2x10^{-7}$ torr. These data clearly demonstrate that the efficiency of collisional activation and dissociation increases with increasing molecular size. Some of this enhanced dissociation can be attributed to increased cross section as a function of size. However, simple estimates of molecular size imply that this can account for at most a factor of two difference and does not fully explain the nearly eight-fold difference in dissociation efficiency observed here.

To account for the marked increase in dissociation efficiency, it is concluded that the efficiency of converting relative translational energy into vibrational excitation

Figure 3-1. Dissociation rates for deprotonated $(ala)_n$ as a function of total internal energy of the molecule at an assumed threshold energy (E_o) of 2.5 eV and a pre-exponential factor of 13.2 where n=2,4,6 and s (the number of internal degrees of freedom)=60,120 and 180.

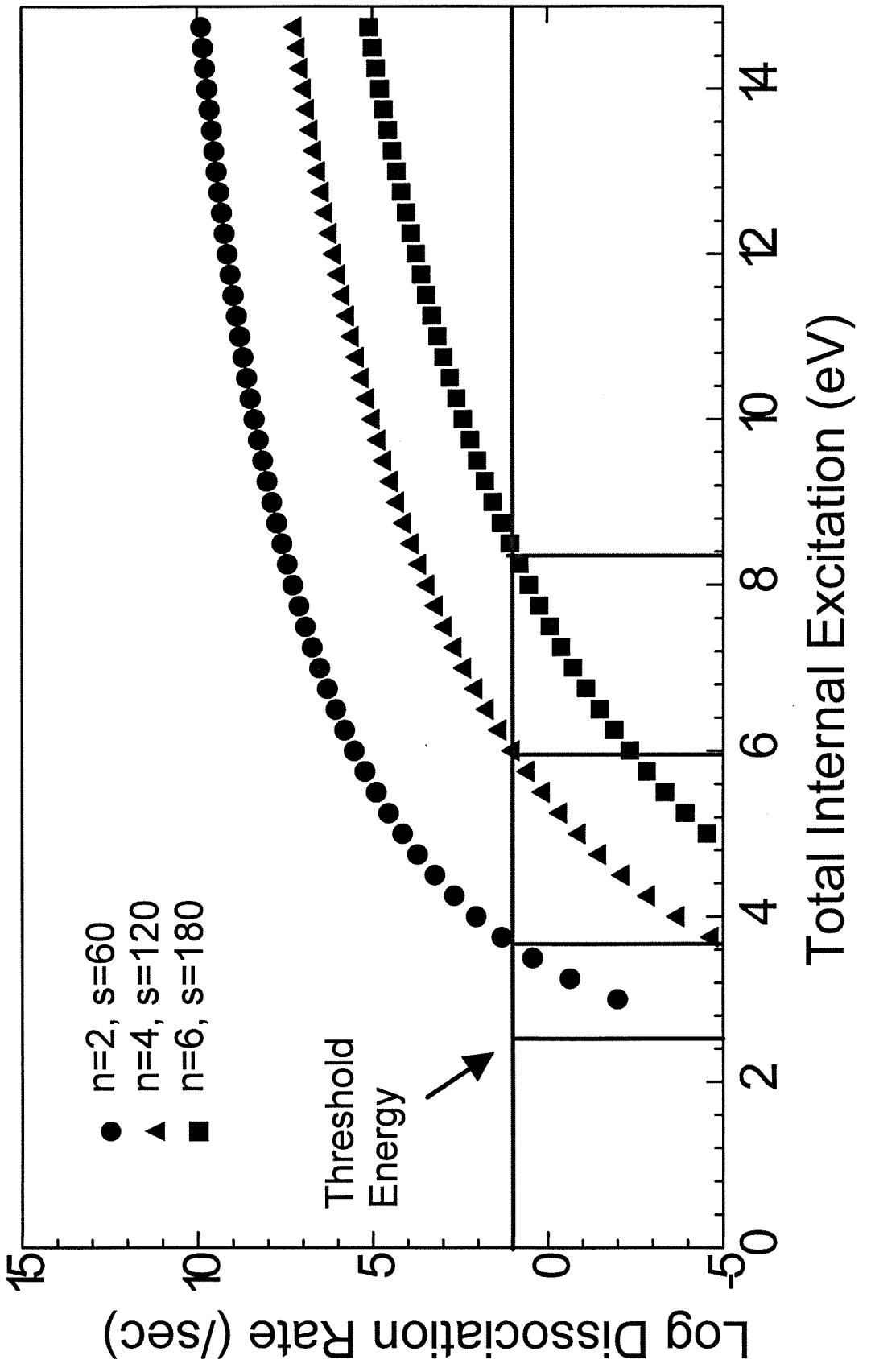
Log Dissociation Rate (/sec)
Total Internal Excitation (eV)
n=2, s=60
n=4, s=120
n=6, s=180
Threshold Energy
15
10
5
0
-5
0
2
4
6
8
10
12
14

Figure 3-2 (a) Effect of molecular size on dissociation efficiency. The extent of dissociation as a function of the number of internal modes of the peptide at a constant average center of mass collision energy of 1.25 eV and nitrogen collision gas pressure of $2x10^{-7}$ torr is shown. The off resonance excitation was applied for a period of 1 second. (b) Effect of collision gas on dissociation efficiency. The extent of dissociation of deprotonated gly-gly-ala was monitored as the average COM collision energy was varied for nitrogen, carbon dioxide, cyclohexane and ammonia collision gases. The off resonance excitation was applied for a period of 1 second. Data are given for nitrogen at two different pressures. Ammonia is more efficient at activating large molecules.

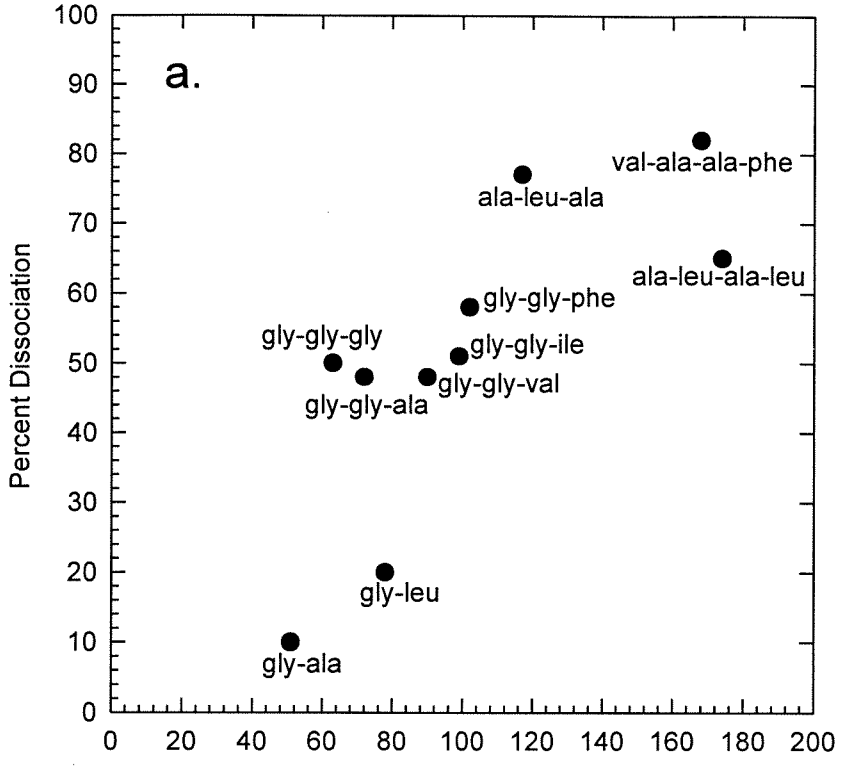
a.
Percent Dissociation
val-ala-ala-phe
ala-leu-ala
ala-leu-ala-leu
gly-gly-phe
gly-gly-gly
gly-gly-ile
gly-gly-ala
gly-gly-val
gly-leu
gly-ala
0
10
20
30
40
50
60
70
80
90
100
0
20
40
60
80
100
120
140
160
180
200

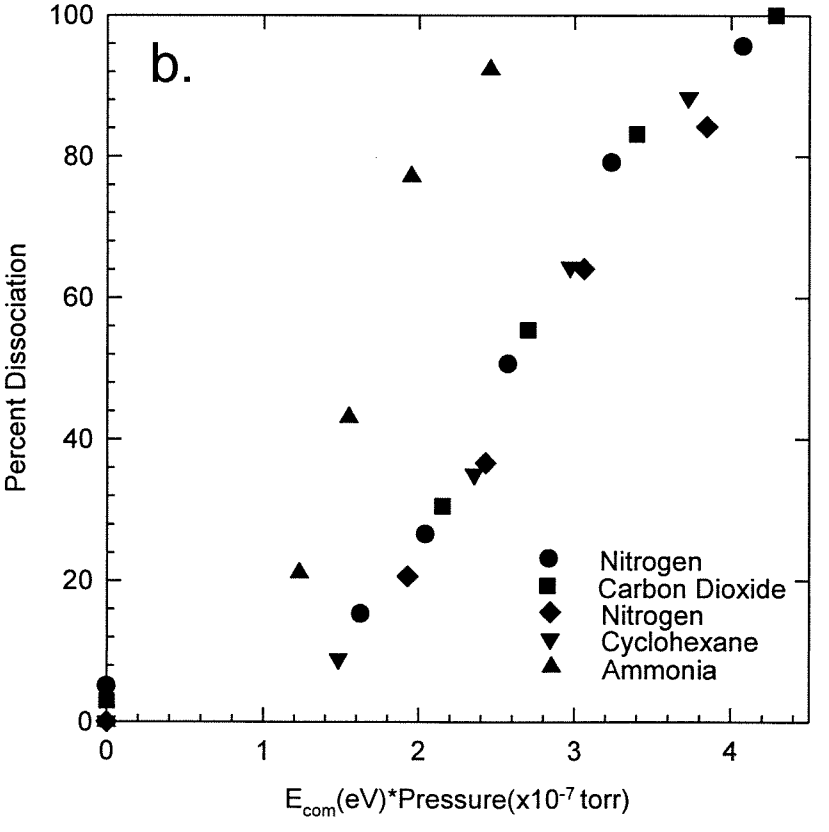
b.
Percent Dissociation
Nitrogen
Carbon Dioxide
Nitrogen
Cyclohexane
Ammonia
0
20
40
60
80
100
0
1
2
3
4
E_com(eV)*Pressure(x10^-7 torr)

increases with increasing molecular size. A simple estimate of the collision efficiency can be obtained by considering deprotonated gly-gly-ile which is 50% dissociated with the conditions indicated in Figure 3-2a. Using a gas kinetic ion-molecule collision rate of $1x10^{-9}$ cm^3 $molecule^{-1}$ sec^{-1}, under these conditions the ion undergoes about 6.5 collisions sec^{-1}. RRKM calculations with an assumed threshold energy of 2.5 eV indicate that it requires about 4.5 eV of total internal energy to induce dissociation at a rate of 10 sec^{-1}. With 6.5 collisions sec^{-1} this corresponds to an average energy transfer of 0.69 eV per collision, which is 55% of the average COM collision energy.

Trajectory calculations using a molecular mechanics force field are consistent with our experimental observations.[6] Figure 3-3 shows the calculated amount of energy transferred per collision as a function of impact position for deprotonated gly-gly-ile colliding with nitrogen at a relative translational energy of 1.25 eV. On average, 41% of the available relative kinetic energy is transferred into internal modes of the peptide, which undergoes extensive deformation during the collisions. No intermediate collision complexes are observed, and the amount of energy transferred is insensitive to impacting nitrogen orientation. The peptide behaves like a compressible energy absorbing medium. This theory predicts that as the molecules get larger, a point will be reached where virtually all of the available collision energy can be transferred into internal modes. Trajectory calculations for nitrogen colliding with protonated bradykinin (a nonapeptide with 444 internal degrees of freedom) typically show, except for glancing collisions which transfer smaller amounts of energy, energy conversions of greater than 90% even at relative collision energies as high as 100 eV. An interesting consequence of the

Figure 3-3. Results of trajectory calculations using a molecular mechanics potential energy surface for deprotonated gly-gly-ile colliding with nitrogen. On the left is the orientation of deprotonated gly-gly-ile with optimized geometry. Nitrogen approaches from above with 1.25 eV relative kinetic energy. On the right is the three dimensional representation of the fraction of energy transferred from translational to vibrational excitation as a function of impact position. The maximum amount of energy is transferred when nitrogen collides with the hydrogen bonded N and C termini. On average 41% of the collision energy is transferred into internal modes.

N_2 Impact from above

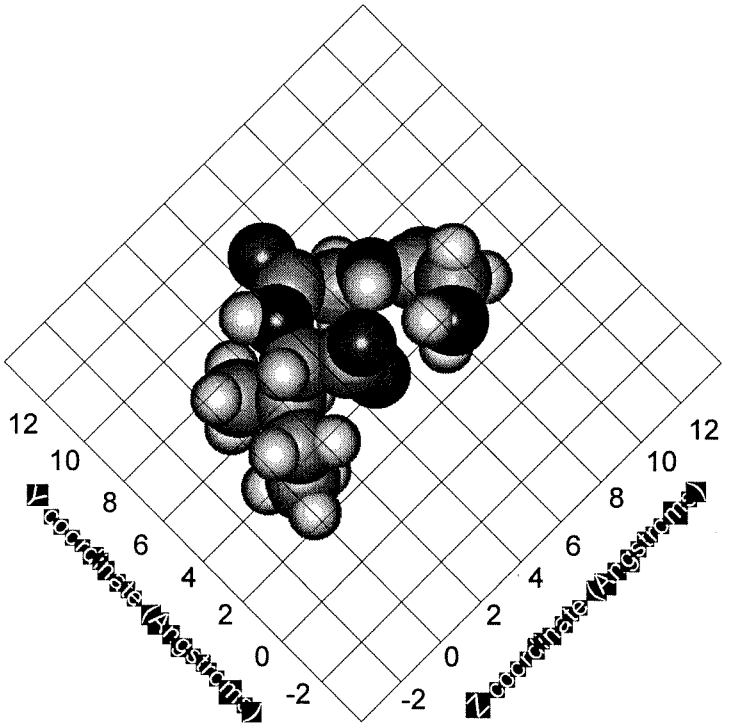

Energy Transfer Efficiency versus Position

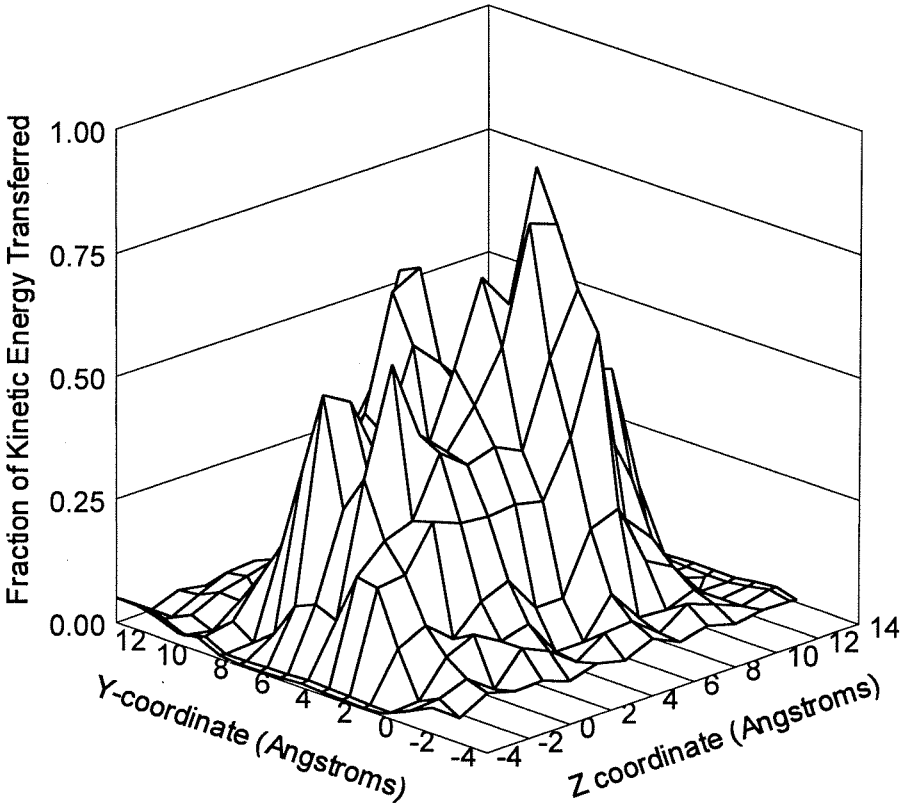

efficient conversion of translational to internal excitation is the ability to deposit reasonably well defined amounts of internal excitation in a large molecule under single collision conditions.[7]

The effect of collision gas on dissociation efficiency was examined using several gases of varying size and complexity. Measurements were carried out at different pressures for nitrogen, carbon dioxide, cyclohexane and ammonia. As shown in Figure 3-2b, we observe that the extent of dissociation with nitrogen, carbon dioxide and cyclohexane is a function of the product of the average COM collision energy and the pressure, which can be regarded as a measure of the energy exposure for multiple collision conditions. The one polar species investigated, ammonia, can be considered to be a "sticky" molecule, and is therefore more efficient at transfer of energy into internal modes.

Characterizing the collisional activation process is a necessary first step in understanding more fully the dynamics and energetics of the dissociation of large, complex molecules. The off resonance collisional activation process is amenable to detailed modeling with a master equation analysis which includes the effects of ion deactivation processes due to collisions and infrared radiative emission.[8] This analysis may yield parameters such as activation energies. Our expectations that this can be done are heightened by the observation that the extent of dissociation observed is not strongly dependent on the choice of collision parameters for non polar species of varying complexity. The largest species we have examined in the present studies has a molecular

weight of 405. It will be of particular interest to extend the present studies to peptides with significantly higher molecular weights.

ACKNOWLEDGMENTS

We gratefully acknowledge the financial support of EMM from a Rainin Fellowship and a NIH-NRSA Human Genome Fellowship, of SC from a NIH-NRSA traineeship in Biotechnology, and of MTR from a California Institute of Technology Consortium grant. We are indebted to the Beckman Foundation and Institute for the initial funding and continuing support of the research facilities. This work was supported in part by the National Science Foundation under grant CHE-9108318. Funds for instrument development have also been provided by ARPA (Advanced Research Projects Agency) and the DOD-URI program (ONR-N0014-92-J-1901).

REFERENCES

[1] a. Alexander, A.J.; Boyd, R.K.; *Int. J. Mass Spec. Ion Processes.* **1989**, 90, 211-240. b. Alexander, A.J.; Thibault, P.; Boyd, R.K.; Curtis, J.M.; Rinehart, K.L. *Int. J. Mass Spec. Ion Processes.* **1990**, 98, 107-134. c. Despeyroux, D; Wright, A.D.; Jennings, K.R. *Int J. Mass Spec. Ion Processes.* **1993,** 126, 95-99.

[2] Marzluff, E.M.; Campbell, S.; Rodgers, M.T.; Beauchamp, J.L. *submitted to JACS.*

[3] Gauthier, J.W.; Trautman, T.R.; Jacobsen, D.B. *Anal. Chim. Acta.* **1991**, 246, 211-225.

[4] Numerous mass spectrometry experiments have made use of multiple low energy collision conditions to accumulate internal excitation and induce rearrangement and dissociation of ions. See for example: Jarrold, M.F.; Honea, E.C. *J. Am. Chem. Soc.*, **1992**, 114, 459-464. Nourse, B.D.; Cox, K.A.; Morand, K.L.; Cooks, R.G. *J. Am. Chem. Soc.* **1992**, 114, 2010-2016.

[5] RRKM calculations were carried out using the Whitten-Rabinovitch approximation to estimate sums and densities of states. Whitten, G.Z.; Rabinovitch, B.S. *J. Chem. Phys.* **1963**, 38, 2466-2473. See also Appendix 1 of reference 2 for more details.

[6] Trajectory calculations were run using MM+, a version of the MM2 force field supplied with Hyperchem (Autodesk, Inc.) to describe the peptide and an exponential-6 potential to describe the projectile-peptide interaction. It is described more fully by Allinger, N.L. *J. Am Chem. Soc.* **1977**, 99, 8127. Atomic charges were initially optimized using semi-empirical methods.

[7] One way to readily accomplish this is by excitation with a fast neutral colliding with a slow ion. This has been proposed by Turecek, F. *Rapid Comm. Mass Spec.* **1991**, 5, 78.

[8] E.M Marzluff; J.L. Beauchamp, to be published.

Chapter 4

The Use of Computational Methods for Understanding Unimolecular Dissociation and Collisional Activation of Large Molecules in the Gas Phase

The previous two chapters included discussions that made use of computational methods to help understand further the reaction dynamics and dissociation energetics of large molecules in the gas phase. These methods include RRKM (Rice, Ramsperger, Kassel, and Marcus) statistical rate calculations, theoretical structure determinations, and collision trajectory calculations. A more detailed description of the application of these methods and results obtained from them will be given in this chapter.

PART I.

RRKM calculations.

To further understand the energetics of unimolecular dissociation reactions of large, biological molecules in the gas phase, RRKM calculations were performed to obtain an understanding of the range of excitation energies necessary to obtain efficient dissociation.[1] For the experiments conducted in this thesis, particularly those employing low energy off resonance collisional activation to effect dissociation, the rates of dissociation that can be easily observed in the FT-ICR occur on timescales of 1-100 per second (or to dissociation rates of 10^0-10^2 per second corresponding to a $\log_{10}k$=0-2). In Chapter 2 it was demonstrated that RRKM calculations can be applied to allow understanding of the energetic changes associated with observed dissociation processes. They are especially useful for helping to distinguish processes arising from competitive as opposed to sequential processes. The methodology and additional findings are described in more detail here.

RRKM calculations were carried out using the Whitten-Rabinovitch approximation.[2] For reference, Figure 4-1 shows an energy diagram for the

Figure 4-1. Schematic diagram of activation and dissociation of molecule A. E is the energy added to A, resulting in formation of an excited complex, denoted A^*. A^* proceeds to products through a transition state $A^{\neq}$ with an RRKM rate constant $k(E)$. E is the total internal energy of A, E_o is the threshold (or activation) energy of the process, and $E^{\neq}$ is the energy over threshold.

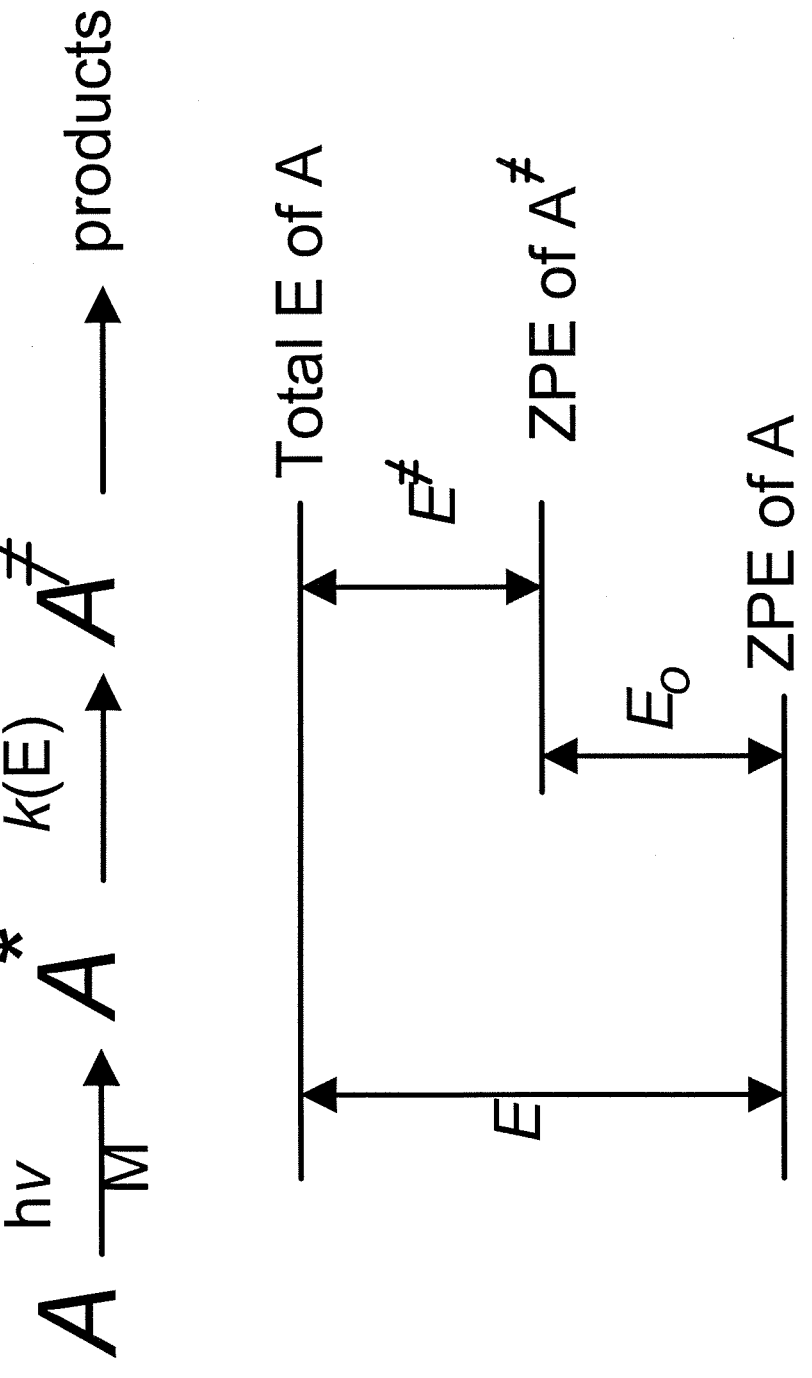
A
hν
M
A*
k(E)
A≠
products
Total E of A
E≠
ZPE of A≠
E0
ZPE of A
E

mechanism of the unimolecular dissociation process for a molecule A activated by either collisions or photon absorption. An internal energy, E, is added to A, resulting in the formation of excited complex, denoted A^*. A^* proceeds to products through a transition state $A^{\neq}$ with an RRKM rate constant $k(E)$ as shown in Equation 1.

$$A \xrightarrow{M} A^* \xrightarrow{k(E)} A^{\neq} \longrightarrow products \qquad (1)$$

Referring to Figure 4-1, E denotes the total internal energy of A, E_0 is the activation energy (threshold energy) of the process, and $E^{\neq}$ is the energy over threshold. E_z denotes the zero point energy (ZPE) of the reactant species and $E_z{}^{\neq}$ denotes the zero point energy of the transition state, $A^{\neq}$.

The RRKM rate constant, $k(E)$, is the micro-canonical transition state theory rate constant given by Equation 2.

$$k(E) = \frac{G(E^{\neq})}{hN(E)} \qquad (2)$$

$G(E^{\neq})$ is the sum of states in the energy range 0 to $E^{\neq}$ of the active degrees of freedom in the transition state and $N(E)$ is the density of states in the energy range 0 to E for the active degrees of freedom of the reactant. For simplicity, in the calculations carried out here, the reactant molecule is assumed to have s active degrees of freedom ($s = 3n\text{-}6$, where n is the number of atoms in the molecule). The transition state is assumed to have one less active degree of freedom ($s\text{-}1$) than the reactant molecule. Using these assumptions, the semi-classical sum of states for the transition state, using the Whitten-Rabinovitch approximation,[2] is given by Equation 3. The semi-classical density of states is the derivative of the sum of states for the reactant and is given by Equation 4.

$$G(E^{\neq}) = \frac{\left(E^{\neq} + aE_z^{\neq}\right)^{s-1}}{(s-1)!\prod_{i=1}^{s-1} hv_i^{\neq}} \qquad (3)$$

$$N(E) = \frac{(E + aE_z)^{s-1}}{(s-1)!\prod_{i=1}^{s} hv_i}\left(1 - \frac{da}{dE}\right) \qquad (4)$$

The rate expression can then be simplified to the form shown in Equation 5.

$$k(E) = \left(\frac{E^{\neq} + a^{\neq}E_z^{\neq}}{E + aE_z}\right)^{s-1} \frac{\prod v_i}{\prod v_i^{\neq}}\left(1 - \frac{da}{dE}\right) \qquad (5)$$

The Whitten-Rabinovitch approximation introduces the empirical correction factor a, which depends on E', ($E' = E/E_z$) and is given by Equation 6.

$$a = 1 - \beta\omega(E') \qquad (6)$$

The parameters β and ω are given by Equations 7 and 8, respectively.

$$\beta = \frac{s-1}{s}\frac{< v^2 >}{< v >^2} \qquad (0.1<E'<1.0) \quad (7)$$

$$\omega = \left[5.00E' + 2.73(E')^{.5} + 3.51\right]^{-1}$$
$$\omega = \exp\left[-2.4191(E')^{.25}\right] \qquad (1.0<E'<8.0) \quad (8)$$

A computer program specifically designed for calculations of large molecules has been written in Windows Visual Basic implementing this methodology. This program calculates the rates of dissociation as a function of internal energy using these equations. It allows the user to easily enter and change data and plots the rates on screen, without the need for use of either a separate editor or plotting program that currently available RRKM programs require.[3]

For the molecules considered in this chapter, the ZPE energies and sums and densities of states are very large, necessitating the simplifying steps shown here to carry out the calculations and to avoid (with very large molecules) overflowing the standard floating point limitations imposed by most computer programs and calculators. To carry out an actual calculation, a reasonable mechanism and activated complex are first proposed. Vibrational frequencies for the reactant molecule are estimated from known vibrational frequencies for functionally similar groups. Any additional frequencies not directly assignable are treated as low frequency vibrations, and internal rotations are assumed to be constrained in the transition state.[4] The chosen frequencies are used to calculate the values of the frequency factors and ZPE's. Typical frequency factors for all calculations are on the order of 10^{13} sec^{-1}.

To get an idea of the effect of molecular size on calculated RRKM dissociation rates of large molecules, calculations were initially carried out on protonated glycine polymers. Table 4-1 gives the ZPE's and required internal energies of the reactant species for dissociation at rates of 1, 10^3 and 10^6 sec^{-1} for a series of protonated glycine polymers with 5, 10, 50, and 100 amino acids (s=144, 249, 1089, 2139 respectively) with an assumed threshold energy, E_0, of 2.5 eV. Figure 4-2 shows the predicted rates as a function of internal energy for these molecules. For reference, Table 4-2 gives the frequencies of the reactant molecule and activated complex used in this calculation. The dissociation reaction in this case is assumed to be a simple dissociation of an arbitrary peptide bond. The corresponding frequency factor for this reaction calculated from these frequencies is 1.68×10^{13} sec^{-1}.[5]

Table 4-1. Internal energy (Internal energy per degree of freedom) required for specific dissociation rate (eV) for dissociation of protonated glycine polymers with an assumed activation energy of 2.5 eV.

	5-mer	10-mer	50-mer	100-mer
s	144	249	1089	2139
ZPE (eV)	10.7	18.2	77.9	151.7
Rate (sec^{-1})				
1	6.0 (.042)	10.0 (.040)	45.5 (.042)	83.0 (.039)
10^3	9.0 (.063)	15.0 (.060)	66.5 (.061)	125 (.057)
10^6	15.0 (.104)	24.0 (.096)	110 (.101)	

Figure 4-2. Calculated rates of dissociation as a function of internal energy using RRKM theory for a series of protonated glycine polymers with an assumed activation energy E_o=2.5 eV. The energies required to effect dissociation at a rate of 100 sec^{-1} are marked.

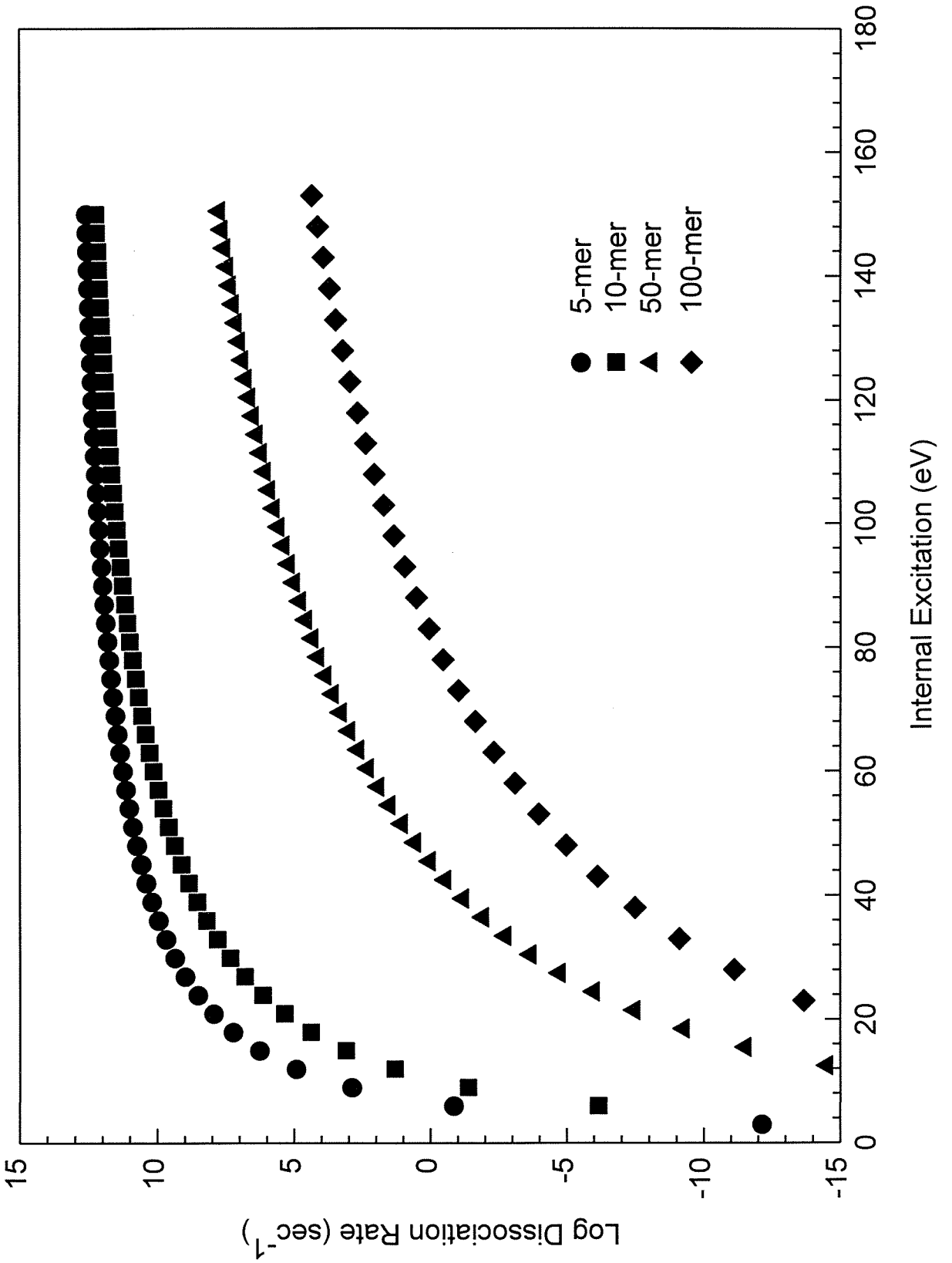
Log Dissociation Rate (sec^{-1})
15
10
5
0
-5
-10
-15
0
20
40
60
80
100
120
140
160
180
Internal Excitation (eV)
5-mer
10-mer
50-mer
100-mer

Table 4-2. Assigned vibrational frequencies used for calculation of dissociation rates of glycine polymers (reactant molecule).

Frequency (cm-1)	5-mer	10-mer	50-mer	100-mer
2800	10	20	100	200
3500	3	8	48	98
3400	2	2	2	2
1680	4	9	49	99
1600	3	3	3	3
1200	7	12	52	102
800	2	2	2	2
1150	7	12	52	102
1300	5	10	50	100
720	13	23	103	203
1500	1	3	3	3
1350	1	1	1	1
600	71	126	566	1116
1550	4	9	49	99
2900	4	4	4	4
3450	1	1	1	1
3100	3	3	3	3
1710	1	1	1	1
Total:	144	249	1089	2139

Table 4-2. (continued). Assigned vibrational frequencies used for calculation of dissociation rates of glycine polymers (transition state).

Frequency (cm-1)	5-mer	10-mer	50-mer	100-mer
2800	10	20	100	200
3500	3	8	48	98
3100	3	3	3	3
1680	3	8	48	98
1200	6	11	51	101
1150	7	12	52	102
1300	4	9	49	99
3475	1	1	1	1
1700	1	1	1	1
600	71	126	566	1116
1220	1	1	1	1
1640	1	1	1	1
2000	1	1	1	1
2900	4	4	4	4
3400	2	2	2	2
1710	1	1	1	1
720	13	23	103	203
1600	2	2	2	2
1500	3	3	3	3
1350	1	1	1	1
700	1	1	1	1
1550	3	8	48	98
1575	1	1	1	1
Total:	143	248	1088	2138

Figure 4-3. Comparison of calculated dissociation rates for the deprotonated peptide gly-gly-ile to lose the C-terminus amino acid using RRKM theory and programs supplied with reference 4.

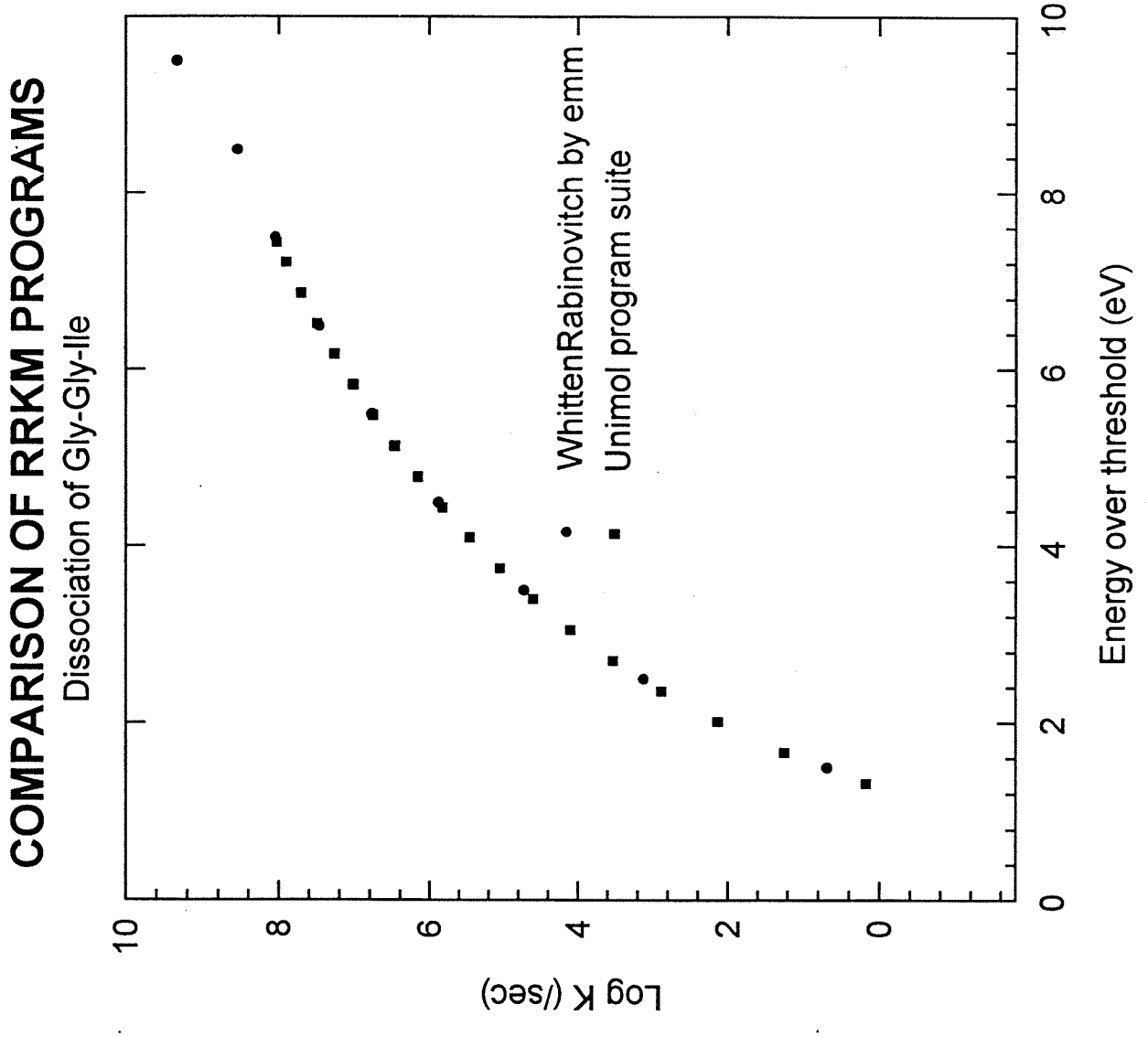
COMPARISON OF RRKM PROGRAMS
Dissociation of Gly-Gly-Ile
WhittenRabinovitch by emm
Unimol program suite
Log K (/sec)
Energy over threshold (eV)
0
2
4
6
8
10

Due to the convenient fact that the rate constants are a function of the ratio of the assumed properties of the activated complex and reactant species, the effect of choice of frequencies which are not directly involved in the dissociation reaction is small, as they cancel each other. This is especially true for the choice of values of low energy modes not directly assignable to vibrations or rotations. Changing the value of these by several hundred wavenumbers has a very slight effect on calculated rates. 600 cm^{-1} is usually assumed to be a good general average value for frequencies not directly assignable. To test the accuracy of the Whitten-Rabinovitch approximation, calculations using the direct count algorithm were performed (again assuming rotations to be inactive) for deprotonated gly-gly-ile dissociating to yield the C-terminus amino acid.[6] For rate constants of less than 10^8 sec^{-1}, the agreement between the two methods was exceptionally good (Figure 4-3).

Choice of a reasonable activation energy is more challenging. The reasoning leading to choice of threshold energies for dissociation of deprotonated peptides was given in Chapter 2. In the calculation of dissociation of the protonated glycines, the ions were assumed to undergo cleavage of the amide bond to give B-type fragments. Homolytic bond cleavage of C-N bonds usually have activation energies of 2.4-2.6 eV.[7] Based on this, we estimate an E_0 of between 2-3 eV for the dissociation of these molecules. The calculations indicate (Table 4-1 and Figure 4-2) that for large molecules there is a large kinetic shift, and that to effect dissociation on a timescale for optimum observance using FT-ICR detection methods (1-10 sec^{-1}), a large amount of internal energy (well over the reaction threshold energy) is required. The amount of energy over threshold required to effect dissociation at the same rate increases as

the number of degrees of freedom of the molecule increases (Figure 4-2 and Figure 3-1).

This result is what is qualitatively expected; the many degrees of freedom of these molecules means the internal energy can be spread out over many internal modes. Dissociation is only observed when the internal energy greatly exceeds the threshold energy, E_0. What is not so obvious is the fact that selectivity between two competing processes with similar activation energies is still observed even when the internal energy greatly exceeds the threshold energy. The branching ratios for two processes differing slightly in activation energy are shown in Figures 4-4 and 4-5 for protonated glycine polymers of length 5 and 100. Even for processes differing in threshold energy by only 0.2 eV at extremely high internal energies (well over the amount necessary even to effect dissociation observable by FT-ICR techniques), high selectivity toward the lower energy process is predicted. This high degree of selectivity has been experimentally observed in the low energy off resonance collisional activation studies carried out in Chapter 2. Very high internal energies are necessary before a significant amount of the higher activation energy pathway would be observed. As will be shown in the next chapter, the radiative relaxation rates of large molecules with large amounts of internal energy are so high it is unlikely any current activation method could be used to accumulate such high internal energies.

As a result of this selectivity for the low energy dissociation pathway, the observation of multiple products in moderate abundance can usually be attributed to continued sequential dissociation of the initial product ion. Since an energy E>>Eo is required to effect dissociation of a large molecule, the internal energy of the products

Figure 4-4. Competitive dissociation pathways of the 5-mer protonated glycine polymer. a. RRKM rates predicted for two processes with the slightly different activation energies 2.5 and 2.7 eV. b. Predicted branching ration of dissociation products as a function of internal energy expected in this instance.

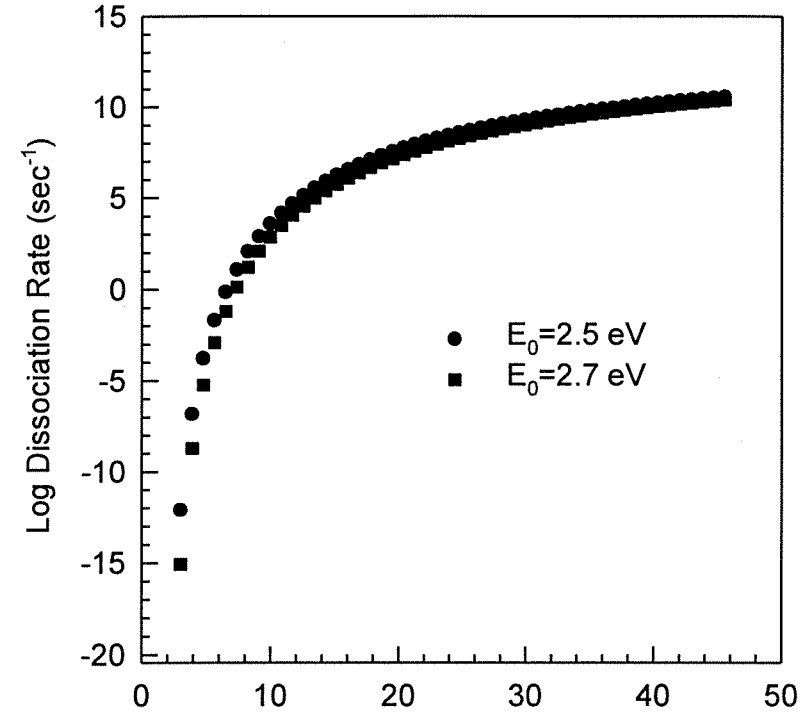
15
10
5
0
-5
-10
-15
-20
0
10
20
30
40
50
Log Dissociation Rate (sec^{-1})
E_0=2.5 eV
E_0=2.7 eV

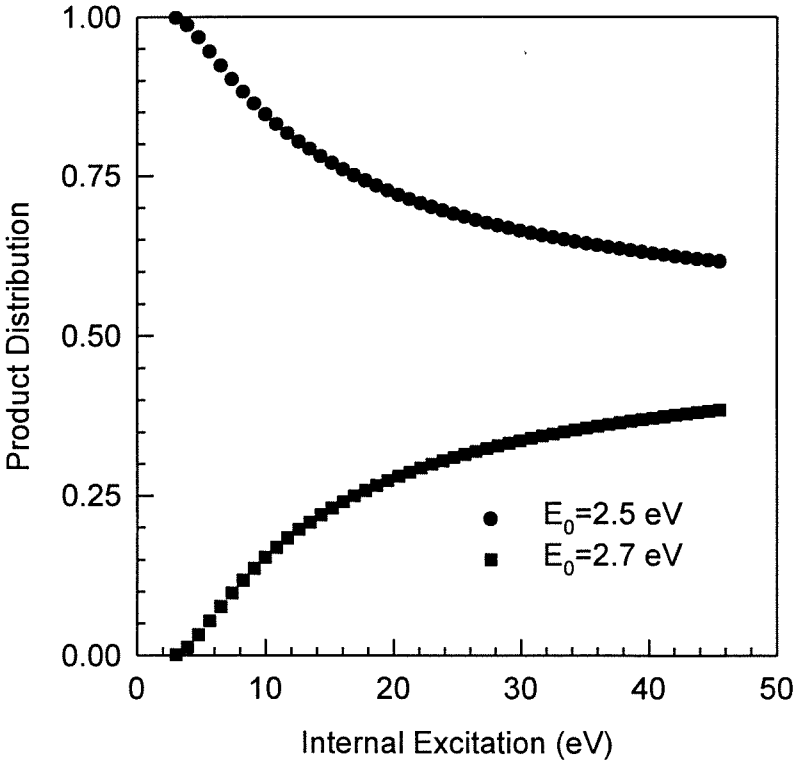
1.00
0.75
0.50
0.25
0.00
0
10
20
30
40
50
Product Distribution
Internal Excitation (eV)
E_0=2.5 eV
E_0=2.7 eV

Figure 4-5. Competitive dissociation pathways of the 100-mer protonated glycine polymer. a. RRKM rates predicted for two processes with the slightly different activation energies 2.5 and 2.7 eV. b. Predicted branching ratios for dissociation products expected in this instance.

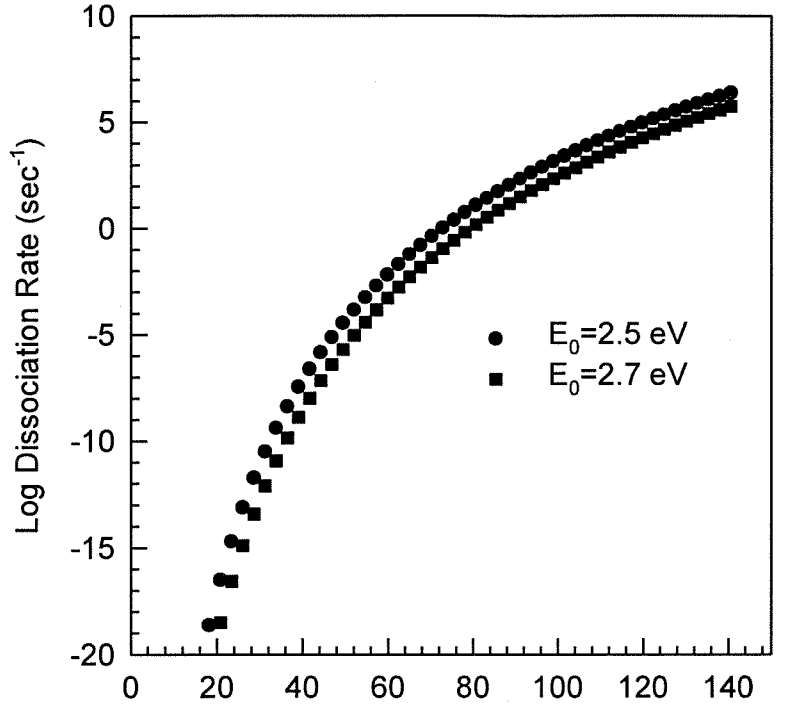
Log Dissociation Rate (sec^{-1})
10
5
0
-5
-10
-15
-20
0
20
40
60
80
100
120
140
E_0=2.5 eV
E_0=2.7 eV

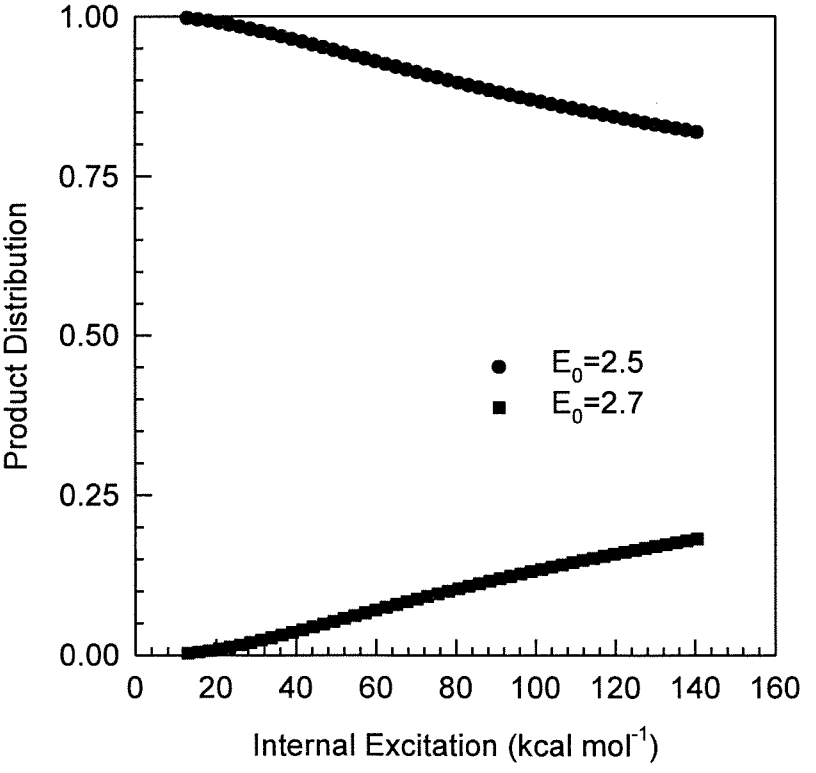
Product Distribution
1.00
0.75
0.50
0.25
0.00
0
20
40
60
80
100
120
140
160
E_0=2.5
E_0=2.7
Internal Excitation (kcal mol^{-1})

will also be high. RRKM analysis shows that, for larger products, if there is a dissociation pathway with a similar or slightly lower activation energy available to the fragment ion, it will continue to dissociate at a comparable rate. The energetics and dynamics of a process yielding two significant products were considered in detail for the deprotonated peptide thr-val-leu in Chapter 2. The observation of significant amounts of products by a direct competition between two pathways has not been observed in our experiments.

Multiple products have also been observed for the slightly different example of protonated met-enkephalin and will be described here. Off resonance activation of protonated met-enkephalin is shown in Figure 4-6, and results in formation of the A_4 and B_4 ions. Isolation and activation of the B_4 ion results in exclusive formation of the A_4 ion, as shown in Figure 4-7. An RRKM analysis for the processes is shown in Figure 4-8. An idea of the energetics for sequential dissociation can be obtained from the RRKM analysis of the sequential dissociation of the B_4 ion of met-enkephalin to yield the A_4 ion. An internal energy of 10 eV leaves about 5.7 eV of energy in the B_4 fragment ion upon dissociation. If the fragmentation to yield the A_4 ion has an activation energy of 2.0-2.5 eV, it will proceed at an appreciable rate (0.1-10 sec^{-1}), explaining the formation of a significant amount of the A_4 ion observed in Figure 4-6. Because of the high pressures employed in this experiment, collisional relaxation would have occurred rapidly, implying the lower activation energy is probably a more reasonable value.

The two examples of thr-val-leu and met-enkephalin dissociating to yield two products are different in a significant manner. In the dissociation of thr-val-leu

Figure 4-6. Low energy dissociation of the protonated peptide met-enkephalin (tyr-gly-gly-phe-met) against a pulsed gas pressure of $1x10^{-6}$ torr nitrogen. a. Isolated parent ion. b. Irradiation at $<E_{com}>$ of 0.335 eV for 3 seconds yields almost complete dissociation and two products (the A_4 and B_4 ions).

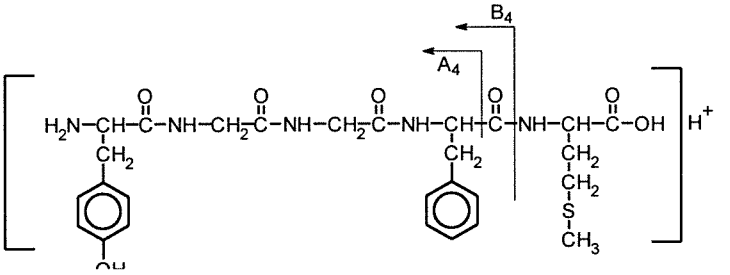
B4
A4
H2N–CH–C–NH–CH2–C–NH–CH2–C–NH–CH–C–NH–CH–C–OH
H+
CH2
CH2
CH2
CH2
S
CH3

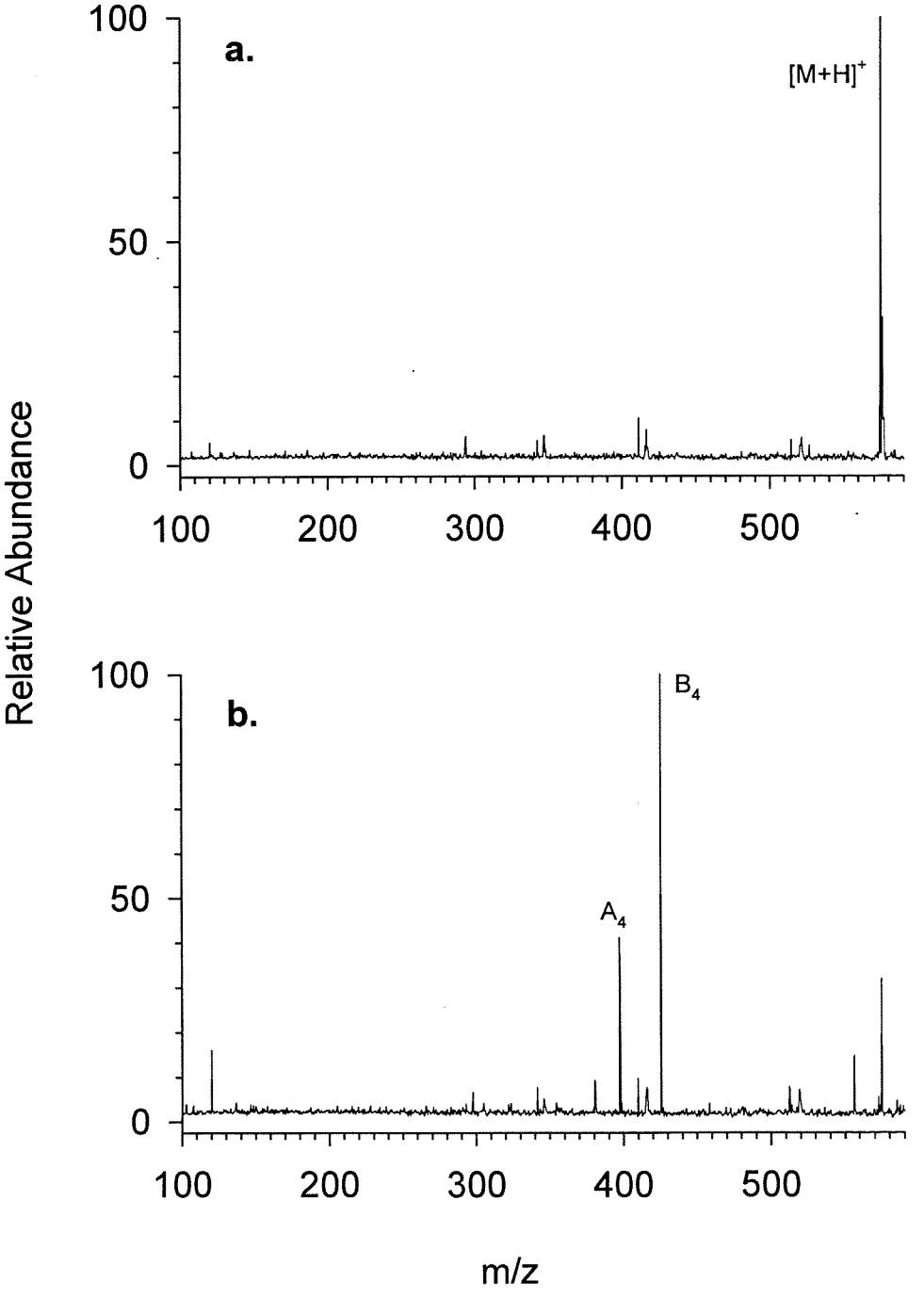
a.
[M+H]+
b.
B4
A4
100
50
0
100
200
300
400
500
Relative Abundance
m/z

Figure 4-7. Low energy dissociation of the B_4 fragment from protonated met-enkephalin. a. Isolated B_4 ion. b. Off resonance activation yields the A_4 ion.

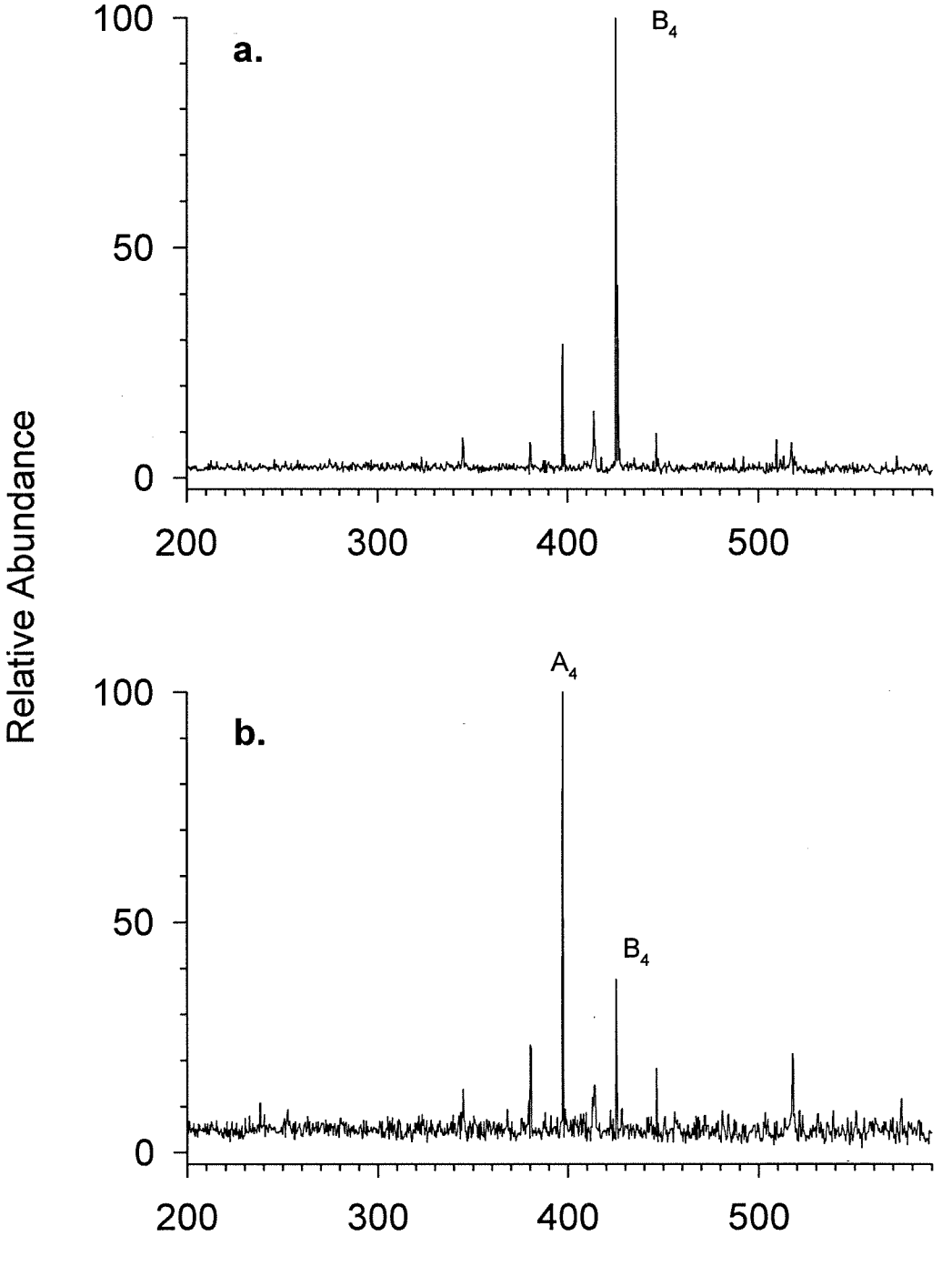
a.
b.
Relative Abundance
100
50
0
200
300
400
500
B_4
A_4
m/z

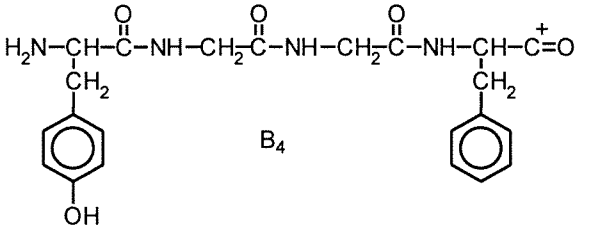
$H_2N-CH(CH_2-C_6H_4-OH)-C(=O)-NH-CH_2-C(=O)-NH-CH_2-C(=O)-NH-CH(CH_2-C_6H_5)-C\equiv O^+$
B_4

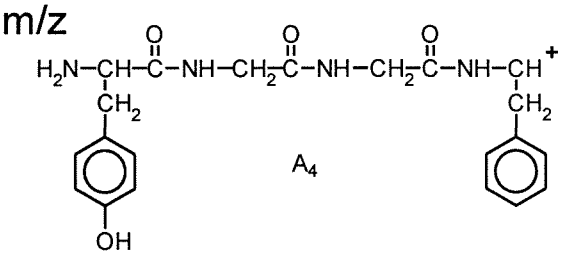
$H_2N-CH(CH_2-C_6H_4-OH)-C(=O)-NH-CH_2-C(=O)-NH-CH_2-C(=O)-NH-CH^+-CH_2-C_6H_5$
A_4

Figure 4-8. RRKM analysis of the dissociation energetics of protonated met-enkephalin. a. Dissociation to form the B_4 fragment ion. b. Dissociation of the B_4 fragment to form A_4 fragment.

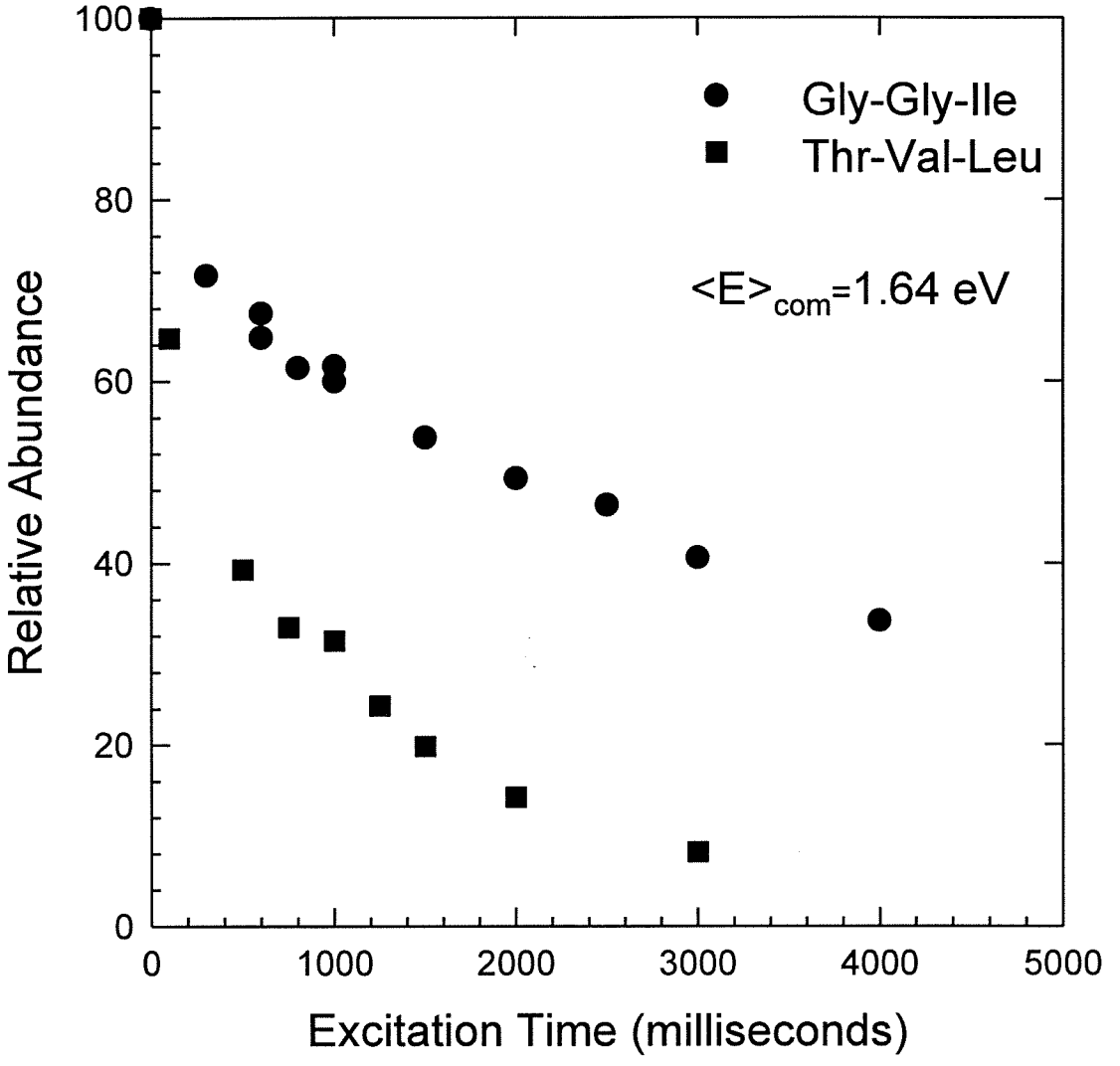
Gly-Gly-Ile
Thr-Val-Leu
<E>com=1.64 eV
Relative Abundance
Excitation Time (milliseconds)
0
20
40
60
80
100
0
1000
2000
3000
4000
5000

considered in Chapter 2, both observed processes can occur independently from the parent ion. The second process (loss of the C-terminal amino acid) is going to have the same activation energy for dissociation from the initial ion as from formation from the product of the initial fragment ion (loss of formaldehyde). Therefore, the initial process must have a lower activation energy than the second process. The dissociation processes and energetics are shown in Scheme I. Figure 4-9 compares the extent of dissociation of thr-val-leu and gly-gly-ile under identical conditions. The two peptides are similar in size, and the relative ease of dissociation of deprotonated thr-val-leu is apparent. For protonated met-enkephalin the processes are different. The formation of the A_4 ion from the parent peptide compared to the B_4 ion will occur by different mechanisms, and thus have different activation energies. Formation of the A_4 ion from the parent peptide must have a higher activation energy than formation of the B_4 ion or else it is unlikely that significant amounts of the A_4 ion would be observed. However, it is possible the sequential process of formation of the A_4 ion from the B_4 ion can actually have a lower activation energy than the formation of the B_4 ion from the protonated parent ion. Given the high pressures employed in these dissociations, and the resulting rapid rate of collisional relaxation, this seems a likely hypothesis. Energetics of these dissociations are not well understood, and further work is currently being done.

RRKM theory and an understanding of collisional activation efficiency can also be used to get an idea of energy transfer. Assuming a gas kinetic ion-molecule collision rate of 1×10^{-9} cm^3 $molecule^{-1}$ sec^{-1} (see Appendix 1), for the case shown in Figure 4-6, met-enkephalin undergoes about 32 collisions sec^{-1} for 3 seconds. With

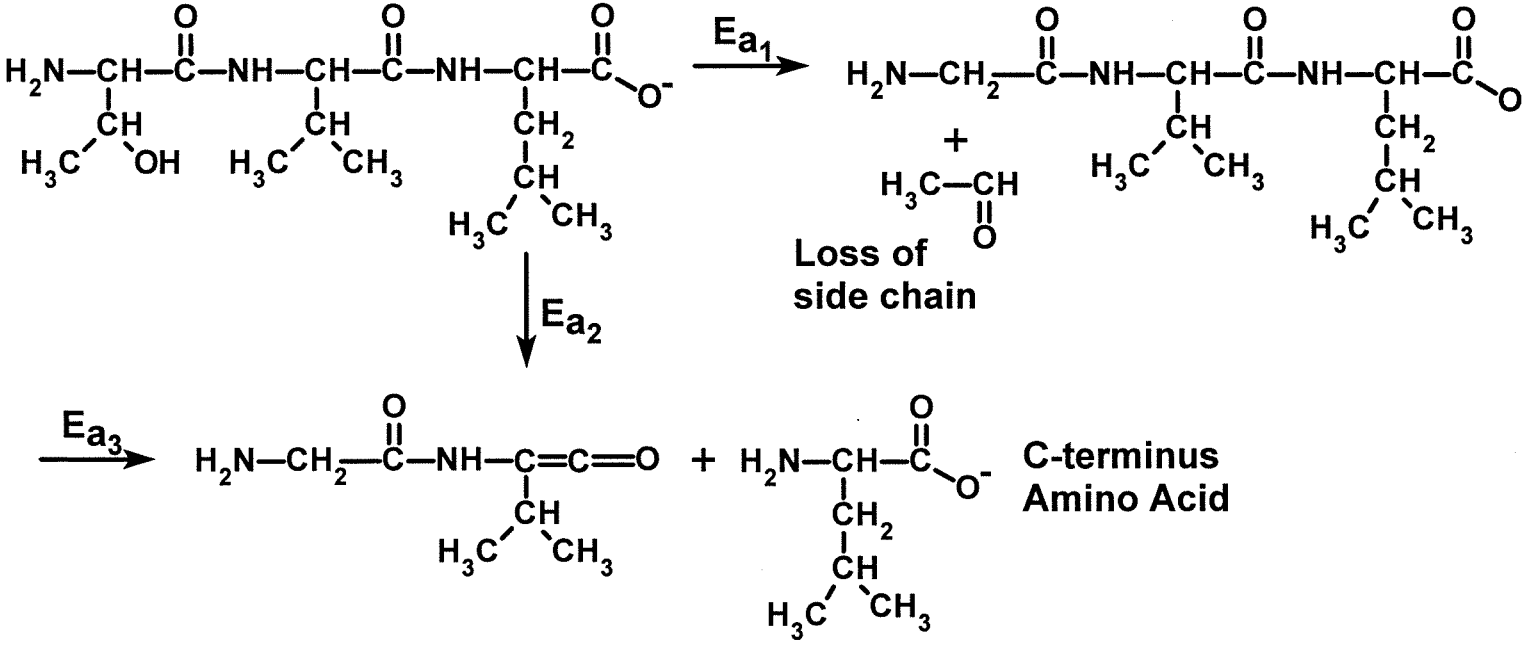

To rationalize the observed product distributions, it follows that:

$$E_{a_1} < E_{a_2} \cong E_{a_3}$$

Scheme 1

Figure 4-9. Comparison of the dissociation energetics of deprotonated peptides gly-gly-ile and thr-val-leu. Extent of dissociation observed with excitation time is shown for both peptides at an <Ecom>=1.64 eV against a static pressure of nitrogen gas.

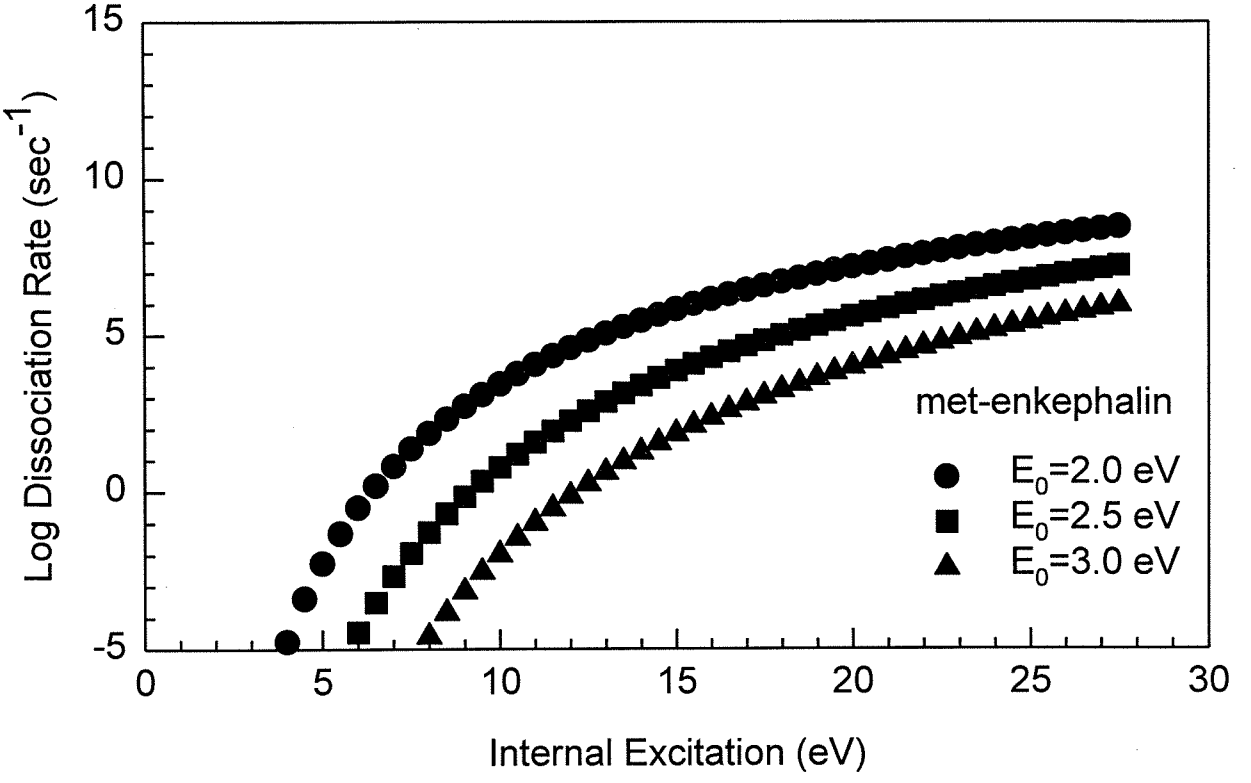
Log Dissociation Rate (sec^{-1})
15
10
5
0
-5
0
5
10
15
20
25
30
Internal Excitation (eV)
met-enkephalin
E_0=2.0 eV
E_0=2.5 eV
E_0=3.0 eV

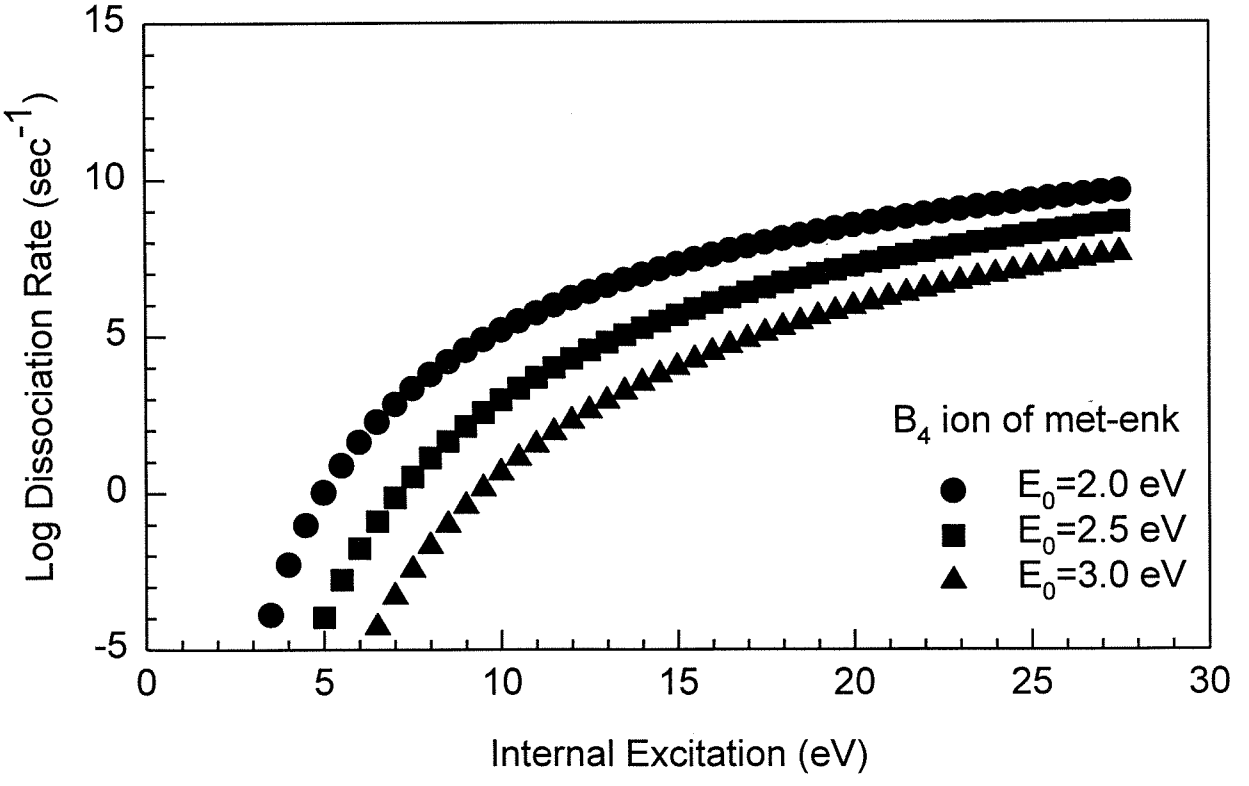
Log Dissociation Rate (sec^{-1})
15
10
5
0
-5
0
5
10
15
20
25
30
Internal Excitation (eV)
B_4 ion of met-enk
E_0=2.0 eV
E_0=2.5 eV
E_0=3.0 eV

an assumed activation energy of 2.5 eV, a dissociation rate of 10 sec^{-1} requires an internal energy of 10.0 eV (Figure 4-8). At 0.335 eV collision energy this corresponds to an average energy transfer of .11 eV or 33% of the average COM collision energy. It should be noted that this experiment was done with pulsed valves and, as a result, the pressure decreases over the course of the experiment. These numbers provide a lower estimate of the energy transfer. In addition, during the 3 seconds of activation, it is possible infrared radiative relaxation occurs. This would also imply a higher energy transfer efficiency. A similar calculation carried out for the dissociation of deprotonated gly-gly-ile in Chapter 3 yielded an average energy transfer of 55% per collision at 1.25 eV relative energy. In these calculations, it has been assumed that the initial internal ion energy is low and all of the internal energy must be supplied by collisions. As will be shown in the next chapter, the internal energy of these large molecules at room temperature, while high, contributes a small fraction of the energy required for dissociation at an appreciable rate.

A limited number of theoretical kinetic analyses of large molecule unimolecular dissociation (RRK, RRKM, and Arrenhius methods) have been published, and deserve some mention here. Schlag and Levine performed RRK analysis on large molecules with s (the number of degrees of freedom) up to 1000.[8] These calculations show that molecules with internal energies significantly above dissociation threshold still have a low average energy per vibrational mode. As a result, large internal energies are required to dissociate these molecules. However, because of the approximations required to perform RRK calculations, these calculations overestimate the amount of internal energy required for significant

dissociation rates compared to the RRKM results presented in this chapter. As a result they conclude that the energy requirements to induce observed fragmentation (specifically photoinduced dissociation) cannot be easily obtained in a mass spectrometer, and so there must be a "bottleneck" to statistical redistribution of energy among the internal modes. Our RRKM results do not support this idea; the amount of fragmentation observed can be accounted for using reasonable activation energies and collisional energy transfers.

Griffen and McAdoo have carried out RRKM calculations (using the Whitten-Rabinovitch approximations) on model peptide polymers.[9] They show that it takes more internal energy to induce dissociation as the size of the molecule (and hence number of degrees of freedom) increase. However, to avoid the "bottleneck" problem of Levine and Schlag, they chose low threshold energies for their reaction (0.1 to 1 eV). Given the inherent strength of the peptide bond, this choice of exceptionally low activation energies make these calculations less valuable, as the calculated rates at a given internal energy are too high. With their assumed activation energy, the "smaller" molecules chosen dissociate at rates of 10^{-10} sec-1 or higher, with the addition of energy corresponding to one 193 nm photon. One interesting observation is that at room temperature, when you add in the thermal energy of the molecule and the energy of 1 photon (193 nm), a plot of the calculated log(k) vs. assumed threshold energy yields a linear relationship. The slopes of the line depend on the number of internal degrees of freedom, and it is not entirely clear what this analysis means. Recently, Bernschtein and Oref have carried out RRKM calculations on large polymers.[10] Their results are very similar to those presented here. They point out that

the RRK calculations of Levine and Schlag overestimate the active degrees of freedom, and hence the internal energy required to dissociate the molecules at a given rate. They have shown that effective RRK and Arrenhius calculations can yield results which are in agreement with RRKM calculations. Their results predict that it is possible to explain the observed dissociation patterns in a mass spectrometer using RRKM theory.

Structural Determinations.

To enhance our understanding of the mechanisms and energetics of dissociation, geometry optimization and energy minimization of peptides was carried out using the Hyperchem program (Hypercube Inc.) suite. This was run on an IBM 486 DX66 computer in the Microsoft Windows environment. The usefulness of this methodology to substantiate likely gas phase structures and dissociation mechanisms has been shown in Chapter 2.

To carry out these calculations, structures are first built using the Hyperchem peptide library and AM1 or PM3 semi-empirical calculations are used to assign initial atomic charges. Simulated annealing with the molecular mechanics force fields is used to probe the probable low energy structures, and peptides were also user manipulated to structures of interest. These manipulations are necessary, for example, to probe the "folded" and "unfolded" structures of peptides. The structures are then optimized with molecular mechanics, typically using MM+ force fields for protonated peptides and AMBER force fields for deprotonated peptides. Final optimization of all structures of interest was carried out using semi-empirical methods, usually at the AM1 level, though similar results for deprotonated peptides

were obtained using PM3 as well. The AM1 model has been found to be a fast and accurate calculation method for ions as well as neutrals. It has been demonstrated to be able to accurately handle intramolecular hydrogen bond interactions.[11] Typical optimization of peptides of 5 amino acids or less require several hours for convergence.

PART II.

Introduction

Studies of the collision dynamics of large molecules in the gas phase have become more feasible as techniques applicable to these investigations have become more sophisticated. Understanding the dynamics of collisions of small inert neutral species with large ions is of fundamental importance, in part because collision induced dissociation is one or the potential methods for obtaining structural information about biological molecules. Until recently, the collisional activation of large molecules was considered to be an inherently inefficient process.[12] Recent experimental evidence has shown that the efficiency of energy conversion for low energy (<5 eV center of mass) collisions from translational to vibrational modes increases as the number of vibrational degrees of freedom of the molecule increase.[13] The efficiency of activation was shown to be a function of the collision energy and independent of collision gas for non-polar gases of various sizes. The enhanced activation efficiency was postulated to be due to the ability of the molecule to deform during the collision, absorbing large amounts of the collision energy.

Ion molecule collision trajectories calculations using molecular mechanics have been shown to support the high energy transfer efficiencies experimentally observed in the above experiments.[13] In addition, trajectory calculations of the collision of helium with peptides at high collision energies have been performed and shown to result in energy transfers in excess of 20 eV.[14] In this paper, further results of trajectory calculations of the collision processes for large molecules will be presented. The effect of energy, ion size, and collision partner have been

investigated. The calculations are consistent to a first approximation with a mechanism of energy transfer through a direct momentum transfer between the neutral collision partner and one atom of the large ion. However, the ability for a molecule to deform and absorb energy also affects the amount of energy transferred. It is shown that part of the increased efficiency of energy transfer as the size of the ion increases can be attributed to multiple interactions of the collision species with the ion.

Computational Methods

Trajectory calculations were run using molecular mechanics force fields (usually MM+) supplied with the Hyperchem program suite (Hypercube, Inc.) MM+, based on the MM2 method developed by Allinger[15], uses an exponential repulsion combined with an R^{-6} attraction to describe the Van der Waals interactions between molecules in addition to using atomic charges to compute electrostatic terms. These calculations are done on an atom by atom basis and no distance cutoffs were employed. Before running the trajectory calculations, the peptide and collision gas were separately optimized using the semi-empirical methods at the AM1 or PM3 level. This provided an initial geometry and charge distribution prior to carrying out the trajectory calculations. For convenience, the ion (peptide) is initially chosen to be at rest and the collision gas is assigned an initial velocity. For small peptides (4 amino acids or fewer) the simulations are usually run with step sizes of 1 femtosecond. Larger peptide simulations are run with step sizes of 0.1 femtoseconds. To determine the extent of collisional energy transfer, the final velocities of both the peptide and collision gas are monitored and used to calculate the final total kinetic

energy, from which the percent of energy transfer into internal modes is computed. To determine the average energy transfer into a molecule, many trajectories evenly sampling the target area of the peptide were run and the energy transfer efficiencies from all of these are averaged. For reported energy transfer estimates in this paper, typically a minimum of 20 collision trajectories were averaged. Running more trajectories did not significantly alter the average energy transfer efficiency observed.

Results

The results of a trajectory calculation of deprotonated gly-gly-ile and nitrogen at a relative energy of 1.25 eV is shown in Figure 4-10. In this particular trajectory the nitrogen approaches and interacts with the peptide, transferring 48% of the relative kinetic energy into internal modes, corresponding to an increase in internal energy of 0.14 kcal mol^{-1} per degree of freedom. Figure 4-11 shows the corresponding kinetic energy and velocity during the course of the trajectory and indicates at what corresponding point during the trajectory the corresponding snapshots shown in Figure 4-10 were taken. At 1.25 eV the observed "duration" of the collision is about 0.1 picoseconds (100 femtoseconds). This is similar to the timescale of a vibration and is indicative of an impulsive collision. On average, at this collision energy 41% of the collision energy is converted into internal modes, corresponding to a 0.12 kcal mol^{-1} increase per degree of freedom. For reference, RRKM calculations with an assumed activation energy of 2.5 eV indicate a requirement of 1 kcal mol^{-1} per degree of freedom to effect dissociation at a rate of 1 sec^{-1}.[16]

Figure 4-10. Snapshots of trajectory calculation of collision of deprotonated gly-gly-ile with nitrogen at 1.25 eV relative energy. The nitrogen interacts with the peptide, transferring 48% of the collision energy into internal modes.

1
2
3
4
5

Figure 4-11. Change in kinetic energy and velocity of nitrogen during a collision with deprotonated gly-gly-ile at 1.25 eV relative energy. The trajectory follows the path shown in Figure 4-10. In this particular trajectory 48% of the collision energy is transferred into internal modes.

Collision of deprotonated GGI with Nitrogen at 1.25 eV relative Energy

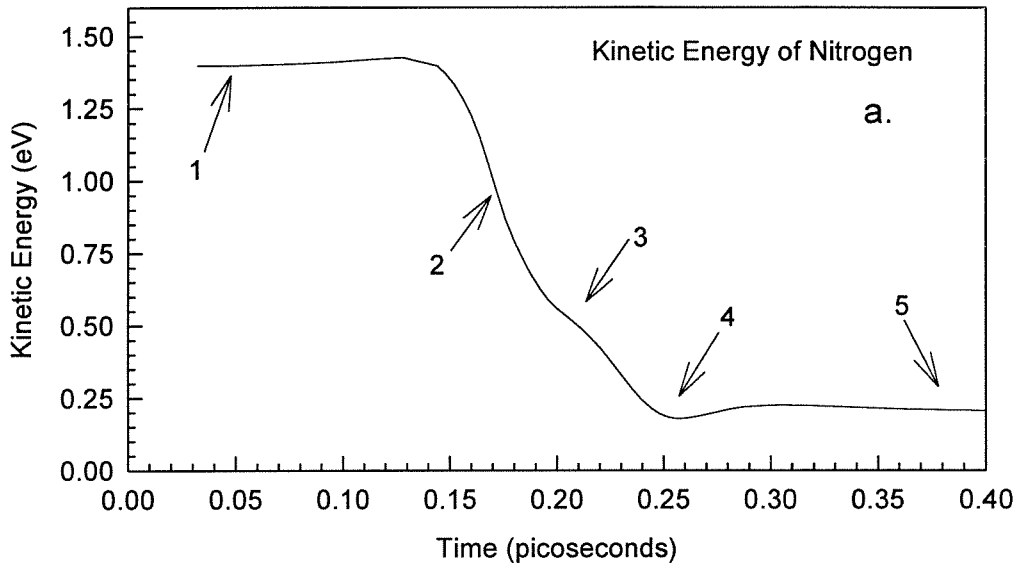

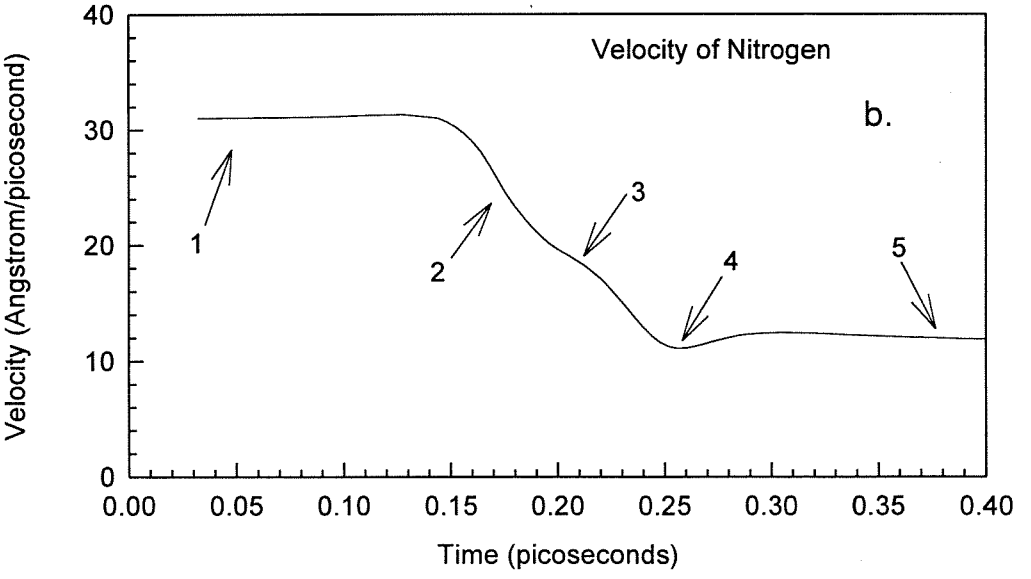

Figure 4-12 shows several snapshots of a representative collision of deprotonated gly-gly-ile with nitrogen at 12.5 eV relative energy. Nitrogen comes in and collides with the peptide, which undergoes extensive deformation during the collision. The post-collision snapshot of the molecule demonstrates the change in structure it has undergone during the collision. This particular trajectory results in transfer of 75% of the collision energy into internal modes; on average 60% of energy is calculated to be converted into internal modes at this collision energy, compared to 41% calculated at 1.25 eV. This demonstrates that the calculated percentage of energy transferred is a function not only of the size of the molecule, but that it is also a function of the collision energy.

Figure 4-13 shows the change in kinetic energy and velocity of the collision partners during the course of the Hyperchem trajectory for the collision of nitrogen with deprotonated gly-gly-ile at 12.5 eV. At 12.5 eV the collision lasts 50 femtoseconds, again indicative of an impulsive collision. In this case 75% of the internal energy is transferred into internal modes. Both of these trajectories follow the same path, reflected in the snapshots shown in Figure 4-12. This particular collision corresponds to 2.18 kcal mol^{-1} of energy transferred per degree of freedom. While this is enough to induce dissociation at a rate greater than 1 sec^{-1}, it should be noted that the molecular mechanics force fields used do not support the ability to dissociate the molecule.

Energy transfer efficiencies as a function of impact position with the ion determined from trajectory calculations of deprotonated ala-leu-ala-leu with nitrogen, argon and carbon dioxide at 1.25 eV, relative collision energy are shown in Figure 4-

Figure 4-12. Snapshots of a trajectory calculation of collision of deprotonated gly-gly-ile with nitrogen at 12.5 eV relative energy. In this particular collision 75% of the collision energy is transferred into internal modes. Note the extensive deformation of the molecule during and after the collision.

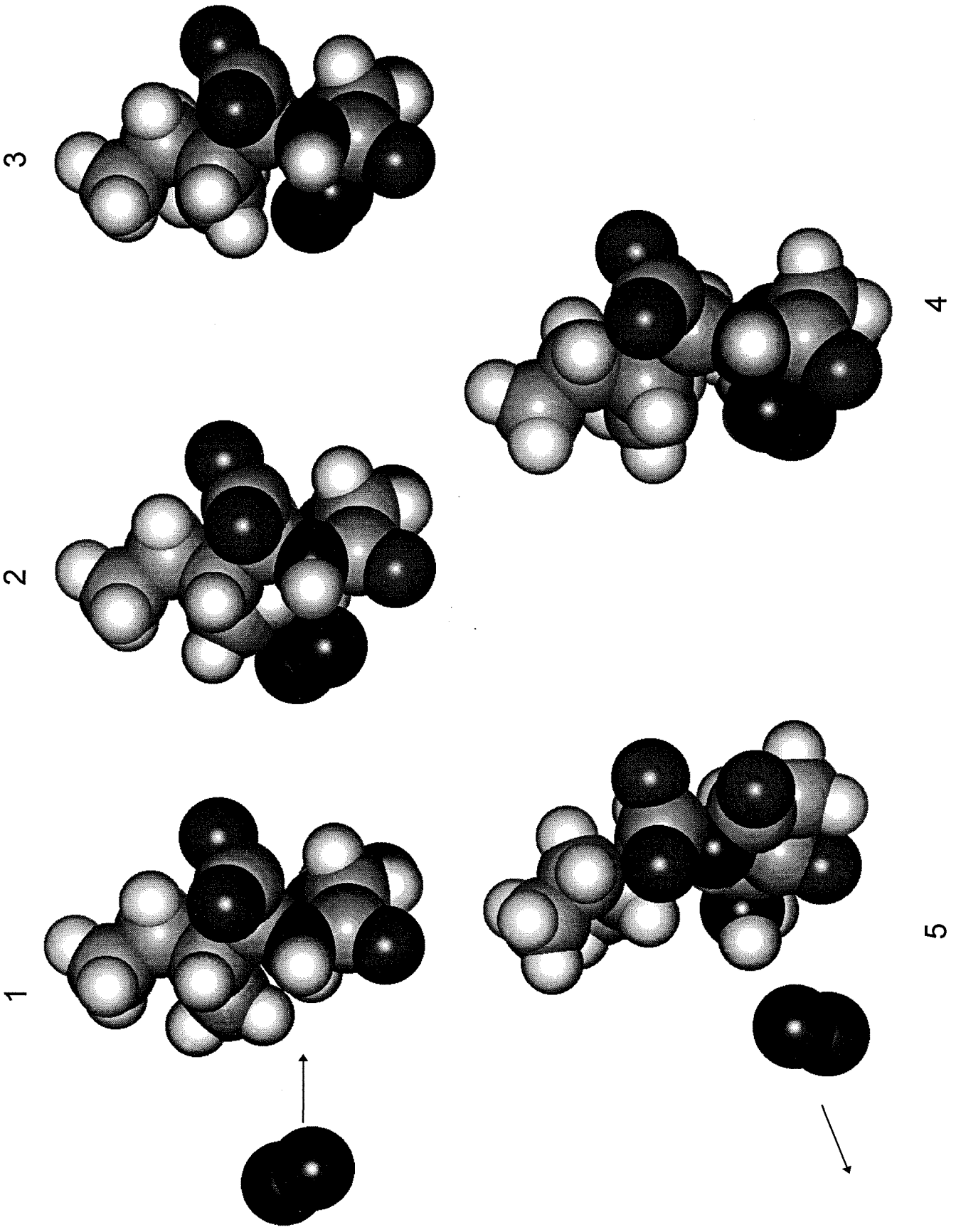
1
2
3
4
5

Figure 4-13. Change in kinetic energy and velocity of nitrogen during the collision with deprotonated gly-gly-ile at 12.5 eV relative energy. The trajectory follow the path shown in Figure 4-12. In this particular trajectory 75% of the collision energy is transferred into internal modes.

Collision of deprotonated GGI with Nitrogen at 12.5 eV relative Energy

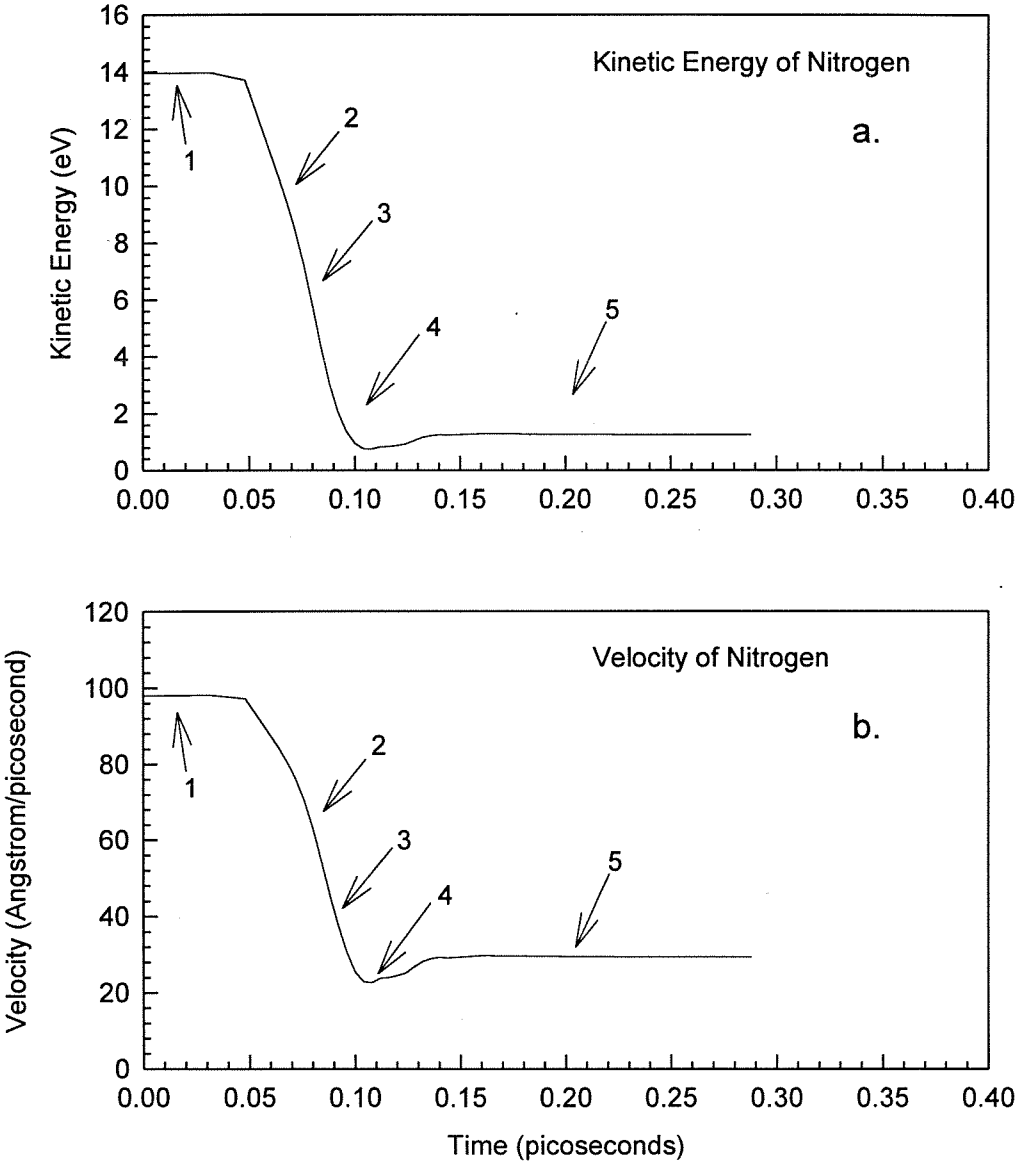

14. Trajectories were calculated for cuts along the x and y axis of one orientation of the molecule, as shown in Figure 4-14c. The amount of energy transferred depends on impact position, but does not depend on choice of collision gas for these non-polar collision gases. For this molecule at a collision energy of 1.25 eV an average of 57% of energy is transferred into internal modes (0.09 kcal mol^{-1} per degree of freedom), compared to 41% for deprotonated gly-gly-ile.

To investigate the extent to which it is possible to increase the collision energy and still effect efficient energy transfer, trajectory calculations of protonated bradykinin (a nonopeptide of molecular weight 1060.1, with 444 internal degrees of freedom) were carried out at 50 eV relative energy. Snapshots of bradykinin undergoing a collision with nitrogen at 50 eV relative energy are shown in Figure 4-15. The bradykinin was initially optimized with AM1, with the proton on an arginine side chain solvated by hydrogen bonds and effectively embedded within the molecule. In this trajectory the nitrogen comes in and undergoes multiple collisions with the bradykinin as it travels through the molecule, finally receding slowly away form the bradykinin after having transferred 96% of its energy into internal modes. This corresponds to an internal energy transfer of 2.5 kcal mol^{-1} per degree of freedom, which would induce dissociation at a rate of 1 sec^{-1} or greater. The extent of vibrational excitation and molecular deformation of the bradykinin resulting from the collision is apparent from the snapshots. This collision with the nitrogen traveling through the bradykinin is somewhat unique; the majority of collisions undergo impacts in which the nitrogen scatters backwards. However, at this collision energy,

Figure 4-14. Calculated energy transfer as a function of impact position for deprotonated ala-leu-ala-leu with a variety of collision gases (nitrogen, argon, carbon dioxide) at 1.25 eV. a. Collision trajectories along the y-axis. b. Collision trajectories along the x-axis. c. Orientation of ala-leu-ala-leu used for this calculation. Collision trajectories were calculated along each line across the molecule. The amount of energy transferred is dependent only on the impact position and not on choice of collision gas. On average, 57% of the relative energy is transferred into internal modes.

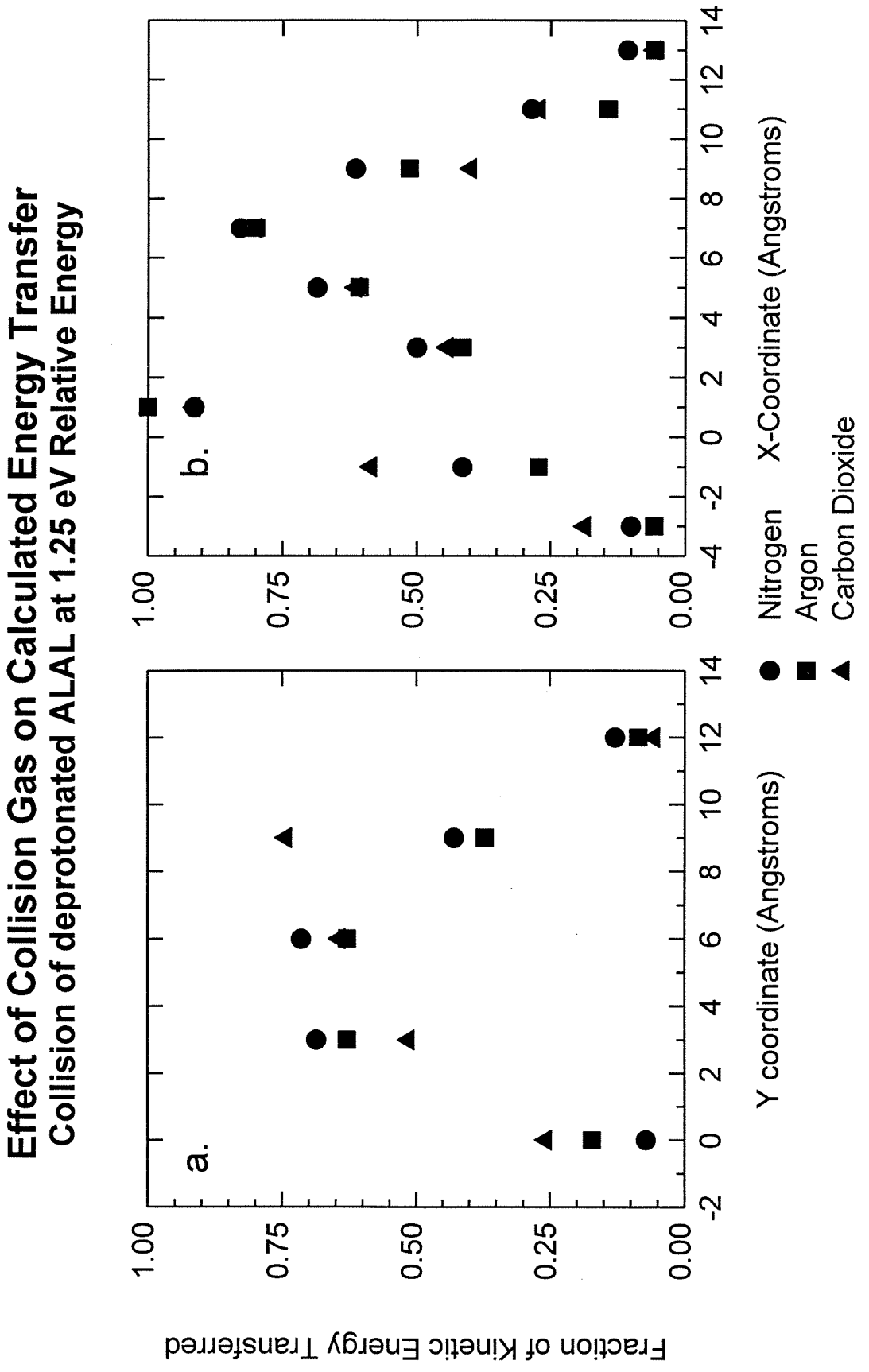
Effect of Collision Gas on Calculated Energy Transfer
Collision of deprotonated ALAL at 1.25 eV Relative Energy
Fraction of Kinetic Energy Transferred
a.
b.
1.00
0.75
0.50
0.25
0.00
-2
0
2
4
6
8
10
12
14
-4
Y coordinate (Angstroms)
X-Coordinate (Angstroms)
Nitrogen
Argon
Carbon Dioxide

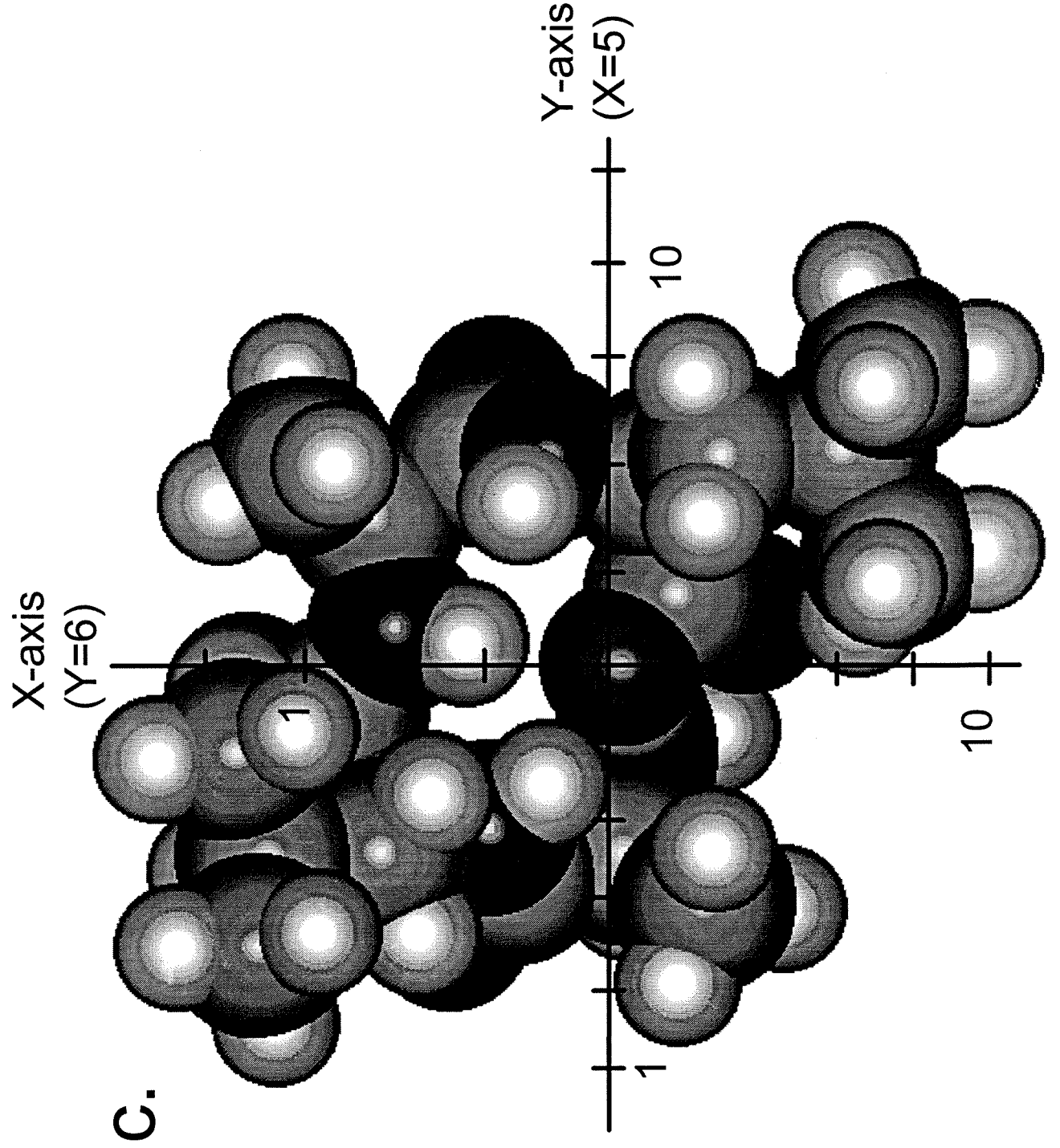
C.
X-axis
(Y=6)
1
10
Y-axis
(X=5)
1
10

Figure 4-15. Snapshots of trajectory calculation of protonated bradykinin (arg-pro-pro-gly-phe-ser-pro-arg, m/z=1061, s=444) colliding with Nitrogen at 50 eV relative energy. Nitrogen collides with the bradykinin, initially optimized with AM1, and travels through the peptide, undergoing multiple encounters before exiting the other side. This particular trajectory results in transfer of 96% of the relative kinetic energy into internal modes. Note the extensive change in structure of the bradykinin after the collision.

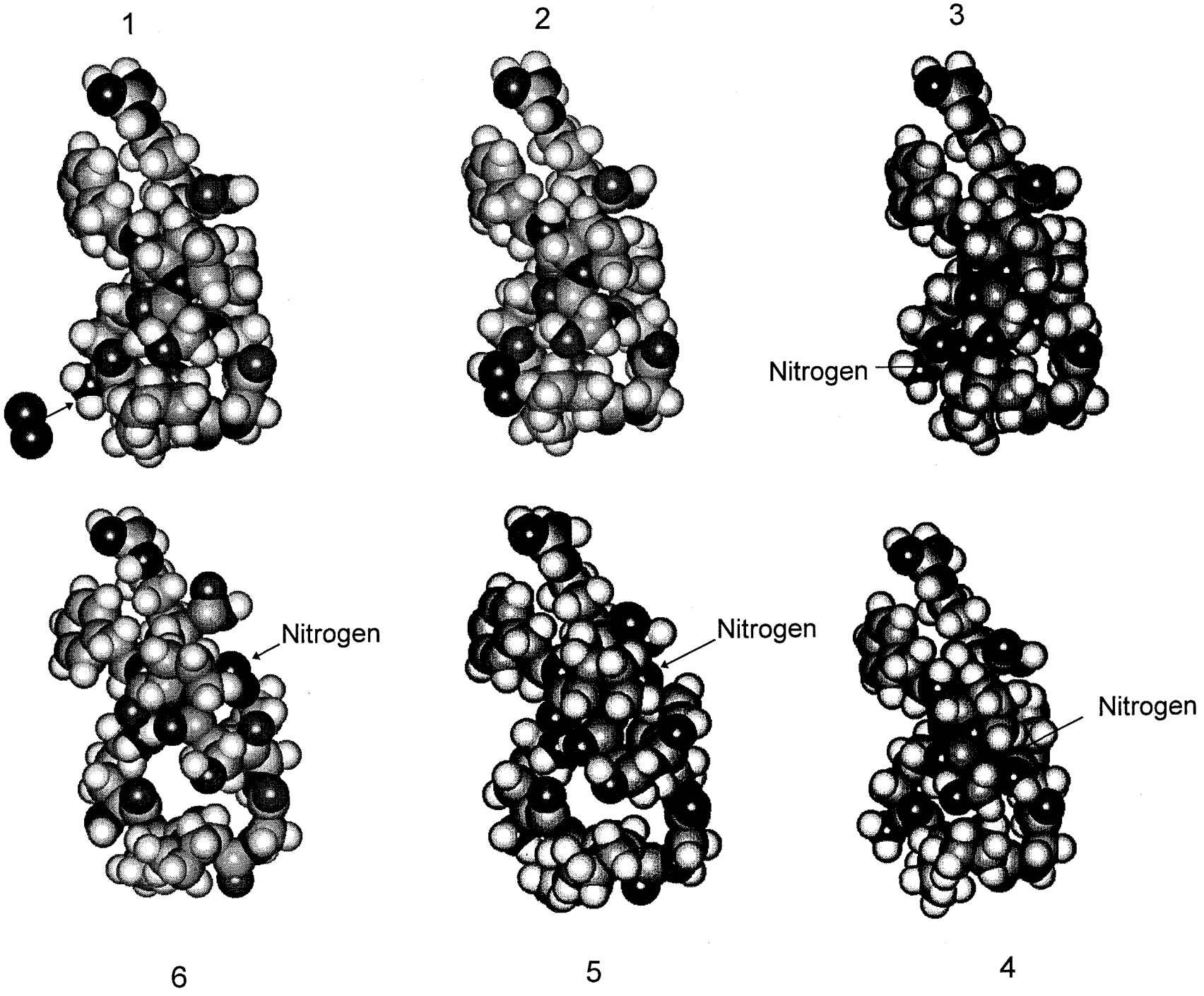
1
2
3
Nitrogen
Nitrogen
Nitrogen
Nitrogen
6
5
4

except for glancing collision which transfer small amounts of energy, most of the collisions result in greater than 90% energy conversion efficiency.

Figure 4-16 shows a plot of the velocities and kinetic energies of the nitrogen and bradykinin during and after the collision. The nitrogen undergoes multiple encounters with the bradykinin, each one resulting in a substantial percentage of energy transfer into internal modes. There are three distinct energy loss regions, each resulting in a loss of kinetic energy over a time of about 10-15 femtoseconds. The time spent between encounters varies depending on where the nitrogen is located within the molecule. After undergoing two encounters on the inside of the peptide (resulting in a loss of about 80% of the initial kinetic energy), the nitrogen is traveling much more slowly. It travels relatively unimpeded for about 75 femtoseconds (corresponding to a distance of 5.5 Angstroms) before undergoing a final collision with a phenylalanine side chain while leaving the molecule (snapshots 5 and 6, Figure 4-15) and losing most of its remaining kinetic energy. While such high energy collision conditions are currently experimentally unfeasible,[17] it is, however, interesting to note the predicted high efficiencies of energy conversion.

These observations imply that it may be possible to take advantage of the efficient energy transfer to deposit well defined amounts of high internal energy under single collision conditions. One proposed way to accomplish this is by excitation of a slow ion by a collision with a fast neutral.[18] However, the formation of an intense neutral beam of atoms with well defined energy is difficult. A commercially available FAB gun will supply a beam of atoms over about a 25 mm^2 area at a flux of about $1x10^{13}$ atoms/second. While this is a reasonably intense beam, it is designed to

Figure 4-16. Change in kinetic energy and velocity of nitrogen colliding with protonated bradykinin at 50 eV relative energy. The trajectory follows the path shown in Figure 4-15. The nitrogen undergoes multiple encounters with the bradykinin, each one transferring energy into internal modes of the peptide. In this particular trajectory, a total of 96% of the collision energy is transferred into internal modes.

Collision of protonated Bradykinin with Nitrogen at 50 eV relative Energy

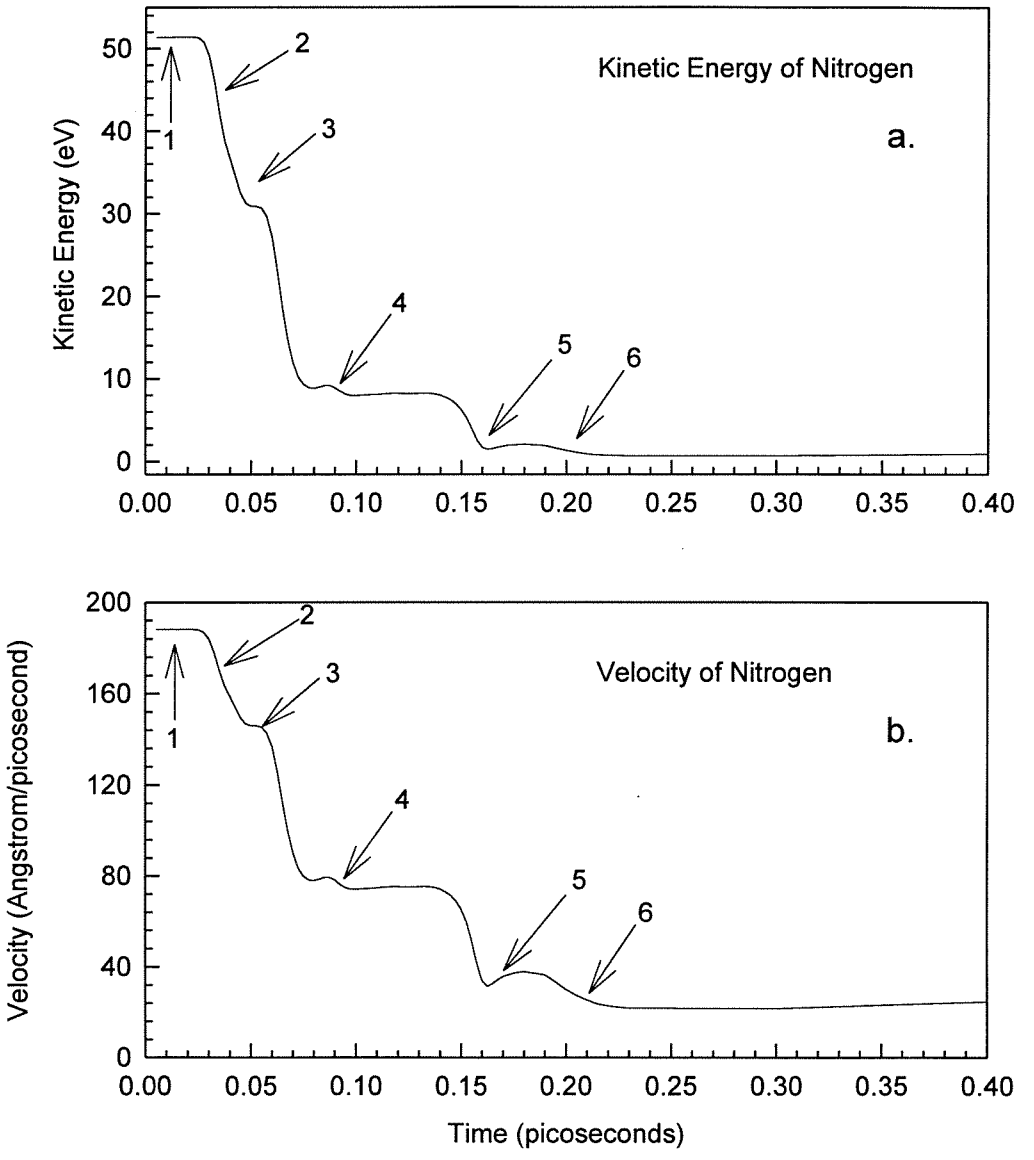

be supplied at several kilovolts, not one hundred volts. A more experimentally viable method would be to use a beam of ions. Trajectory calculations of Na^+ with peptides indicate this would also be a potentially efficient method for excitation. At low energies (<2 eV) collision of Na^+ with a protonated peptide show that the Na^+ is repelled by the charge on the peptide and reflects away from the molecule with little to no energy transfer. At high energies the trajectory calculations indicate that this coulomb repulsion can be overcome and large amounts of energy transferred into internal modes.

Trajectory calculations with protonated bradykinin colliding with Na^+ near the charge center at 50 eV relative energy result in large predicted energy transfers. Figure 4-17 shows snapshots of a collision, where the Na^+ collides with the molecule, with a resultant 96% of the energy transferred into internal modes. The initial Na^+ orientation and velocity is the same as that for Nitrogen in Figure 4-15. However, due to different interactions with the bradykinin, the Na^+ does not travel through the molecule, but ultimately rebounds, having lost most of its kinetic energy. Figure 4-18 shows the change in kinetic energy and velocity of the Na^+ during the trajectory. Again, similar to the collision with nitrogen, there are three distinct encounters of the Na^+ with the peptide. The initial loss of velocity is slow (40 femtoseconds) compared to the nitrogen encounter (Figure 4-16) and is due in part to the slowing down and deflection of the Na^+ by coulomb repulsion with the protonated site. The Na^+ is deflected away from the charge center and collides with other parts of the peptide, resulting in loss of a significant amount of its kinetic energy. An interesting point of this trajectory is that the Na^+ velocity increases after its initial encounters as it

Figure 4-17. Snapshots of a trajectory calculation of the ion-ion collision of Na^+ with protonated bradykinin at a relative energy of 50 eV. The Na^+ ion interacts strongly with the protonated bradykinin for a net energy transfer of 95% of kinetic energy into internal modes.

1
2
3
Sodium
4
Sodium
5
6

Figure 4-18. Change in kinetic energy and velocity of Na^+ colliding with protonated bradykinin at 50 eV relative energy. The trajectory of the Na^+ follows the path shown in Figure 4-17, undergoing multiple encounters with the bradykinin. In this particular trajectory 95% of the collision energy is transferred into internal modes.

Collision of protonated Bradykinin with Sodium at 50 eV relative Energy

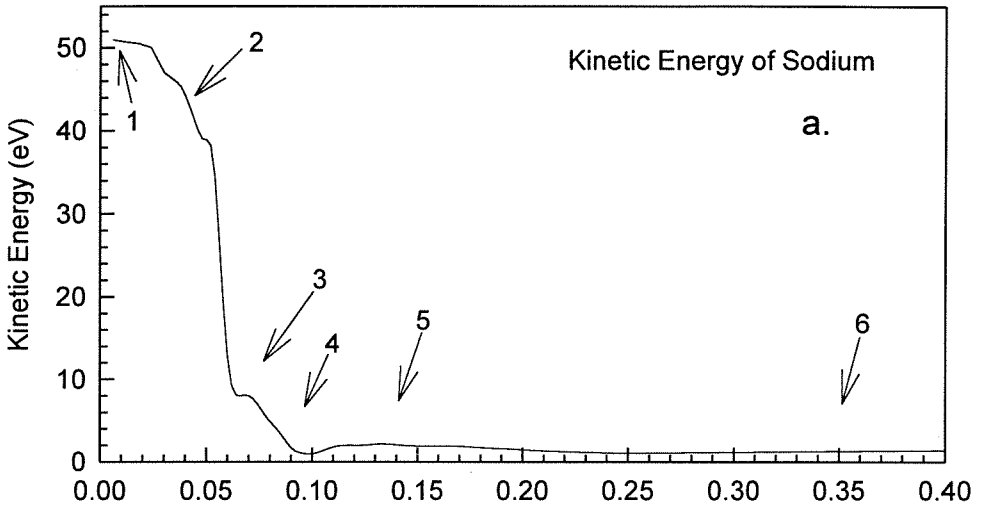

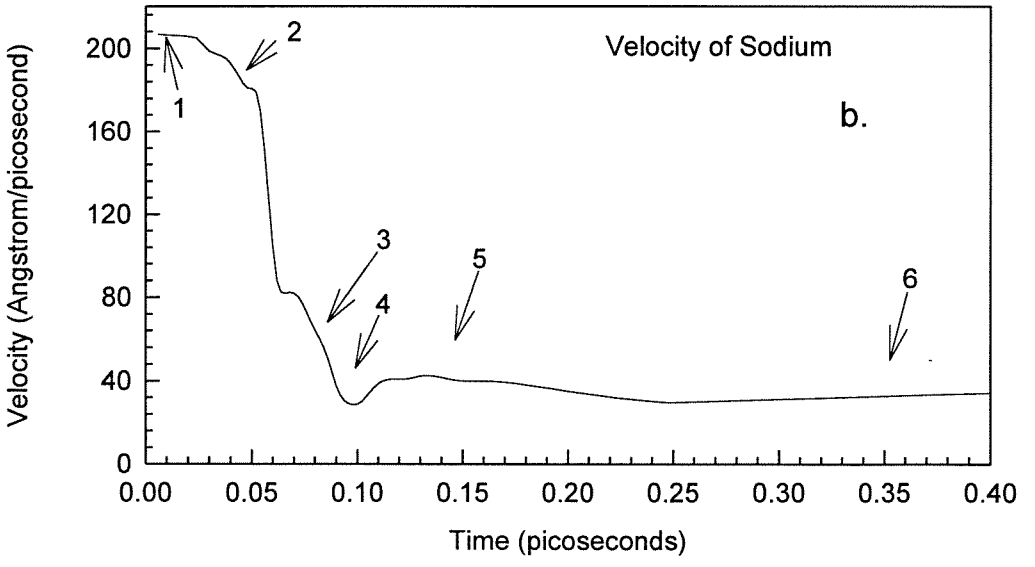

responds to the coulomb repulsion. It is still within the peptide at this point (Figure 4-18, snapshot 5) and undergoes one more encounter before exiting the molecule having lost most of its initial kinetic energy.

Discussion

These trajectory calculations demonstrate that the percentage of energy transfer into internal modes increases both as the size of the molecule increases and as the collision energy increases. This is in good agreement with experimental results.[13] The percentage of energy transfer is independent of collision gas for the non-polar gases (Figure 4-15), nitrogen, argon and carbon dioxide, also in good agreement with available experimental data.[13] The percentage of energy transferred is a function of impact position within the molecule.

The mechanism of collisional excitation has been proposed to occur by direct momentum transfer between colliding atoms.[19] To get a qualitative understanding of this process, the simplest case of two atoms undergoing a head on completely elastic collision conserving energy and momentum can be considered. One can solve these two equations to get the final velocities of the colliding partners given in Equation 9, assuming the atom in the ion is initially at rest. $v_i(final)$ is the final velocity of the atom in the ion, $v_g(final)$ is the final velocity of the collision gas atom, and v_g is the initial velocity of the collision gas.

$$v_i(final) = \frac{2m_g}{m_i + m_g} v_g$$
$$v_g(final) = \frac{m_g - m_i}{m_i + m_g} v_g \qquad (9)$$

In this instance, the energy transfer is predicted to be a strong function of the mass of the interacting atoms. When the masses of the colliding partners are equal, the first atom will hit the second atom and stop, transferring all of its energy to the second atom. If a heavier atom hits a lighter atom, for example if $3m_i=m_g$ (Argon) significantly less energy should be transferred. While the situation for molecules is obviously more complicated, the simplest case of an atom-atom impulsive collision resulting in energy transfer is supported by the trajectory calculations, which predict large amounts of energy transfer in collisions involving nitrogen. A maximum of 80% efficiency of translational energy is observed to be transferred into internal modes in single encounters. This would also explain the similar energy transfer efficiencies for nitrogen, carbon dioxide and cyclohexane which have been experimentally observed.[13]

The total amount of energy transfer is a strong function of internal degrees of freedom. The ability of a large molecule to convert collision energy into internal excitation is evident form watching a simulated trajectory. The large number of internal modes allow the ion to deform during the collision, and it acts as a compressible energy absorbing medium (see Figure 4-16, for example). In addition, as the peptide size increases, so does the possibility of multiple encounters of the collision species with the peptide in a single collision event, with each encounter resulting in a significant loss of internal energy. The impulsiveness of the collision would indicate that a collision at high energies along the periphery could result in atom stripping. In recent work by Fenselau and co-workers, it was observed that at relative collision energies of 15-25 eV, a small fraction of products corresponding to

loss of H_2 and capture of collision molecule were observed when methane was used as a collision gas.[20]

CONCLUSIONS

The utility of using molecular dynamics calculations to understand the dissociation of large molecules has been demonstrated. Estimates of energy transfer from trajectory calculations of ion molecule collisions are in good agreement with experimental data. The collisions appear to be impulsive in nature, and the energy transfer occurs on a timescale similar to a vibrational period. Trajectory calculations indicate the utility of using fast ions as a collision partner instead of a neutral gas to effect efficient energy transfer. This would provide a unique opportunity to generate large molecular ions with reasonable well defined internal energies, permitting study of the dynamics of the subsequent unimolecular dissociation processes.

APPENDIX 1

Ion-Molecule Collision Theory. The Shulz-Phelps Ion Gauge results in very accurate pressure measurements, from which collision rates can be calculated. The Langevin cross section, σ_L, for ion-molecule collisions is given by Equation 10, where b^* is the impact parameter, α is the polarizability of the collision gas, e is the electronic charge, and E_C is the collision energy.

$$\sigma_L = \pi (b^*)^2 = \pi \left(\frac{2\alpha e^2}{E_c} \right)^{1/2} \qquad (10)$$

Plugging in a value of α=1.76x10^{-24} cm^3 for the polarizability of nitrogen yields a collision cross section $\sigma \approx$ 2x10^{-14} cm^2 or 200 Angstroms^2. It should be noted that this provides a lower limit for a collision cross section for a peptide, which is physically larger than the small molecules to which these equations are usually considered valid. However, when considering the effect of size on collision cross section, the values of the impact parameters must be looked at in more detail. The impact parameter as a function of collision energy for a molecule-ion collision is given by Equation 11. A plot of this function is given in Figure 4-19. At typical collision energies employed in the off resonance collisional activation process, the corresponding impact parameter ranges from 2-3 Angstroms. This is significantly smaller than the size of the peptides studied. As a result trajectories that result in the collision gas passing close to the charge center will probably be deflected towards it slightly.

$$b^* = \left(\frac{2\alpha e^2}{E_c} \right)^{\frac{1}{4}} \qquad (11)$$

Figure 4-19. Calculated impact parameter as a function of collision energy for the collision of an ion with nitrogen.

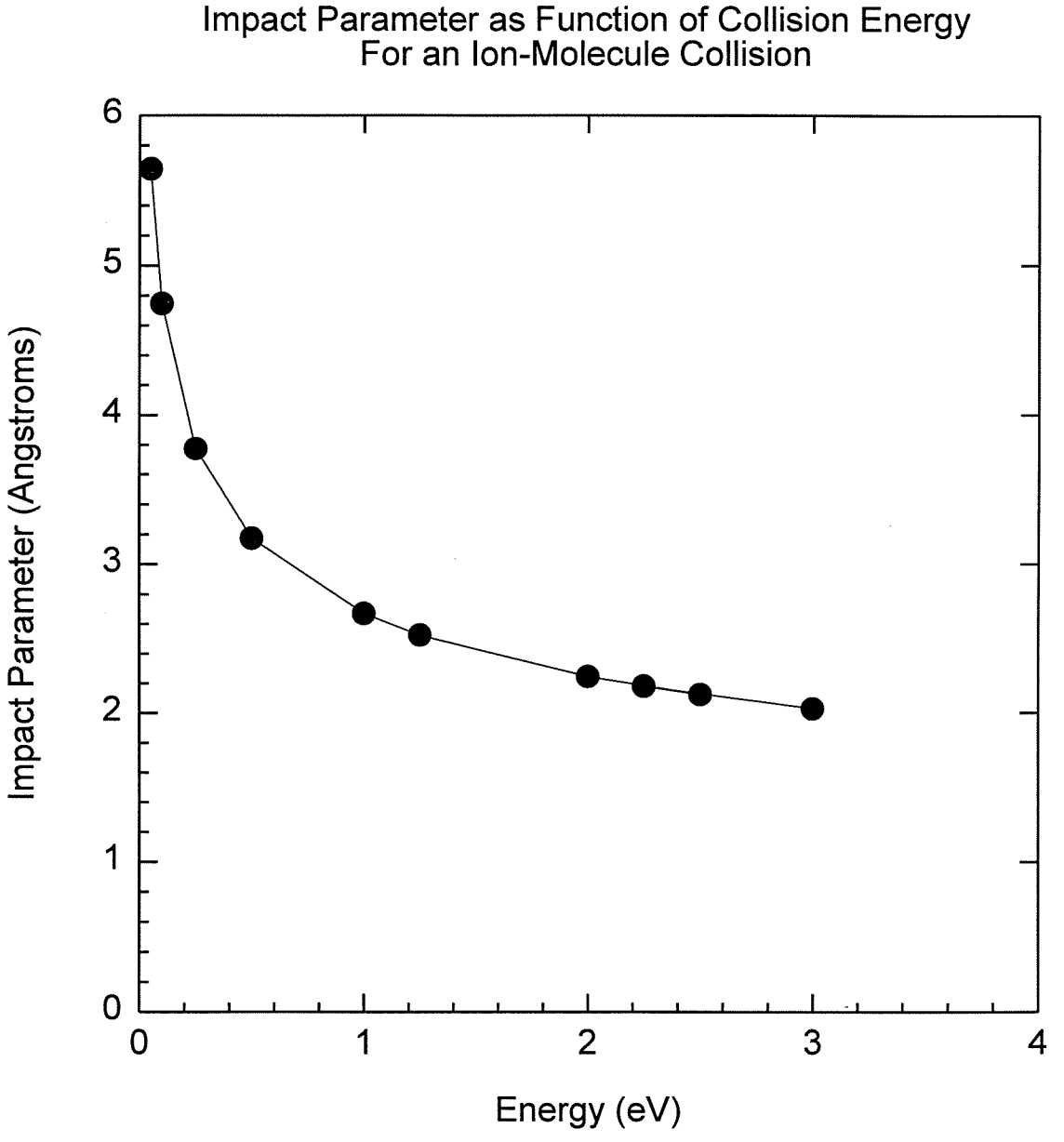
Impact Parameter as Function of Collision Energy
For an Ion-Molecule Collision
Impact Parameter (Angstroms)
Energy (eV)
0
1
2
3
4
5
6
0
1
2
3
4

Indeed, our calculations show that there is a well defined point, corresponding with the size of the molecule, at which point very little energy is transferred. As the size of the molecule increases, the collision cross section will increase; however, the ability of these molecules to fold up and form internal hydrogen bonds results in compact structures, and this effect will not directly scale with the number of atoms. For peptides with five or fewer amino acids, the cross section estimate given by Equation 10 appears to be a good value.

The collision rate, which is independent of collision energy, is given by Equation 12, where μ is the reduced mass of the colliding products.

$$k = \left(\frac{4\pi^2 \alpha e^2}{\mu}\right)^{1/2} \qquad (12)$$

Plugging in values of μ=26.70 AMU (1.66×10^{-24} g/AMU) for met-enkephalin colliding with nitrogen, the above polarizability and using cgs units ($e=4.8 \times 10^{-10}$ esu) yields a collision rate of 6.0×10^{-10} cm^3 $molec^{-1}$ sec^{-1}, comparable to the "typical" gas kinetic collision rate of 1×10^{-9} cm^3 $molec^{-1}$ sec^{-1}, which is used in all collision rate calculations. Using n/V=P/RT, one can calculate that a pressure of 2×10^{-7} torr=6.5×10^9 molecules/cm^3. To simplify this to a usable expression, values of R=.08206 l-atm $mole^{-1}$ K^{-1}, $N_a=6.02 \times 10^{23}$ molecules $mole^{-1}$, T=300 K, 1 liter = 1000 cm^3, and 760 torr/atm are plugged in to yield the expression shown in Equation 13 where P is in Pressure and n/V has units of molecules cm^{-3}.

$$\frac{n}{V} = 3.218 \times 10^{16} * P(torr) \qquad (13)$$

For reference, a pressure of $1x10^{-6}$ torr corresponds to $3.2x10^{10}$ molecules cm^{-3} and a collision rate of 32 collisions sec^{-1}. A pressure of $2x10^{-7}$ torr corresponds to 6.5 collisions sec^{-1}.

REFERENCES

[1] For more details about statistical calculations see, for example, Seinfeld, J.I.; Francisco, J.S.; Hase, W.L. *Chemical Kinetics and Dynamics.* Prentice Hall: New Jersey, 1989, Chapter 11.

[2] Whitten, G.Z.; Ravinovitch, B.S. *J. Chem. Phys.* **1963**, 38, 2466-2473.

[3] A copy of this program is available from the authors on request. It requires an IBM compatible computer with Windows 3.1 and a math co-processor.

[4] For large molecules undergoing a small structural change of one bond dissociation, this is a very reasonable assumption.

[5] The frequency factor is given by $\frac{ek_bT}{h}\frac{Q_v^{\neq}}{Q_v}$ and can be calculated from the vibrational partition functions for the reactant and activated complex.

[6] The programs used (entitled UNIMOL) are associated with the text by Gilbert, R.G. and Smith, S.C. Theory of Unimolecular and Recombination Reactions. Blackwell Scientific Publications: Oxford, 1990.

[7] Benson, S; O'Neal, E. *Kinetic Data on Gas Phase Unimolecular Reactions* (1970).

[8] Shlag, E.W.; Levine, R.D. *Chem. Phys. Letters*, **1989**, 163, 523-530.

[9] Griffen, L.; McAdoo, D. *J. Am. Soc. Mass Spectrom.* **1992**, 4, 11-15.

[10] Bernshtein, V.; Oref, I. *J. Phys. Chem.* **1994**, 98, 136-140.

[11] (a) Dewar, M.J.S.; Zoebisch, E.G.; Healy, E.F.; Stewart, J.J.P. *J. Am. Chem. Soc.*, **1985**, 107, 3902-3909. (b) Dewar, M.J.S.; Dieter, K.M. *J. Am. Chem. Soc.*, **1986**, 8075-8086.

[12] (a) Alexander, A.J.; Boyd, R.K. *Int. J. Mass Spectrom. Ion Processes.* **1989**, 90, 211-240. (b) Alexander, A.J.; Thibault, P.; Boyd, R.K.; Curtis, J.M.; Rinehart, K.L. *Int. J. Mass Spectrum. Ion Processes.* **1990**, 98, 107-134.

[13] Marzluff, E.M.; Campbell, S.; Rodgers, M.T.; Beauchamp, J.L. *J. Am. Chem Soc.* **1994**, 116, 6947-6948.

[14] Gilbert, R.G.; Sheil, M.M.; Derrick, P.J. *Org. Mass Spectrom.* **1985**, 20, 430-431.

[15] Allinger, N.L. *J. Am. Chem. Soc.*, **1977**, 99, 8127.

[16] For "large" molecules (50 or more degrees of freedom) undergoing unimolecular dissociation at a rate of 1 sec^{-1} with an activation energy of 2.5 eV and frequency factor of 2x1013, an internal energy of 1 kcal mol-1 can be used to obatin an idea of the energy requirements for dissociation.

[17] Dissociation kinetics of 1-10 sec^{-1} are easily detected using FT-ICR techniques; however, inducing collisions of large molecules at greater than 10 eV relative energy is experimentally difficult. While such collisions are possible in a sector instrument, much higher dissociation rates are required to observe product formation.

[18] Turecek, F. *Rapid Comm. Mass Spectrom.* **1991**, 5, 78.

[19] (a) Uggerud, E.; Derrick, P.J. *J. Phys. Chem.*, **1991**, 95, 1430-1436. (b) Bradley, C.D.; Curtis, J.M.; Derrick, P.J.; Shell, M.M. *J. Chem. Soc. Faraday Trans.* **1994**, 90, 239-247. (c) Uggerud, E.; Derrick, P. *Z. Narurforsch*, **1989**, 44a, 245.

[20] Cheng, X.; Fenselau, C. J. Am. Chem. Soc., 1993, 115, 10327-10333.

Chapter 5

Kinetic Modeling of the Collisional Activation Process

The previous three chapters have used results from RRKM calculations and Hyperchem molecular dynamics simulations to understand the unimolecular dissociation and collisional energy transfer processes of large molecules. In the cases considered the dissociation rates and activation energies were estimated using knowledge about similar chemical systems. In this chapter, an attempt will be made to analyze the unimolecular dissociation dynamics more quantitatively by using a master equation analysis to calculate the internal energy distribution of the ion population as a function of time during the off resonance collisional activation process, taking into account all of the processes which can add or remove energy from the stored ion population, including radiative relaxation. The dissociation of deprotonated gly-gly-ile to yield the deprotonated C-terminus amino acid will be used as the model process, as this compound has been experimentally and theoretically investigated in prior chapters.

RRKM analysis of deprotonated gly-gly-ile. The dissociation mechanism of deprotonated gly-gly-ile to give the C-terminus amino acid (discussed in more detail in Chapter 2) is shown in Scheme 1. Gly-gly-ile is a tripeptide with 35 atoms and 99 degrees of freedom. The assumed vibrational frequencies for the reactant and activated complex used to calculate the unimolecular dissociation rate constant as a function of energy are given in Table 1. The ability of an RRKM analysis to adequately describe the dissociation energetics of large molecules is supported by its ability to qualitatively explain our dissociation results (see Chapter 3 and 4). For reference, RRKM curves for the dissociation of gly-gly-ile as a function of activation energy are shown in Figure 5-1. The assumed activation energies were chosen to lie

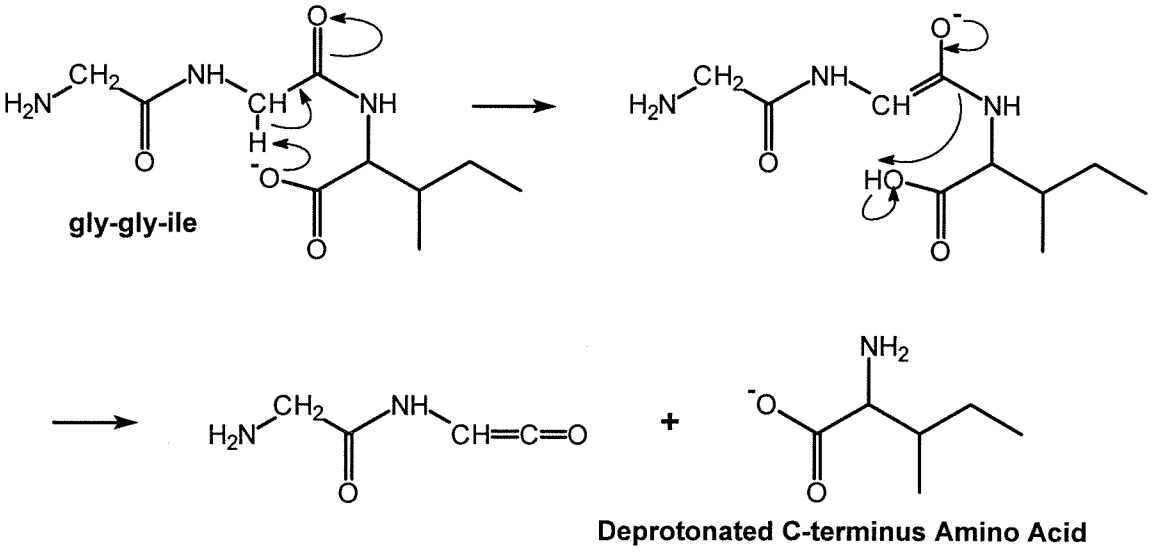

Scheme 1

Table 1. Frequencies (cm^{-1}) assumed for the dissociation reaction of deprotonated gly-gly-ile to give the deprotonated C-terminus amino acid.

Reactant Molecule/99 total active modes		Transition State/98 total active modes	
Frequency	Degeneracy	Frequency	Degeneracy
1610	1	1200	1
1400	1	900	1
1680	2	1400	1
3400	2	1500	1
3500	2	1580	1
2800	14	1680	1
1150	4	3400	1
1200	3	2800	13
1300	2	1150	3
1150	3	1200	3
720	3	1300	2
1380	2	1150	3
1400	7	720	2
1600	2	1380	2
1550	3	1400	6
600	48	1600	2
		1550	3
		3500	2
		600	50
Total:	99	Total:	98

Figure 5-1. RRKM curves for the unimolecular dissociation of gly-gly-ile as a function of threshold energy. Curves were calculated using the Whitten Rabinovitch approximation assuming a dissociation mechanism shown in Scheme 1, with vibrational frequencies given in Table 1.

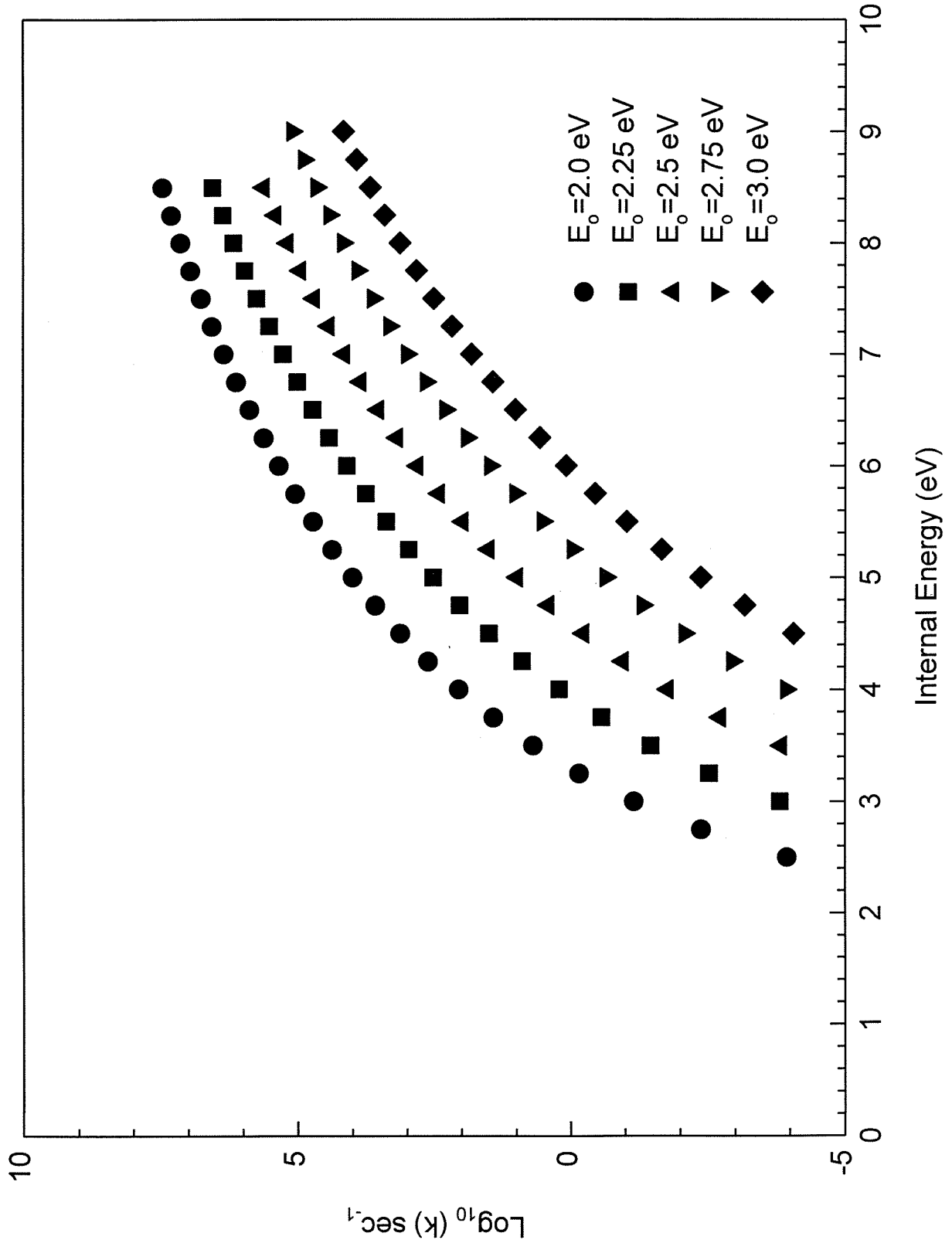
Log10 (k) sec-1
10
5
0
-5
0
1
2
3
4
5
6
7
8
9
10
Internal Energy (eV)
Eo=2.0 eV
Eo=2.25 eV
Eo=2.5 eV
Eo=2.75 eV
Eo=3.0 eV

between 2.0 and 3.0 eV. The upper limit is based on thermochemical data available for dissociation of acetamide, which undergoes a non charge assisted four-center elimination reaction with a $\log_{10}A=13.0$ and $E_o=68$ kcal mol^{-1} (2.9 eV),[1] and the lower limit is slightly above the estimated reaction endothermicity of 1.7 eV.[2] All of the analysis in previous chapters averaged these values and used an assumed activation energy of 2.5 eV to explain observed product distributions and activation efficiencies. For reference, at this energy an internal energy of 5.0 eV is required for dissociation at a rate of 10 sec^{-1}.

Correlation of Internal Energy with Temperature. In prior analysis the thermal energy of the molecule has been neglected. The internal energy of the molecule as a function of temperature can be calculated assuming a canonical ensemble of oscillators each with a temperature T_v. The internal energy can then be related to temperature by Equation 1, where T_v is the temperature and Q is the partition function.

$$E = RT_v^2 \frac{\partial \ln Q}{\partial T_v} \qquad (1)$$

For computational purposes, the partition function is assumed to be given by the vibrational partition function. This is given by Equation 2 for an ensemble of i oscillators each with an associated frequency ν_i. In this expression the zero of energy is taken to be the zero point energy (ZPE) of the molecule. For reference, the deprotonated peptide gly-gly-ile has a calculated ZPE of 7.7 eV.

$$Q = \prod_i q_{v_i} \text{ where } q_{v_i} = \frac{1}{1 - e^{-h\nu_i/kT}} \qquad (2)$$

By taking the derivative of this expression and simplifying, we can rewrite Equation 1 into a more usable form, shown in Equation 3.

$$E = \sum_i \frac{h c \bar{\nu}_i}{e^{\frac{h c \bar{\nu}_i}{kT}} - 1} \qquad (3)$$

Plugging in the assumed oscillator frequencies for the reactant molecule of deprotonated gly-gly-ile given in Table 1, this expression yields a calculated internal energy at 300 K (room temperature) of 0.23 eV. This is a small fraction (≈5%) of the internal energy required to dissociate this molecule at a rate of 1-10 sec^{-1}.[3] As the molecules of interest get larger, the internal energies of these molecules at room temperature can become quite high. However, this energy is typically a small fraction of the total energy required for dissociation. At room temperature only the low energy modes are significantly populated. A good rule of thumb for estimating the internal energy of a large biological molecule (three amino acids or more) at room temperature is to assume an average contribution towards the internal energy of 0.07 kcal mol^{-1} for each degree of freedom in the molecule.

Using Equation 3, the "temperature" of the molecule as a function of internal energy can be calculated. Figure 5-2 shows this for deprotonated gly-gly-ile. It is noteworthy to observe that an internal energy of 5.0 eV corresponds to a temperature of 1125 degrees Kelvin. This implies that the dissociation of these molecules requires very high internal temperatures. Using the parameters given in Table 1 for deprotonated gly-gly-ile, the frequency factor for the reaction at room temperature is

Figure 5-2. Calculated internal energy as a function of temperature for deprotonated gly-gly-ile.

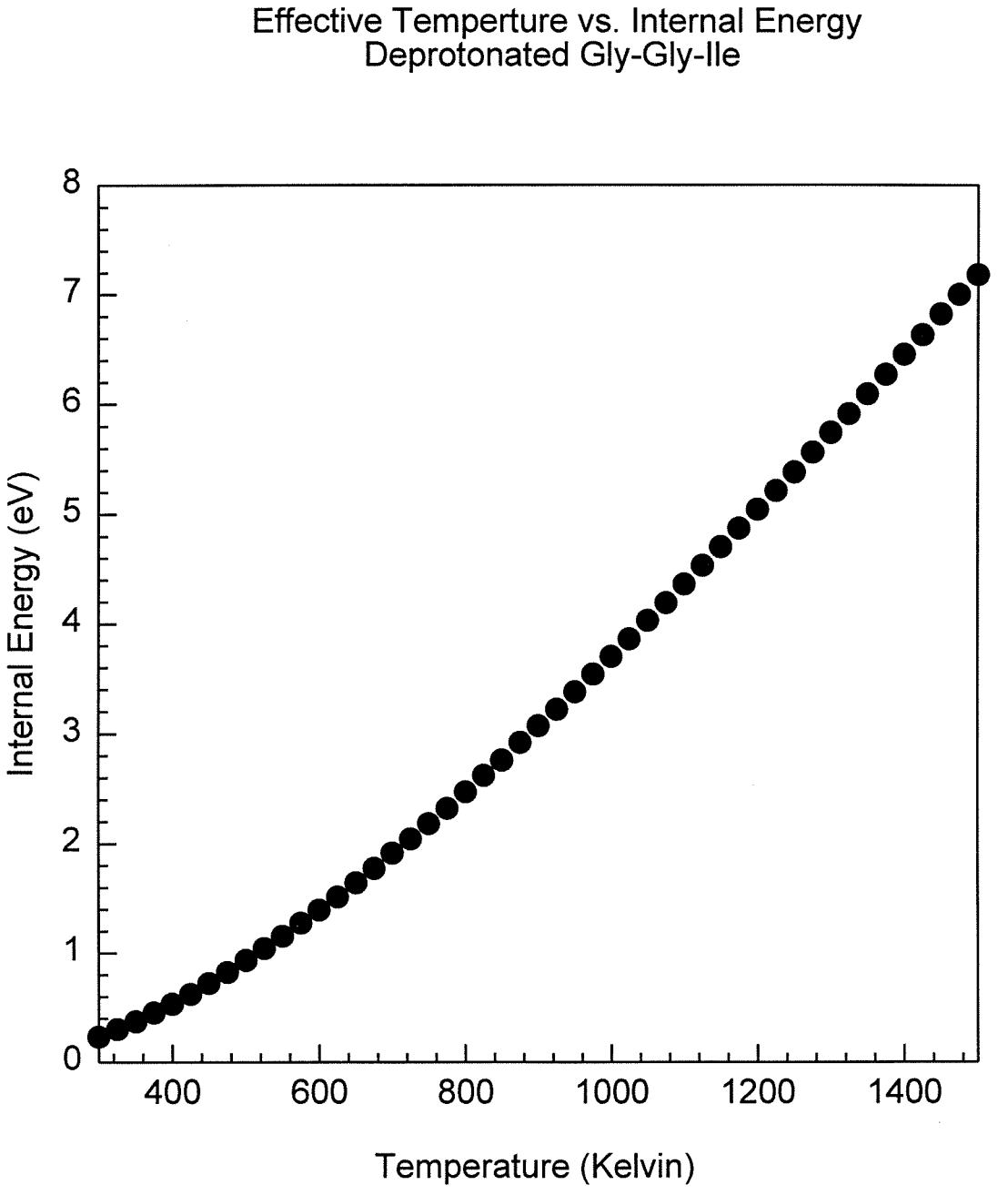
Effective Temperture vs. Internal Energy
Deprotonated Gly-Gly-Ile
Internal Energy (eV)
0
1
2
3
4
5
6
7
8
400
600
800
1000
1200
1400
Temperature (Kelvin)

calculated to be 1.3×10^{13} sec^{-1}. This is a typical value for a transition state which is not unduly constrained.

The extent of fragment formation observed in the collisional dissociation of deprotonated gly-gly-ile as a function of time at five different collision energies is shown in Figure 5-3. The time required to obtain 50% dissociation for each of the collision energies is also shown. The collision energies vary from 0.94 to 1.36 eV center of mass (COM), and activation was carried out against a static pressure of nitrogen at 2×10^{-7} torr (6.5 collisions sec^{-1}). The excitation energy was changed by varying the amplitude of the applied radio frequency (rf) excitation. At all energies a significant amount (≈15-20%) of dissociation is observed at sufficiently short time to be attributed to a single collision event.

In a naive attempt to determine the activation energy of the dissociation process directly from this data, an attempt was made to analyze the dissociation energetics assuming that at long times each collision energy corresponded to an effective internal temperature of the molecule. If each excitation energy corresponded to a temperature, then a plot of ln$k$ vs. $1/\langle E_{com} \rangle$ (see Equation 4) should give a line with a slope related to E_o. This analysis has been applied to the time dependent data shown in Figure 5-3. Figure 5-4 shows plots ln[gly-gly-ile] vs. time for the data in Figure 5-3, assuming a fist order rate of dissociation. A plot of ln[k] versus $1/\langle E_{com} \rangle$ is shown in Figure 5-5 and yields a straight line with a slope of -6.89. The difficult part of this analysis is assigning a meaning to the slope of that line. Even if each energy corresponded to a temperature, it is unclear if such a dependence would be

Figure 5-3. The extent of deprotonated C-terminus amino acid formation as a function of time for off resonance excitation of deprotonated gly-gly-ile at various collision energies. The collision gas was nitrogen at a pressure of $2x10^{-7}$ torr (6.5 collisions sec^{-1}). The amount of time to induce 50% dissociation for each energy is marked.

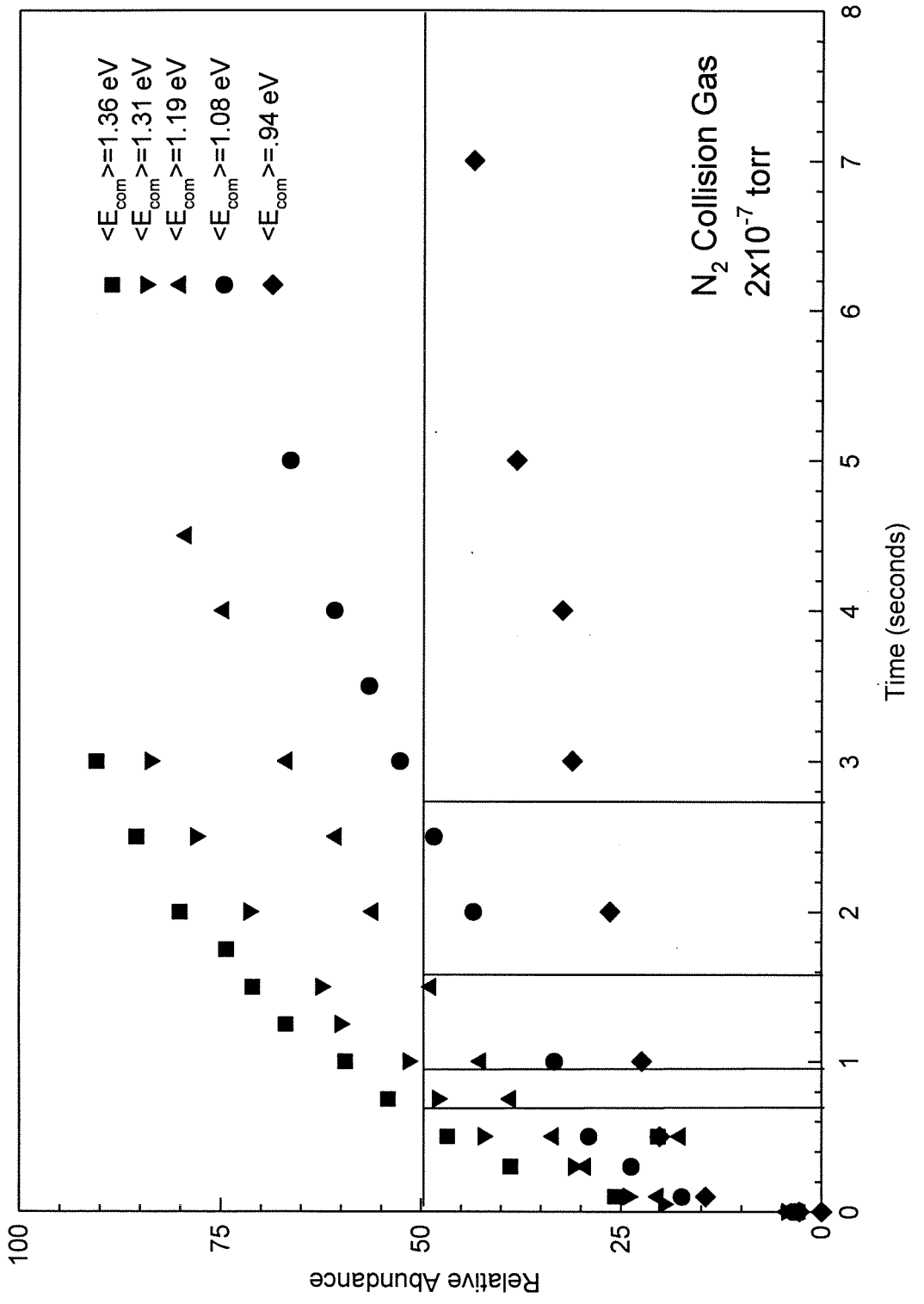
$<E_{com}>$=1.36 eV
$<E_{com}>$=1.31 eV
$<E_{com}>$=1.19 eV
$<E_{com}>$=1.08 eV
$<E_{com}>$=.94 eV
N_2 Collision Gas
$2x10^{-7}$ torr
Relative Abundance
Time (seconds)
0
25
50
75
100
0
1
2
3
4
5
6
7
8

Figure 5-4. Analysis of rate of dissociation of the deprotonated gly-gly-ile as a function of time for each collision energy shown in Figure 5-3.

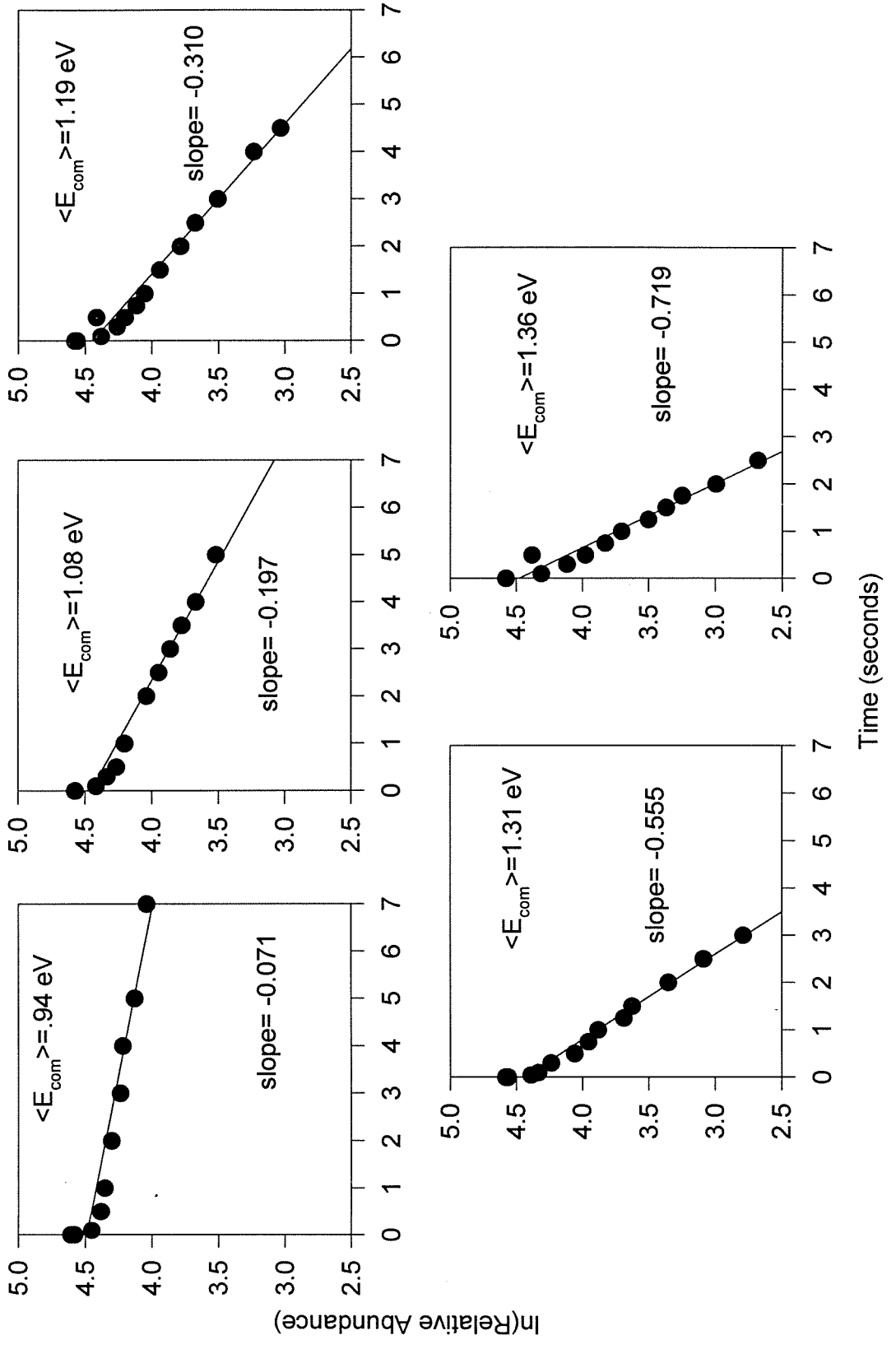
ln(Relative Abundance)
Time (seconds)
<E_com>=.94 eV
slope= -0.071
<E_com>=1.08 eV
slope= -0.197
<E_com>=1.19 eV
slope= -0.310
<E_com>=1.31 eV
slope= -0.555
<E_com>=1.36 eV
slope= -0.719

Figure 5-5. A plot of *ln*(dissociation rates) obtained from the data shown in Figure 5-4 as a function of *1/E*.

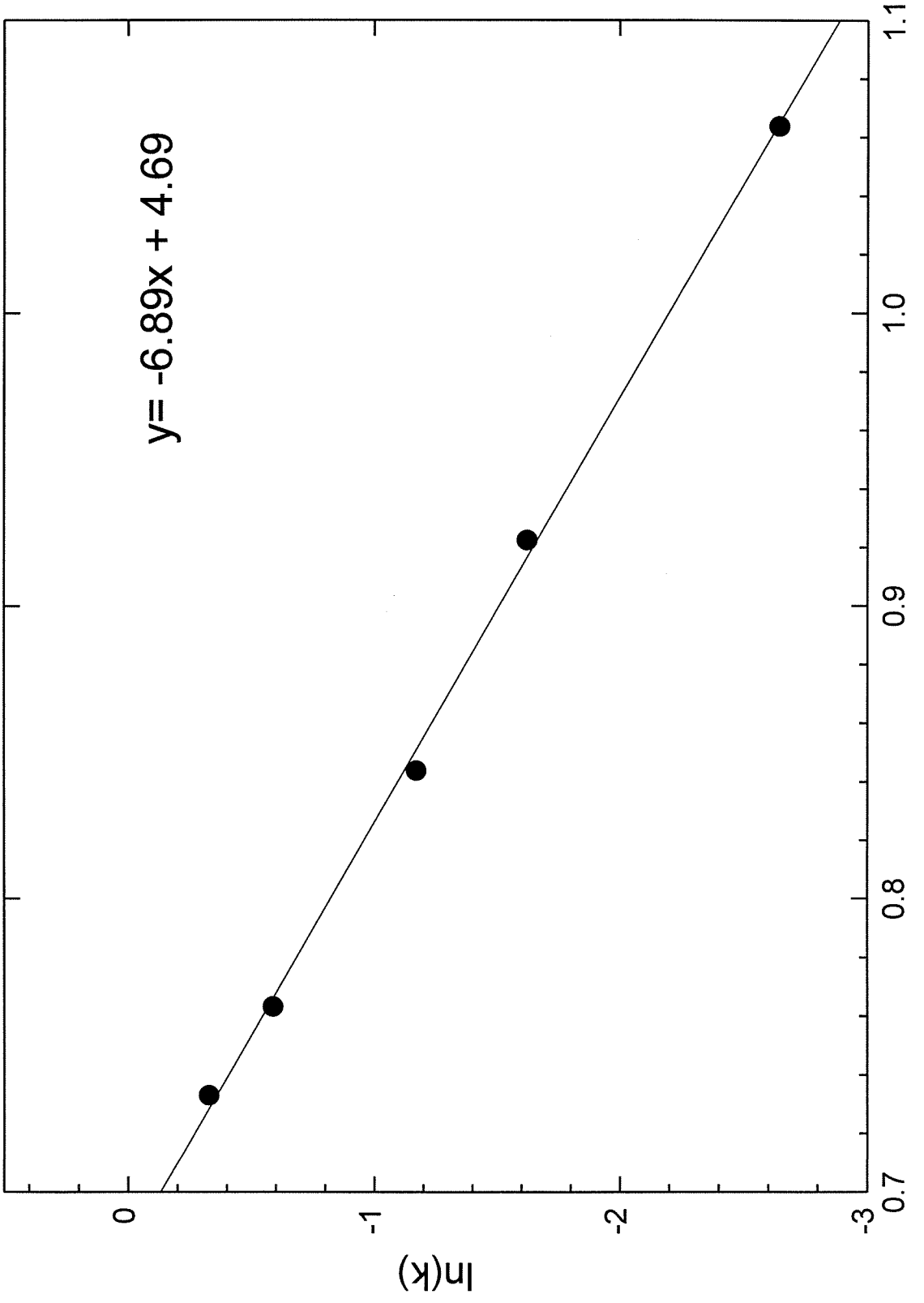
y= -6.89x + 4.69
ln(k)
0
-1
-2
-3
0.7
0.8
0.9
1.0
1.1
1/<Ecom>
0
-1
-2
-3

linear. Nor is it clear how to determine what temperature each collision energy would correspond to. For this data analysis to yield useful numbers, a more complete understanding of the internal energy distributions of these molecules, and how they vary with collision energy, pressure, and time, is necessary.

Master Equation Analysis. Several processes contribute to the change in the internal energy distribution as a function of time for a species *x(E,t)* during off resonance collisional activation. The population of energy levels of the molecule *x* are affected by collisional activation, collisional deactivation, radiative relaxation and unimolecular reaction. This is shown schematically in Figure 5-6. The internal energy of the species *x(E,t)* at any time can be determined by using information about each of these processes to solve the time dependent master equation, given by Equation 4.

$$\frac{\partial x(E,t)}{\partial t} = \int_0^\infty \Big([M]R(E,E')x(E',t) - [M]R(E',E)x(E,t) - K(E',E)x(E,t)\Big)dE - k(E)x(E,t) \quad (4)$$

The four processes involved in changing the internal energy population are accounted for. *R(E,E')* is the collisional activation rate constant for energy transfer from levels *E'* to level *E*, *R(E',E)* is the collisional deactivation rate constant for energy transfer from level *E* to levels *E'*, and *K(E',E)* is the radiative relaxation rate constant from level *E* to levels *E'*. These three processes are integrated over all energy levels *E'*. *k(E)* is the unimolecular dissociation reaction rate constant, and can be determined from RRKM theory.

Figure 5-6. Schematic diagram of the processes contributing to the change in internal energy of a species *x(E)*.

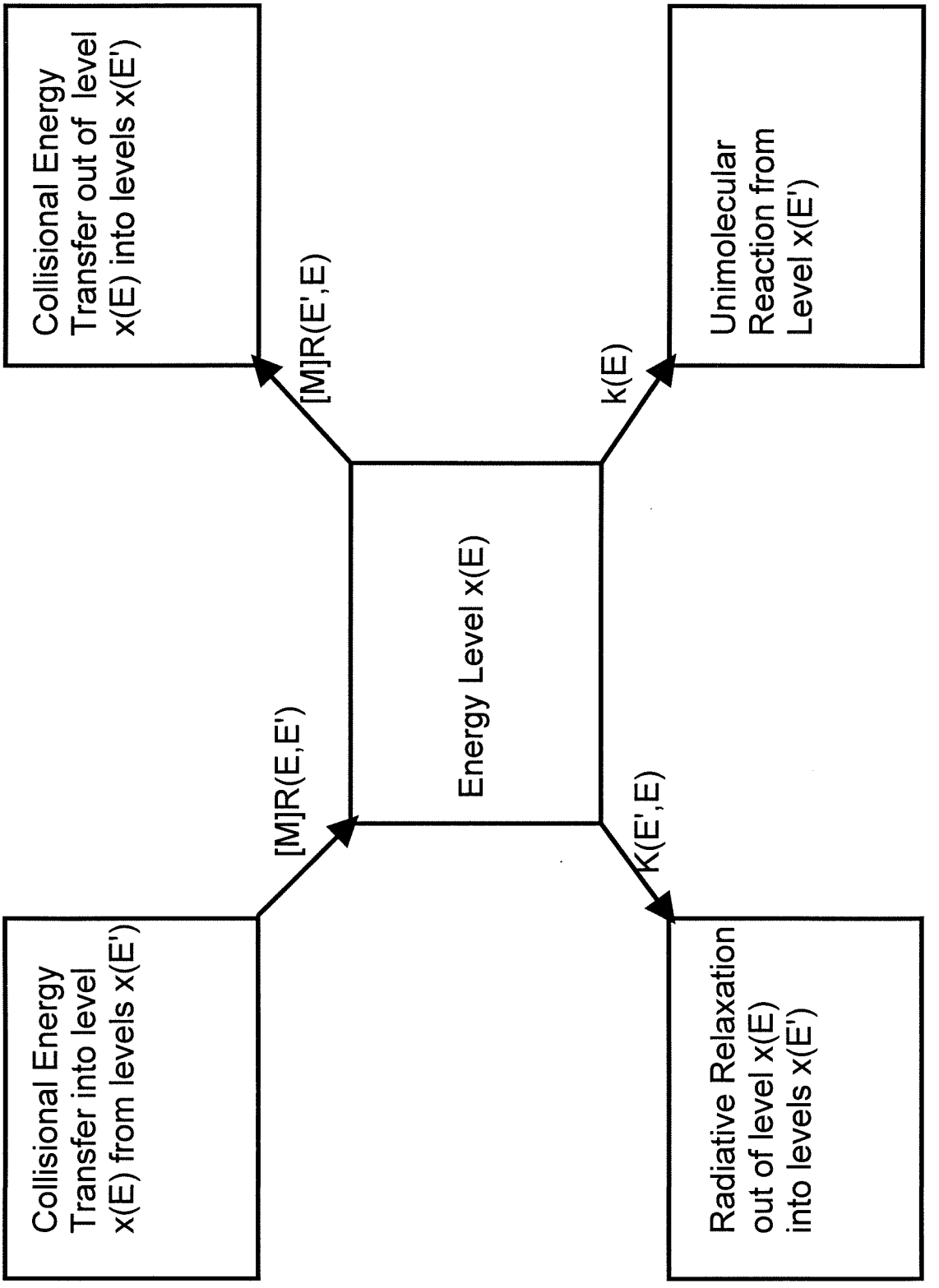
Collisional Energy Transfer out of level x(E) into levels x(E')
[M]R(E',E)
Unimolecular Reaction from Level x(E')
k(E)
Energy Level x(E)
[M]R(E,E')
K(E',E)
Collisional Energy Transfer into level x(E) from levels x(E')
Radiative Relaxation out of level x(E) into levels x(E')

To mathematically solve the time dependent master equation, it is useful to approximate the continuum integral form given in Equation 4 as a discrete summation.[4] This is done in Equation 5, where the indices *i* and *j* are used to represent energy levels *E'* and *E*, respectively.

$$\frac{dx_i(t)}{dt} = \delta E \sum_{j=0}^{\infty} \left([M] R_{ij} x_j - [M] R_{ji} x_i - K_{ji} x_i \right) - k_i x_i(t) \quad (5)$$

This equation can be re-expressed in the matrix form shown in Equation 6.

$$\frac{d\mathbf{x}}{dt} = \mathbf{J}\mathbf{x} \quad (6)$$

The coefficients of the matrix J are given by Equation 7.

$$\begin{aligned} \mathbf{J}_{ij} &= [M]\delta E R_{ij} \text{ for } i \neq j \\ \mathbf{J}_{ii} &= -k_i - \sum_{i \neq j} [M]\delta E R_{ji} \end{aligned} \quad (7)$$

x is a column vector with elements x_i representing the distribution of each energy state, x_i. $\mathbf{J}_{ij}$ is the matrix term that expresses the rate of change from state *j* to state *i*. More specifically, $\mathbf{J}_{21}$ is the rate of upward energy change from state 1 to state 2 and $\mathbf{J}_{35}$ is the rate of downward energy change from state 5 to state 3. The diagonal terms of each column are the negative of the sum of all the elements of the column and the rate constant for reaction from that level; this allows for conservation of the reactant abundance. Equation 6 is a simple differential equation and has the solution given by Equation 8.

$$\mathbf{x}(t) = e^{\mathbf{J}t}\mathbf{x}(t=0) \quad (8)$$

Finding the exponential of a matrix is not always an easy task. We choose to take advantage of the properties of the matrix **J**, which can be diagonalized by finding its eigenvalues and eignenvectors. This allows us to rewrite the matrix **J** as shown in Equation 9, where **A** is a diagonal matrix with the eigenvalues λ_i the diagonal elements, and **Q** is a matrix with the corresponding eigenvectors, $\mathbf{e}_i$, as its column vectors.[5]

$$\begin{aligned}[\mathbf{J}] &= [\mathbf{Q}]\,[\mathbf{A}][\mathbf{Q}]^{-1} \Rightarrow \\ [\mathbf{J}t] &= [\mathbf{Q}][\mathbf{A}t][\mathbf{Q}]^{-1}\end{aligned} \qquad (9)$$

The exponential of **J** can be shown to be related to the exponential of the diagonal matrix **A**, as given in Equation 10.

$$e^{[\mathbf{J}t]} = [\mathbf{Q}]e^{[\mathbf{A}t]}[\mathbf{Q}]^{-1} \qquad (10)$$

The exponential of a diagonal matrix is just the exponential of its individual terms, and this allows a straightforward method to compute the internal energy distribution $\mathbf{x}(t)$, by defining the matrix **J** and then computing its eigenvectors and eigenvalues. The population of $\mathbf{x}(t)$ contains the internal energy distributions as a function of time. The depletion of populations can be determined by summing over all values $\mathbf{x}(t)$ as a function of time.

Maple V employs a function for determining the exponential of a matrix in this manner and was employed in this analysis to determine the population distributions. Appendix 1 contains the code used to set up the matrix and determine the final population distributions. Computationally, using arrays of size greater than 30x30 was impractical due to slowness of the routine. For matrices of size 30x30,

each time point required 15 minutes of computational time on an IBM DX2 66 MHz computer running Maple V in the Windows environment. For the peptide gly-gly-ile this allowed an energy grain size of 0.25 eV to be employed. As available fitting routines do not allow the proper constraints to be implemented, all data fitting was done by observation and user modification to the matrix **J**. We next consider the parameters required for the matrix **J**.

The determination of *k(E),* the unimolecular rate constant, using RRKM theory has been described in detail in Chapter 4. The other activation and deactivation rate constants are not so straightforward to determine. In an attempt to determine the efficiency of collisional energy transfer into internal modes, the effect of molecular size on dissociation efficiency was investigated, as detailed in Chapter 3. It was shown that Hyperchem trajectory calculations can be used to predict energy transfer efficiencies, which can be quite high. The primary mechanism of energy transfer appears to be via impulsive collisions with multiple encounters of the neutral collision gas possible with larger peptides resulting in ≈40-90% of relative collision energy transferred into internal modes during a collision event (see Chapter 4). As a first approximation, the rate of collisional deactivation during the off resonance activation process will be considered to be small relative to the rates of excitation and reaction.

In an effort to determine the magnitude and importance of the rate of radiative relaxation, the data for rate of dissociation of gly-gly-ile as a function of collision energy shown in Figure 5-3 was qualitatively analyzed. Assuming a dissociation rate

of 1-10 sec^{-1} and a corresponding internal energy of 4.5 eV to induce dissociation, the required collision efficiency to obtain this internal energy can be calculated. At a pressure of $2x10^{-7}$ torr, there are approximately 6.5 collisions/second. The amount of time to induce 50% dissociation was used to determine the average amount of energy that must be transferred per collision to yield a total internal energy of 4.5 eV. The results are summarized in Table 2. It is noteworthy that the efficiencies for activation for energies that induce significant dissociation in less than a second are similar to those determined in Chapter 3 experimentally and supported by Hyperchem collision trajectories. The implied activation efficiency decreases dramatically as a function of collision energy. Over this narrow energy range, this dependence is not fully explained by the trajectory calculations. Instead, these results imply that energy loss processes play an important role, especially at the long times required to effect dissociation with lower collision energies.

The primary loss pathway available to these molecules during the excitation process is infrared radiative relaxation. A recent review of ion-molecule radiative association reactions summarizes the theoretical and experimental results relating to radiative stabilization processes.[6] Very little is known about the process for large molecules. A recent study of the cooling of tri-tert-butylbenzene ions by Dunbar *et. al.* attempts to address this.[7] In this study, it was found that a radiative rate of 1.06 sec^{-1} at an internal temperature of 506 K could be used to adequately model observed unimolecular dissociation data. It was pointed out that radiative cooling rates should be independent of size for a given internal temperature. However, as the molecule size increases for a given internal energy, this should result in a slower radiative

Table 2. Time required to effect 50% dissociation of deprotonated gly-gly-ile as a function of energy against a collision gas of nitrogen at $2x10^{-7}$ torr (6.5 collisions/second). Implied energy transfer/collision to reach an internal energy of 4.5 eV.

Collision Energy (COM) (eV)	Time for 50% dissociation (seconds)	Percent transfer/collision
0.94	>7	10%
1.08	2.65	24%
1.19	1.55	37%
1.31	.95	56%
1.36	.65	72%

cooling rate. This is due to the decrease in effective temperature with size at a constant energy. At high temperatures, more high energy internal modes (which tend to radiate more strongly) are populated, and this is expected to result in an increased radiative stabilization rate.

The calculated internal temperatures required for dissociation of deprotonated gly-gly-ile are significantly higher than those used in Dunbar's experiments.[7] It is expected that the radiative stabilization rate should be a function of temperature, increasing rapidly with increasing internal temperature. Furthermore, this is consistent with the strong dependence of dissociation efficiency on collision energy observed in Figure 5-3. For the master equation modeling, the radiative relaxation rate was taken to be an energy dependent rate. Above 3 eV internal energy the radiative relaxation was assumed to occur at a rate of 1 sec^{-1} with a resulting energy loss of 0.25 eV. Above 4 eV (1050 degrees K) the relaxation rate was increased to 5.5 sec^{-1}. It should be noted that the same effect could be brought about by either having a lower dissociation rate with a larger energy loss, or by assuming the energy transfer efficiency of each collision is dramatically reduced at high internal energies. In fact, since the two parameters have a net cancellation effect, it should be noted that what we are really varying is an "effective" activation efficiency at each energy in our modeling process, especially at high energies where dissociation is the predominant process.

By using the radiative relaxation rate described above, and putting in a collision efficiency based on the Hyperchem trajectory calculations, the dissociation process was modeled for deprotonated gly-gly-ile at collision energies of 1.36 eV and

1.08 eV based on data shown in Figure 5-4. A matrix was set up with a grain size of 0.25 eV. An average energy transfer efficiency of 43% for 1.36 eV and 39% for 1.08 eV was assumed for each collision, with a small fraction of collisions resulting in up to 75% of the collision energy being transferred into internal modes. This was done in an attempt to account for energy dependence of the collisional energy transfer process observed in Chapter 4. A slight energy dependence was built into the activation efficiency, and above an internal energy of 3 eV, the efficiency of energy transfer was dropped to 35% (32%), and above 4 eV the efficiency was further decreased to 30% (26%). The effect of this on the predicted distribution is negligible, as above 4 eV dissociation begins to be the dominant process.

The experimental data could be fit using these reasonable parameters and the RRKM unimolecular dissociation rate constants calculated with E_o=2.5 eV. However, to explain the large fraction of dissociation observed at short times, it was necessary to assume a fraction of the ions are formed from the FAB process with very high internal energies. Once this assumption is made, the calculated fit shown in Figure 5-7 can be obtained. The predicted dissociation curve at 1.36 eV assuming an initial thermal ion population is also shown. The long induction period observed in this case could only be modeled to adequately fit the data by assuming a fraction of the molecules are formed with high internal energy. Unfortunately, the internal energy distributions of ions generated in the FAB process are not known. Collisional cooling is a slow process, and as a result we cannot easily relax the ion population to thermal energies during an experiment. As a result of our inability to fix this parameter, there are too many variables to determine an activation energy. In this

Figure 5-7. Comparison of experimental and calculated dissociation efficiency as a function of time for deprotonated gly-gly-ile at an $<E_{com}>$=1.36 eV. Calculated curves were determined from a master equation analysis. See text for details on assumed parameters.

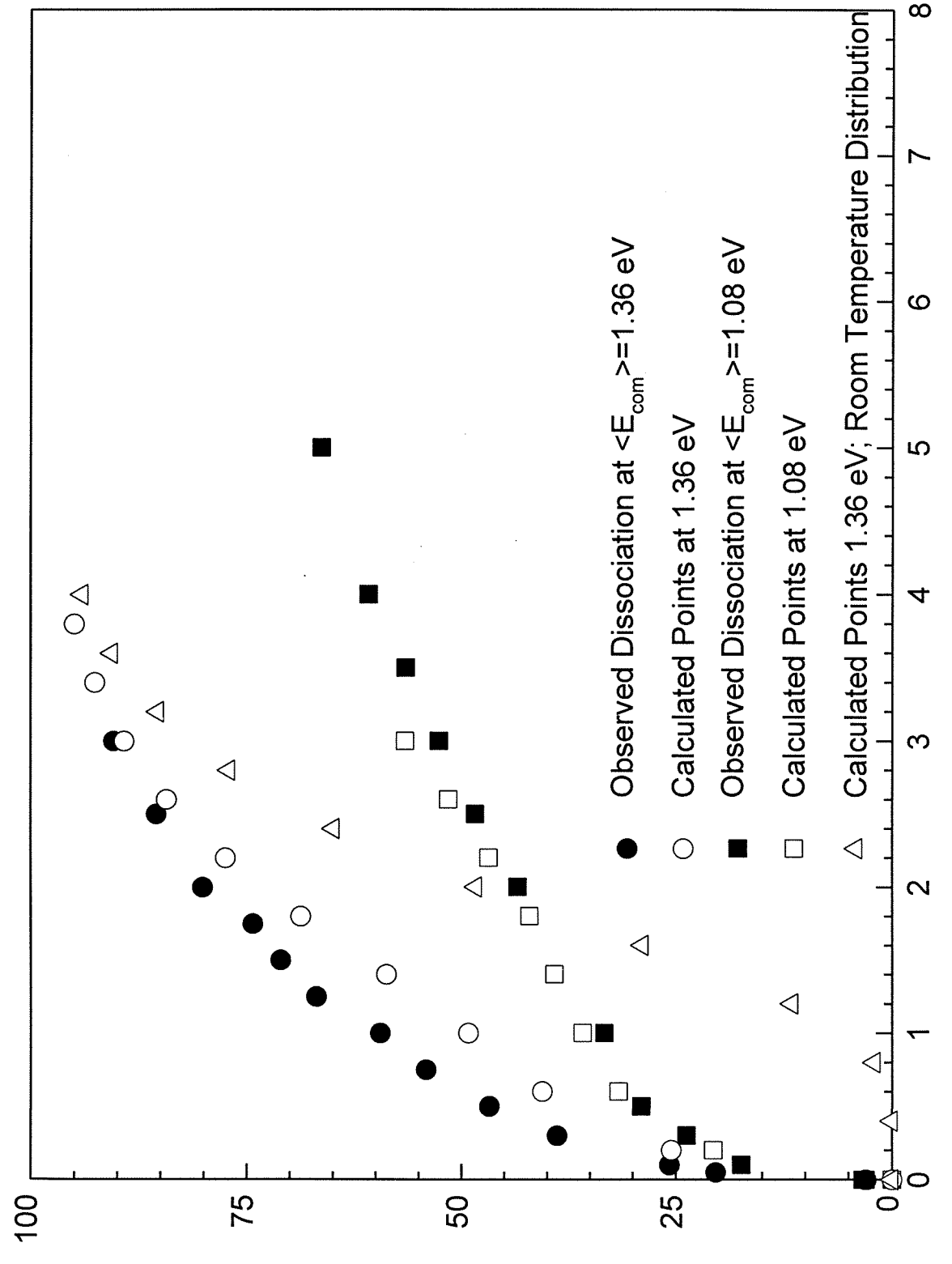
Relative Abundance
Time (seconds)
Observed Dissociation at <E_com>=1.36 eV
Calculated Points at 1.36 eV
Observed Dissociation at <E_com>=1.08 eV
Calculated Points at 1.08 eV
Calculated Points 1.36 eV; Room Temperature Distribution

particular case, to fit the data, 50% of the molecules were assumed to have an initial internal energy of 4.5 eV and 15% were assumed to have an internal energy of 4.0 eV. The remainder were assumed to have thermal energies (0.25 eV). With this assumption the fits observed in Figure 5-7 are obtained. Were this initial distribution to be varied slightly, the same data could have been fit to a lower activation energy with similar assumptions about the radiative relaxation and collisional activation terms. Likewise, a slightly lower initial energy distribution and more efficient activation can account for the observed dissociation.

Figure 5-8 shows the time evolution of the internal energy distribution of the above fit for 1.36 eV and 1.08 eV. At short times (0.1 seconds), the distribution still resembles the starting distribution. However, after 1 second it has reached essentially a steady state, where the only changes are due to ion losses by unimolecular dissociation reaction. This process is slightly slower for the 1.08 eV population. This is experimentally supported by the observations in Figure 5-4, where it is shown that after the initial depletion of high energy species, the dissociation follows first order kinetics. Changes in the starting ion energy distribution, particularly assuming the ions have a lower energy, or a distribution with a more uniform population density among all of the energies do not allow an accurate fitting of the observed short time dissociation. While the results of the calculation method are sensitive to variation in the activation energy and assumed activation and deactivation efficiencies, without knowing the details of the initial distribution, it is impossible to fit the data and obtain meaningful information about these. The primary conclusion that can be drawn from this analysis is that a significant fraction of the ions generated by the FAB process are

Figure 5-8. Calculated energy distributions as a function of time for the data shown in Figure 5-7. a. For a 1.36 eV excitation energy. b. For 1.08 eV excitation energy.

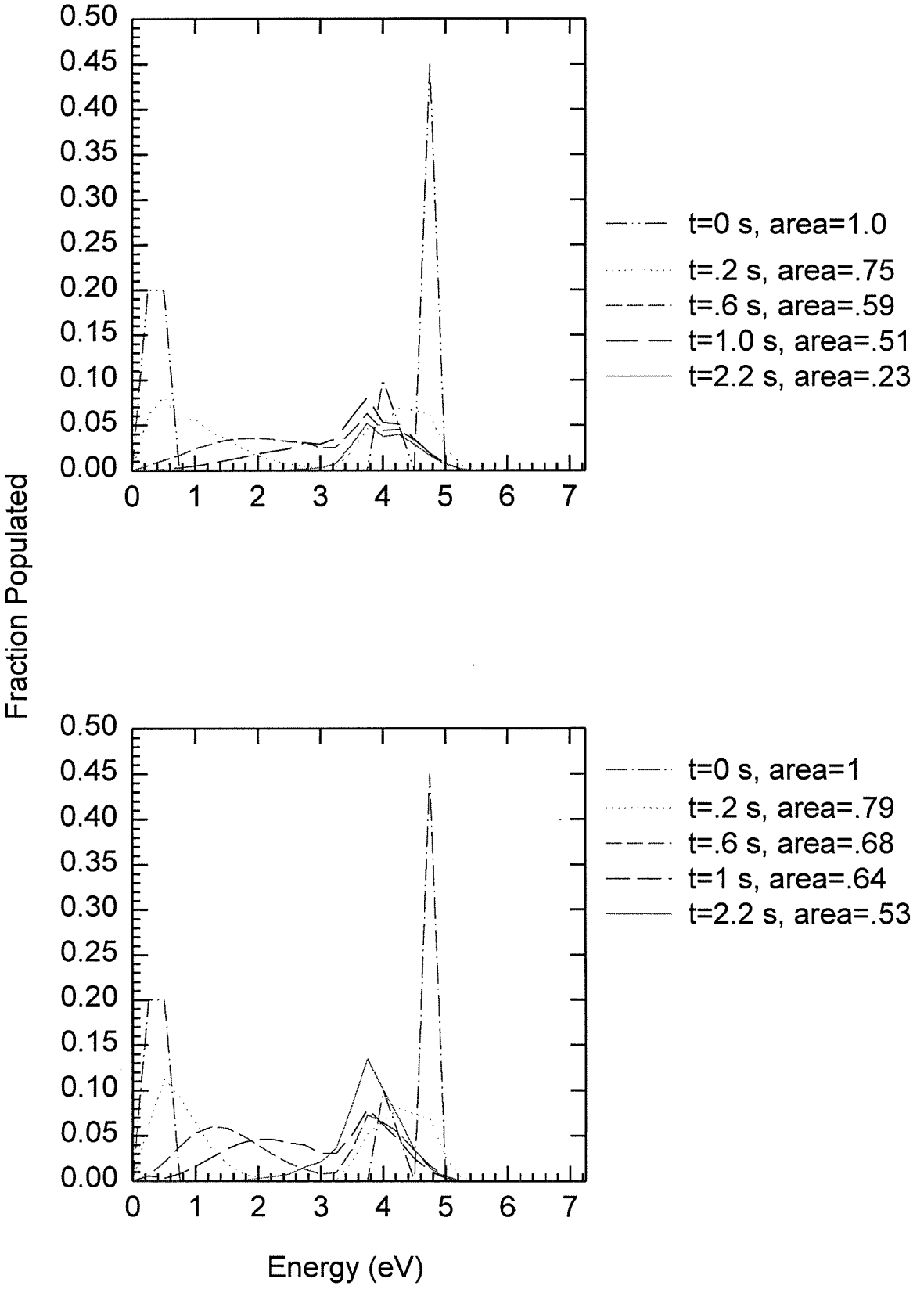
Fraction Populated
0.50
0.45
0.40
0.35
0.30
0.25
0.20
0.15
0.10
0.05
0.00
0 1 2 3 4 5 6 7
t=0 s, area=1.0
t=.2 s, area=.75
t=.6 s, area=.59
t=1.0 s, area=.51
t=2.2 s, area=.23
0.50
0.45
0.40
0.35
0.30
0.25
0.20
0.15
0.10
0.05
0.00
0 1 2 3 4 5 6 7
t=0 s, area=1
t=.2 s, area=.79
t=.6 s, area=.68
t=1 s, area=.64
t=2.2 s, area=.53
Energy (eV)

formed with high internal energies and that they relax slowly on the time scale and collision gas pressures available to us.

A few experimental notes deserve mention. Chapter 1 and 2 describe in detail the parameters and methodology of the off resonance process. After the initial ion isolation following the FAB pulse, the remaining ion population does not possess enough internal energy to undergo spontaneous unimolecular dissociation and in the absence of an off resonance activation pulse no dissociation is observed, even at detection delays as long as several seconds. Typically the activation pulse is applied 500-1000 ms after ion formation, and the detection event occurs 500 milliseconds after the end of the activation pulse. Increasing the delay before activation to several seconds in an attempt to thermalize the ions has a very slight effect on the observed extent of dissociation. Activation at very low energies typically results in dissociation of up to 25% of the ions, and increasing the activation time does not further increase the observed extent of dissociation. This implies that at very low collision energies, radiative cooling competes with the unimolecular activation at long times, making dissociation of the ions difficult. Because of this evidence two discrete ion populations were assumed in the calculations here.

CONCLUSIONS

A master equation analysis of the off resonance collisional activation process has the possibility of yielding useful information about the activation efficiencies and energetics required for dissociation. A prerequisite for obtaining useful information from this analysis is a knowledge of the initial internal energy distribution of the ions. Since this information is not currently available, there are too many variables to fit the

data in a manner that will yield quantitative information. The one thing which is apparent from these calculations is that a significant fraction are formed with high internal energy and undergo dissociation after one collision event. It is also clear that, as was proposed, the activation efficiencies of these molecules are large. It appears that the radiative relaxation rate is also significant. However, while the data can be fit using reasonable parameters, more quantitative information cannot be obtained at this time. A method of forming ions with a known internal energy distribution is necessary before further analysis of this type can be attempted. One method of doing this with ions generated by FAB in an FT-ICR would be to use a pulsed collision gas at high pressures to collisionally relax the ions, followed by quadrupolar axialization to collect the ions back into the center of the cell.[8] After this step, which could take up to a minute, the activation process could be carried out.

APPENDIX 1. Code for Maple V master equation analysis.

```
with(linalg):
k:=array(1..30):
for i from 1 to 30 do
k[i]:=0:
od:
k[12]:=0:
k[13]:=1.3223e-7:
k[14]:=6.5521e-6:
k[15]:=1.4462e-4:
k[16]:=1.8717e-3:
k[17]:=.0165:
k[18]:=.1090:
k[19]:=.5735:
k[20]:=2.5127:
k[21]:=9.4735:
k[22]:=31.5030:
k[23]:=94.1905:
k[24]:=257.0857:
k[25]:=648.4672:
k[26]:=1526.7854:
k[27]:=3383.3272:
k[28]:=7105.4404:
k[29]:=1.4225e4:
```

```
k[30]:=2.7283e4:

mat:=array(1..30,1..30):
for i from 1 to 30 do
for j from 1 to 30 do
mat[i,j]:=0:
od:
od:



for j from 1 to 30 do

if j=1 then
mat[j+1,j]:=1.75:
mat[j+2,j]:=2.5:
mat[j+3,j]:=1:
mat[j+4,j]:=.5:
mat[j+5,j]:=.25:
mat[j+6,j]:=.00:
mat[j+7,j]:=0:
mat[j+8,j]:=.0:
mat[j+9,j]:=.0:
elif j>1 and j<13 then
mat[j-1,j]:=.0:
```

```
mat[j+1,j]:=1.75:
mat[j+2,j]:=2.5:
mat[j+3,j]:=1:
mat[j+4,j]:=.5:
mat[j+5,j]:=.25:
mat[j+6,j]:=.00:
mat[j+7,j]:=.0:
mat[j+8,j]:=.0:
mat[j+9,j]:=.0:
elif j<17 and j>12 then
mat[j-1,j]:=1:
mat[j-2,j]:=0:
mat[j+1,j]:=2.25:
mat[j+2,j]:=3.0:
mat[j+3,j]:=0.75:
mat[j+4,j]:=0:
mat[j+5,j]:=0:
elif j<22 and j>16 then
mat[j-2,j]:=2.5:
mat[j-1,j]:=3.5:
mat[j+1,j]:=3.5:
mat[j+2,j]:=2.5:
```

```
mat[j+3,j]:=0.:
elif j<28 and j>21 then
mat[j-2,j]:=3:
mat[j-1,j]:=4:
mat[j+1,j]:=5.5:
mat[j+2,j]:=.50:
mat[j+3,j]:=.0:
else
mat[j-2,j]:=5:
mat[j-1,j]:=5:
fi:
sum1:=0:
od:

for j from 1 to 30 do

s1:=0:
for i from 1 to 30 do
s1:=s1+mat[i,j]:
od:
x:=k[j]:
```

```
mat[j,j]:=(-1*s1+(-1*k[j])):
od:
print(mat):
```

mat

```
xo:=array(1..30):
for i from 1 to 30 do
xo[i]:=0:
od:
xo[1]:=.0:
xo[2]:=.20:

xo[3]:=.20:
xo[4]:=.0:
xo[5]:=.0:
xo[6]:=.0:
xo[7]:=.0:
xo[8]:=.0:
xo[9]:=.0:
xo[10]:=.0:
xo[11]:=.0:
xo[12]:=.0:
xo[13]:=.0:
xo[14]:=.0:
```

```
xo[15]:=.0:

xo[16]:=.0:

xo[17]:=.10:

xo[18]:=.05:

xo[19]:=.0:

xo[20]:=.45:

xo[21]:=.0:

print(xo):
```

$$xo$$

```
t:=.2:



for i from 1 to 10 do

evalm(exponential(mat*t)&*xo);

t:=t+.4;

od;
```

REFERENCES

[1] (a) Hunt, M.; Kerr, J.A.; Trotman-Dickensen, A.F. *J. Chem. Soc.* **1965**. 5074-5080. (b) Benson, S.W.; O'Neal, H.E. in *Kinetic Data on Gas Phase Unimolecular Reactions.* National Bureau of Standards. United States, 1970.

[2] The endothermicity of the initial abstraction process can be estimated from the difference in acidities between a carboxylic acid site and a model ketone. Likewise, the endothermicity of the reaction was estimated by a thermodynamic analysis of the bonds broken and formed during reaction.

[3] For the off resonance activation process, this is the rate regime of interest. It should be noted that single collision dissociation techniques require even higher internal energies to effect detectable dissociation and that the initial internal energy is a correspondingly smaller fraction of the required dissociation energy.

[4] Gilbert, R.G.; Smith, S.C *Theory of Unimolecular and Recombination Reactions.* Blackwell Scientific Publications: Oxford, 1990.

[5] For more on properties of diagonal matrices, see Friedberg, S.H.; Insel, A.J.; Spence, L.E. *Linear Algebra.* Prentice Hall: New Jersey, 1979, Chapter 5.

[6] Dunbar, R.C. in *Unimolecular and Bimolecular Reaction Dynamics*, Chapter 5. Edited by Ng, C.Y.; Baer, T.; Powis, I., John Wiley: New York, 1994.

[7] Ho, Y.; Dunbar, R.C. *J. Phys. Chem.* 1993, 97, 11474-11479.

[8] Speir, J.P.; Gorman, G.S.; Pitsenberger, C.C.; Turner, C.A.; Wang, P.P.; Amster, I.J. *Anal. Chem.* **1993**, 65, 1746-1752.

Chapter 6

Implementation of an Electrospray Ionization Source with a Quadrupole Mass Spectrometer

Electrospray Ionization (ESI) is a recently developed method for producing large multiply charged species in the gas phase.[1] A spray of fine droplets of typically methanol/water mixtures is produced by applying a high electric field (typically 3kV/cm) between a needle and plate. The sample of interest is dissolved in the solvent and the droplets are sampled into vacuum through a hole in the plate. Several stages of differential pumping and various combinations of heating, drying gases and collisions are used to desolvate the species, resulting in highly charged species. The result is a very soft ionization method capable of producing ions with molecular weights above 100,000 daltons with little or no fragmentation. Several recent reviews demonstrate the advances in this field.[2,3,4]

To obtain experience with the electrospray ionization process and to have available an electrospray mass spectrometry system for routine analysis in our laboratory, a Vestec electrospray ionization source has been interfaced to an existing Extrel quadrupole mass spectrometer system capable of mass analysis up to 2000 amu. The source interface was designed to allow maximum flexibility of choice of lens systems, with the ultimate aim of interpolating an ion mobility mass spectrometer between the electrospray ionization source and the quadrupole mass analyzer. In addition, the existing arrangement allows the addition of a collision cell as well.

The electrospray source was obtained from Vestec Corporation (now Perspective Biosystems, Houston, TX). Its design and use has been described in detail in the literature. [5] This source was originally purchased for use with the Beckman Institute FT-ICR (described in more detail in Chapter 1) but proved

unsuitable due to its tendency to form ions with a large distribution of kinetic energies. A broad ion energy distribution leads to inefficient trapping in FT-ICR experiments. This is not as much of a problem in quadrupole mass spectrometers, which can operate with a broad range of ion energies. A schematic design of the source assembly is shown in Figure 6-1. A retarding potential analysis (described in more detail in Chapter 1) of the ions formed from this source is shown in Figure 6-2. The source uses a nozzle with a 0.4 mm orifice to sample ions from atmosphere into the first differentially pumped region, evacuated to approximately 5 torr with a Balzers UNO016B mechanical pump. The needle to nozzle and nozzle to skimmer distances can both be easily adjusted. Once optimum values for these distances have been determined, they are rarely changed. Ions pass through a skimmer (0.6 mm) into the repeller region pumped to 100-150 millitorr with an Edwards E2M12 mechanical pump. To aid in ion desolvation, this region is typically heated to 150-175 degrees Celsius. Ions are sampled through a skimmer into the first high vacuum region (10^{-4} torr) pumped with a Leybold 250 liter/second turbomolecular pump. At this point typically about 10 picoamps of ion current can be detected.

A diagram of the source interfaced with the quadrupole mass spectrometer located in 37 Noyes is shown in Figure 6-3. To obtain adequate pressures for operation of the quadrupole mass spectrometer ($<10^{-5}$ torr), multiple differential pumping regions are employed. The source region is separated from the rest of the instrument by a gate valve. This allows isolation of the main chamber from the high pressures of the electrospray ionization source when the instrument is not in use. The main chamber is pumped with a 6-inch diffusion pump equipped with a liquid

Figure 6-1. Schematic diagram of Vestec Electrospray source assembly.

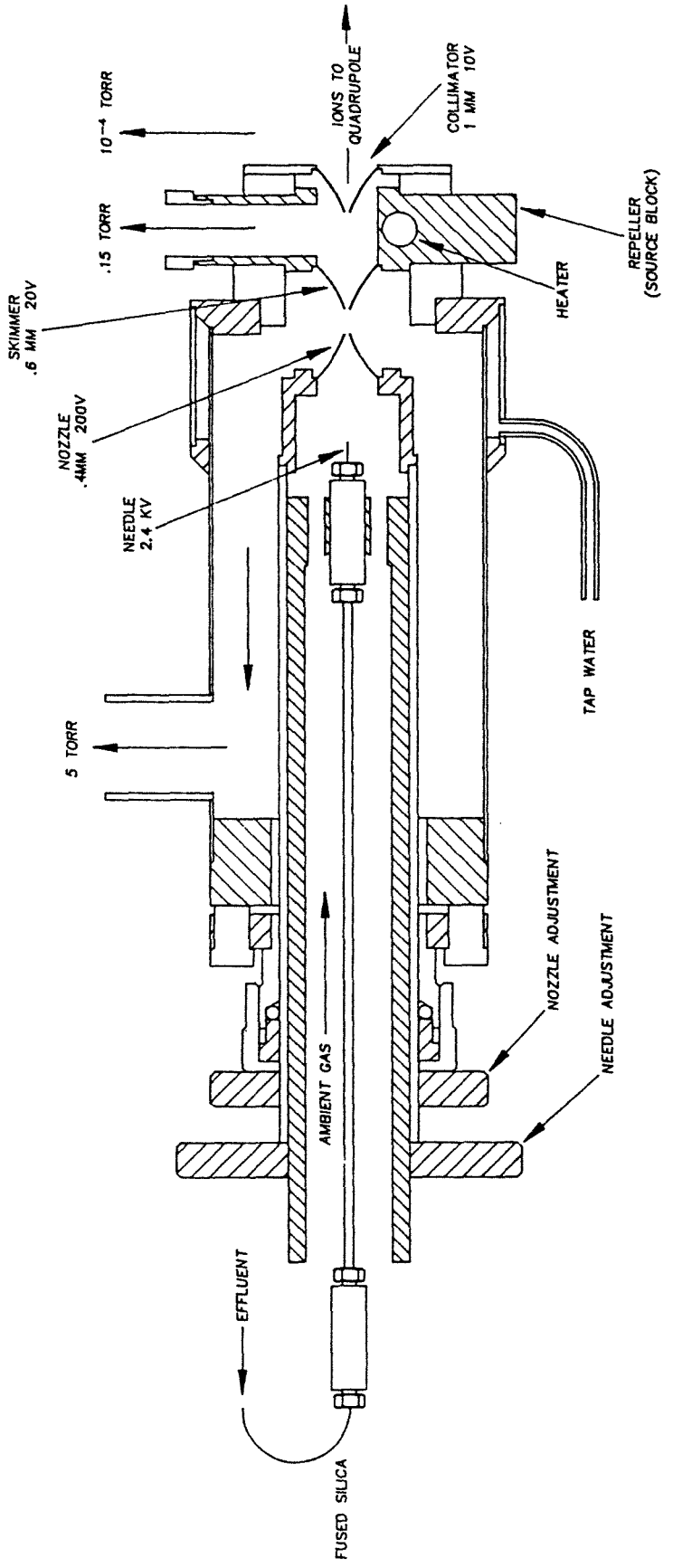
IONS TO QUADRUPOLE
COLLIMATOR 1 MM 10V
10⁻⁴ TORR
.15 TORR
REPELLER (SOURCE BLOCK)
HEATER
SKIMMER .6 MM 20V
NOZZLE .4MM 200V
NEEDLE 2.4 KV
5 TORR
TAP WATER
NOZZLE ADJUSTMENT
NEEDLE ADJUSTMENT
AMBIENT GAS
EFFLUENT
FUSED SILICA

Figure 6-2. Energy analysis of ions generated with electrospray ionization source as measured with the energy analyzer described in Chapter 1.

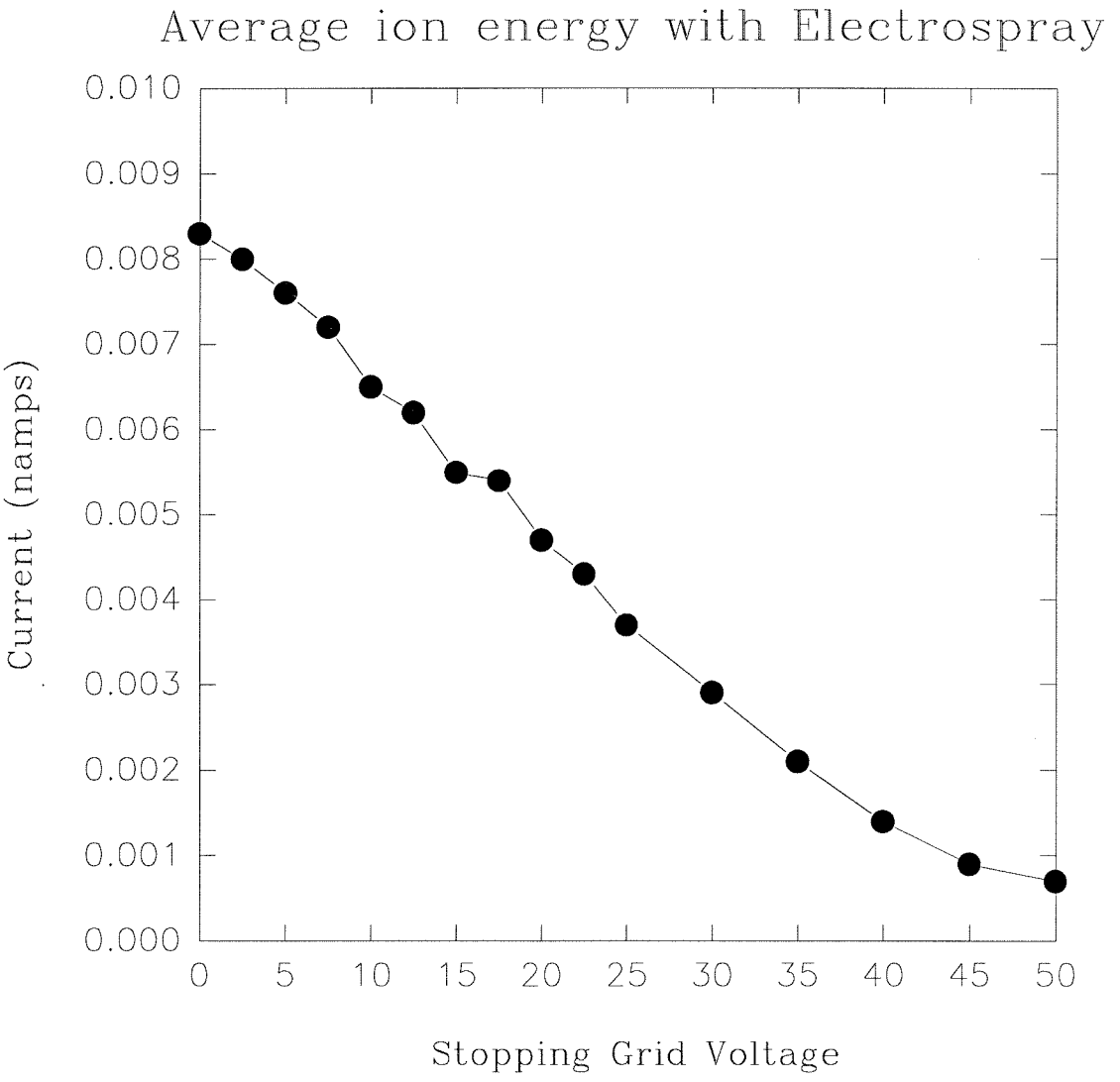
Average ion energy with Electrospray
Current (namps)
0.010
0.009
0.008
0.007
0.006
0.005
0.004
0.003
0.002
0.001
0.000
0
5
10
15
20
25
30
35
40
45
50
Stopping Grid Voltage

Figure 6-3. Schematic diagram of electrospray ionization source interfaced with quadrupole mass spectrometer.

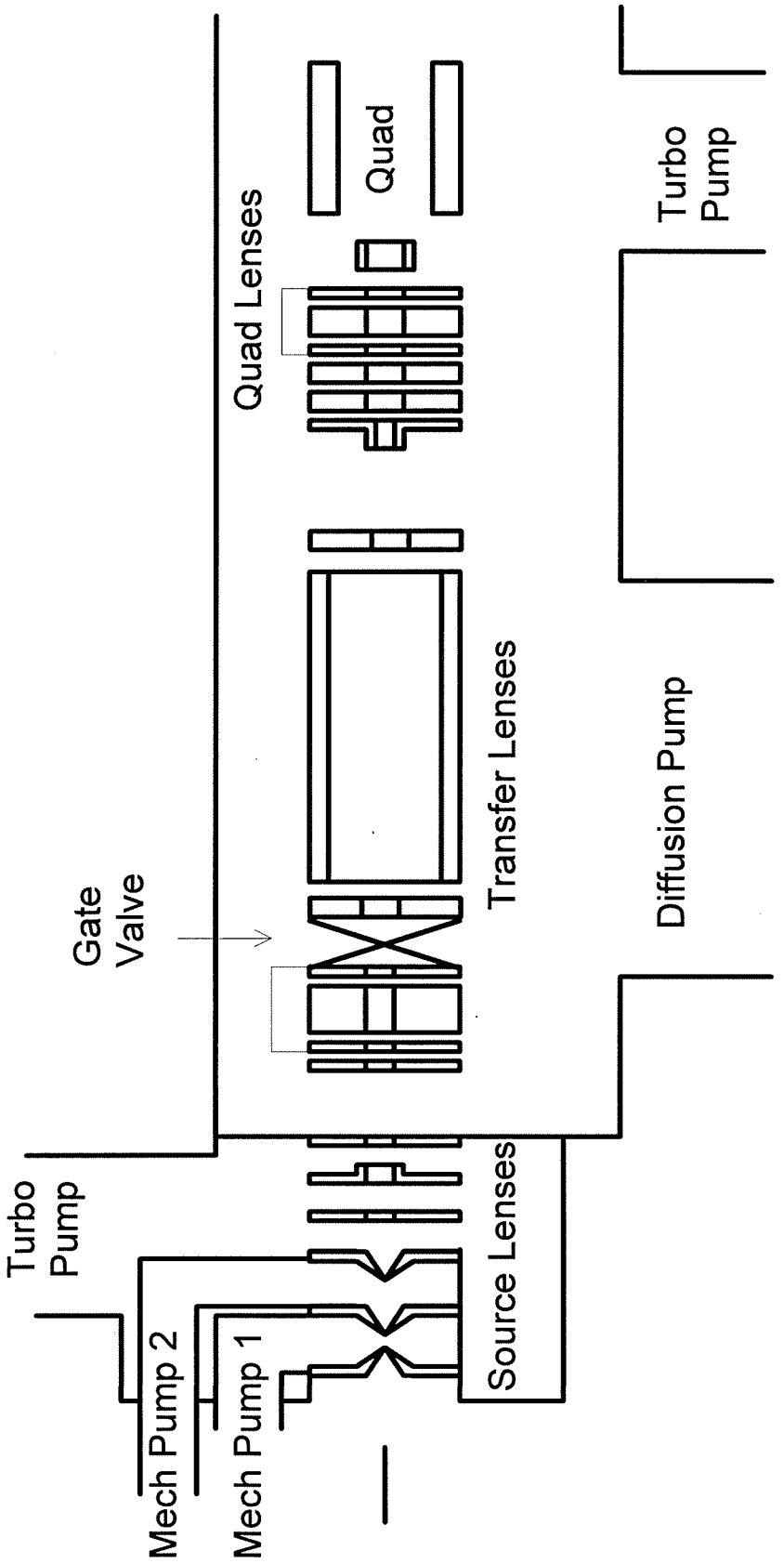
Turbo Pump
Mech Pump 2
Mech Pump 1
Source Lenses
Gate Valve
Transfer Lenses
Quad Lenses
Quad
Diffusion Pump
Turbo Pump

nitrogen trap (Varian VHS-4) and a Leybold 250 Liter/second turbomolecular pump. While not currently implemented, the system is designed to allow incorporation of an additional gate valve between the ion transfer lenses and quadrupole entrance lenses to allow isolation of the quadrupole region. There is currently no differential pumping constrictions between the transfer and quadrupole regions. It will be necessary to modify the instrument to incorporate differential pumping between these two regions before any high pressure ion mobility or collision dissociation experiments can be carried out. Ion gauges are present on both the transfer and quadrupole region. In addition, the main chamber is plumbed with gas inlet lines and outlet lines to a Baratron capacitance manometer for measurement of higher pressures (typically 1-5 torr) that are employed in collisional activation and ion mobility experiments.

The lens assembly, including typical voltages, is shown in more detail in Figure 6-4. Ions exiting the source region are accelerated and then focused with an einzel lens into the entrance of a cylindrical lens (7/8 inch ID, 6 inches long) which transports them through the chamber and into the quadrupole. The entrance to the quadrupole is equipped with its own lens stack mounted on the housing of the quadrupole as shown. The transfer lens system in the main chamber is modular in nature and it can be changed as desired. The current lens components in this region are mounted on three ceramic rods running the length of the chamber, and additional lens elements can be added and existing ones removed as desired. It should be noted that materials needed to create a variety of lens assemblies and collision cells in the main chamber are available. In addition, for testing of the quadrupole system, an

Figure 6-4. Schematic diagram of lens assembly for transport of ions generated with electrospray ionization source into the qaudrupole mass spectrometer.

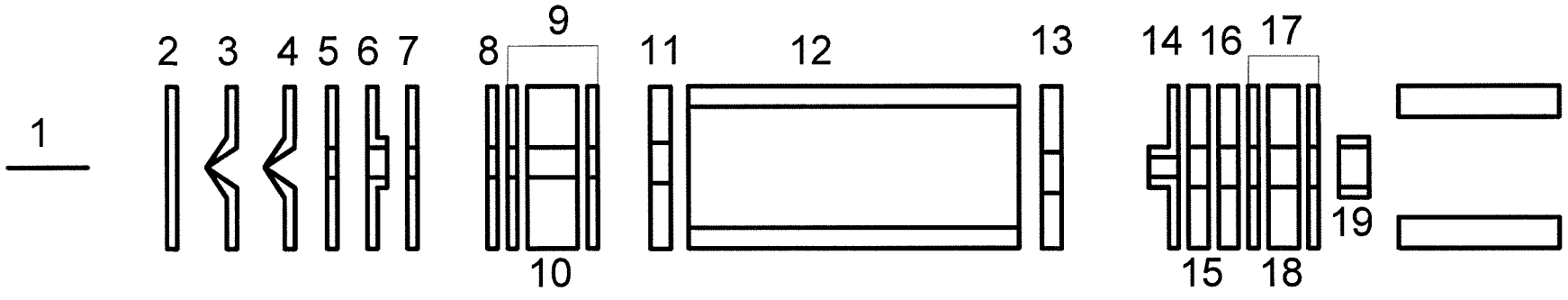

	Lens Name	Typical Voltage		Lens Name	Typical Voltage
1	Needle	2500-3000	11	Entrance	-77
2	Nozzle	+212	12	Cylinder	-111
3	Repeller	+53	13	Exit	-81
4	SRC	+31	14	Extractor	-133
5	Lens 1	-161	15	Accelerator 2	-83
6	Lens 2	-37	16	Decelerator	-14
7	Lens	-174	17	Einzel Lens 2	-38
8	Accelerator	-467	18	Einzel Lens 2 Focus	-6
9	Einzel Lens 1	-329	19	ELFS	24
10	Einzel Lens 1 Focus	-388		ELFS2	-18

electron impact source is available for mounting on these rods (see Appendix 1 for more details). By trial and error it was discovered that the simplest design of a cylindrical tube was most efficient for ion transport through the chamber.

To interface the electrospray source with existing vacuum and electronic components, it was necessary to construct several pieces. Diagrams of these are included here with dimensions for future reference. Figure 6-5 shows a schematic design of a stainless steel mating piece constructed by MDC for mounting the electrospray ionization source. Figure 6-6 shows a schematic design of a stainless steel quad, also constructed by MDC for mounting the quadrupole mass spectrometer, turbomolecular pump and ion gauge to the instrument. In addition, a gate valve for isolating the quadrupole spectrometer and a capacitance manometer for measuring pressures of 0.01-10 have been obtained and can be mounted on the instrument without further modification.

Figure 6-7 shows a schematic of the electronic connection box for providing power to the electrospray ionization source. Voltages to the needle assembly are provided through a 14 pin AMP connector. This provides high voltage connections to the needle and connections to a J-type thermocouple mounted near the needle tip for monitoring the temperature in the vicinity of the needle. Power is provided to the rest of the electrospray apparatus (including AC heater, another J-type thermocouple and lenses) through a 37 pin AMP connector. An electronic interface box allowing connection of standard thermocouple and voltage inputs was constructed with pin connections shown in Figure 6-7. Because the needle assemble slides into a stainless steel housing, the spray cannot be directly observed. Instead, the only way to insure a

Figure 6-5. Schematic diagram of mating piece designed to interface electrospray ionization source with existing vacuum pieces.

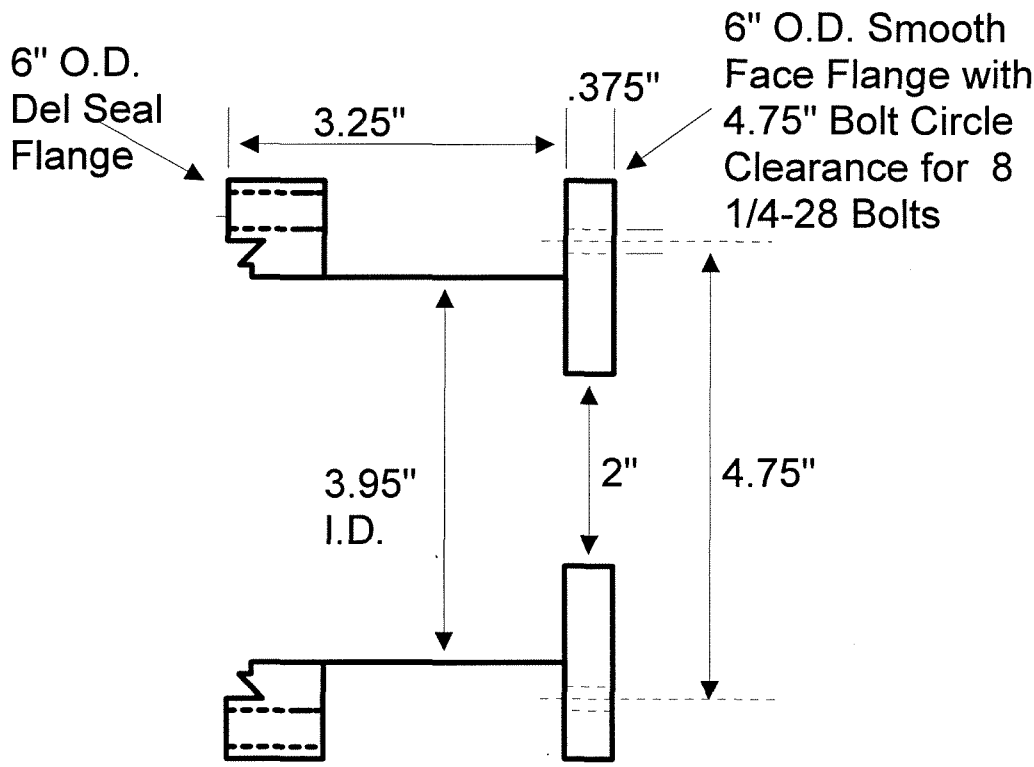
6" O.D.
Del Seal
Flange
3.25"
.375"
6" O.D. Smooth
Face Flange with
4.75" Bolt Circle
Clearance for 8
1/4-28 Bolts
3.95"
I.D.
2"
4.75"

Figure 6-6. Schematic diagram of stainless steel quad constructed for mounting quadrupole mass analyzer to existing vacuum assembly.

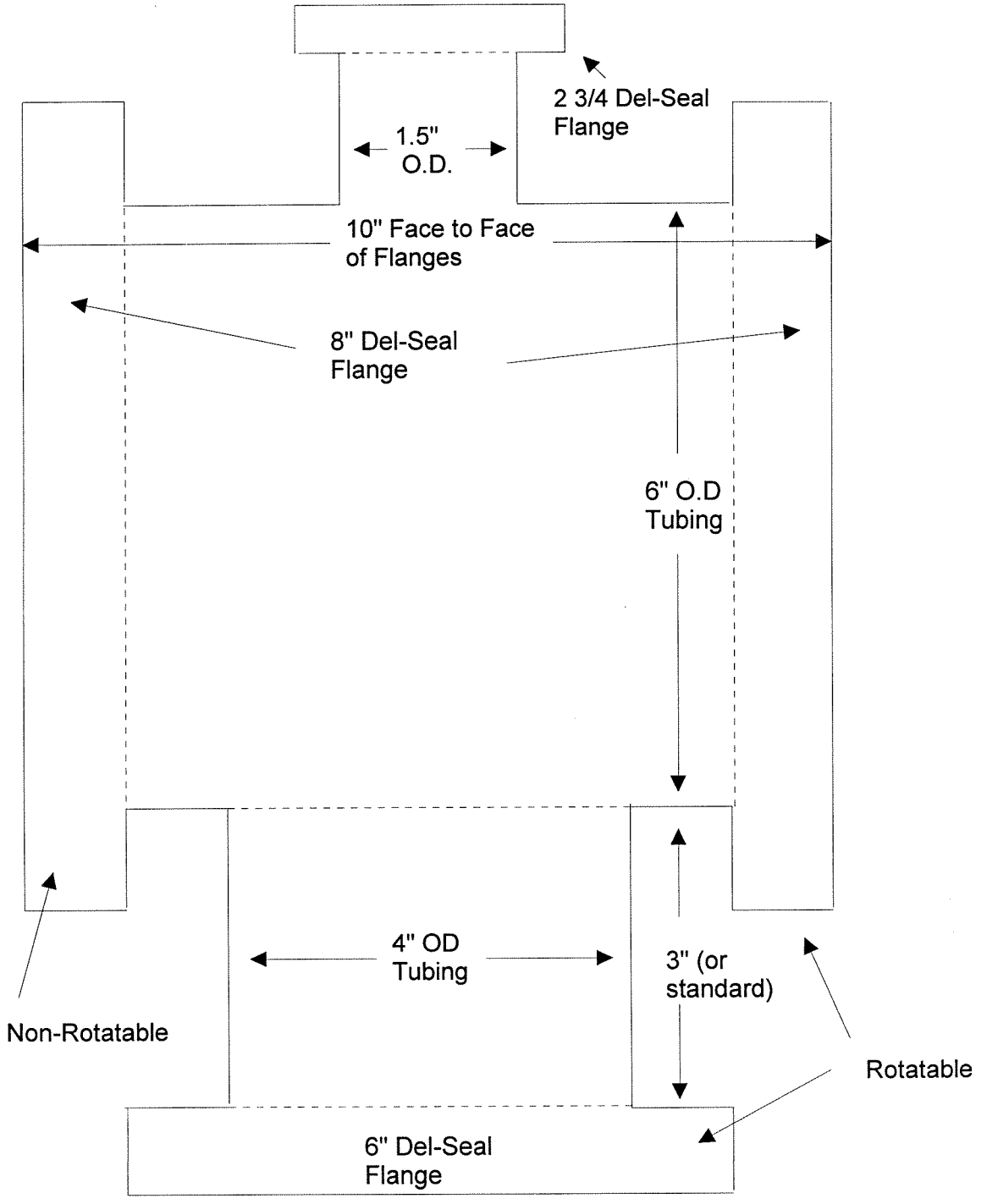
2 3/4 Del-Seal Flange
1.5" O.D.
10" Face to Face of Flanges
8" Del-Seal Flange
6" O.D Tubing
4" OD Tubing
3" (or standard)
Non-Rotatable
Rotatable
6" Del-Seal Flange

Figure 6-7. Schematic diagram of electronic interface box to supply power to the electrospray source.

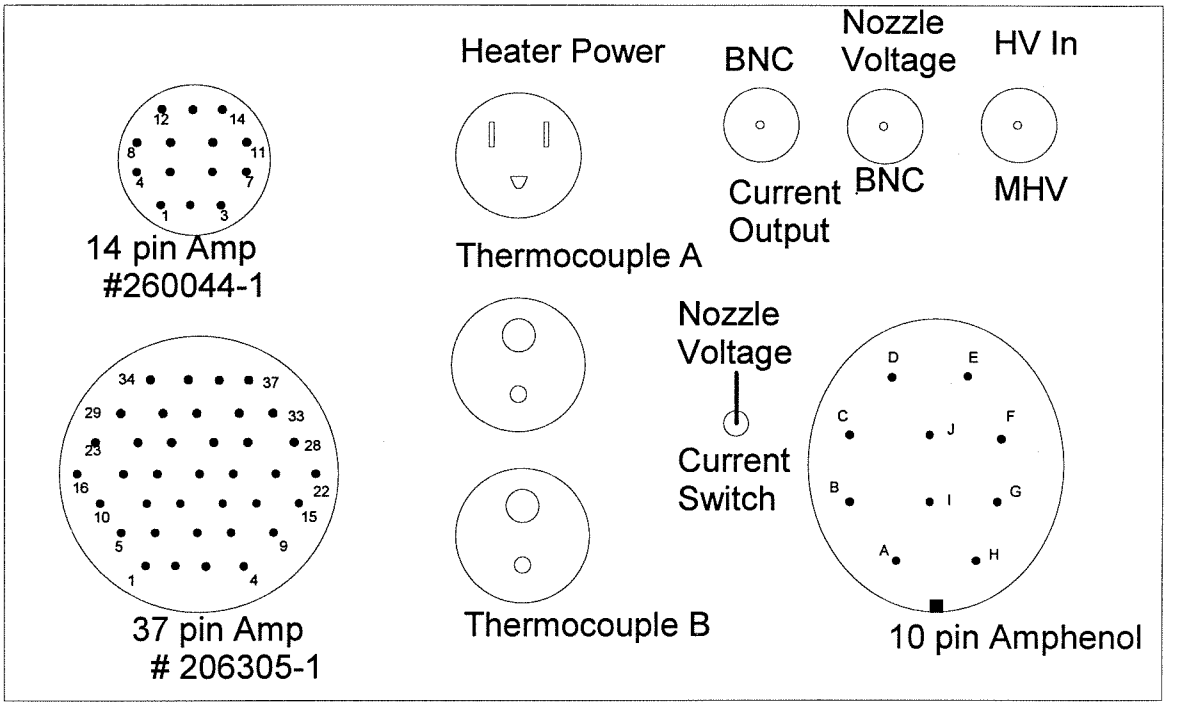

37 Pin Amp Connections
(Output)
Pin

1	Ground
4	SRC
5	Thermocouple B +
6	Lens 2
7	Lens 1
8	Lens
10	Thermocouple B -
16	Heater
17	Heater
23	Nozzle
34	Repeller

14 Pin Amp Connections
(Output)
Pin

1	Thermocouple A +
2	Thermocouple A -
9	Needle High Voltage
14	Ground

10 Pin Amphenol Connections
(Input)
Pin

A	SRC
C	Lens
D	Repeller
E	Lens 1
I	Lens 2

stable uniform spray is through monitoring the ion current. To monitor this an electrometer is connected to the BNC connection labeled "Current Output" on the interface box and the selection switch turned to the setting for current measurement. This allows detection of the ion current impinging on the nozzle, which should be about 0.3 microamps for optimum operation. Because there is no voltage applied to the nozzle during current detection, the source is not in optimum mode for ion transport. Mass detection should only be carried out when the switch is set to supply voltage to the nozzle.

A mass spectrum of doubly protonated gramicidin S, a cyclic peptide with sequence -leu-phe-pro-val-orn-leu-phe-pro-val-orn-, is shown in Figure 6-8. To obtain this spectrum a 10 picomole/microliter solution of equal parts water and methanol and 2% acetic acid was prepared. The solution was introduced into the source using a syringe pump at a flow rate of 8 microliters/minute. This spectrum is a good example of the typical signal intensity that can be observed for peptide species. Primarily the double protonated ion is observed.

By adjusting the repeller voltage, the electrospray source can be used to effect collisional dissociation. Increasing the repeller voltage with respect to the other lenses causes the ions to undergo collisions in this region with higher energy, which can result in fragmentation. An example of this is shown in Figure 6-9 for protonated met-enkephalin. By carefully tuning the source voltages, the protonated peptide can be observed with no fragmentation. Increasing the repeller voltage by 20 volts results in extensive fragmentation (Figure 6-9b). These results can be compared to the low energy dissociation spectrum of met-enkephalin shown in Figure 1-23 carried out

Figure 6-8. Electrospray mass spectra of doubly protonated gramicidin S, a cyclic decapeptide (-leu-phe-pro-val-orn-leu-phe-pro-val-orn-) with protonated MW=1142.5), and doubly protonated m/z=571.75. a. Complete mass spectrum. b. Region around the double protonated peak.

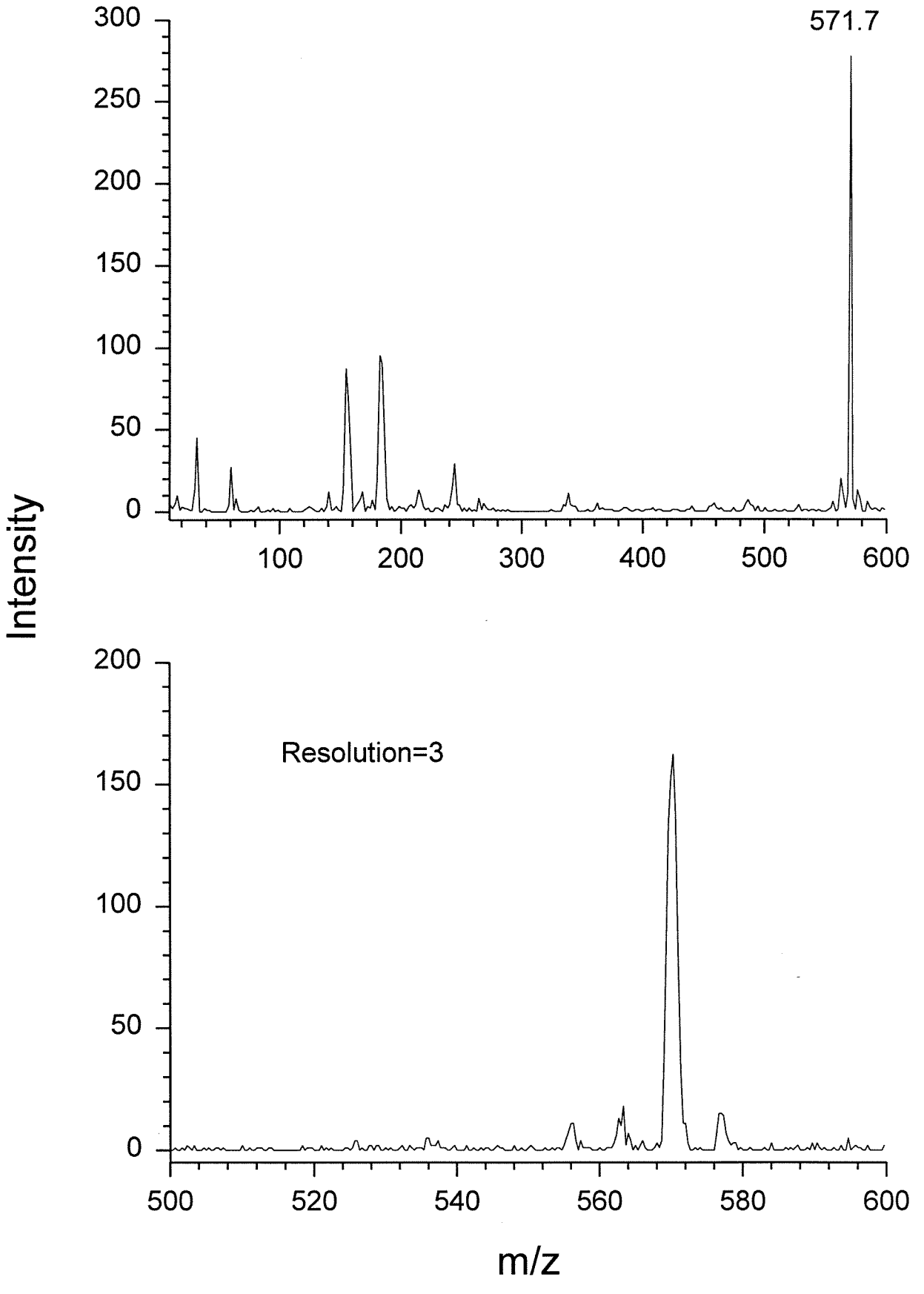
571.7
Resolution=3
Intensity
m/z
300
250
200
150
100
50
0
100
200
300
400
500
600
200
150
100
50
0
500
520
540
560
580
600

Figure 6-9. Electrospray mass spectra of protonated met-enkephalin at m/z 574.6. a. Parent ion. b. Collisional dissociation spectrum obtained as a result of increasing the repeller potential by 20 Volts.

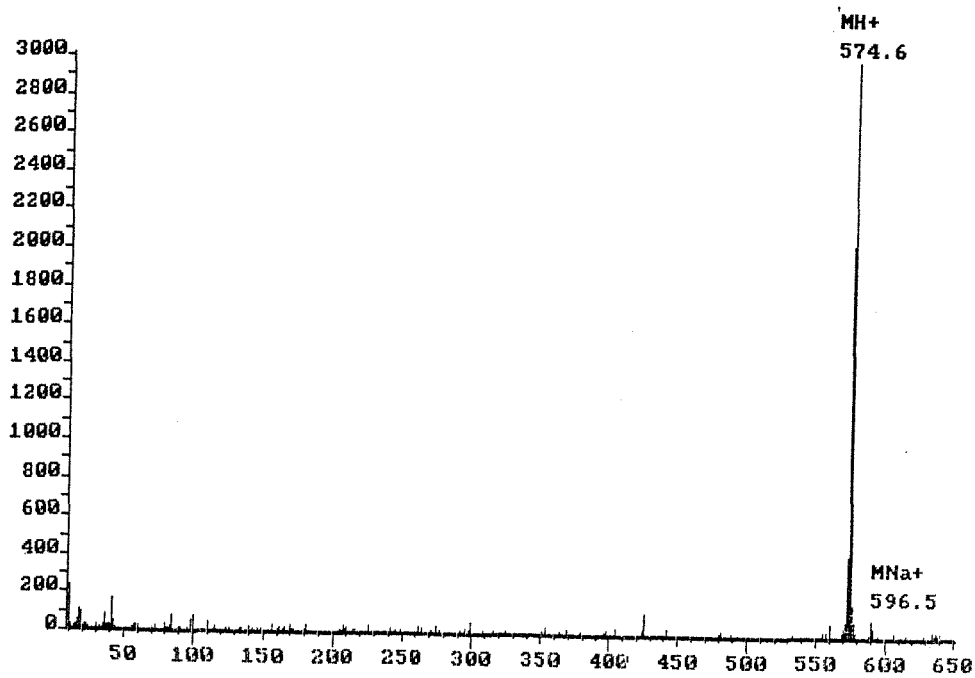
MH+
574.6
MNa+
596.5
3000
2800
2600
2400
2200
2000
1800
1600
1400
1200
1000
800
600
400
200
0
50
100
150
200
250
300
350
400
450
500
550
600
650

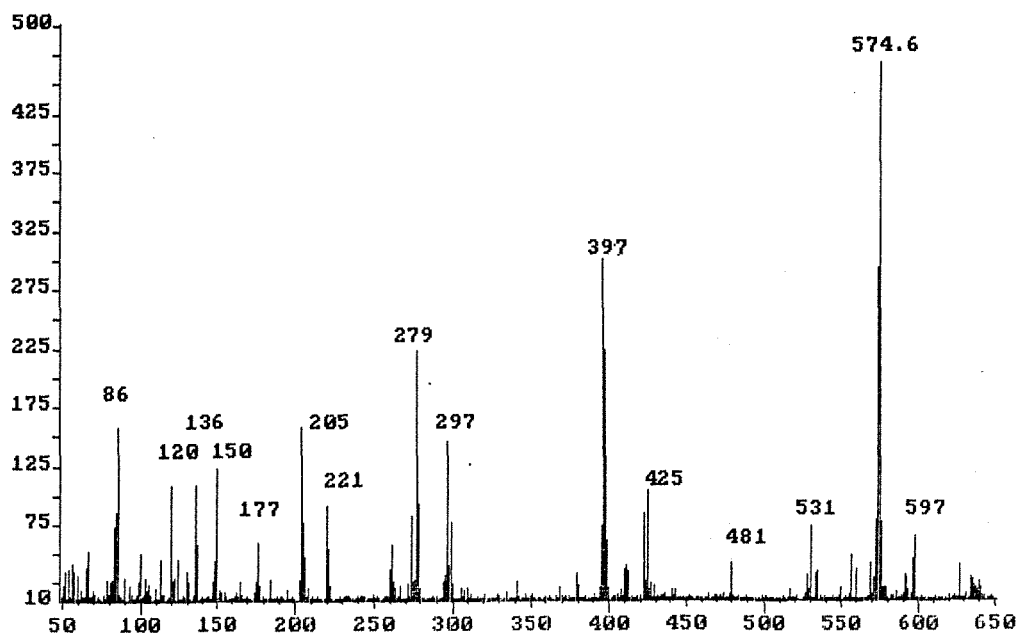
574.6
397
279
86
136
120
150
205
297
221
177
425
481
531
597
500
425
375
325
275
225
175
125
75
10
50
100
150
200
250
300
350
400
450
500
550
600
650

using off resonance excitation in the FT-ICR spectrometer. The fragementation using the collisions within the source region of the electrospray ionizer is much more extensive than that observed in either the Liquid SIMS process of ionization or the off resonance collisional activation experiments. Based on previous discussions (Chapter 4) of the unimolecular dissociation of this species, this extensive fragmentation is indicative of the formation of species with high internal energies. A nice feature of the electrospray source is the ability to tune for this.

APPENDIX 1

An electron impact source which can be used for generation of ions with a controlled energy spread from a gaseous sample is shown in Figure 6-10. In addition a diagram for an easily constructed circuit that can be used to generate a non-regulated emission current from a filament is shown. The 6 amp power supply is used to supply current to the filament, and a bias supply controls the electron energy. By implementing an analog current meter as shown, the emission current from the filament can be monitored. Emission currents as high as 100 microamperes are easily obtained. The source consists of a chamber that can be attached to the gas inlet line. Electrons emitted from a filament travel through the chamber ionizing any gas present and are collected on an electron collector. The emission current can be monitored here as well. The chamber potential determines the ion energy (15 Volts) and the filament bias determines the electron energy (40 Volts). A repeller plate within the chamber is biased slightly more positive than the chamber itself (18 Volts), causing the ions to exit the chamber, where they can be detected by a mass spectrometer. The voltages given in parenthesis are for guidance only.

Figure 6-10. Diagram of an electron impact source and simple circuit for obtaining a non-regulated electron emission from the filament.

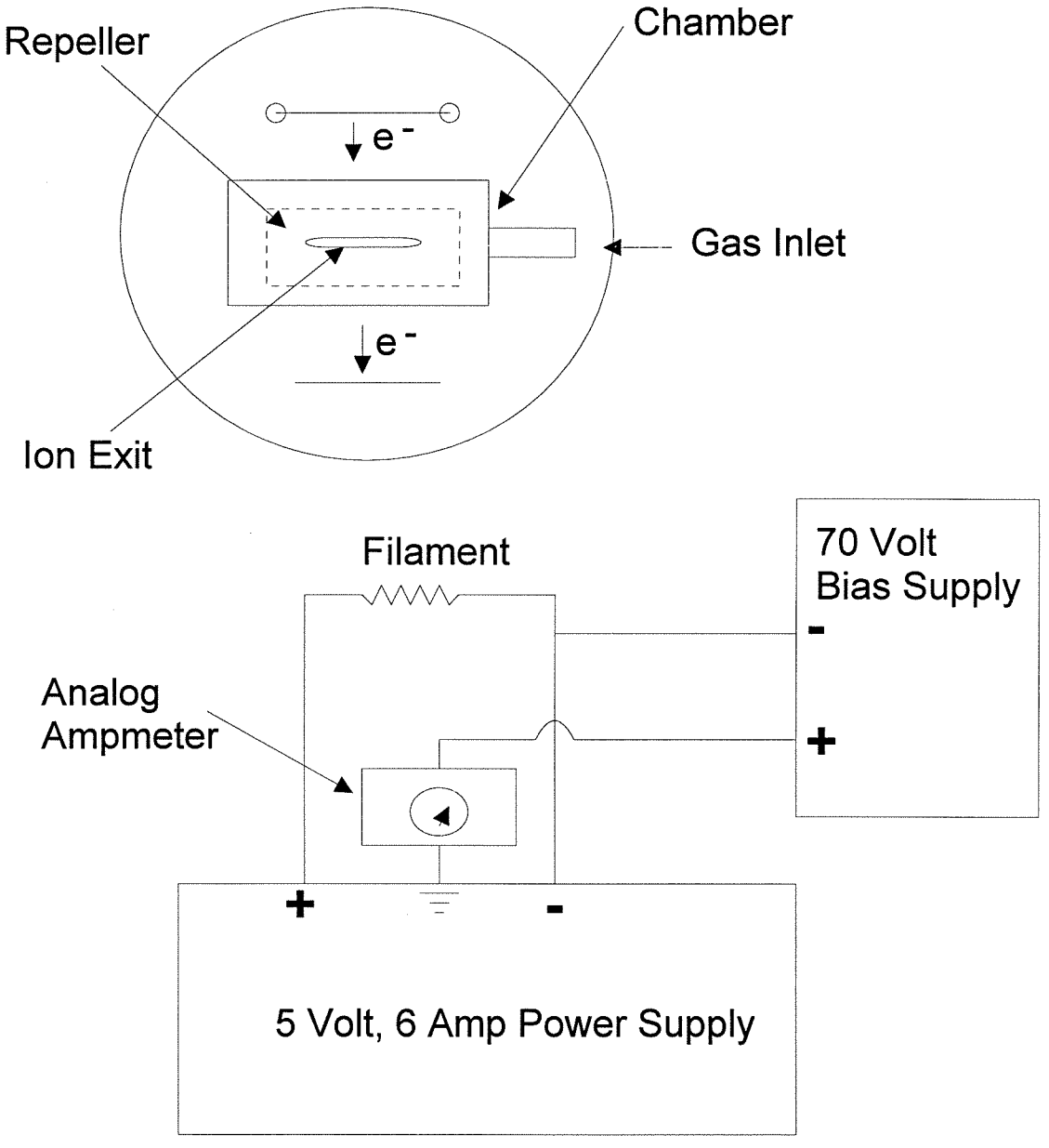
Repeller
Chamber
e -
Gas Inlet
e -
Ion Exit
Filament
70 Volt
Bias Supply
-
Analog
Ampmeter
+
+
-
5 Volt, 6 Amp Power Supply

REFERENCES

[1] Fenn, J.B.; Mann, M.; Meng, C.K.; Wong, S.F.; Whitehouse, C.M. *Science.* **1989**, 64-74.

[2] Fenn, J.B.; Mann, M.; Meng, C.K.; Wong, S.F.; Whitehouse, C.M. *Mass Spectrom. Rev.* **1990**, 9, 37-70.

[3] Huang, E.C.; Wachs, T.; Conboy, J.J.; Henion, J.D. *Anal Chem.* **1990**, 62, 713A-725A.

[4] Smith, R.D.; Loo, J.A.; Edwards, C.G.; Baringa, C.J.; Udseth, H.R. *Anal Chem.* **1990**, 62, 882-899.

[5] Allen, M.H.; Vestal, M.L. J. Am. Soc. Mass Spectrom. **1992**, 3, 18-26.